



**The creation of a platform for investigating the
network function of human pluripotent stem cell
derived neurons in development and disease**

A thesis presented for the award of

Doctor of Philosophy

William Plumbly

2017

Acknowledgements

Firstly, I would like to thank my supervisors in Cardiff, Adrian and Jeremy. Your guidance throughout this project has been invaluable and your faith in me has been incredibly appreciated. Thanks also to Nick at AstraZeneca. Yours and Tarek's help and continued interest over last few years has been greatly appreciated and much needed.

Thank you to everyone in the institute with whom I have worked and has given me help and guidance. Thanks in particular must go to Jenny, Nick, Amy and Matt. Thanks also to Adam for my training in single-cell electrophysiology - your guidance with this part of the project has been vital. A special thanks to Emma and Trudy – your tireless work running and maintaining the institute makes everybody's lives much easier than it would otherwise be.

Thank you to my family and friends for your encouragement and support over the last few years, without which this work would not have been possible.

A very special thank you must go to Hayley. I know that I could not have been without your unwavering support and continued sacrifice over the best part of ten years.

Finally, a thank you to AstraZeneca for part-funding the work in this project.

Abstract

The formation and function of neural networks is a key aspect of normal brain development, while a converging body of evidence from human genetic and clinical/preclinical studies strongly implicates altered synapse and network function in the aetiology of mental health disorders, including autism spectrum disorder (ASD). The advent of induced pluripotent stem cells (iPS cells) and protocols to differentiate them into functional neurons provides exciting opportunities for modelling human development and disease *in vitro*, although until recently the possibilities for investigating network function in such neurons have been limited. The work in this project describes the development of a platform for the analysis of network behaviour in iPS cell derived neuron cultures, based upon the use of multi electrode arrays (MEAs). The project also looks at the function of neurons derived from ASD patient iPS cells with heterozygous deletions of SHANK3, a post-synaptic density protein, mutations of which are strongly associated with ASD.

Chapter 3 describes the formation of a pipeline for the analysis of MEA data. It focuses on producing key statistics of basal excitability (e.g. Spike rate, number of bursts) and the analysis of synchronised activity states.

Chapter 4 describes the adaptation of a neuron differentiation protocol using astrocyte conditioned medium (ACM) and hypoxic (2% O₂) incubator environments to increase the functional maturity of iPS cell derived neurons. Cells cultured in ACM/2% conditions had hyperpolarised resting membrane potentials and increased induced and spontaneous action potential activity compared to neurons cultured in standard conditions.

Chapter 5 describes the profiling of spontaneous network-driven activity in iPS cell derived neurons. MEA recordings of cultures showed that spontaneous activity changes markedly over development: up to 30 days post plating (DPP) activity is uncoordinated; between 30-40DPP, coordinated activity emerges in the form of synchronised burst firing; activity from 50DPP is characterised by synchronised oscillating periods of high and low activity each lasting > 5 seconds. Coordinated behaviour required both AMPA and NMDA receptor function and the interval between more active periods was attenuated by inhibitors of GABA_A receptors and L-type voltage gated calcium channels, possibly via a common mechanism.

Chapter 6 studies the function of iPS cell derived neurons from ASD patients with deletions of SHANK3. Patients neurons were less spontaneously active than control neurons as observed with both MEA recordings and calcium imaging, while also showing changes in the shape of calcium transients. Analysis of the shape of extracellular spikes from MEA recordings revealed a small population of spike shapes, characterised by a 'double-peak', that were unique to SHANK3 mutant neurons.

This project presents a platform for the recording and analysis of network behaviour in iPS cell derived neuron over both development and in disease states. While the focus here has been on modelling ASD, the work provides a framework for the modelling of human neuron network behaviour in a range on neurodevelopmental disorders and, importantly, as method of screening novel therapeutics in a human cell context.

Abbreviations

(m)EPSC	<i>(mini) Excitatory post synaptic current</i>
4-AP	<i>4-Aminopyridine</i>
ACM	<i>Astrocyte conditioned medium</i>
aCSF	<i>Artificial cerebral spinal fluid</i>
AMPA	<i>α-amino-3-hydroxy-5-methyl-4-isoxazolepropionic acid</i>
ANOVA	<i>Analysis of variance</i>
APV	<i>((2R)-amino-5-phosphonovaleric acid</i>
ASD	<i>Autism spectrum disorder</i>
ASDR	<i>Array wide detection rate</i>
BDNF	<i>Bone derived neurotrophic factor</i>
bFGF	<i>Basic fibroblast growth factor</i>
Bic	<i>Bicuculline</i>
BSA	<i>Bovine serum albumin</i>
CI	<i>Confidence intervals</i>
CNQX	<i>6-cyano-7-nitroquinoxaline-2,3-dione</i>
CNV	<i>Copy number variation</i>
DAPI	<i>4',6-Diamidino-2-Phenylindole, dihydrochloride</i>
DAPT	<i>N-[N-(3,5-Difluorophenacetyl-L-alanyl)]-(S)-phenylglycine t-butyl ester</i>
DBSCAN	<i>Density-based spatial clustering of applications with noise</i>
DMEM	<i>Dulbecco's Modified Eagle's medium</i>
DMSO	<i>Dimethyl sulfoxide</i>
DNA	<i>Deoxyribonucleic acid</i>
DPBS	<i>Dulbecco's phosphate buffered saline</i>
DPP	<i>Days post plating</i>
EB	<i>Embryoid body</i>
ECF	<i>Extra cellular fluid</i>
EDTA	<i>Ethylenediaminetetraacetic acid</i>
EGF	<i>Epidermal growth factor</i>
ES cell	<i>Embryonic stem cell</i>

FBS	<i>Foetal bovine serum</i>
GABA	<i>γ-Aminobutyric acid</i>
HEPES	<i>4-(2-hydroxyethyl)-1-piperazineethanesulfonic acid</i>
hPS cell	<i>Human pluripotent stem cell</i>
iAP	<i>Induced action potential</i>
ICC	<i>immunocytochemistry</i>
iPS cell	<i>Induced pluripotent stem cell</i>
IPSC	<i>Inhibitory post synaptic current</i>
ISI	<i>Inter spike interval</i>
KO	<i>Knock out</i>
LAP	<i>Less active period</i>
LTCC	<i>L-type (voltage gated) calcium channel</i>
LTD	<i>Long term depression</i>
LTP	<i>Long term potentiation</i>
MAD	<i>Median absolute deviation</i>
MAP (interval)	<i>More active period (interval)</i>
MEA	<i>Multi electrode array</i>
MEF	<i>Mouse embryonic fibroblasts</i>
mGluR	<i>Metabotropic glutamate receptor</i>
MHD	<i>Mental health disorder</i>
MRS	<i>MAX rise slope</i>
NHA	<i>Normal human astrocytes</i>
NMDA	<i>N-methyl-D-aspartate</i>
NPC	<i>Neural precursors</i>
PCA	<i>Principle components analysis</i>
PDL	<i>Poly-d-lysine</i>
PFA	<i>Paraformaldehyde</i>
Picr	<i>Picrotoxin</i>
PMDS	<i>Phelan McDermid syndrome</i>
PSD	<i>Post synaptic density</i>
R_i	<i>Neuron input resistance</i>
RNA	<i>Ribonucleic acid</i>
ROI	<i>Region of interest</i>
sAP	<i>Spontaneous action potential</i>
SBF	<i>Synchronised burst firing</i>

SD	<i>Standard deviation</i>
SEM	<i>Standard error of the mean</i>
SHANK3	<i>SH3 and multiple ankyrin repeat domains 3</i>
SNV	<i>Single nucleotide variation</i>
Std	<i>Standard</i>
Tau or τ	<i>Neuron membrane capacitance</i>
VGCC	<i>Voltage gated calcium channels</i>
vGlut	<i>Vesicular glutamate transporter</i>
V_{rest}	<i>Neuron resting membrane potential</i>
WT	<i>Wild type</i>

Contents

Declarations	i
Acknowledgements	ii
Abstract	iii
Abbreviations	v
1. Introduction	1
1.1 Overview	1
1.2 Stem cells and neuronal differentiation	2
1.2.1 Human pluripotent stem cells	2
1.2.2 Neuronal differentiations and neuron maturity.....	4
1.2.3 Co – culturing neurons and astrocytes	9
1.2.4 Culturing neurons in hypoxic conditions	11
1.3 Autism spectrum disorders	13
1.3.1 Clinical overview of ASD.....	13
1.3.2 Genetic overview of ASD.....	14
1.3.3 Converging evidence of synapse and network dysfunction in ASD.....	17
1.3.4 SHANK3 and ASD	23
1.3.5 SHANK3 as a model of ASD	25
1.4 Studying networks <i>in vitro</i> and multi electrode arrays	27
1.4.1 Studying neural networks in vitro	27
1.4.2 Overview of MEAs	28
1.4.3 MEAs for studying network function in vitro.....	32
1.5 Summary	35
1.6 Project aims	36
2. Materials and methods	37
2.1. Plasticware and Consumables	37
2.2. Stem Cell Culture	38
2.2.1. Cell line and maintenance	38
2.2.2. iPS cell passaging	39
2.2.3. iPS cell freezing	39
2.4. Neural media formulations	43
2.5. Differentiation of glutamatergic neurons from IBJ4 iPS cells	44
2.5.1. Neural induction and formation of neural precursors.....	44
2.5.2. Terminal differentiation of forebrain precursors	45
2.5.3. Freezing of neural precursors.....	47

2.5.4.	Thawing of neural precursors and terminal differentiation	47
2.6.	Culture and differentiation of ASD (SHANK3) patient cell lines	48
2.7.	Culture of primary normal human astrocytes and medium conditioning	49
2.8.	Single-cell patch clamping of iPS cells derived neurons	50
2.8.1.	Patching pipettes and solutions	50
2.8.2.	Current – clamp recording of neurons	51
2.8.3.	Patch-clamp analysis	52
2.9.	Immunocytochemistry	53
2.9.1.	Cell preparation and staining	53
2.9.2.	Imaging and analysis	54
2.10.	Calcium Imaging	56
2.10.1.	Cell preparation and imaging	56
2.10.2.	Analysis	57
2.11.	Multi electrode array culturing and recordings	58
2.11.1.	Equipment	58
2.11.2.	Preparing arrays and care	58
2.11.3.	Culturing cells for use on arrays	59
2.11.4.	Recording and analysis	60
2.11.5.	MEA cleaning	61
2.12.	Statistical analysis	62
3.	The development of a pipeline for the analysis of iPS cell derived neuron	
	multi electrode array data	63
3.1	Introduction	63
3.2	Chapter Aims	65
3.3	Development and description of analysis measures	66
3.3.1	General Overview	66
3.3.2	Online data acquisition	68
3.3.3	Spike detection	72
3.3.4	Spike waveform extraction	77
3.3.5	Basic Statistics	76
3.3.6	Network Analysis	83
3.3.7	Wave feature extraction and clustering	87
3.4	Summary	90

4. Optimising culturing conditions to improve the physiological maturity of hPS cell - derived neurons	91
4.1 Introduction.....	91
4.2 Chapter Aims	93
4.3 Results.....	94
4.3.1 Intrinsic electrophysiological properties of neurons.....	94
4.3.2 Cell classification by induced action potentials.....	102
4.3.3 Intrinsic properties grouped by AP classification	104
4.3.4 Action potential analysis	109
4.3.5 Spontaneous action potentials.....	113
4.4 Discussion	115
5. Profiling network development in iPS cell derived neurons	124
5.1 Introduction.....	124
5.2 Chapter Aims	126
5.3 Results.....	127
5.3.1 Differentiations of IBJ4 iPS cells produce neurons with a cortical neuron identity	127
5.3.2 Development of network behaviour in iPS cell derived neuronal cultures	131
5.3.3 Pharmacological profiling of iPS cell derived neurons during early development	137
5.3.4 Excitatory pharmacological profiling of iPS cell neurons in late development.....	144
5.3.5 Inhibitory pharmacological profiling of iPS cell derived neurons in late development	149
5.3.6 IBJ4 iPS cells derived neuronal cultures contain GABAergic interneurons	154
5.3.7 Synchronised network activity is regulated by L-type calcium channels	156
5.4 Discussion	165
6. Functional phenotyping of ASD patient derived neurons	173
6.1 Introduction.....	173
6.2 Chapter Aims	177
6.3 Results.....	178
6.3.1 Identification of precursor and neuron fate	178
6.3.2 Investigating the development of spontaneous activity in SHANK3 mutant neurons	184
6.3.3 Interneuron populations in SHANK3 mutant and control cultures	192
6.3.4 Pharmacological profiling of SHANK3 mutant and control neurons	194
6.3.5 Investigating the shape of spikes produced by SHANK3 mutant neurons	198
6.3.6 Pharmacological profiling of spike shapes in SHANK3 mutant neurons	204
6.3.7 Investigating spontaneous calcium events in SHANK3 mutant iPS cell neurons.....	206
5.4 Discussion	215

7. General Discussion	223
7.1 Results chapter summaries.....	223
7.1.1 Chapter 3 – Development of a pipeline for the analysis of MEA data	223
7.1.2 Chapter 4 – Optimising culturing conditions to improve the physiological maturity of hPS cell derived neurons.....	224
7.1.3 Chapter 5 – Investigating network development in iPS cell derived neurons	225
7.1.4 Chapter 6 – Functional phenotyping of autism spectrum disorder patient iPS cell derived neurons.....	226
7.2 Context and points of discussion.....	227
7.2.1 Modelling network behaviour with hPS cells derived neurons.....	227
7.2.1 L-type calcium channels, network function and mental health disorders.....	230
7.2.2 Network function and iPS cell modelling in ASD	232
7.2.3 hPS cell derived neuron maturity	236
7.3 Study limitations.....	237
7.3.1 Neuron maturity and patch-clamping.....	237
7.3.2 Variability in MEA recordings.....	238
7.3.3 SHANK3 expression in ASD patient derived neurons	238
7.4 Future directions	240
7.4.1 L-type calcium channels	240
7.4.2 Observing network behaviour in SHANK3 mutant (and control) neurons.....	240
7.4.3 Unique spike shapes of SHANK3 mutant neurons	241
7.4.4 Extending the analysis of networks	242
7.4.5 Conclusions	243
 References	 244
 Appendix.....	 259

1. Introduction

1.1 Overview

Over the last few years technological advances and improvements in methodological processes have substantially increased the opportunities for modelling neurological diseases *in vitro* with human pluripotent stem cells (hPS cells). In particular, the use of induced pluripotent stem cells (iPS cells) derived from individual patients allows studying the influence of particular genetics to disease aetiology while opening up the potential for personalised therapeutics. The advent of large-scale genetics studies has provided a wealth of novel insights into the complex genetics of several mental health disorders (MHDs), including autism spectrum disorders (ASD). Together with iPS cell technologies and protocols to differentiate these cells into neurons, this provides a unique opportunity to study the cellular and molecular aspects of ASD in a model human system. However, as with other MHDs, converging genetic and experimental evidence strongly implicates a role for aberrant synaptic singling and circuit function in ASD. Advances in multi-electrode array (MEA) technologies have opened up opportunities to study network function in a iPS cell model system, which has, until more recently, been limited. However, a key obstacle in investigating network function of iPS cell derived neurons is their relative immaturity compared to adult or primary rodent neurons, a limitation which must be addressed to observe complex network behaviour *in vitro*.

This chapter provides a background to the use of hPS cells for modelling neuronal function *in vitro* and focuses on methods to improve the immaturity of hPS cell derived neurons. It subsequently then provides an overview of ASD and highlights the converging evidence implicating altered network function in the disorder. Finally, the chapter offers a background to the use of MEAs for studying neuron electrophysiology with an emphasis on the use of MEAs to record the activity of hPS cell derived neurons.

1.2 Stem cells and neuronal differentiation

1.2.1 Human pluripotent stem cells

The *in vitro* modelling of human neurons is based upon the use of human pluripotent stem cells (hPS cells). For several years this referred solely to human embryonic stem cells (ES cells), pluripotent cells derived from the inner cell mass of blastocysts (Thomson *et al.*, 1998). The 'stem' nature of these cells was shown by their ability to differentiate into teratomas encompassing cells from all three germ layers and their ability to be self-renew indefinitely *in vitro* (Richards *et al.*, 2003). ES cells have provided a great deal of information about the nature of *in vitro* development and have been the basis for the creation of protocols to differentiate cells in to range of fates, including cardiomyocytes (Mummery *et al.*, 2003), hepatocytes (Rambhatla *et al.*, 2003), osteoblasts (Sottile *et al.*, 2003) and a range of neuronal fates (see section 1.2.2). However, the use of ES cells is not without controversy (Orive *et al.*, 2003). The derivation of the inner cell mass firstly requires a source of embryos, most of which are donated following *in vitro* fertilisation; and the collection of the inner cell mass requires destruction of the embryo. Never the less, ES cells have remained an important part of cell culture research and continue to be used for range of applications, especially as they are still regarded as the 'gold standard' hPS cells by some researchers.

In 2006-07, a landmark series of studies by a number of groups showed the generation of hPS cells derived from adult somatic cells (Takahashi and Yamanaka, 2006; Okita *et al.*, 2007; Wernig *et al.*, 2007; Takahashi *et al.*, 2007; Yu *et al.*, 2007). These induced pluripotent stem cells (iPS cells) were generated by forced expression of a combination of the pluripotency associated transcription factors OCT3/4, SOX2, KLF4, c-MYC, NANOG and LIN28 in fibroblasts and produced stem cells which were very similar to ES cells, most importantly by demonstrating both self-renewal and differentiation into lineages from all three germ layers. In subsequent years the methods to produce iPS cells has continually improved to address some of the potential issues associated with the early incarnations. This includes includes the use of non-integrating methods of gene delivery (Okita *et al.*, 2008; Stadtfeld *et al.*, 2008) , reduction and regulation of oncogene expression and methods to increase the efficiency of iPS cell production (Huangfu *et al.*, 2008; Luo *et al.*, 2013) . However, despite these improvements, there is still some debate over whether iPS cells are as 'true' a stem cell as ES cells. In particular, there is

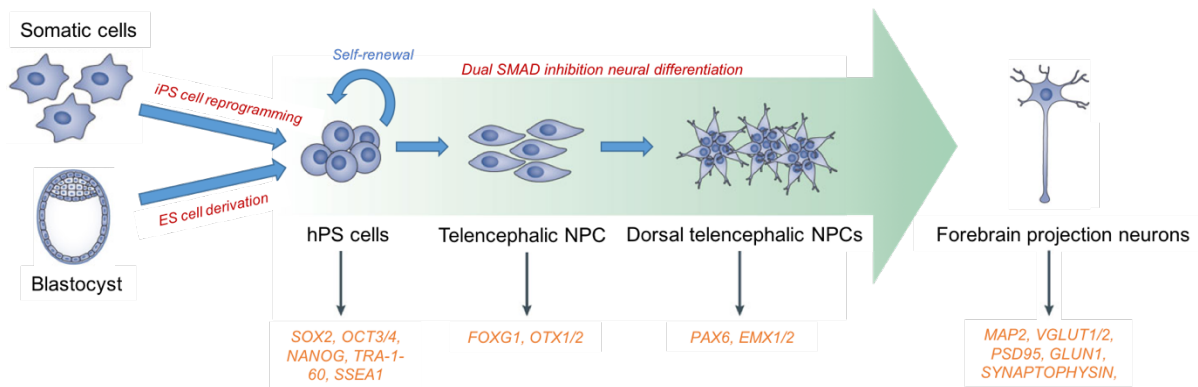
some concern over differences in gene expression (Chin *et al.*, 2009; Ghosh *et al.*, 2010) and changes at the level of the epigenome. Both ES and iPS cells should possess a 'reset' epigenetic landscape, however it has been shown that some iPS cell lines show remnants of a DNA methylation signature characteristic of the somatic cells from which they were derived (Kim *et al.*, 2010; Doi *et al.*, 2009). Furthermore, epigenetic differences have been noted in different clones of iPS cells derived from the same pool of somatic cells, suggesting that inappropriate methylation may be the result of incomplete reprogramming (Polo *et al.*, 2010). Finally, it has also been suggested that sporadic de novo mutations and larger chromosomal alterations occur in iPS cells more frequently than ES cells (Hussein *et al.*, 2011; Laurent *et al.*, 2011).

Despite these reservations, the research potential of iPS cells was recognised immediately and they have become a routine part of human cell based research. The use of iPS cells from healthy individuals has provided a valuable alternative source of 'WT' stem cells without much of the controversy associated with the creation of ES cells. However, the biggest application of iPS cells is their use in disease modelling and especially for those diseases with complex genetic aetiologies. As well as being able to derive iPS cells from patients for whom specific causative mutations are known, they also allow the comparison between different patient derived cell lines with the same disease-implicated mutations, in the context of different genetic backgrounds. To enhance the use of iPS cells for disease modelling, technologies have been continuously developed to improve their accessibility from an increasing number of patients. Specifically, while early methods were based upon the use of fibroblasts as the source cells, which requires the collection of a skin biopsy, protocols have been optimised to allow of the reprogramming of a range of somatic cells, including keratinocytes (Aasen *et al.*, 2008), blood tissues (Loh *et al.*, 2010; Staerk *et al.*, 2010) and renal epithelial cells present in urine samples (Zhou *et al.*, 2012). The use of these less invasive cells is of particular interest in the study of developmental diseases where cells are ideally sourced from younger patients.

1.2.2 Neuronal differentiations and neuron maturity

Although iPS cells can, in theory, be used to model any adult tissue system, perhaps their biggest application over the last few years has been in the modelling of neurons for studying both human development and disease. Protocols for differentiating stem cells into neurons were developed initially with ES cells but have been transferred successfully for use with iPS cells. Indeed, to date iPS cells have been used to create a wide array of neuronal subtypes including dopaminergic (Kwon *et al.*, 2014), serotonergic (Lu *et al.*, 2016b), medium spiny neurons (Arber *et al.*, 2015), hypothalamic neurons (Wang *et al.*, 2015) and GABAergic interneurons (Nicholas *et al.*, 2013; Maroof *et al.*, 2013). However, by far the most developed protocols are those used to produce ‘forebrain cortical neurons’, which, while encompassing an array of possible neuron types, has become a somewhat standard term to describe the production of mostly glutamatergic, excitatory neurons of a cortical fate (Muratore *et al.*, 2014; Espuny-Camacho *et al.*, 2013; Shi *et al.*, 2012; Chambers *et al.*, 2009). Unless otherwise stated, for the following sections ‘hPS cell derived neurons’ refer to neurons of this fate.

The differentiation of neurons from hPS cells is based upon the *in vitro* modelling of the early embryonic environment in such a way as to promote the formation of (neuro)ectoderm, followed by neural progenitors and finally terminally differentiated neurons (Figure 1.1). This involves mimicking the expression of particular morphogenic signals present in the developing neural tube to produce a patterning of cells according to their eventual fate. The various stages of development can then be traced by the expression of certain protein markers in the cells. For excitatory forebrain neurons, this first requires the production of telencephalic precursors expressing FOXG1 and OTX1/2; followed by PAX6 / EMX1/2 positive *dorsal* telencephalic progenitors; and finally determined cortical projection neurons which express a variety of proteins, including MAP2, TBR1 and VGLUT1/2 (Watanabe *et al.*, 2005; Rakic, 2009). In general, there are two main routes to produce neurons from iPS cells, one based upon the formation of 3D embryoid body aggregates (EBs) and another based upon monolayer cultures. EB methods were originally developed from protocols used to differentiate neurons from mouse ES cells and while they still remain an important part of stem cell culture methods, have perhaps been superseded in more routine differentiations by monolayer protocols. These are based upon inhibiting SMAD signalling in hPS cells, via two independent routes

A**B**

	hPS cell neurons	Mouse cortical neurons
Passive		
V_{rest} (mV)	-42.9	-70
Input resistance ($G\Omega$)	1.7	0.2
Membrane capacitance (pF)	32.9	80
Action potentials		
AP threshold (mV)	-32.1	-53
Amplitude (mV)	53.4	93
Half – width (ms)	5.2	0.8

Figure 1.1 – Differentiation of neurons from human pluripotent stem cells (hPS cells). (A) hPS cells are derived from two sources: embryonic stem cells (ES cells) are isolated from the inner cell mass of a blastocyst; induced pluripotent stem cells (iPS cells) are derived from adult somatic cells (e.g. fibroblasts or keratinocytes) by reprogramming cells using forced expression of pluripotency transcription factors, typically OCT3/4, SOX2 and NANOG. hPS cells can self renew *in vitro* and can be used to produce neurons via differentiation protocols. Monolayer protocols to produce cortical projection neurons are based upon inducing a neural fate by dual – SMAD signalling inhibition. At each stage of the protocol, the fate of the cells can be determined by analysing their expression of certain patterning markers (orange writing). Produced neurons are routinely described as ‘mature’ if they show expression of a number of neuronal and synaptic markers. However, electrophysiologically they remain immature compared to cortical mouse neurons (B). A was produced using graphics adapted from Mertens et al., 2016. The hPS cell neuron data in B was calculated by taking an average of the statistics presented in Shi *et al.*, 2012, EspunyCamacho *et al.*, 2013 and Bardy *et al.*, 2015. The mouse data in B was taken from the Cell Types Database @ The Allen Brain Atlas and represents data from a typical layer IV pyramidal neuron.

(termed dual SMAD inhibition), which, in the presence of pro-neural medium, is sufficient to induce a neural fate in a high proportion of stem cells (Chambers *et al.*, 2009; Muratore *et al.*, 2014).

One of the key outstanding issues surrounding hPS cell derived neurons is that of maturity. While almost all protocols and studies describe the end point neurons as mature, this is relative in the context of developing hPS cell neurons. In real terms, these neurons are still immature when compared to adult human neurons and rodent primary neurons across a number of physiological measures. For example, hPS cell neurons rarely have resting membrane potentials (V_{rest}) below -50 mV, compared to around -70 mV for adult glutamatergic cortical neurons (Kandel, 2013); possess high input resistances greater than around 500 M Ω , compared to under 200 M Ω for cortical pyramidal neurons (input resistance is a key measure of neuronal maturity and describes the extent to which cells express functional ion channels; (Allen Brain Atlas, 2015; Figure 1.1); and while hPS cell neurons can possess functional NMDA receptors, these very rarely contain GluN2A, the subunit expressed in the majority of cortical synapses in adult brain (Cull-Candy *et al.*, 2001). The relative immaturity of hPS cell neurons is perhaps not a surprise given the nature of culturing procedures and the fact that even an 80-day protocol going from stem cells to post mitotic 'mature' neurons lasts only around a third of the typical human gestation period. Indeed, comparison of hPS cell neuron (derived using a monolayer protocol) and human developmental transcriptomes revealed that stem cell neurons most closely resembled human neurons from the late first to early second trimester (Brennan *et al.*, 2014).

Overall, neuronal differentiation protocols are relatively long, taking on average around 8 weeks for the development of mature neurons, potentially introducing productivity limitations into any planned experiments. Furthermore, many of the earlier protocols in particular showed highly variable conversion efficiencies, produced heterogeneous populations of cells and could be inconsistent between different cell lines. As such, the attention of many protocol optimisation studies has been on the homogeneity of cultures, the production of purer neuronal populations and efforts to improve the timescale of neuron production. This includes using combinations of small molecules (Li *et al.*, 2011), heterologous expression of transcription factors (Zhang *et al.*, 2013) and the direct conversion of fibroblasts into neurons using

transcription factors (Tian *et al.*, 2012; Pfisterer *et al.*, 2011) or microRNAs (Yoo *et al.*, 2011). However, although studies usually present results regarding the maturity of neurons, this has often primarily been determined by the expression of proteins, for example which mark neuron 'maturity' (e.g. MAP2, NEUN), mark cortical layer fate (e.g. SATB2, CTIP2) or mark the development of synapses (e.g. PSD-95, Synaptophysin and GluN1).

It is only more recently where a functional analysis of neurons in terms of their electrophysiological properties has become more routine and the optimisation of protocols has focused more on physiological maturity. An interesting study explicitly looking at maturity over neuronal development using a standard protocol highlighted that while hPS neurons do functionally mature over time, this development is slow, variable and ultimately often limited (Prè *et al.*, 2014). A number of subsequent studies have developed protocols which have shown impressive improvements in hPS cell-neuron maturation. Bardy *et al.* identified a number of compounds present in more standard differentiations basal mediums (almost all of which are based upon DMEM/F12 and/or neurobasal) which may impair the development and function of physiological neuron activities (Bardy *et al.*, 2015). Consequently, they developed a basal medium centred upon replicating the physiological characteristics of aCSF, which was shown to improve the functional maturity of hPS cell neurons, including increased induced and spontaneous activity, increased synaptic events and reduced input resistance, although this was still relatively high ($>1 \text{ G}\Omega$). Taking a different approach, Telezhkin *et al.* described a protocol based upon the development of a batch of novel media formulations, with a DMEM/F12 base, containing a range of small molecules including mitotic inhibitors, the BDNF receptor agonist LM22A4, the GSK3 β inhibitor CHIR99021 and GABA (Telezhkin *et al.*, 2016). Neurons produced with this protocol showed good spontaneous and induced action potential formation, relatively hyperpolarised resting membrane potentials and input resistances often below $800\text{M}\Omega$, all of which appeared within 21 days of the start of differentiations. Finally, Gunhanlar *et al.* recently described the development of relatively simple protocol, based upon DMEM/F12 / neurobasal medium, which in their hands produced neurons with impressively hyperpolarised resting membrane potentials of $< -55 \text{ mV}$, some spontaneous action potentials and spontaneous post-synaptic currents (Gunhanlar *et al.*, 2017).

While these three studies together present good progress in terms of neuron physiology, it is clear that certain properties may be enhanced by the specific optimisation methods used and that there is a certain degree of variation seen depending on the source cell lines (Bardy *et al.*, 2015; Bardy *et al.*, 2016). Furthermore, some of these protocols require non-standard reagents and the use of multiple small molecules which may be prohibitive in some research circumstances. Instead, there has been some interest in the use of more simple and accessible protocol modifications, based upon improving the physiological nature of the culturing system. The following sections will focus on two of these protocol manipulations: culturing neurons with medium pre-conditioned by primary astrocytes and maintaining developing cultures in hypoxic conditions.

1.2.3 Co – culturing neurons and astrocytes

Over the last few years a strong body of evidence has developed implicating astrocytes in the functional maturation of neurons and especially in the development of the synapse (Ullian *et al.*, 2004; Hama *et al.*, 2004 and reviewed in Clarke and Barres, 2013). At the most basic level, astrocytes are essential for neuron survival throughout development *in vivo*, as they regulate both blood flow and metabolic resources (Attwell *et al.*, 2010; Pellerin *et al.*, 2007). At the synapse, support can be in the form of physical contacts between astrocytes and developing neurons, where local interactions promote synaptogenesis via activation of protein kinase C (Hama *et al.*, 2004). Astrocytes also provide support via the secretion of pro-synaptogenesis molecules, including those which promote synapse formation (e.g. thrombospondins; Risher and Eroglu, 2012 and hevin; Kucukdereli *et al.*, 2011), the activation of ‘silent’ synapses early in development via the requirement of functional AMPA receptors (glypicans; Allen *et al.*, 2012); and molecules which may regulate functional synapses by the *inhibition* of synapse formation (e.g. SPARC; Kucukdereli *et al.*, 2011). Interestingly, there is also evidence to suggest that astrocytes secrete different molecules depending on the type of synapse being formed (excitatory/inhibitory; Hughes *et al.*, 2010; Elmariah *et al.*, 2005). Finally, astrocytes are also involved in the activity-dependent pruning of synapses, via mechanisms involving phagocytosis (Chung *et al.*, 2015).

The role of astrocytes in developing hPS cell neurons is less understood. In hPS cell neural differentiations, astrocytes do form natively but the process is delayed such that during early neuron development and synaptogenesis, there is few astrocytes present and those that are there are likely to be immature (Roybon *et al.*, 2013; Itsykson *et al.*, 2005; Serio *et al.*, 2013). Protocols have been specifically developed for the differentiation of astrocytes from hPS cells, involving a range of molecules including BMPs (Krencik and Zhang, 2011), CNTF (Shaltouki *et al.*, 2013) and the undefined combination of factors present in fetal bovine serum (FBS) (Hayashi *et al.*, 2011). However, while some of these have been adapted into neuron differentiation protocols to produce a mixed population of cells, it is very hard to control the continued growth of astrocytes over that of the post-mitotic neurons. Another approach involves co-culturing astrocytes and neurons by introducing exogenous astrocytes, either primary rodent or human, into neurons. This method has shown to increase the maturity of cultures by a

number of measures, including promoting more physiological resting membrane potentials, increased synapse formation and enhanced spontaneous excitability (Kaczor *et al.*, 2015; Hu *et al.*, 2016; Odawara *et al.*, 2014 and reviewed in Livesey *et al.*, 2015). Again however, it can be difficult to control the proliferation of astrocytes relative to neurons, and without the use of mitotic inhibitors there can be a tendency for astrocytes to overwhelm the culture and form astrocyte-only aggregates. Finally, for larger differentiations of neurons the requirement to set up co-culture systems may become logistically prohibitive.

Using a different approach, several studies have shown that pre-conditioning neuron differentiation medium with human or rodent astrocytes can enhance the development and maturation of neuron cultures (Hama *et al.*, 2004; Rushton *et al.*, 2013). In this way, astrocytes are cultured in differentiation medium for several days allowing them to secrete the pro-maturation factors described above (thrombospondins, hevin etc.) and others including GDNF, TGF β and CCL5 (Chang *et al.*, 2003). The conditioned medium (astrocyte conditioned medium; ACM), is then used as usual on neuronal cultures, exposing the developing neurons to these factors. Of course, this approach does not allow any physical interactions between neurons and astrocytes and therefore prevents any potential benefits that contact may provide. However, by hopefully exposing neurons to pro-maturation factors, in particular those which promote functional synapse formation, ACM aids in the development of hPS cell derived neurons which can be easily adapted and scaled to a range of differentiation protocols.

1.2.4 Culturing neurons in hypoxic conditions

Typically, all cell cultures including neuron differentiations are incubated at 37°C in an atmosphere of 95% air and 5% CO₂, leading to a chamber O₂ concentration of around 20%. This level of oxygen is highly un-physiological compared to that of mammalian brain tissue and especially the developing brain (Erecińska and Silver, 2001; Goda *et al.*, 1997; Silver and Erecińska, 1998). Indeed, the average partial pressure of O₂ in the rat is between 0.1% and 5.3%, depending on brain region. The reason for this discrepancy is perhaps partly one of protocol routine and partly one of logistics, as differentiating neurons are often cultured in the same incubator as stem cells, which do require the higher oxygen levels. Nevertheless, several studies dating back a number of years have reported the benefits of reduced oxygen on neuron culturing, including on neuron/progenitor survival (Studer *et al.*, 2000; Cheng *et al.*, 2014; Brewer and Cotman, 1989) and neuron maturation, dendrite arborisation and synaptogenesis (Studer *et al.*, 2000; Liu *et al.*, 2009). While the exact mechanisms for these responses are not clear, it has been suggested that the low O₂ conditions promote the expression and production of neuroprotective and pro-maturation trophic factors, including FGF8 and erythropoietin (Epo; (Studer *et al.*, 2000)). FGF8 is most commonly thought of as one of the key morphogens involved in the fate determination of midbrain dopaminergic neurons (for a review see Arenas *et al.*, 2015) and indeed FGF8 is thought to be essential for the differentiation of stem cell derived dopaminergic neurons *in vitro* (Lim *et al.*, 2015; Barberi *et al.*, 2003). However, there is evidence to suggest that FGF8 is also involved in cortical neuron development, after prosencephalic/mesencephalic specification. At this point, FGF8 may act to control localised cortical populations, acting with EMX2 and PAX6 to control the development of cortical progenitors (Grove and Fukuchi-Shimogori, 2003; Rebsam *et al.*, 2002). Epo is the primary hormone that regulates the production of red blood cells in bone marrow. Epo and its associated receptor are known to be expressed in the developing mammalian brain, although its function during this period is not well understood (Yu *et al.*, 2002; Juul *et al.*, 1998). However, several studies have shown that Epo has neuroprotective effects on several different neuronal types, especially following hypoxia-induced excitotoxicity (Lykissas *et al.*, 2007; Celik *et al.*, 2002; Morishita *et al.*, 1997). The mechanism by which Epo acts in this way is again, not well understood, however work has shown that multiple signalling pathways could be implicated, including those involving PI3-K, ERK1/2 and AKT-1/PKB (Sirén *et al.*, 2001; Chong *et al.*, 2002).

Importantly, several studies have reported the improved survival of hPS cell derived neural progenitors with hypoxic (or 'normoxic'; 2.5 – 5% O₂) compared to 'standard' (20% O₂) incubator atmospheres (Bilican *et al.*, 2014; Santilli *et al.*, 2010; Stacpoole *et al.*, 2011). Furthermore, Bilican *et al.*, also report that neurons cultured in lowered O₂ conditions display enhanced functional maturation compared to cells in ambient oxygen, as shown by increases in cell excitability, cell capacitance and functional excitatory synapse formation.

1.3 Autism spectrum disorders

1.3.1 Clinical overview of ASD

Autism spectrum disorder (ASD) represents a group of related heterogeneous developmental neurological conditions with onset typically in early childhood. Symptoms are broadly characterised into two key domains: social and communicative, including delayed speech development, limited vocabulary and an unwillingness to interact with peers; and repetitive and restrictive behaviours including limited and recurring routines, uncreative playing and highly specific and limited interests. ASD is associated with a range of comorbidities including motor deficits (McPartland and Klin, 2006), sleep abnormalities (Malow *et al.*, 2012) and seizures (Tuchman and Rapin, 2002), along with other neurological disorders including anxiety (White *et al.*, 2009) and ADHD (Reiersen and Todd, 2008). However, the most common comorbidity is that of intellectual disability (ID), which is thought to occur in around 30-40% of ASD patients (Emerson and Baines, 2010).

ASD affects around 1 in 100 people in the UK, however diagnosis rates are around 4 times higher in males than females (Brugha *et al.*, 2009; Baird *et al.*, 2006). The reason for this difference is currently unknown but a concept gaining increasing interest is the idea of a female protective effect (FPE). Under this model, females are protected from risk of developing ASD by an as yet unidentified trait absent in males, while carrying an increased etiological burden than even affected males (Werling and Geschwind, 2013; Robinson *et al.*, 2013). While evidence for this model remains inconclusive, genetic studies have shown that the incidence of rare deleterious mutations (see next section) is higher in female than male ASD patients (Sanders *et al.*, 2012; Gilman *et al.*, 2011).

1.3.2 Genetic overview of ASD

In common with other mental health disorders (MHDs), the broad aetiology of ASD is thought to be a combination of genomic and environmental factors. Studies with families and twins have shown that ASD is a highly heritable disorder with concordance rates ranging from 5-14% in siblings up to 70-90% in monozygotic twins (Hallmayer *et al.*, 2011; Sandin *et al.*, 2014; Ronald and Hoekstra, 2011). Genetic risk in ASD is conferred by a range of different types of variation which have unique patterns of inheritance and disease penetrance. Figure 1.2 shows examples of the major types of genetic mutations that may contribute to ASD, with their respective inheritance patterns. By far the most researched component of ASD genetic risk is that conferred by rare and *de novo* single nucleotide variation (SNVs; Yuen *et al.*, 2016; Neale *et al.*, 2012; Sanders *et al.*, 2012; De Rubeis *et al.*, 2014b; lossifov *et al.*, 2014b) and copy number variations (CNVs; Levy *et al.*, 2011; Bucan *et al.*, 2009; Szatmari *et al.*, 2007; Sebat *et al.*, 2007). A large number of studies have shown an enrichment of SNVs and CNVs in ASD patients compared with healthy controls, or, in the case of *de novo* variation, protein disrupting mutations identified in the patient but not in either parent (lossifov *et al.*, 2014a). In some cases, individual genes have been identified which harbour strongly ASD associated mutations, including *CHD8* (Bernier *et al.*, 2014), *SCN2A* (Weiss *et al.*, 2003), *TBR1* (Chuang *et al.*, 2015) and *GRIN2B* (Pan *et al.*, 2015). It should be noted though that due to study sample sizes and the rarity of these mutations, no single gene mutation has reached genome-wide significance for ASD association.

Rare and *de novo* deleterious mutations are thought to have high penetrance for ASD – i.e. their presence in an individual is likely to be a key aetiological factor in disease development. However, across the ASD population, these mutations can explain only a very small amount of the genetic risk for disease development. For example, mutations in *CHD8* are some of the most strongly associated with development of ASD and indeed may even confer a subtype of the disorder (Bernier *et al.*, 2014; Barnard *et al.*, 2015). *CHD8* mutations therefore have high disease penetrance but are estimated to only be present in around 0.21% of the ASD population (De Rubeis *et al.*, 2014a). Instead, it is thought that the biggest contributor of genetic risk for ASD is inherited common variations (Gaugler *et al.*, 2014; Klei *et al.*, 2012). These are mostly non-exonic SNVs with a population wide minor allele frequency of > 0.05, each which may contribute a tiny degree of risk for developing ASD (i.e. have low penetrance). However, when

many of these mutations are inherited, the risk burden increases and, together with environmental influences, contribute to the development of disease. While this polygenic model is shared with other MHDs such as schizophrenia and depression (Lee *et al.*, 2013; Schizophrenia Working Group of the Psychiatric Genomics Consortium, 2014), unlike those disorders no single loci has reached genome wide significance for ASD association.

The genetic variations which show the highest penetrance for disease are those which are known to be causative in a range of complex developmental syndromes. These consist of both specific exonic point mutations (e.g. Timothy syndrome, *CACNA1C*; Tuberous sclerosis complex, *TSC1 & TSC2*) and CNVs (e.g. Phelan McDermid syndrome, Velo-cardial facial syndrome), which can be both inherited and *de novo*. While these conditions are rare in the ASD population as a whole, they show up to 80% penetrance in individuals (Phelan *et al.*, 2001; Splawski *et al.*, 2004). These syndromic disorders are highly heterogeneous both in the specifics of their genetics and in the presentation of symptoms, such that patients with differing mutations may present with very similar symptoms, while other patients with identical mutations may not share identical indications. Furthermore, due to the nature of these disorders, a diagnosis of ASD can be precluded by or difficult to dissociate from other neurological presentations.

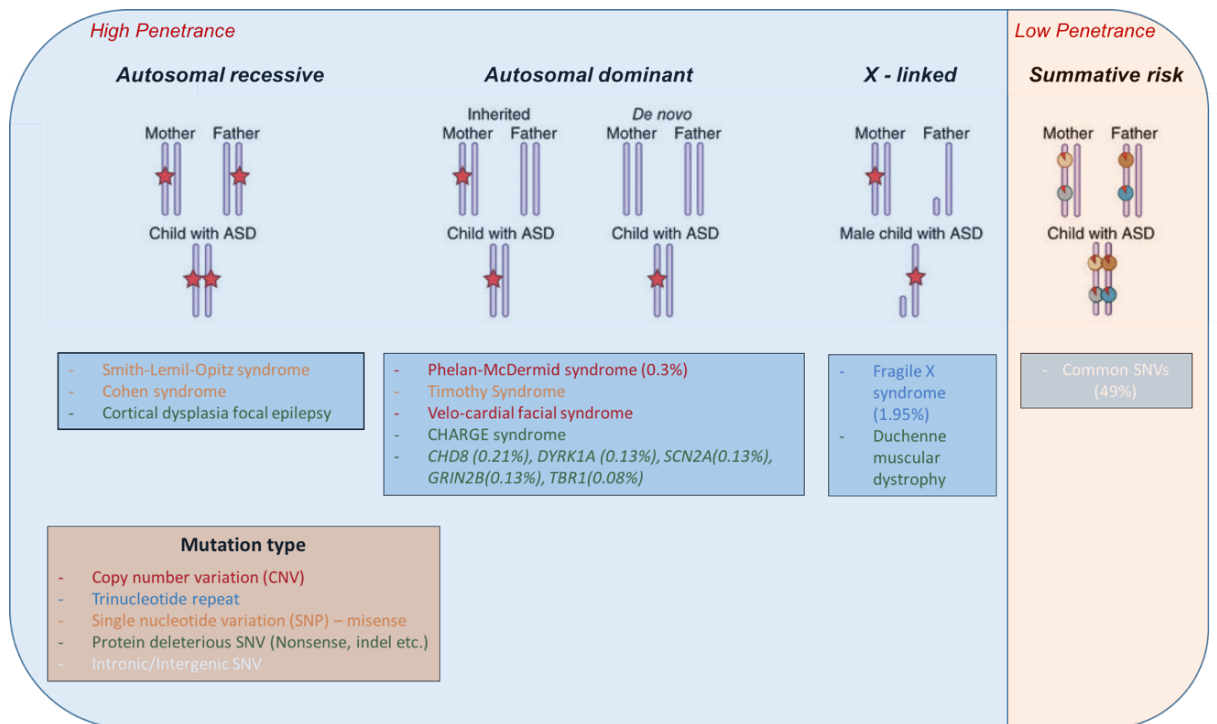


Figure 1.2 - Overview of the genetic variation identified in autism spectrum disorder. The genetics of autism spectrum disorder (ASD) is complex and involves various methods of inheritance and types of mutations. A number of rare inherited and de novo mutations (exonic single nucleotide variations; SNVs) have been identified in several genes including *CHD8*, *DYRK1A* and *SCN2A*. Along with several syndromic conditions with known causative mutations (Phelan-McDermid, Timothy, CHARGE syndromes etc), these represent genetic variation, with various methods of inheritance, which have strong ASD penetrance but account for only a very small percentage of ASD cases. In contrast, inherited mutations in the form of common intronic/intergenic single nucleotide variants (SNVs) provide a tiny degree of risk individually, but can provide summative burden of risk when many are inherited together. This low penetrance common variation thought to explain around 49% of genetic risk in ASD. Figure is adapted from one appearing in DeLaTorreUbieta *et al.*, 2016.

1.3.3 Converging evidence of synapse and network dysfunction in ASD

To date, over 800 genes have been implicated to varying degrees in increased risk for ASD, including single genes part of CNVs for which associative evidence is available (Abrahams *et al.*, 2013). However, recent focus has been on the convergence of these implicated loci on a few molecular pathways, namely protein translation (e.g. *NF1*, *MAPK1*, *RPS6KA3*), WNT signalling (e.g. *PRICKLE1/2*, *CTNNB1*, *CHD8*) and, importantly, synaptic signalling (e.g. *SHANKs*, *SYNGAP1*, *NRXN1*, *NLGN1*; *Figure 1.3A*). Together with the genetic evidence, there has also been a convergence of evidence from a range of human patient and model sources implicating aberrant synaptic signalling and network function in ASD.

Studies in patients have provided a range of evidence implicating aberrant circuit and network behaviour and the level of whole brain function. Several EEG studies using event-related potentials have reported deficits in the way that children with ASD respond to various audio cues, suggesting that there is disturbances in the way that such cues are processed in the brain (Gomot *et al.*, 2002; R *et al.*, 2003; Oram Cardy *et al.*, 2005). Using similar approaches, other studies have shown that ASD patients have deficits in the dissociation of faces from other objects and in the spatiotemporal processing of emotional facial expressions (Akechi *et al.*, 2010; Wong *et al.*, 2008; Dawson *et al.*, 2002). These findings have been corroborated by fMRI studies which have shown that deficits in face- and expression-recognition in ASD are associated with aberrant circuit activity involving several brain regions, including the fusiform gyrus and the amygdala (Kleinmans *et al.*, 2011; Dalton *et al.*, 2005). Other brain imaging studies have focused on executive functioning and have reported that decreased connectivity of cortical inhibition networks may be responsible for alterations to executive processing, which may manifest as inflexible cortical processing leading to the repetitive and restrictive behaviours often observed in ASD (Hill, 2004; Schmitz *et al.*, 2006; South *et al.*, 2007). Similar studies have shown decreased connectivity between language centres and higher processing regions of the frontal cortex and in areas associated with the comprehension of sentences (Just *et al.*, 2004; Kana *et al.*, 2006). A number of reports have implicated aberrant circuit behaviour involving anterior cingulate networks (Mundy, 2003) and orbitofrontal-amygdala connections in deficits seen in the self regulation of socio-emotional behaviour (Bachevalier and Loveland, 2006). Finally, there is evidence to suggest that ASD can be thought of as a more global disconnection disorder caused by irregular neurodevelopmental processes (Geschwind and Levitt, 2007), with

recent diffusion tensor imaging studies reporting altered cortical axonal connectivity (Conturo *et al.*, 2008; Solso *et al.*, 2016). For reviews of human studies of networks in ASD see Belger *et al.*, 2011 and Hernandez *et al.*, 2015.

Human neuropathological studies using post-mortem tissue have also provided evidence of altered neural structure in ASD, although it should be noted that these studies can often be limited by comorbidities and small sample sizes. Several studies have reported altered numbers of neurons, neuron size and positioning of neurons in ASD. These changes have been consistently identified in the hippocampus and amygdala (Bauman and Kemper, 1985; Lawrence *et al.*, 2010; Raymond *et al.*, 1996; Schumann and Amaral, 2006) but have also been reported in several regions of the cortex (Courchesne *et al.*, 2011; van Kooten *et al.*, 2008; Simms *et al.*, 2009). Altered neuronal morphology including aberrant dendritic arbor formation has also been identified in limbic regions and the cortex (Wegiel *et al.*, 2010; Zikopoulos and Barbas, 2010; Hutslar and Zhang, 2010), a region which has also showed altered minicolumn formation (Casanova *et al.*, 2002; Buxhoeveden *et al.*, 2006). Finally, altered glial structure in ASD brains has also been reported, including inappropriate microglia infiltration (Vargas *et al.*, 2005; Tetreault *et al.*, 2012), which may lead to impaired connectivity (Rodriguez and Kern, 2011).

Single gene rodent models of ASD have delivered a good body of evidence that implicates aberrant synaptic signalling and circuit function in ASD. As with all rodent models of disease however, phenotypes have to be viewed in the context of their association to the mutation used as the model, rather than directly to the disease itself. This is especially important when modelling ASD as genetic rodent models are based upon those genes for which clear associations are known. This therefore generally limits ASD rodent modelling to those rare and *de novo* mutations which, while having high disease penetrance, are overall rare in the ASD population. Furthermore, models are often used because of the associated behavioural phenotypes purported to mimic certain ASD symptoms including impaired social interactions, repetitive behaviours and altered communications.

Deficits in neurogenesis and neuronal migration have been reported in a number of genetic rodent models including *CADPS2* (Sadakata and Furuichi, 2009), *CNTNAP2* (Peñagarikano *et al.*, 2011), *FMR1* (Irwin *et al.*, 2000) and *TSC1* (Tsai *et al.*, 2012). All of these models also had

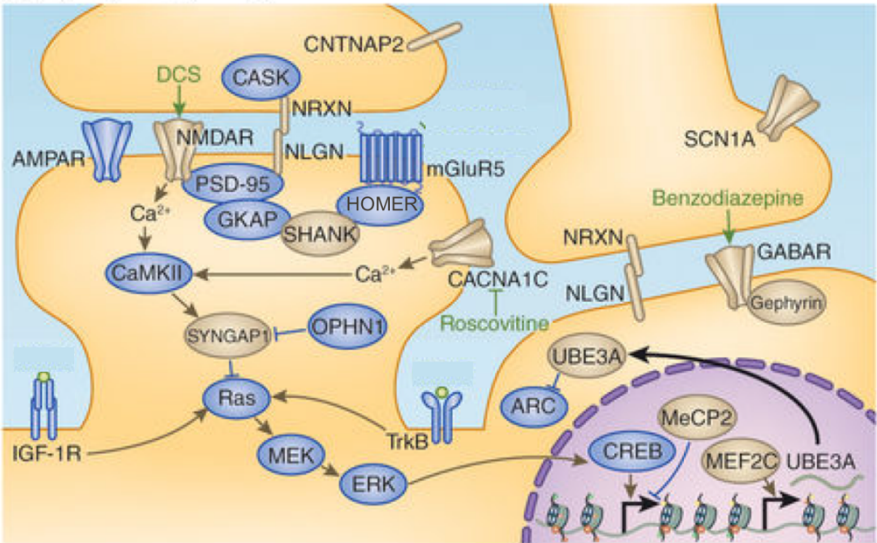
neurons with aberrant dendritic arborisation, a feature that was also seen in *MECP2* (Jiang *et al.*, 2013), *PTEN* (Kwon *et al.*, 2006) and *SHANK2* (Schmeisser *et al.*, 2012) deficient mice. *SHANK2* mutant mice also had altered synaptic signalling, specifically showing changes to NMDA and AMPA receptor signalling and altered excitatory post synaptic potentials (Schmeisser *et al.*, 2012; Won *et al.*, 2012). Aberrant synaptic signalling in the form of both excitatory and inhibitory post synaptic potentials was a hallmark of *SCN1A* (Han *et al.*, 2012), *EXT1* (Irie *et al.*, 2012), *NRXN1* (Etherton *et al.*, 2009), *NRXN2* (Born *et al.*, 2015) and *UBE3A* (Smith *et al.*, 2011) mutant models, while an overall shift in the E/I balance was reported by a number of studies across a range of models (Etherton *et al.*, 2009; Etherton *et al.*, 2011; Smith *et al.*, 2011; Won *et al.*, 2012; Schmeisser *et al.*, 2012). Importantly, one of the most common findings across rodent studies is impaired LTP, having been reported with *NF1* (Molosh *et al.*, 2014), *FMR1* (Irwin *et al.*, 2000), *SHANK2* (Schmeisser *et al.*, 2012) and *TSC2* (Auerbach *et al.*, 2011) mutant mice. Together, this evidence strongly supports an important role for altered synaptic and network function in ASD, as all of these models are based upon genes for which strong genetic associations to ASD exist. It should be noted however that except for the *TSC2*, *FMR1* and *UBE3A* mice (the latter being a duplication), all of these models involved homozygous deletions of the gene of interest.

Modelling ASD using iPS cells is an attractive proposition as it allows the potential to study cellular and molecular aspects of the disease in a human setting. As well as the possibility of studying the disease impact of specific mutations (hetero- or homozygous) in the context of a controlled isogenic background, for example by using CRISPR-Cas9 technology with ES or WT iPS cells, there is perhaps greater potential in studying the behaviour of neurons derived from ASD patient iPS cells. This not only allows studies using cells from patients with identified rare, *de novo* mutations and syndromic ASDs with high penetrance but also from the majority of patients where there is no such identified mutations. A number of studies have used these approaches to model ASD with hPS cell neurons and have provided molecular and cellular evidence in a human context which corroborates some of the rodent findings.

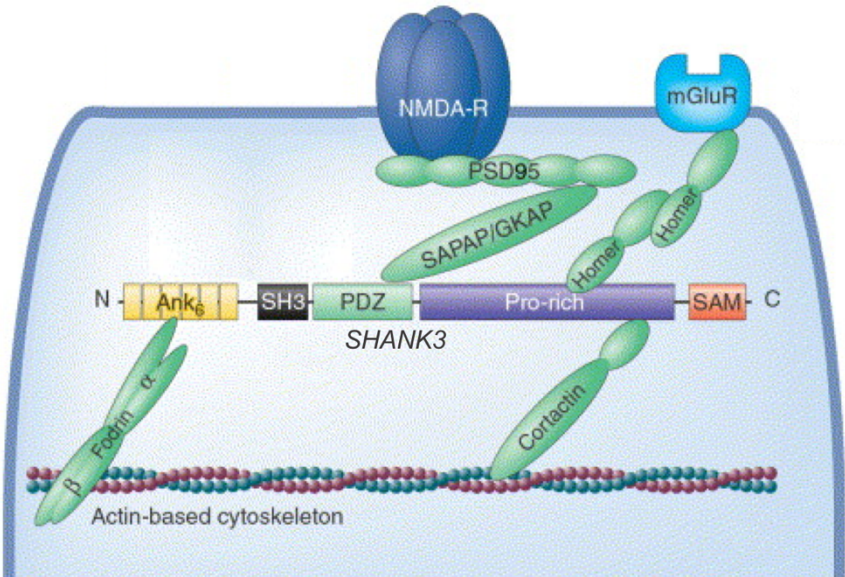
iPS cell derived neurons from Rett syndrome patients with mutations in *MECP2* showed reduced synapse number, spine density and soma size compared to controls (Marchetto *et al.*, 2010). Moreover, these neurons also had reduced excitatory and inhibitory PSPs and reduced spontaneous activity. Similar dendritic changes and reduced synaptic activities were also

reported by two studies using iPS cells derived from Timothy Syndrome patients with gain-of-function mutations in *CACNA1C* (Paşca *et al.*, 2011; Krey *et al.*, 2013), while a striking reduction in neuron process formation was found in neurons derived from Fragile X patients with trinucleotide expansions in FMR1 (Sheridan *et al.*, 2011). Finally, an interesting study using iPS cells from patients with idiopathic ASD reported altered neurogenesis, changes in synaptic signalling and changes to the number of GABAergic interneurons (Mariani *et al.*, 2015).

A



B



C

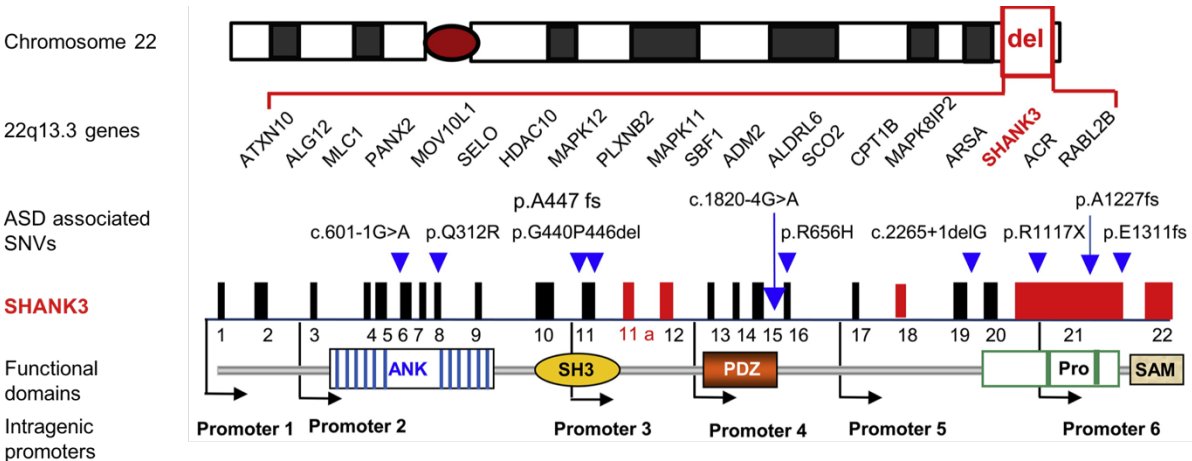


Figure 1.3 - The role of synaptic proteins and SHANK3 in ASD. Converging genetic evidence strongly implicates synaptic dysfunction in the aetiology of ASD. While most genetic risk for ASD is conferred by common variation, many of the rare and de novo mutations with high penetrance for ASD development are found in synaptic proteins (**A**). These include proteins involved in synapse formation (NRXN, NLGN), NMDA receptors (GRIN2B), L-type voltage-gated calcium channels (CANCA1C), voltage-gated sodium channels (SCN1A), synaptic translation (UBE3A) and post-synaptic density scaffolding (SHANKs). Mutations in SHANK3 are some of the most strongly associated with ASD. SHANK3 is a key scaffolding protein at the excitatory synapse, involved in linking glutamate receptors to the actin cytoskeleton via multiple functional domains (**B**). SHANK3 lies at the distal end of chromosome 22 and is one of the key genes deleted in most cases of Phelan McDermid Syndrome (PMDS; also called 22q13.3 deletion syndrome) which is the syndrome with the highest penetrance for ASD (**C**). SHANK3 also harbours several point mutations associated with increased risk for ASD development, several of which are within the functional domains. Two isoforms of SHANK3 have been confirmed in humans but the presence of several intragenic promoters suggests that there could be several more, possibly with as yet unknown unique functions. **A** is adapted from de la Torre Ubieta *et al.*, 2016; **B** is adapted from Kreienkamp, 2002; **C** is adapted from Jiang *et al.*, 2013.

1.3.4 *SHANK3* and ASD

One of the implicated genes most commonly modelled is SH3 and multiple ankyrin repeat domains 3 (*SHANK3*). Mutations involving *SHANK3* are, except for FMRP (mutations in which cause Fragile X syndrome), the most strongly associated with development of ASD. Rare and *de novo* deleterious SNVs in *SHANK3* have been identified in ASD patients (Waga *et al.*, 2011; Moessner *et al.*, 2007; Durand *et al.*, 2012; Boccuto *et al.*, 2013; Gauthier *et al.*, 2009) and small CNVs, (both deletions and duplications) have been associated with sub-types of ASD (Levy *et al.*, 2011; Okamoto *et al.*, 2007; Durand *et al.*, 2007). Importantly, heterozygous deletions of *SHANK3* are thought to be the key aetiological factor in the majority of cases of Phelan-McDermid syndrome (Phelan and McDermid, 2012).

Phelan-McDermid syndrome (PMDS; also known as 22q13.3 deletion syndrome) is a complex developmental disorder characterised symptomatically by neonatal hypotonia, delayed speech, moderate to severe developmental delay, ASD or autistic traits, dysmorphias and, in rare cases, seizures (Phelan and McDermid, 2012). The genetics of PMDS is also complex: in ~80-85% of patients it is caused by a *de novo* deletion of chromosome 22 (around 22q13.3) but the exact location and size of these mutations varies considerably, such that deletions have been observed that range from 150 kb to >8.5 Mb (Wilson *et al.*, 2003). Moreover, while simple deletions are most common, PMDS is also caused by translocations and the formation of ring chromosomes (MacLean *et al.*, 2000). Around 90 genes have been implicated in deletions associated with PMDS but by far the most commonly involved is *SHANK3* – indeed, PMDS diagnosis have been given to patients with deletions that only effect the *SHANK3* gene (Leblond *et al.*, 2014). It should be noted however that there is still no consensus as to whether the involvement of *SHANK3* is required for PMDS diagnosis (Phelan *et al.*, 2015; Disciglio *et al.*, 2014). Importantly, while PMDS is thought to account for < 1% of ASD cases, *SHANK3* associated PMDS is the genetic alteration which has the strongest penetrance for ASD, with around 80% of *SHANK3* PMDS individuals having an ASD diagnosis.

SHANK3 is a member of the SHANK family of post-synaptic density scaffolding proteins. The *SHANK3* gene has 22 exons which code for a multi-domain protein of around 184 kDa. Alternative splicing produces two confirmed functional isoforms in humans, although the presence of several intragenic promoters allows the prediction of up to ten (Wang *et al.*, 2014). The key functional domains include a region of ankyrin repeats, an SH3 region, a PDZ domain, a homer binding region, an actin binding region and a SAM domain (Figure 1.3B&C). In humans, SHANK3 is strongly expressed in the heart, lungs, spleen and the brain, where it is expressed almost universally, with an enrichment of expression in the hippocampus (Uhlén *et al.*, 2015). SHANK3 expression is low in early human development, progressively increases throughout gestation and reaches adult levels around birth (Miller *et al.*, 2014). In rodents, the pattern of regional and developmental expression has been shown to vary between isoforms, raising the prospect of isoform specific functions (Lim *et al.*, 1999).

SHANK3 is localised to the PSD of glutamatergic excitatory neurons, where it acts as a key scaffolding molecule linking glutamatergic signalling complexes to the underlying actin cytoskeleton via its various functional domains (Figure 1.3B). The six ankyrin repeat domain has been shown to interact with alpha II-spectrin (SPTAN1), which may in turn be involved in actin cross-linking (Böckers *et al.*, 2001). The PZD domain is the key region involved in the binding to the NMDAR complex, where it interacts with GKAP1, which in turn forms associations with the NMDAR-linked PSD95 (Naisbitt *et al.*, 1999). Interestingly, the PDZ region has also been shown to directly interact with the GluR1 subunit of AMPA receptors (Uchino *et al.*, 2006). SHANK3 also interacts with mGluR receptors via homer proteins, which bind to the eponymous domain of the protein (Tu *et al.*, 1999; Hayashi *et al.*, 2009). Directly next to this region is a domain which binds to cortactin, which acts as the primary link between SHANK3 (and indeed the 'upper' PSD elements) to the cytoskeleton (Naisbitt *et al.*, 1999). Finally, the SAM domain has been shown to bind to other SHANK3 molecules in the formation of protein oligomers and is also known to be involved in the correct assembly and localisation of the protein to the PSD (Baron *et al.*, 2006).

1.3.5 SHANK3 as a model of ASD

The strong genetic evidence implicating various risk mutations together with the key role of the protein at the synapse has meant that SHANK3 mutant rodents have been one of the most studied ASD models. In fact, it is probably more accurate to say that these are primarily models of SHANK3 – associated PMDS, as they almost all involve deletions of at least part of the gene. Moreover, homozygous SHANK3 KO mice are viable and, as with the other ASD models previously described, is the approach taken by several studies meaning that phenotypes must, in some cases, be viewed in the context of absent SHANK3 expression. Both hetero- and homozygous SHANK3 models have however provided evidence for ASD-like behavioural phenotypes in mice, including reduced social interactions (Bozdagi *et al.*, 2010; Zhou *et al.*, 2016), alterations in ultrasonic vocalisations (Wang *et al.*, 2011; Yang *et al.*, 2012), an increase in repetitive behaviours (Peça *et al.*, 2011; Wang *et al.*, 2011) and impaired hippocampal–dependent learning (Bozdagi *et al.*, 2010; Jaramillo *et al.*, 2016; Kouser *et al.*, 2013). While reported behaviours vary between these studies, an interesting common finding is an increase in repetitive self grooming, which in some cases is self-injurious (Jaramillo *et al.*, 2016; Yang *et al.*, 2012; Wang *et al.*, 2011; Bozdagi *et al.*, 2010; Peça *et al.*, 2011). Of course, as with all rodent models, the extent to which these behaviours are representative of human ASD symptoms is worth consideration. However, it is noticeable that very similar if not identical mutations of SHANK3 confer varying phenotypes in mice in a manner not dissimilar to the heterogeneity seen in the human condition.

SHANK3 KO mice also recapitulate several of the cellular and molecular phenotypes seen with other ASD genetic models. SHANK3 KO mice show changes to dendritic density, reduced spine formation, including reduction to activity-dependent spine plasticity (Wang *et al.*, 2011), (Peça *et al.*, 2011; Hung *et al.*, 2008; Durand *et al.*, 2012) and also a reduction in the thickness of the PSD (Wang *et al.*, 2011). Many studies have shown altered excitatory synaptic signalling, including changes to mEPSC amplitudes and frequencies (Bozdagi *et al.*, 2010), and reduced AMPA and NMDA signalling (Wang *et al.*, 2011; Yang *et al.*, 2012; Jaramillo *et al.*, 2016). NMDA hypo-function has also been identified in a rat *in vitro* model using SHANK3 knock-down (Duffney *et al.*, 2013). Several studies also report changes in the expression of other PSD proteins, including Homer1b/c, GKAP, PSD93, PSD95, GluA1/2 (AMPA receptors) and GluN2A/B (NMDARs) (Bozdagi *et al.*, 2010; Wang *et al.*, 2011; Peça *et al.*, 2011; Jaramillo *et al.*, 2016);

although the region and level of change differs considerably throughout the reports. Interestingly, SHANK2 expression (a related key PSD scaffolding protein) was shown to be increased in a full SHANK KO model, providing the possibility of a degree of compensation (Schmeisser *et al.*, 2012). Importantly, another consistent finding from these mouse studies has been the reduction in hippocampal LTP across a range of plasticity protocols (Kouser *et al.*, 2013; Jaramillo *et al.*, 2016; Bozdagi *et al.*, 2010), strongly suggesting that these mice may have deficits in excitatory network signalling. Indeed, it has also been shown that alterations to activity dependant signalling mechanisms in development may lead to aberrant cortical connectivity. Moreover, there is good evidence to suggest that loss of SHANK3 causes an increase in the excitatory/inhibitory balance in the cortex, possibly due to developmental changes to interneuron maturation and function. Importantly, a recent study involving dissociated primary cortical neurons cultured on and recorded using multi electrode arrays (MEAs) showed altered network-driven firing patterns in neurons from SHANK3 KO mice, which relied on both excitatory and inhibitory signalling (Lu *et al.*, 2016a; see section 1.4.3).

To date there have been two full reports on studies involving neurons derived from iPS cells with SHANK3 haploinsufficiency. The first is currently the only study to use neurons derived from iPS cells from PMDS patients (diagnosed with ASD) and found several phenotypes which corresponded well with rodent studies. PMDS neurons were produced in few numbers than control neurons, with remaining neurons showing reduced expression of AMPA and NMDA receptors, increased cell input resistance, increased evoked excitability (action potentials), and decreased AMPA and NMDA dependent EPSCs (Shcheglovitov *et al.*, 2013). The deficits in excitatory neurotransmission could be rescued with both SHANK3 overexpression and IGF1 treatment. The second study introduced heterozygous conditional mutations of SHANK3 into ES cells and produced neurons which showed reduced dendritic arborisation, increase input resistance, increased evoked excitability, decreased spontaneous excitability, a reduction in excitatory EPSCs, and decreased amplitude of mEPSCs (Yi *et al.*, 2016). While this second report does not use ASD patient cells, it is important as it corroborates several of the findings from the Shcheglovitov study, supporting the suggestion that many of the phenotypes seen in PMDS are caused by a reduction of SHANK3.

1.4 Studying networks *in vitro* and multi electrode arrays

1.4.1 Studying neural networks *in vitro*

In vitro studies of neural networks using patch clamping methods, such as those described in section 1.3.3, are limited by the number of neurons that can be patched simultaneously. While there have been studies reporting the patching of eight cells concurrently, realistically only up to four is probably routine for most research groups. Furthermore, in rodent slice work the probability of patching only two synoptically connected cells, while variable depending on brain regions, is unlikely to be greater than 50% (Debanne *et al.*, 2008). These probabilities are decreased further for dissociated primary neurons although it should be noted that dual-pipette plasticity protocols have been accomplished successfully in dissociated hippocampal cultures (Molnár *et al.*, 2011). To date, there have been no reports of multiple pipette patch clamping or successful induction of LTP/LTD in hPS cell derived neurons. Finally, patch clamp based studies of network interactions in cultures are also limited by the stability of individual recordings and the fact that the same cultures cannot be used multiple times, meaning that developmental experiments required several different

Over the last few years, the use of multi electrode arrays (MEAs) for studying neuronal network *in vitro* has gained a significant amount of interest. MEAs are actually not a new technology, having been first developed in the 1970's and 1980's to record extracellular field potentials from invertebrate neurons and mammalian heart and CNS tissue (Thomas *et al.*, 1972; Gross *et al.*, 1982; Regehr *et al.*, 1989). However, it is only more recently with the advent of more accessible and user friendly systems, increases in computing power and advances in analysis techniques that the technique has been more routinely exploited. MEA systems are based upon the culturing of neurons (or other excitable tissues) directly on or within a panel of substrate-embedded electrodes. In general, MEAs record the local extracellular ionic movements associated with neuron activity, although there have been a number of methods developed which allows the engulfment of protruding electrodes by neurons, providing, to various degrees intracellular-like recordings (Duan *et al.*, 2011; Robinson *et al.*, 2012; Hai *et al.*, 2009). For the purposes of this project, the following sections will focus only on planar based MEA systems

which are by far the most widely used and are the only format which currently allows reliable and stable long-term (> 1 week) recordings of mammalian neuron populations.

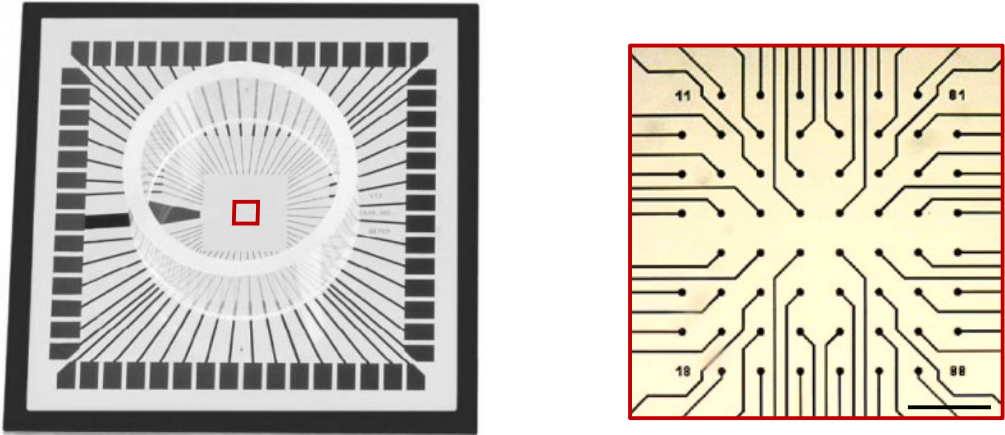
1.4.2 Overview of MEAs

Planar MEAs have become the method of choice largely down to the ease of which neurons can be cultured on them without drastic changes to culturing protocols. Typically, flat inert-metal electrodes (around 50 – 200) are embedded within a glass or plastic culturing surface allowing neurons to be cultured directly above with the aid of standard cell coatings (e.g. poly-d-lysine/lammin). Figure 1.4A shows a typical single MEA with 60 titanium electrodes embedded within a glass culturing surface. As mentioned, MEAs record neuronal activity by detecting the extracellular potentials caused by localised changes in ionic concentrations. The properties of MEA recordings therefore differ to patch-clamp recordings in a number of ways. Figure 1.4B presents schematic diagrams showing the equivalent electrical circuits for the standard whole-cell patch clamping technique and for planar MEA recordings. In whole cell patch clamping, a tiny region of neuron membrane is disrupted, after formation of a high-resistance seal, leading the intracellular fluid of the cell to become in direct contact with the pipette solution and therefore an electrode. A simple series circuit of resistors is established comprising the resistance of the pipette (R_{pipette}), the resistance of the patch (more strictly, the access to the cell; R_{access}) and the resistance of the neuronal membrane (R_m). Providing that the leak (seal) resistance is high (R_{leak}), this circuit therefore allows full amplitude detection of currents flowing through the neuron membrane as R_m is much greater than the combined resistance of R_{pipette} and R_{access} . For MEAs, the neuron-electrode interface is more complex and consists of three elements: a neuron with multiple compartmentalised membranes, including one at the neuron-electrode junction, each with individual parallel RC circuits (simplified to two compartments in Figure 1.4B); a cleft comprising of the gap between the neuron and the electrode, filled with extracellular fluid or culture medium; and the embedded electrode with its own resistance and capacitance. Action potentials in neurons cause localised extracellular conductances which causes fractional differences in the potentials at each membrane compartment. A voltage is created between the membrane junction and the non-junctional membrane which is directly regulated by a resistance formed by the fluid containing cleft (R_{seal}). As such, the degree to which these voltages are successfully detected is largely due to the value of R_{seal} , which

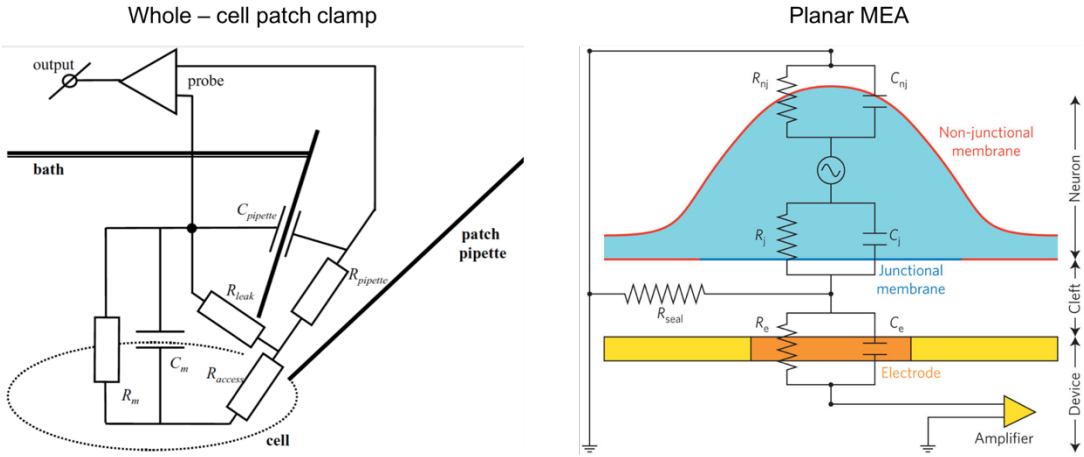
practically is determined by the quality of the adherence of the neuron to the electrode/substrate.

The consequence of the differences described above is that while patch-clamping provides a full scale recording of changes in cell currents, MEA recordings are severely limited in their amplitude resolution, such that an action potential recorded with patch clamping will be detected by MEAs with an amplitude of, at best, around 100x less (Spira and Hai, 2013). Moreover, MEA recordings are not able to detect sub-threshold events, meaning that without pharmacological interventions, they cannot provide any information about the nature of any produced action potentials (Figure 1.4C). While these limitations of MEA recordings should be acknowledged, they perhaps allow the benefits of MEAs to be utilised more effectively. Specifically, unlike patch-clamping, MEAs allow the simultaneous recording of action potentials from large populations of neurons, which in turn can provide information surrounding possible networked behaviour; allow recordings of the same cells over an extended period of time; and provide the potential for simplified large scale screening of pharmacological agents.

A



B



C

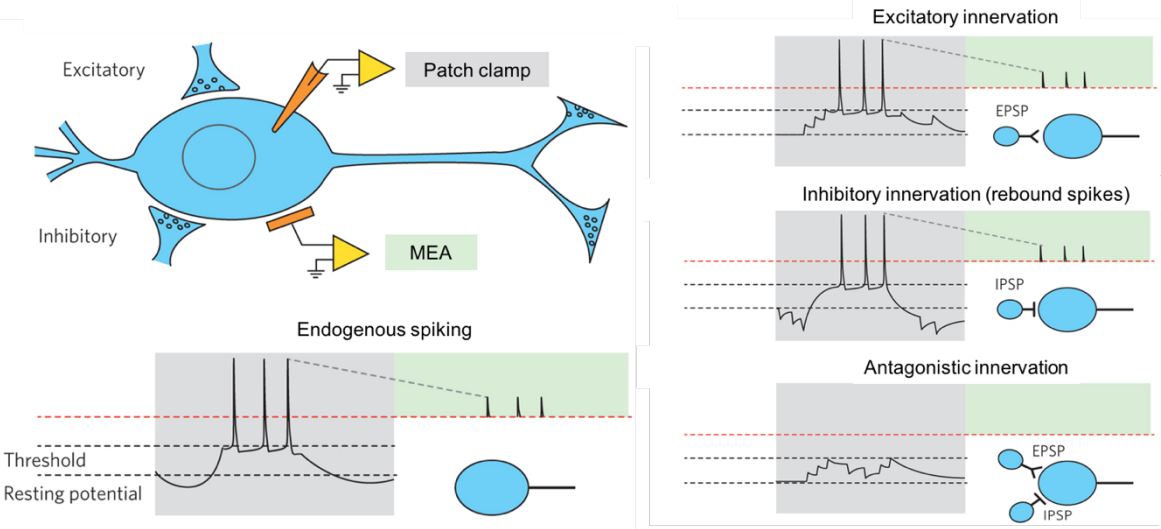


Figure 1.4 – Using Multi electrode arrays (MEAs) for neuron electrophysiology. Planar MEAs have a grid of electrodes embedded into a culturing surface, onto which neurons can be attached. In **A**, a grid of 59 titanium electrodes, each with a diameter of 20 μm , spaced 200 μm apart are integrated into a glass culturing surface. The red inset highlights the arrangement of the electrodes. Scale bar = 400 μm . MEAs record neuron activity as extracellular potentials, in contrast to patch clamp techniques which record intracellular ionic changes. As such, the electronics involved in the recording methods differ substantially. **B** shows schematic diagrams for the equivalent circuits for the whole-cell method of patch clamping and planar MEAs. In patch clamping, the intracellular fluid of the cell is in direct contact with the pipette solution and an electrode. A series circuit forms comprising the resistance of the pipette (R_{pipette}), the resistance of the patch (R_{access}) and the resistance of the neuronal membrane (R_{m}). A high seal resistance (R_{leak}) allows full amplitude detection of whole-cell currents as $R_{\text{m}} > R_{\text{pipette}} + R_{\text{access}}$. In MEA recordings, the neuron-electrode interface consists of a neuron with several compartmentalised membranes, including one at the neuron-electrode junction, each with individual RC circuits (simplified here to two compartments); an extracellular fluid filled cleft comprising of the gap between the neuron and the electrode; and an electrode with its own RC circuit. Localised extracellular conductances cause fractional differences in the potentials at each membrane compartment, which creates a voltage between the membrane junction and the non-junctional membrane. The size of this voltage is directly related to the resistance formed by the fluid containing cleft (R_{seal}). As a result of the difference in recording methods, MEAs are limited in their ability to record sub-threshold events and detect voltage changes with around 100x less resolution (**C**). Unlike patch-clamping, MEAs cannot be used to determine the source of action potentials (excitatory innervations, rebound spikes etc.). In **A**, the full MEA image is taken from Multi Channel Systems; In **B**, the patch clamp circuit is adapted from Molleman, 2003; the MEA circuit in **B** and **C** is adapted from Spira *et al.*, 2013.

1.4.3 MEAs for studying network function in vitro

In recent years, MEAs have been used to study a range of in vitro models of both developmental and disease states. Rodent studies using acute slices were the some of the first to show that network behaviours could be observed using MEAs (Maeda *et al.*, 1995). This behaviour manifested as coordinated high-frequency bursts which, in some cases, could be traced to a particular layer of the cortex (Sanchez-Vives and McCormick, 2000). This synchronised behaviour was extended further in a more recent slice model of epilepsy which reported extended coordinated firing of neurons in response to 4-AP application (Grosser *et al.*, 2014). Using a similar approach, a highly technical study showed that similar coordinated inter-ictal like discharges could be induced in acute hippocampal slices from tissue resected from patients with temporal lobe epilepsy (Hsiao *et al.*, 2014). Several studies have reported observations of network like behaviour in dissociated rodent neurons. While in some studies this behaviour is limited to short, culture-wide synchronised burst firing (SBF; Chiappalone *et al.*, 2003; Raichman and Ben-Jacob, 2008), other studies have shown the establishment of more complex network driven behaviour in the form of slow, culture wide oscillations comprising periods of high activity and low activity, each lasting tens of seconds (Wagenaar *et al.*, 2006; Sun *et al.*, 2010; Mok *et al.*, 2012; Lu *et al.*, 2016a). The establishment of such behaviour is likely to be driven by the balance between excitatory and inhibitory neuronal activity: while excitatory transmission forms the majority of connections, synchronised firing is regulated by feedback mechanisms acting via GABAergic interneurons. Indeed, it has been shown that the dynamics between these oscillatory states can be regulated by changing the ratio of interneurons present in primary cultures (Chen and Dzakpasu, 2010).

More recently, a number of studies have built upon the work reviewed above to use MEAs to investigate networked behaviour in rodent models of ASD. The first of these explored spontaneous network activity in hippocampal neurons from mice harbouring expanded trinucleotide repeats in FMR1 (FMRP) as a model of fragile X syndrome (Cao *et al.*, 2012). It reported that mutant neurons showed hyper-excitation and hyper-synchronisation caused by an imbalance in excitatory/inhibitory signalling, possibly by a mechanisms involving interneuron mGluR1/5 receptors. A second study found strikingly similar phenotypes in a mouse model of Tuberous Sclerosis Complex (TSC), where mutant hippocampal neurons showed an m-TOR signalling dependant increase in spontaneous SBF (Bateup *et al.*, 2013). This again was

attributed to an increase in the E/I balance, driven by a reduction in the amplitude and frequency of inhibitory PSCs. It should be noted that this study was performed with homozygous *Tsc1* KO mice. Finally, an important recent MEA study evaluated the network behaviour of cortical neurons dissociated from mice with homozygous deletions of *Shank3* (Lu *et al.*, 2016a). This reported that as well as mutant neurons showing reduced basal rates of spontaneous activity, they also showed alterations in slow, synchronised culture wide oscillations, with both the period of high activity (More Active Period; MAP) and the interval between these periods (MAP interval) attenuated compared to WT neurons. These phenotypes could be rescued back to WT only by using a combination of AMPAR and GABA_AR positive modulators, strongly suggesting impairment to both inhibitory and excitatory network signalling.

The three studies reviewed above are important as they highlight the clear potential for investigating network behaviour in ASD models using MEAs. They also highlight the potential for using MEAs to study hPS cell models. While, as previously described, there are alternatives to MEAs to investigate circuit behaviour in rodent models, except in very rare cases there is no access to 'intact' human neural tissues which would allow similar experiments. Therefore, the application of hPS cell derived neurons, especially those derived from patient iPS cells, together with MEAs provide exciting opportunities to investigate aspects of neural behaviour which would otherwise be unattainable. However, to date only a small number of studies have investigated hPS cell activity using MEAs. The first such study reported that hES cell derived neurons developed spontaneous activity and fired high frequency bursts which were sensitive to AMPA and NMDA receptor inhibition (Heikkilä *et al.*, 2009). However, coordinated activity was rare and limited to sporadic, short burst firing. In the following years a number of studies using similar approaches reported improved spontaneous activity which matured over development (Ylä-Outinen *et al.*, 2010; Kapucu *et al.*, 2012; Odawara *et al.*, 2014; Amin *et al.*, 2016). Importantly, these studies highlighted that, later in development, much of this activity was driven by AMPA and NMDA synaptic activity. It was only in 2016 that a study showed consistent culture-wide synchronised firing in iPS cell derived neurons which was sensitive to AMPA inhibition (Odawara *et al.*, 2016). However, this behaviour took over 20 weeks to develop and was limited to SBF lasting no more than 2 seconds. As such, to date there have been no reports of the more complex oscillatory network behaviour seen in rodent studies having been observed in hPS cell derived neuron cultures. This can possibly be partly attributed to the immaturity of the neurons in the culture – indeed, in all of the studies above, differentiation protocols were largely

standard. It therefore remains to be determined whether increasing the maturity of the neurons produced could promote the development of more complex network patterns detected in hPS cell MEA cultures. Finally, to date there have been no studies investigating hPS cell ASD model function using an MEA approach.

1.5 Summary

The use of hPS cells and, in particular, iPS cells provide unique opportunities to study the function of human neurons in development and disease states. However, while protocols to differentiate hPS cells into neurons have improved over the last few years to allow more rapid and efficient neuron production, it is only more recently that focus has shifted on to the physiological maturity of hPS cell derived neurons, which, compared to adult neurons, remains immature. While a number of more recent studies have described protocols which show good improvements in a number of electrophysiological properties, these were, in general, based upon the use of non-standard mediums or multiple small molecules. Instead, a body of evidence over number of years supports a role of astrocyte co-culture and hypoxic incubator atmospheres in neuron maturation, two relatively simple physiological protocol manipulation which, in theory, can be adapted to arrange of differentiation methods.

Recent genetics studies have highlighted the strong role of a range of inherited and *de novo* variations have on increased risk for the development of ASD, a group of common related neurodevelopmental conditions. Importantly, many of the genes which harbour these mutations are those that produce proteins with functions at the excitatory post-synaptic density. One of the genes most strongly associated with ASD is SHANK3, which codes for a key PSD scaffolding protein involved in linking glutamate receptors with the actin cytoskeleton. This genetic evidence together with that from human and model studies strongly implicates impaired synaptic signalling and aberrant network function in ASD aetiology.

While several methods exist for the observation of circuit behaviour in rodent models, there is less opportunities to study similar function in hPS cell derived neurons. The advent of more user-friendly MEA systems has provided an opportunity for the long-term culturing and recording of hPS cell derived neuron activity using mostly routine protocols. However, while MEA studies with dissociated rodent neurons show a wide and complex array of single unit and coordinated network activity, to date similar activity in hPS cell neurons has not been observed, perhaps largely owing to the maturity of the neurons used in MEA cultures. Finally, using an MEA approach to investigate network function in a iPS cell model of ASD has not been reported.

1.6 Project aims

Based upon the work reviewed above, the overall objective of this project is to develop a platform for the investigation of network behaviour in iPS cell derived neurons over both development and in an *in vitro* model of ASD. To achieve this, the project has the following four key aims:

1. To optimise a neuronal differentiation protocol to increase the physiological maturity of iPS cell derived neurons. This will be based upon the use of astrocyte-conditioned medium (ACM) and hypoxic culturing environments to develop a protocol that can be adapted for a range of applications.
2. To develop a pipeline for the analysis of data from MEA experiments. This will focus on the analysis of both basal excitability and network driven characteristics
3. To establish an *in vitro* platform for the observation and recording of network driven behaviour in iPS cell derived neurons. This will be based upon the use of planar MEAs and will build upon the work of the previous aims to provide a reliable method of monitoring the change in activity across development.
4. To investigate the network behaviour of iPS cell derived neurons from ASD patients with heterozygous deletions of SHANK3. This will involve the use of the developed MEA platform to monitor such activity over neuronal development and will be supported by other functional assessments.

2. Materials and methods

2.1. Plasticware and consumables

Item	Supplier	Catalogue number
<i>Cell culture treated multiwell plates</i>	Thermofisher (Nunc)	
4 well		176740
6 well		140675
12 well		150628
24 well		142475
<i>Polypropylene centrifuge tubes (sterile)</i>	Thermofisher (Fisherbrand)	
15 ml		14-959-70C
50 ml		06-443-19
1.5 ml Polypropylene microcentrifuge tubes	Thermofisher	11569914
0.5 ml polypropylene microcentrifuge tubes	VWR	211-0027
0.2 ml polypropylene PCR tubes	VWR	732-0546
30ml polystyrene universal tubes	Thermofisher (Sterilin)	128C
<i>Cell culture treated single well dishes</i>	Thermofisher (Nunc)	
10cm		172958
6cm		150326
<i>Cell culture treated flasks</i>	Thermofisher (Nunc)	
25 cm ²		163371
80 cm ²		153732
<i>Serological pipettes</i>	VWR	
2 mL		612-3704
5 mL		612-3702
10 mL		612-3700
25 mL		612-3698
50 mL		612-3696
<i>Pipette tips</i>	Clearline	
10 µL filter		028200CL
20 µL filter		035220CL
200 µL filter		035230CL
200 µL non-filter		DD713140
1250 µL filter		134000CL
1250 µL non-filter		DD713137
1.8 ml Cryovials	Thermofisher (Nunc)	479-6843
2 well chamber slide	Sigma-Aldrich	C6682
20 cm petri dishes	VWR	391-0561
Costar Spin-X tube filters (500 µL; 0.22 µm pore)	Sigma - Aldrich	CLS8161
<i>Round glass coverslips</i>	VWR	
13 mm		631-0150
18 mm		631-0153
Microscope slides	ThermoFisher	P4981
0.22 µm PVDF syringe filter	Millipore	SLGV004SL
<i>Transfer pipettes</i>	VWR	
5 mL		612-5549
1.5 mL		612-4468

2.2. Stem Cell Culture

2.2.1. Cell line and maintenance

The IBJ4 iPS cell line used for the work in Chapter 4 and Chapter 5 in this project was a gift from Josh Chenoweth from the Lieber Institute for Brain Development, MD, USA. The iPS line was derived by that group from the BJ fibroblast line (ATCC, #CRL-2522) using the non-integrating STEMCCA Cre-Excisable Constitutive Polycistronic Lentivirus Kit (Millipore, #SCR531). Figure 2.1 shows representative images of IBJ4 iPS cells, stained with the key markers of pluripotency, SOX2, OCT3/4, NANOG, Tra-1-60, Ssea-4 and KI-67.

All iPS cells were maintained as feeder-free cultures in mTeSR1 medium (Stem Cell Technologies, #05850; prepared according to the manufactures instructions) and on a matrix layer of Matrigel (Corning, #354234). To prepare all cultureware for iPS cells (see Table 2.1), slowly thawed aliquots of frozen 100% Matrigel stock were diluted 1:85 in DMEM/F12 1:1 (Thermo Fisher, #12634-010) and plated onto plastic culture ware at 1 mL/9.6 cm². Coated plates were incubated for at least 1 hour at 37°C, after which plates were washed with DPBS (Thermo Fisher, #14190094) and maintained with DPBS until use. Used diluted Matrigel was reused once on a further plate before being discarded.

Frozen 1 mL vials of iPS cells were rapidly thawed at 37°C, before being added into 9 mL of mTeSR1 medium containing 10 µM of the Rock/Rho pathway inhibitor Y27632 (referred to herein as Y27; Stem Cell technologies, #72302) and centrifuged at 200g for 6 mins. Y27 has been shown to improve the survival of human pluripotent stem cells after thawing and single-cell dissociation (Li *et al.*, 2009; Watanabe *et al.*, 2007). After aspirating all the medium, cells were resuspended in 3 mL of mTeSR1 with Y27 and plated into 1 well of a 6 well plate pre-coated with Matrigel as described. After 24 hours, the medium was aspirated; cells were washed twice with DPBS to remove cell debris and replenished with 3 mL of fresh mTeRS1 without Y27. iPS cells were maintained in mTeSR1 with media changes every other day until 70-80% confluency, at which point cells were passaged using the enzyme free reagents Gentle Cell Dissociation Reagent or ReLeSR (both Stem Cell Technologies, #07174 and #05872 respectively).

2.2.2. *iPS cell passaging*

For standard passaging, following aspiration of medium and washing with DPBS, 1 mL Gentle cell dissociation reagent was added per well of cells and incubated at 37°C for 2 mins. The reagent was then aspirated; cells were carefully washed with DPBS and then covered with 1 mL mTeSR1. Cells were then lifted from the culture surface by scratching with a 2 mL stereological pipette and were collected into a 30 mL universal centrifuge tube. Cells were then diluted to the desired concentration by adding an appropriate amount of mTeSR1. For routine maintenance of the line, cells were passaged and diluted based on the number of wells being passaged and the number of wells required.

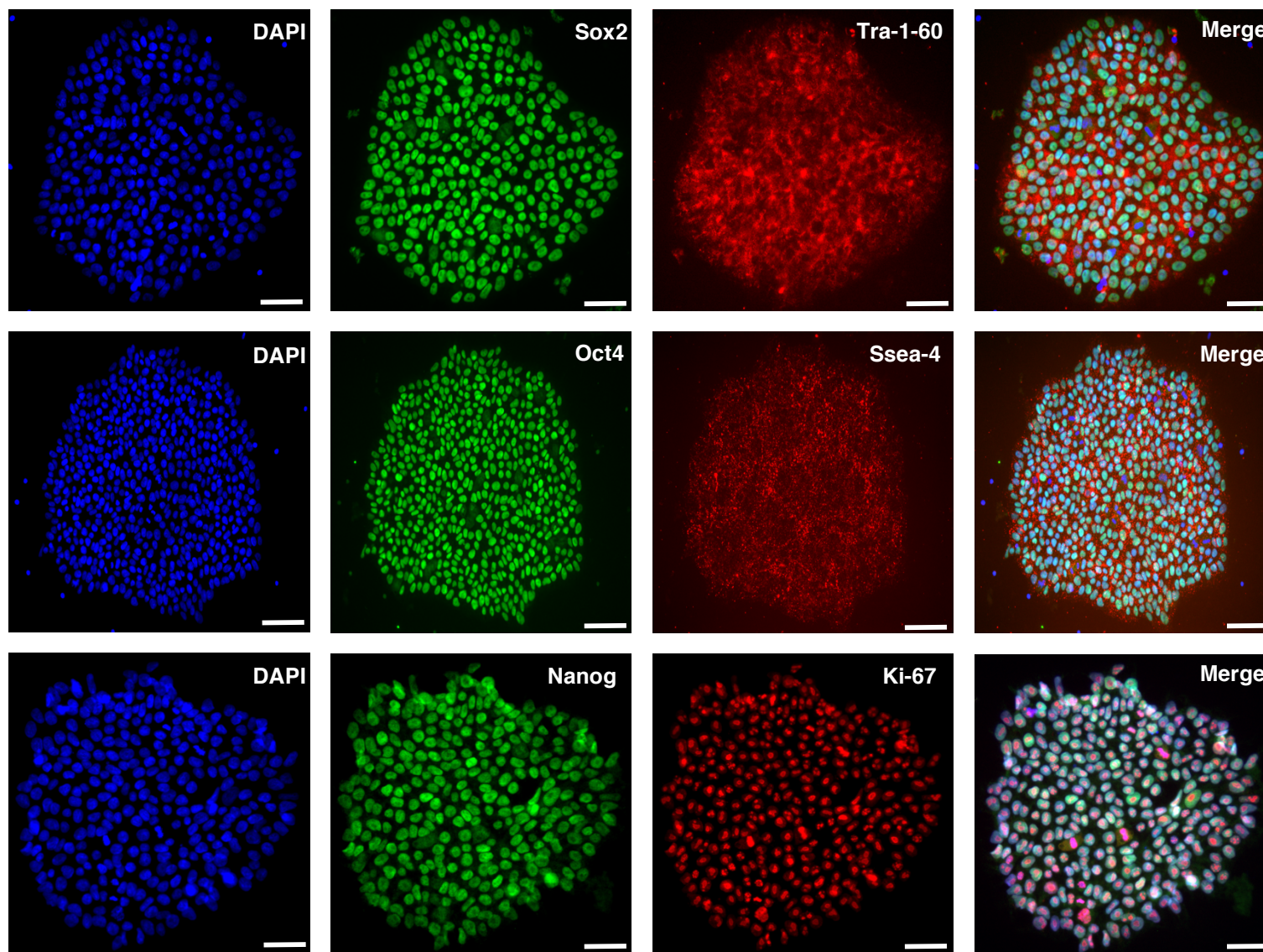
In situations when cell colonies were uneven or regions of cells were undergoing spontaneous differentiation, ReLeSR was used to isolate the pluripotent cells from those that were differentiating. Following aspiration of medium, 1 ml ReLeSR was added to each well and then rapidly aspirated off after around 50 seconds. Cells were then incubated without any medium for 1.5 – 2 mins, after which 1 ml of fresh medium was added. To selectively remove pluripotent cells, the plate was firmly tapped against the palm of a hand for 60 seconds, after which detached cells were collected up and then diluted and plated in the way described above.

2.2.3. *iPS cell freezing*

To freeze IPS cells for storage, 10 μ M Y27 was first added to cells 2 hours before freezing. Cells were frozen in a cryoprotection medium of mTeSR1 containing a final concentration of 10% dimethyl sulfoxide (DMSO; Sigma-Aldrich, #D2650). An initial freezing medium containing 20% DMSO in mTeSR1 was made fresh and stored at 4 °C for 2 hours before cell freezing. Cells were dissociated for freezing following the same protocol as that described for standard cell passaging with gentle cell dissociation reagent. Once collected, cells were then centrifuged at 200g for 6 mins. After aspiration of medium, cells were gently re-suspended in half of the total medium required for freezing. Cells were not counted prior to freezing – instead, one confluent well of a 6 well plate was frozen into 1 ml final volume of cryoprotection medium. In this way, pooled wells of cells were frozen according to the number of wells being frozen. After cell resuspension, the same volume of cryoprotection medium was then added dropwise, giving a final DMSO concentration of 10%. 1 ml of re-

2. Materials and methods

suspended cells were added per cryovial and vials were placed in a CoolCell freezing box (Biocision) and transferred to a -80 °C freezer. Cells were transferred to liquid nitrogen for long terms storage within 48 hours.



2. Materials and methods

Figure 2.1 – IBJ4 iPS cells show expression of key markers of pluripotency. IBJ4 cells were fixed and stained to determine the expression pattern of six key pluripotency markers. Oct4, Sox2 and Nanog are the three primary transcription factors that regulate the pluripotency pathways in stem cells. Tra-1-60 and Ssea-4 are both proteins expressed on the membrane of pluripotent stem cells. Ki67 is a nuclear protein present in all dividing cells. Panels show representative images of IBJ4 iPS cells. Fixed cells were of passage number 5-8. Scale bars show 50 μm .

2.4. Neural media formulations

Component (stock concentration)	Supplier	Cat.#	Volume for 150 mL total medium (+ final concentration supplement)				
			<i>N2B27-RA</i>	<i>N2B27+RA</i>	<i>Shank3</i>	<i>Brainphys</i>	<i>Astrocyte</i>
DMEM/F12 1:1 (1x)	ThermoFisher	12634010	97.5 mL	97.5 mL	-	-	133.5 mL
Neurobasal (1x)	ThermoFisher	21103049	49 mL	49 mL	145.5 mL	-	-
BrainPhys Basal (1x)	StemCell	05790	-	-	-	145.5 mL	-
B27-RA supplement (50x)	ThermoFisher	12587010	1 mL (1x with respect to neurobasal)	-	-	-	-
B27+RA supplement (50x)	ThermoFisher	17504044	-	1 mL (1x with respect to neurobasal)	3 mL (1x)	3 mL (1x)	-
N2 supplement (100x)	ThermoFisher	7502001	1 mL (1x with respect to DMEM/F12)	1 mL (1x with respect to DMEM/F12)	-	-	-
FBS (100%)	Biowest	S1810	-	-	-	-	15 mL (10%)
PSG (100x)	ThermoFisher	10378016	1.5 mL (1x)	1.5 mL (1x)	1.5 mL (1x)	1.5 mL (1x)	1.5 mL (1x)
β -mercaptoethanol (100mM)	Sigma-Aldrich	M3148	150 μ L (0.1 mM)	150 μ L (0.1 mM)	-	-	-
Ascorbic acid (200 mM)	Sigma-Aldrich	A4403	-	-	75 μ L (100 μ M)	15 μ L (20 μ M)	-
BDNF (20 μ g/mL)	Tocris	2837	-	150 μ L (20 ng/mL; when required as per protocol)	150 μ L (20 ng/mL)	150 μ L (20 ng/mL)	-

2.5. Differentiation of glutamatergic neurons from IBJ4 iPS cells

Presented here is the basic protocol used within the research group for the production of forebrain glutamatergic projection neurons. This is a well characterised protocol based upon the dual-SMAD inhibition methods described by Chambers *et al.* 2009 and Shi *et al.* 2012. The basic outline of the protocol is shown in Figure 2.2.

2.5.1. Neural induction and formation of neural precursors

Two days before the start of neural induction (D0), confluent wells of iPS cells were collected with GCD reagent as described and plated onto 12 well plates pre-coated with reduced growth factor Matrigel (Corning, #354230) as required (standard passage ratios were around 1:6 – 1:8). Cells were maintained with mTeRS1 until 80% confluent after which cells were washed once with DPBS and refilled with N2B27-RA (Table 2.4) containing 100 nM LDN193189 (LDN; Sigma-Aldrich, #SML0559) and SB431542 (SB; Sigma-Aldrich #S4317). Both these molecules act through the TGF- β signalling pathway and are indirect inhibitors of R-SMAD proteins; receptor-regulated transcription factors which regulate the expression of over 500 genes (Massagué *et al.*, 2005), the inhibition of which has been shown to induce neural fate in human pluripotent stem cells (Chambers *et al.*, 2009; Elkabetz *et al.*, 2008; Lee *et al.*, 2007). LDN acts through the BMP/GDP branch of the pathway to prevent the phosphorylation (activation) of SMADs1, 5 and 8 via the inhibition of the BMP type 1 receptors ALK2 and ALK3 (Yu *et al.*, 2008). SB acts via the TGF- β /activin/nodal branch of the pathway to prevent the phosphorylation and nuclear translocation of SMAD2 and 3 (Hjelmeland *et al.*, 2004).

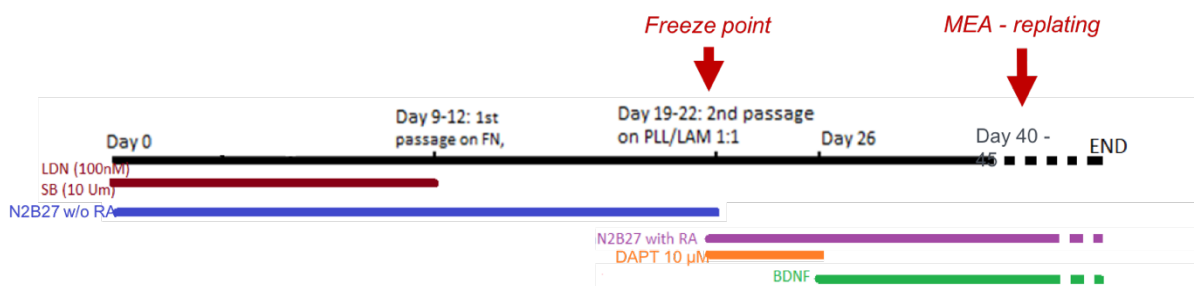


Figure 2.2 – Overview of the protocol to differentiate iPS cells to cortical forebrain neurons. Neural induction of iPS cells is achieved by dual-SMAD inhibition using LDN193189 and SB431542 in N2B27-RA medium. At day 9-12, cells are passaged onto fibronectin (FN) – coated plates at a ratio of 1:1.5 (with respect to culture area). After a further 10 days, cells were deemed precursors (NPCs) were either passaged onto coverslips coated with poly-D-lysine (PLL)/laminin (LAM); or frozen for later use. From this point, cells were cultured in N2B27 + RA with 10 μ M DAPT for 5 days. At day 26, DAPT was removed and BDNF was added to medium until the end of the culture. For multi electrode array (MEA) experiments, cell were re-plated onto arrays at Day 40-45.

2. Materials and methods

iPS cells were maintained in this neural induction medium, with half medium changes every 2 days, for around 9-12 days after which point multi-layered colonies of cells could be seen. For the 1st passage, cells were initially pre-treated for 2 hours with 10 μ M Y27, after which the medium was removed from cells and kept for use later. After washing with DPBS, 500 μ L of 0.05 mM EDTA (Sigma-Aldrich #E8008) was added to each well and cells were incubated for 10 mins at 37 °C. After EDTA aspiration and DPBS washing, 500 μ L of fresh N2B27-RA with 10 μ M Y27 was added to each well and cells were detached from the plate by scratching using a 2 mL stereological pipette. All collected cells were then pooled into a 50 mL tube(s) and diluted with the conditioned medium and/or fresh medium to obtain a passage ratio of 1:1.5 (with respect to culture area) and to allow plating of 1.5 ml of cells per well. Medium was added such that final composition of the diluted cells contained fresh medium (with Y27) and conditioned medium at a ratio of 1:1. 1.5 ml of cells were then plated onto fresh 12 well plates pre-coated with fibronectin (Millipore; #FC010). After 24 hours, all medium was aspirated from cells and replaced with 2 ml fresh N2B27-RA alone. Cells were maintained in this way with half medium changes every two days for around 9-10 days, after which multilayer colonies comprising neural rosettes were visible. At this point (D18-22), cells were deemed to be neural precursors (NPCs) and differentiations were either continued to produce neurons or NPCs were frozen for storage and later use.

2.5.2. Terminal differentiation of forebrain precursors

To continue differentiations, the 2nd passage was performed as described above for the 1st passage with the following alterations: depending on the future application of the neurons, cells were either passaged with EDTA as described or with Accutase (Thermo Fisher, #A1110501), which allows single – cell dissociation and passaging. Accutase was generally used for applications such as single cell electrophysiology and immunocytochemistry where clear separation of individual cells was required, while EDTA was used for cells that were earmarked for RNA or protein extraction. For single cell dissociation, cells were first pre-treated 2 hours before passaging with 10 μ M Y27. Following medium aspiration and DPBS washing, 500 μ L of accutase was added to each well and cells were incubated for 10 mins at 37°C. 500 μ L of medium was then added to each well and cells were dissociated by gently triturating with a 1 ml pipette tip. After collection, cells were centrifuged at 200g for 6 mins, counted using a haemocytometer and subsequently re-suspended in appropriate volumes of medium obtain the required densities for the application (see Table 2.4). For EDTA

2. Materials and methods

passaging, cells were split at a ratio of 1:4. Following either dissociation method, cells were plated onto 13 mm glass coverslips (in 24 well plates; 1ml per well) or 12 well plates (1.5 ml per well) coated with 0.1 mg/mL poly-D-Lysine (Sigma-Aldrich, #P7886) and 20 μ g/ml laminin (Roche, #11243217001). To promote the terminal differentiation of neurons, 24 hours after plating all medium was replaced with N2B27+RA (Table 2.4) and 10 μ M DAPT. DAPT is an indirect inhibitor of the notch signalling pathway acting via γ -secretase. This action has been shown to control cell proliferation (Androutsellis-Theotokis *et al.*, 2006) and promotes the formation of neurons during stem cell differentiation (Crawford and Roelink, 2007; Elkabetz *et al.*, 2008). After 5 days, DAPT was removed from the medium and neurons were maintained in N2B27+RA supplemented with 2 μ g/ml BDNF until the end of the culture, with half-medium changes every other day.

Table 2.3 – Plating density of iPS cell derived neurons as required for different applications

Application	Dissociation reagent	Plating density cells/mm ²
RNA extraction	EDTA	1300
Immunocytochemistry	Accutase	750
Patch Clamping	Accutase	400
Calcium imaging	Accutase	400
Multi electrode arrays	Accutase	1800*
<i>*Estimated density - see text for MEA plating methods</i>		

2.5.3. Freezing of neural precursors

The freezing of NPCs was carried out following the same protocol as that for iPS cells with the following alterations: Cells were dissociated from plates using EDTA as described for passaging, with cells kept as much as possible as larger aggregates rather than single cells; cells were frozen in a medium of N2B27-RA with 10% DMSO (and N2B27 was used for all stages of the freezing); wells of NPCs were pooled and were then frozen such that 2 or 3 wells of cells were frozen together (in 1 mL total medium) to increase cell density and viability after thawing.

2.5.4. Thawing of neural precursors and terminal differentiation

Frozen 1 mL vials of NPCs were rapidly thawed at 37°C, before being added into 9 mL of N2B27-RA with 10 µM of Y27 and centrifuged at 200g for 6 mins. After aspirating medium, cells were resuspended in 1.5 mL of N2B27 with Y27, 20 ng/mL bFGF and 20 ng/mL EGF. These growth factors have been shown to promote the proliferation of neural precursors and therefore allows the expansion of NPCs after thawing (Cheng *et al.*, 2014; Li *et al.*, 2011). 1 vial of NPCs was plated into 1 well of a 12 well plate pre-coated with PDL/laminin 1:1 as described in section. After 24 hours, the medium was aspirated; cells were washed twice with DPBS to remove cell debris and replenished with 2 mL of fresh N2B27-RA with bFGF and EGF but without Y27. Cells were expanded and maintained as precursors until the desired number of cells was available, however bFGF and EGF were only used for a maximum of 7 days. In general, one vial of thawed NPCs could successfully be expanded 1:4, so for example a to get a full 12 well plate of NPCs, 3 vials of cells were required to be thawed. Any passaging required during this step was done with EDTA as described in section 2.2.1. Once all wells of NPCs were confluent, terminal differentiation was carried out as described in section 2.2.2. At this point, cells were deemed to be precursors equivalent to day 19-22.

2.6. Culture and differentiation of ASD (SHANK3) patient cell lines

The Two ASD patient lines and two control lines of NPCs used in this study (Chapter 6) were a gift from with Jack Price from the Institute of Psychiatry, King's College London as part of an ongoing collaboration. The genetic lesions present in the patient lines are presented in Chapter 6 but both include heterozygous deletions of SHANK3. iPS cells from two control and two ASD patients were derived from keratinocytes as described in Cocks *et al.*, 2014. Briefly, cells were cultured on a MEF feeder layer in a low-calcium serum-free keratinocyte growth medium. Reprogramming was achieved using a polycistronic lentivirus co-expressing OCT4, SOX2, KLF4 and c-MYC, excisable with Cre recombinase. Cells were then gradually switched to ES cell medium before colony isolation.

All four cell lines used in this study were received as frozen vials of NPCs. The protocol for the production of the precursors can be found in appendix 1. As with the protocol described in section 2.5, this protocol is based upon monolayer differentiation and dual-SMAD inhibition.

Vials of NPCs were thawed following the protocol in section 2.2.4, with the only alterations being the use of Shank3 medium instead of N2B27 (Table 2.4) and the thawing of cells into 1 well of 6 well plate, pre coated with PDL/laminin 1:1. After 72 hours, cells were re-plated onto glass coverslips in 24 well plates. Cells were first dissociated into single cells using accutase as described. Cells were counted and re-suspended in Shank3 medium with Y27 to allow a plating density of 500 cells/mm², when plated at 1 ml per well. After 24 hours, cells were topped up with 1 ml extra Shank3 medium without Y27 and half the medium was changed following a further 2 days culture. After 5 days, the medium was gradually changed to astrocyte conditioned BrainPhys (Table 2.4; see section 2.7) by half – medium changes every 2 days over a period of 6 days. BrainPhys is a defined medium for the culture and differentiation of stem cell derived neurons that provides a much more physiological extracellular environment that media based on Neurobasal alone (Bardy *et al.*, 2015). This allowed the recording of extracellular spikes without the need for changing into recording medium. Neurons were maintained in BrainPhys for a total of 14 days before being re-plated onto MEAs for analysis (see section 2.11).

2.7. Culture of primary normal human astrocytes and medium conditioning

Primary normal human astrocytes (NHAs) were bought initially from Lonza (#CC-2565). Vials of the original stock were thawed as described for previous cell lines into astrocyte medium (Table 2.4) onto un-coated 6 well plates. Once confluent, cells were passaged using TrypLE Express (ThermoFisher #12604021). After DPBS washing, 1 mL TrypLE was added to each well and cells were incubated for 10 min at 37°C. 1 mL Astrocyte medium was then added to each well and cells were dissociated and collected by triturating with a 1 ml pipette tip. After spinning at 220g for 6 mins, cell pellets were re-suspended in astrocyte medium and plated in T75 flasks (20 ml cells+medium/flask). Astrocytes were then maintained and expanded in T75 flasks and for up to 5 passages. Flasks of astrocytes were frozen up to P3 in astrocyte medium as described for NPCs. 5x 1 mL vials of astrocytes were frozen from a confluent T75 flask. Subsequent vials of expanded astrocytes were then thawed and used as described.

For astrocyte conditioning of differentiation media, 60-80% confluent flasks of <P5 NHA were used. After aspiration of astrocyte medium and 2x DPBS washes, 50 mL of medium (either N2B27+RA or BrainPhys) was added to flasks and astrocytes were cultured in this medium for 72 hours at 37°C in 20% O₂. After this period, the conditioned medium was removed from flasks, sterilised using a 0.22 µm syringe PVDF filter and stored at 4°C for use with 7 days or -20°C for longer storage. Astrocytes were then used again to condition further medium (after a 2 day recovery period with astrocyte medium), passaged as described or discarded. Conditioned medium was used 1:1 with fresh medium for neural differentiations as required.

2.8. Single-cell patch clamping of iPS cells derived neurons

Neurons for patch clamping were plated on glass coverslips as described in section 2.5. Patch clamping was performed on neurons between days 30-34 and 50-54 after single cell passaging onto coverslips. These time periods represented two distinct maturation points, simplified as 30PP and 50DPP, with 4 days allocated for data collection of that time point. For example, cells patched on D54 were collected as part of the D50 time point. This 4-day window allowed the collection of enough data for each time point, while keeping the neurons as similar possible in terms of their maturity.

Cells were patched using the following electrophysiology rig:

- Olympus BX51 WI upright microscope with brightfield, IR-DIC and epi-fluorescence
- Olympus 10x objective and 40x water immersion objective
- Olympus TH4-200 halogen light source
- CoolLED pE-300 LED source
- Q-imaging Rolera Bolt CMOS camera
- Luigs and Neumann motorised stage and table
- Luigs and Neumann Junior manipulators
- Axon Instruments HS-2 Unity gain headstages
- Axon Instruments Multiclamp 700B amplifier
- Axon Instruments Digidata 1550B
- PC running Multiclamp commander; pClamp v10 and Q-image

2.8.1. Patching pipettes and solutions

Cells were patched using borosilicate filament glass (Sutter; BF100-58-15) forged into pipettes using a Flaming/Brown puller (Sutter Instruments, #P97), resulting in resistances of 5-8 M Ω . All cells were patched at room temperature (around 22°C) in a basic physiological extracellular fluid (ECF) comprising 142 mM NaCl, 2.5 mM KCL, 2 mM CaCl₂, 1 mM MgCl₂, 10mM HEPES buffer and 30 mM D-glucose; pH adjusted to 7.4 with 4 M NaOH. The intracellular solution for pipettes consisted of 142 mM potassium gluconate, 1 mM CaCl₂, 2 mM MgCl₂, 10 mM HEPES and 11 mM EGTA; adjusted to pH7.4 with KOH. The osmolality

of internal solutions was adjusted to 290 mOsm, using a Vapour pressure osmometer (ELITech).

2.8.2. Current – clamp recording of neurons

Initial cell patching was done in voltage-clamp mode, $V=0$. After identifying target cells and correcting for electrode off-sets, patch pipettes were brought into close contact with cells and giga-ohm seals were made by applying negative pressure to the pipette. Appropriate seals were determined by applying a 5 mV, 50 Hz square wave through the electrode. After applying compensation for fast and slow capacitive transients and setting holding voltage of around -40 mV, cell break in was achieved by applying short bursts of negative pressure and/or short (50-200 μ s) 50 pA pulses of current at 50 Hz ('Zap' function of Multiclamp Commander). Immediately after break in, the commander was switched to current-clamp mode, $I=0$. Series resistance (bridge balance) values were corrected after break in and were monitored throughout experiments. Typical compensation values = $15.68 \pm 1.31 \text{ M}\Omega$ (mean \pm SEM, $n = 11$).

For basic recording of intrinsic properties and action potentials, the following protocols were applied for each cell:

1. To determine resting membrane potential: 2 minutes gap free recording, $I=0$; assessed immediately after cell break-in.
2. For I-V characteristics: episodic recording (10 s sweep), 1 s current injections beginning at - 100 pA, $\Delta 10$ pA steps, total 20 sweeps; followed by -10pA 1 s step to determine input resistance; cell held at -70 mV (current required dependent on cell, typically around -30 pA)
3. For rheobase and action potential characteristics: episodic recording (5 s sweeps), 1 s current injections beginning at + 10 pA, $\Delta 10$ pA steps, total 20 sweeps; cell held at - 70 mV (note other starting and delta currents were sometimes used. e.g. + 5 pA and $\Delta 5$ pA).
4. Spontaneous action potentials were observed with gap free recording with cells at resting membrane potential, $I=0$.

Recordings were taken using Clampex 10 (Molecular Devices, USA) and were subsequently analysed using Clampfit 10 (Molecular Devices, USA), Excel and Graphpad Prism.

2.8.3. Patch-clamp analysis

Resting membrane potentials (V_{rest}) for each cell were determined as the mean observed voltage across the 2 min gap-free recording. Input resistance (R_i) was determined by injecting small current steps into cells and recording the voltage response. At least 10 sweeps were performed for each cell and the R_i was determined as $R = V/I$, where V was the mean maximum voltage deflection for the sweeps and I was the input current step. Membrane time constant (τ) values for each cell were calculated by determining the time at which the voltage fell to $1/e$ (~63%) of the final voltage following a current step. This was done by using the equation $V_t = V_{max}e^{(-t/RC)}$ where $\tau = RC$. Membrane capacitance values were not reported in this project but none the less calculated as $C = \frac{\tau}{R}$. Occurrence of induced action potentials (iAPs) was determined by holding cells at around -70mV and injecting positive current steps ($\Delta 5$ -10pA) until APs were seen. If no APs were seen when the membrane potential reached -10 mV, it was assumed none would be seen at all. iAP categorisation of cells was based on visual assessment of traces. To be deemed a full AP, the overshoot had to be greater than 0 mV otherwise they were deemed as 'attempted'. AP trains were determined as two or more full APs (as described) seen within the stimulus time period (1 second in all cases).

Action potential events for analysis were detected using a threshold based method in Clampfit. The baseline for detection was set as the threshold for AP initiation of each individual cell. This was found by taking the first derivative of the first induced action potential seen in each cell, ($y = \frac{\Delta V}{\Delta t}$), finding the point of major upward deflection and aligning this to the voltage trace of the action potential (see Chapter 4). As for cell classification, the threshold for individual event detection was set as 0 mV. There was no minimum rate of upward deflection or maximum event time used, although individual events were manually inspected after detection to remove noise. Along with the AP threshold for each cell, three properties were recorded for each event: amplitude, half-width (the *width* of the event at half the maximum *height*), and the maximum velocity of the rising slope (Max Rise Slope). As the number of events detected in each cell was highly variable (following the same current step protocols for each cell), the average values for each property per cell were subsequently weighted relative to the number of events detected in that cell and averaged to give a single value for each time point or condition. The same approach was used to calculate the average variances.

2.9. Immunocytochemistry

2.9.1. Cell preparation and staining

Coverslips of cells for immunocytochemistry (ICC) were fixed as required using 4% paraformaldehyde solution (PFA; Sigma #P6148). After medium aspiration, cells were washed three times with DPBS. 0.5 mL of PFA was then added to each coverslip and incubated at room temperature for 15 mins. After aspirating PFA, coverslips were washed 3 times in DPBS before storing in DPBS at 4°C in the dark until use.

For staining, cells were first permeabilised using 0.1% Triton X-100 (Sigma; X100PC) diluted in DPBS, incubated at room temperature for 10 minutes. Cells were subsequently washed three times with DPBS. Coverslips of cells were then blocked to prevent non-specific binding by incubating with 1% bovine serum albumin (BSA; Sigma #A2153) in PBST (DPBS + 0.1% Tween 20; Sigma #P1379) for 30 mins at room temperature. Primary antibodies were then diluted as required (Table 2.4) in PBST + 1% BSA. Cells were incubated in primary antibody solutions over night at 4°C. The next day, cells were washed three times with DPBS, each for 5 minutes with gentle agitation. Cells were then incubated with secondary antibodies diluted in DPBS + 1% BSA as required (Table 2.4) for 1 hour at room temperature in the dark. Following three 5 minute washes with DPBS, cells were counter stained by incubating for 1 minute with 0.1 µg/ml DAPI (ThermoFisher #62248) and subsequently washed twice with DPBS. Before mounting, cells were firstly rinsed with distilled water to remove salts and subsequently dried to remove excess liquid. Coverslips were then mounted onto slides using DAKO fluorescence mounting medium (Agilent # S3023), sealed with clear nail polish and then stored at 4°C in the dark until visualisation.

2.9.2. *Imaging and analysis*

Stained cells were imaged using the following microscope set up:

- Leica DMI6000 inverted microscope with automated x, y and z movement
- Leica 10x, 20x, 40x and 100x (oil immersion) objectives
- Leica DMC3500 CCD camera
- Leica EL6000 light source
- PC running LAS X

In some cases, images were acquired using the microscope system described in section 2.10

Regions of interest were imaged at the desired magnification using stacks of z-planes to capture an increased focal range. Captured images were processed initially using the deconvolution plugin of LAS X to correct for multiple plains of focus. Images were then processed for presentation using Fiji.

2. Materials and methods

Table 2.4 – Primary and secondary antibodies used for immunocytochemistry

Antibody	Species	Supplier	Cat #	Dilution	
Primary antibodies					
Nestin	Rabbit	Millipore	ABD69	1/500	
FOXP1	Rabbit	Abcam	Ab18259	1/250	
PAX6	Mouse	Abcam	Ab78545	1/300	
TBR1	Rabbit	Abcam	Ab31940	1/500	
TBR2	Rabbit	Abcam	Ab23345	1/300	
SOX2	Mouse	Abcam	Ab97959	1/400	
OCT4	Goat	Santa Cruz	sc8628	1/500	
NANOG	Goat	R&D systems	AF1997	1/200	
KI-67	Mouse	BD Biosciences	550609	1/ 200	
Tra-1-60	Mouse	Millipore	MAB4360	1/500	
SSEA4	Rat	Millipore	MAB4303	1/500	
MAP2	Chicken	Millipore	AB5622	1/1000	
TUJ1	Chicken	Neuromics	CH23005	1/200	
GABA	Rabbit	Sigma - Aldrich	A2052	1/500	
GAD67	Mouse	Millipore	mab5406	1/500	
CTIP2	Rat	Abcam	ab18465	1/500	
SATB2	Mouse	Abcam	ab51502	1/250	
PSD95	Mouse	Antibodies Inc.	73-028	1/40*	
GLUN1	Mouse	Antibodies Inc.	73-272	1/40*	
VGLUT1	Mouse	Antibodies Inc.	75-066	1/500	
*Note TC supernatant					
Secondary antibodies					
Alex Fluor 488					
α mouse	Goat	ThermoFisher	A32723	All 1/10000	
α rabbit	Goat		A11034		
α rabbit	Donkey		A21206		
α Goat	Donkey		A11055		
α chicken	Goat		A11039		
α rat	Goat		A11006		
Alex Fluor 594					
α mouse	Goat		A11032		
α rabbit	Goat		R37117		
α rabbit	Donkey		R37119		
α Goat	Donkey		A11058		
α rat	Goat		A11007		
Alex Fluor 647					
α mouse	Goat		A32728		
α rabbit	Goat	A21244			

2.10. Calcium Imaging

2.10.1. Cell preparation and imaging

Single cell calcium imaging of neurons was performed using Fluo-4 AM (ThermoFisher; #F14201). Coverslips of cells were initially transferred into a 2-well chamber slide to allow compatibility with the heating system described below. Cells were then exposed to a cocktail of reagents comprising of 1 μ l/ml of Fluo-4 AM, 1 μ l/ml of 20% pluronic acid (ThermoFisher; # P3000MP) and 0.5 μ l/ml of cell loading reagent (ThermoFisher; #I14402) diluted into 1 mL of culture medium (Brainphys). After 30 minutes incubation at 37°C, medium was aspirated and cells were washed three times with DPBS. 1 mL of fresh medium was then added to cells and incubated for a further 30 minutes. After this incubation, medium was aspirated and replaced with 1 mL fresh Brainphys in which cells were recorded.

Cells were calcium imaged using the following microscope rig:

- Zeiss Axio Observer inverted microscope
- Zeiss 40x objective (LD Plan-Neofluar 40x/0.6)
- Zeiss 38 HE filter set
- Lumencor SpectraX LED light source
- Hamamatsu Orca-Flash 4.0 CMOS camera
- Multi channel Peristaltic pump for solution exchange
- Ibidi chamber heating system
- Zeiss Zen software

Chambers of cells were transferred to the microscope room, placed onto into the plate heated at 37°C and covered with a lid heated at 40°C to prevent the formation of condensation. After identifying regions of cells, fluorescent images were taken at a rate of 10 Hz using the constant streaming mode of the camera at a resolution of 1000x1000 pixels (2000x2000 with 2x binning). Regions were imaged for 5 minutes per experiment.

2.10.2. Analysis

Recorded stacks of images were imported into Fiji (Schindelin *et al.*, 2012) and four equal square sub-regions were extracted and saved as .tif files (full stacks were extracted for each sub-region with each region around 500x500 pixels). Region of interests (ROIs) were then identified in each sub-region using the Matlab based NeuroCa package (Jang and Nam, 2015), which adopts an approach based upon circular Hough transforms (Jiang and Ehlers, 2013). ROIs were limited to cell bodies only and were detected using a radius threshold of 2 – 7 pixels. While ROI masks were created with NeuroCa, the actual analysis of calcium events was performed with the Matlab based FluroSNAAP (Patel *et al.*, 2015). In order to use the ROI mask created with NeuroCa in FluroSNAAP, mask files were converted accordingly using a custom written Matlab script. Files were then processed in FluroSNAAP using the batch processing function to analyse single ROI events only. No network or connectivity analysis was performed. Results from the analysis were then imported into Excel for processing and subsequently into Prism for statistical evaluation.

2.11. Multi electrode array culturing and recordings

2.11.1. Equipment

60MEA200/30iR-Ti-gr MEAs were used throughout this project (Multi channel systems; MCS). These are planar MEAs with a grid of 60 titanium nitrate electrodes (59 + 1 internal reference) embedded within a silicon nitrate substrate. Each electrode has a diameter of 30 μm , with 200 μm spacing between electrodes (an image of the MEAs used can be seen in Chapter 3). MEAs were recorded using a MEA2100-HS2x60 headstage amplifier, attached into MSC-IFB-3.0 analogue/digital interface board. Cultures were recorded using the MC_Rack data acquisition software running on a high-performance PC.

The following MEA hardware settings were used throughout the project:

<i>Amplifier</i>	MEA 2100
<i>Signal voltage range (μV)</i>	-2000 – 2000
<i>Gain</i>	5
<i>Input voltage range (mV)</i>	-9.8 – 9.8
<i>Sampling frequency (Hz)</i>	25000
<i>Sample depth</i>	16 bit

Amplifier offsets were checked every month and corrected when required. Cultures were kept at 37°C with a TC02 temperature regulator controlled by the PC-based TCX software. The recording head stage was isolated within a custom made faraday cage.

2.11.2. Preparing arrays and care

Clean MEAs (see below for cleaning procedures) were stored at 4°C in the dark, with the cultured area submerged in distilled water. Before cell plating, MEAs were first pre-treated with 1 ml FBS for at least 1 hour at 4°C in the dark. This made sure the culturing surface of the array was as hydrophilic as possible. After FBS, MEAs were washed 3 times with distilled water. Culture surfaces were then treated with 0.01% PEI (50% stock; Sigma; #03880) and incubated for 1 hour at 37°C. Arrays were then washed once with distilled water and left to dry completely in a sterile cell culture hood.

2.11.3. *Culturing cells for use on arrays*

Coverslips of cells earmarked for extracellular electrophysiology were re-plated onto MEAs at D40-45 (D0 = iPS cells; see Figure 2.2). 1 hour prior to re-plating, revitacell was added to wells (final concentration = 1x) and cells were incubated at 37°C until use. Neurons were dissociated from coverslips by aspirating medium (which was saved), washing cells once with DPBS, adding 0.5 ml accutase and incubating for 10 minutes at 37°C. Coverslips were then visualised under a phase contrast microscope to check cell detachment. If neurons remained secure, cells were incubated for a further 3-5 minutes. After addition of 0.5 ml fresh medium, cells were collected by gently pipetting the medium until all cells were dissociated from the coverslips (this was checked with microscope observation). Cells from each coverslip were then pooled into a 30 ml universal tube and cells were further dissociated by gentle pipetting. Cells were then centrifuged at 200g for 6 minutes. After medium aspiration, the cell pellet was re-suspended in 1 or 2 ml of fresh medium depending on the number of cells. Cells were then counted using a haemocytometer and preparations were diluted/concentrated as required to allow a high plating density of 50,000 cells / 20 μL , which equated to around 1800 cells / mm^2 . 3 μL revitacell (100x) and 3 μL of 500 $\mu\text{g}/\text{mL}$ laminin was then added to each 20 μL of cell/medium suspension. 25 μL of cell/medium mix were then dropped directly on top of the electrode grid of each MEA. Ideal drops were those that formed small domes of cells which remained self-supporting (Figure 2.3). MEAs were then each placed in a standard 20 cm petri dish with the lids replaced and carefully transferred into an incubator for 1 hour at 37°C. After 1 hour, 1 mL of a 1:1 mix of the saved conditioned medium and fresh medium with 1x revitacell was then carefully flooded into each MEA. After a further 24 hours incubation, 1 ml of fresh medium was added to each array, bringing the total to 2 mL. 1 mL of medium was then replaced every 3 days with fresh/ACM medium at a 1:1 ratio as described in section 2.6.

2.11.4. Recording and analysis

Raw MEA data was recorded with MC Rack at a sample rate of 25000 Hz. Electrode data was filtered online with a 200 Hz high pass and a 5000 Hz low pass filter (both 2nd order butterworth). A maximum of two arrays could be recorded simultaneously and arrays were kept at 37°C throughout recordings. Recordings typically lasted for 5 or 10 minutes. Data was stored as .mcd files which contained the filtered continuous traces for each electrode together with the spikes detected using the online threshold detection built into MC_Rack. After selecting electrodes for analysis (between 15-30), chosen data was then converted to ascii files for offline analysis using the MC Data tool (MCS). Offline analysis was achieved with custom scripts written in Matlab. A detailed description of the analysis measures developed and employed in the project for the processing of MEA data is presented in Chapter 3. Briefly, spikes were detected from filtered data using an automatic threshold-based method set at $-5.5 \times \hat{\sigma}$, where $\hat{\sigma}$ is an estimate of the noise of each electrode. Spike timestamps were analysed to provide statistics on the general excitability of cultures. Network activity was analysed by creating array-wide spike detection rate (ASDR) plots with a bin width of 200 ms. ASDR peaks were detected using a threshold of 70-80% of the maximum sized bin. All data was processed for comparative statistics using Graphpad Prism.

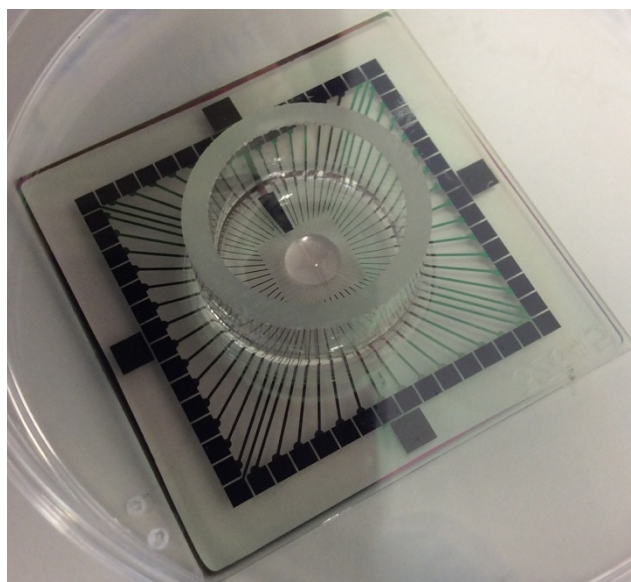


Figure 2.3 – Plating iPS cell derived neurons onto MEAs. To achieve the required density and survival of cells, neurons were plated onto MEAs as drop cultures. 50000 cells were resuspended in 20 μ L of medium, together with 3 μ L of laminin and 3 μ L of revitacell. Cells were then dropped onto completed dry MEAs, pre coated with PEI, to create a drop of cells/medium directly above the electrode area. After 1 hour of incubation at 37C, the culture well was flooded with 1 mL medium.

2.11.5. MEA cleaning

After use, TrypLE was used to dissociate cell cultures from array surfaces. One cell debris was removed, MEAs were washed with Alconox Tergazyme (ThermoFisher; #16-000-199), an anionic and protease based detergent. Arrays were placed into a large volume of 1% Tergazyme solution and soaked overnight with very gentle agitation. The next day, arrays were rinsed with distilled water and left to soak in fresh water for a further 24 hours. MEAs were rinsed for a final time before being steam-autoclaved, in individual autoclave pouches, for 15 minutes at 120°C in a bench-top autoclave. After cooling, the well of each array was filled with distilled water and stored at 4°C in the dark until use.

2.12. Statistical analysis

All descriptive and comparative statistics in this project were completed with Prism 6 (Graphpad). However, to determine the route of analysis (parametric or non-parametric), data was first processed using histograms, q-q plots and normality tests (kurtosis and skew tests) in R (RDevelopment, 2012). Where groups of data from the same experiment, presented with contrasting distributions, parametric tests were used as they are, in general, better equipped to cope with non-gaussian distributed data. The statistical tests used for each of the experiments are described in the results of each chapter. While the significance or otherwise of each relevant comparison is reported where appropriate, in general only significant differences were detailed in tables along with the average differences and corresponding variance. All p values reported are two-tailed. Unless otherwise stated, all summary plots of data show means + standard deviation. N numbers for each experiment vary and are reported in individual figures. However, except in a couple of cases involving smaller experiments, all results presented here were collected from at least three differentiations.

3. The development of a pipeline for the analysis of iPS cell derived neuron multi electrode array data

3.1 Introduction

The advent of more user-friendly and reliable multi-electrode array (MEA) systems together with advances in techniques for multi-unit recording *in vivo* has led to renewed interest in the development of methods to process the captured neuronal activity. In particular, one of the primary advantages of planar MEAs over single cell patch clamping is the ability to culture neurons following a relatively standard protocol but which allows the simultaneous recording of activity from a large population of neurons. This extends the analysis of single unit behaviour to the level of small networks, therefore providing an opportunity for the study of the functional development of neuron populations *in vitro* and investigating the behaviour of cell based models of disease. This opportunity is extended further with the use of iPS cell derived neurons, allowing the study of how these cells behave throughout their development and allowing the possibility to investigate network function in human models of disease.

The analysis of MEA data is inherently complex and computationally challenging. The arrays used throughout this project have 60 electrodes, each recording raw data at a rate of tens of kilo hertz (kHz) leading to very large data files (>3 Gbs) which need to be processed offline. Decisions are then required about the analysis of the raw data at several points, most noticeably surrounding how spikes are identified, quality control of spike data, how statistics are inferred from spikes, the analysis and handling of spike waveforms and finally, the processing of data concerning the activity of neural networks. Over the last few years, there have been a number of both proprietary and open source tools made available for the analysis of multi-channel electrophysiological data (including MEA data, *in vivo* extracellular recordings etc.) many of which package a range of analysis measures aimed at providing a comprehensive solution to the processing challenge (Wagenaar *et al.*, 2005; Georgiadis *et al.*, 2015; Hazan *et al.*, 2006; Vato *et al.*, 2004; Egert *et al.*, 2002; Quian Quiroga *et al.*, 2004).

3. Development of an MEA analysis pipeline

At the onset of this project, a number of these tools were tested to identify one which would be suitable for the types of analysis required. However, a number of issues were identified which limited their potential use. Firstly, although the majority of the tools are written in Matlab and therefore, theoretically should be functional across platforms and releases, several procedural errors were encountered which either prohibited analysis or introduced a sufficient enough hurdle as to limit the speed of processing. This was especially an issue with the open source tools as these tended to lack the documentation and support to allow useful troubleshooting. Secondly, the beginning of this project and the development of the protocols for successful MEA culturing and recording was in parallel with the learning of the analysis techniques and the Matlab coding language. The existing Matlab based tools are, in general, fairly comprehensive in their analysis scope and have been written by experienced researchers and informaticians, often meaning that the level of coding complexity is high. This therefore meant that it was difficult in some circumstances to determine how certain parameters were controlled, how specific analysis measures were performed and how particular statistics were arrived at. Thirdly, many of the existing tools place an emphasis on the analysis of spike waveforms and in particular, feature extraction and shape clustering, being a key factor in the analysis of multi electrode recording *in vivo*. While the analysis of spike shapes was something which was of potential interest, it was not the primary aim of the process to be used here. Finally, the existing tools had all been developed based upon data recorded from rodent neurons, either *in vivo* or dissociated cultures *in vitro*. For some analysis measures, the use of iPS cell derived neurons did not affect the outcome measure. However, for others, such as the determination of baseline noise and the identification of bursts, these tools often mis-represented the true activity. In fact, it is perhaps more accurate to say that certain characteristics were mis-represented in the context of their nature as iPS derived neurons, owing to their relatively immaturity and therefore inactivity compared to primary neurons.

In light of the limitations of existing analysis tools described above, it was decided to develop a new analysis pipeline tailored for the types of analysis that were required throughout this project. As well as providing a way of controlling every aspect of the analysis process, this would also provide a greater understanding about the nature of the activity being recorded from iPS cell derived neurons, which in turn would inform some of the key decisions being taken about how the analysis should take shape to best suit this type of cell.

3.2 Chapter Aims

This chapter aims to develop a pipeline of computational tools for the analysis of MEA data, focusing on the processing of extracellular recordings from iPS cell derived neurons. The chapter will aim to produce a toolkit which focuses on the calculation of two key groups of statistics, those based upon the general excitability of individual neurons and those based upon the development of network driven behaviours in the cultures. The pipeline will also aim to provide a clear and intuitive set of analysis steps which will allow accessible processing of data for users relatively new to MEA recordings.

3.3 Development and description of analysis measures

3.3.1 General Overview

The development of an analysis platform was based upon four key steps: online data acquisition, spike detection, spike waveform extraction and analysis of network behaviour. This was supplemented with an additional step to extract feature information from waveforms and performing clustering to identify specific populations of spike shapes. Figure 3.1 presents a schematic of the general approach taken for the development of the pipeline and highlights the key decisions required regarding the methodological approach within each step. From these steps, primary analysis outcomes will be devised based around two areas of focus: basic excitatory properties of the cultures based around single unit statistics and analysis of network function based around patterns of coordinated firing.

For several reasons the pipeline was developed and written entirely within Matlab (Mathworks Inc., 2010; except for the acquisition and filtering of data). Firstly, although a proprietary software, Matlab is widely available through institutional licences and is supported by an extensive recourse database, including many user-created plugins, toolboxes and guides. Secondly, the type of data to be analysed, essentially large databases of continuous data which is then manipulated within the rows and columns, is a strong feature of Matlab. Finally, a number of aspects of the analysis are based upon those developed elsewhere, either as part of similar Matlab based electrophysiology packages, or from tools available from various Matlab resource databases.

3. Development of MEA analysis pipeline

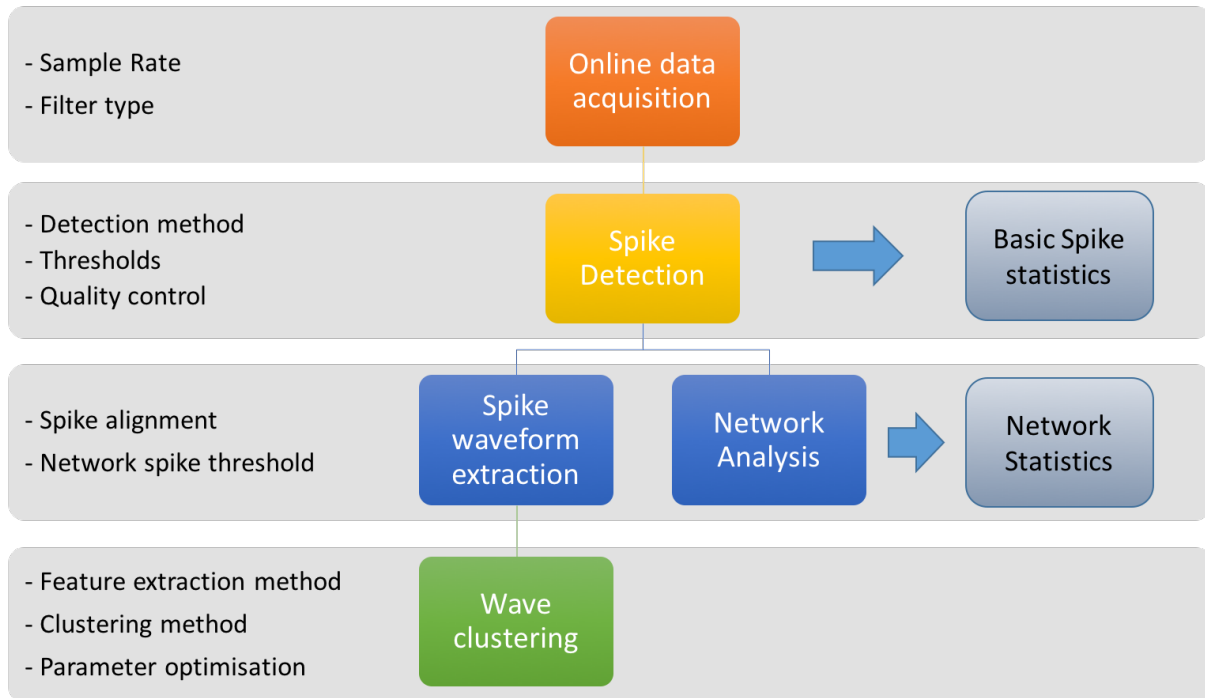


Figure 3.1 - Workflow of the analysis pipeline developed in this project. The pipeline was based around 5 key areas of processing: online data acquisition, spike detection, extraction of spike waveforms, analysis of network behaviour and clustering of spike waveforms. Each of these steps has numerous decisions associated with them regarding the development of the analysis methods (left side of grey panels). The pipeline will be used to deliver two primary sets of outcome measures, statistics based around general excitability at the level of single units ('Basic Spike Statistics') and those concerning the activity of culture-wide networks ('Network Statistics').

3. Development of an MEA analysis pipeline

3.3.2 Online data acquisition

As described in Chapter 2, iPS cell derived neurons were cultured on 60 electrode planar MEAs and recorded using an equipment package from Multi Channel Systems (MCS). Recordings were taken from arrays using the MC Rack tool (MCS) which allows fully customisable acquisition of data from up to four MEAs simultaneously (note a maximum of two were recorded concurrently in this project). Hardware settings were as described in Chapter 2 and were not altered throughout all of the MEA recordings.

Data arriving from each electrode of an MEA is in the form of continuous raw time-voltage traces. In all cases, raw data was sampled at a rate of 25000 Hz. In order to perform spike detection and subsequent analysis, the data must first be filtered. A high pass filter is required to remove low frequency field-potentials and any potential 50 Hz AC noise, while a low pass filter provides 'cleaning' of the signal for higher frequencies. For all experiments used in this project, raw electrode data was filtered online through a butterworth 2nd order high-pass filter, set at 200 Hz, followed by a butterworth 2nd order low-pass filter at 5000 Hz. Figure 3.2A&B shows the gain attenuation and phase plots for each of the filters used. Although it has been shown that filters of different types and parameters, particularly causal filters such as that used here, can in some circumstances affect the shape of detected spikes (Quiñero Quiroga, 2009), using the online filtering was chosen as it allowed the filtered data to be the basis of the subsequent offline analysis. Furthermore, building the spike detection algorithms with an additional step of retrospective filtering proved to be computationally challenging due to the size of the files being handled. Figure 3.2C shows a trace of data from one electrode before and after band pass filtering. The variable baseline of the unfiltered signal is due to slow field potentials (<100 Hz) and hinders the reliable detection of extracellular spikes. Filtering the signal using the parameters described above produces a stable baseline from which spikes can be easily identified and readily detected computationally and without supervision.

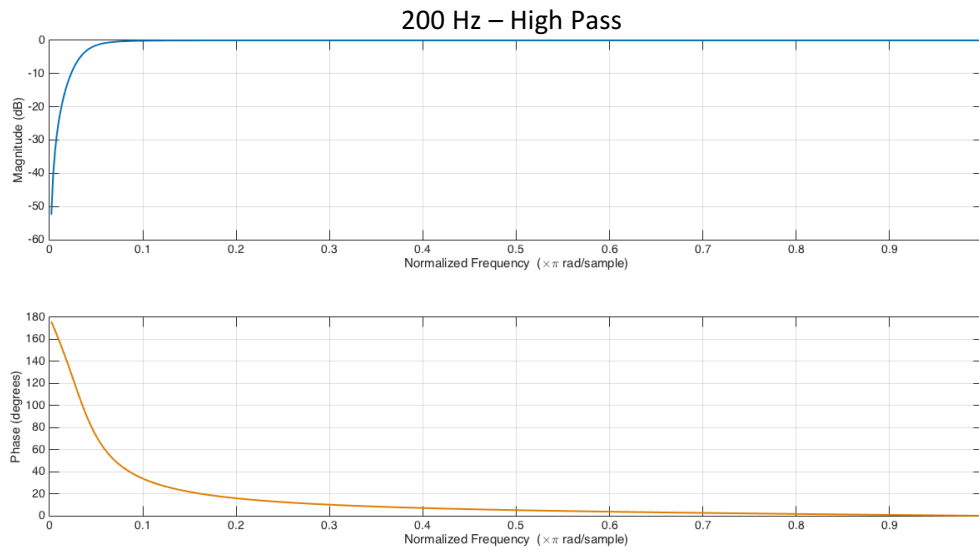
For each electrode of an array, filtered data was recorded and stored in .mcd format, the standard file associated with all MCS software. To allow offline analysis of data with Matlab, data was then converted to tab-delimited ASCII format using the MC Data tool (MCS). It was at this point that electrode data from each array experiment was chosen to be taken forward for analysis. With a sample rate of 25000 Hz and recordings up to 10 minutes long, analysing the

3. Development of an MEA analysis pipeline

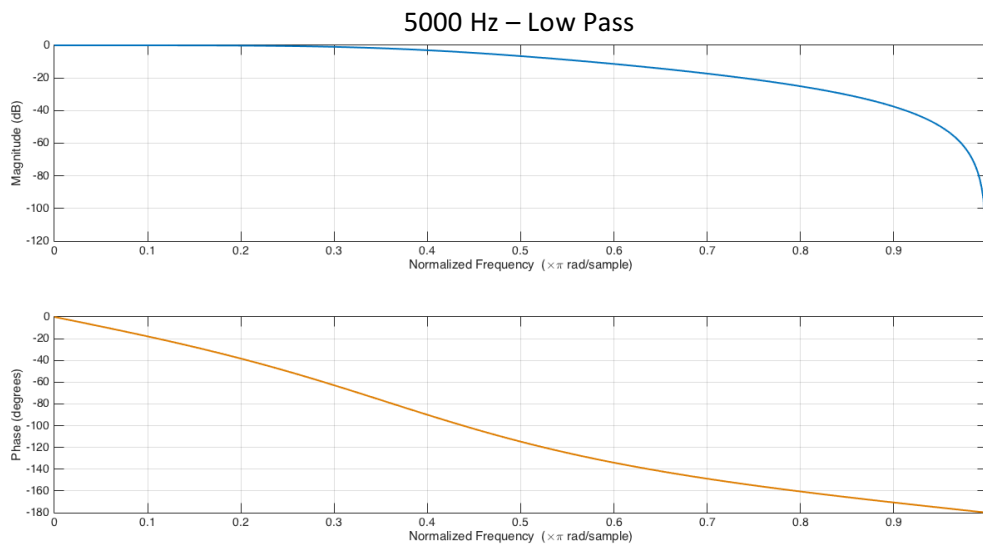
data from all 60 electrodes of an array was prohibitive as files were > 20 Gb. Moreover, it was also almost always unnecessary, as despite the optimisation of culturing protocols described elsewhere in this project, very rarely did all 60 electrodes record neuron activity. Instead, for each recording experiment, a selection of between 16-25 electrodes were taken forward for analysis. Electrodes were chosen to represent the activity of the cultures as a whole and as such were taken from across the array. At least 2 electrodes were taken from each column and no two electrodes could be adjacent, whether between columns or rows. This was to control for the possibility that adjacent electrodes were recording activity from the same neuron, although this has been shown to be very unlikely (Lin *et al.*, 2005). The chosen electrodes for each experiment are shown where required throughout the project.

3. Development of MEA analysis pipeline

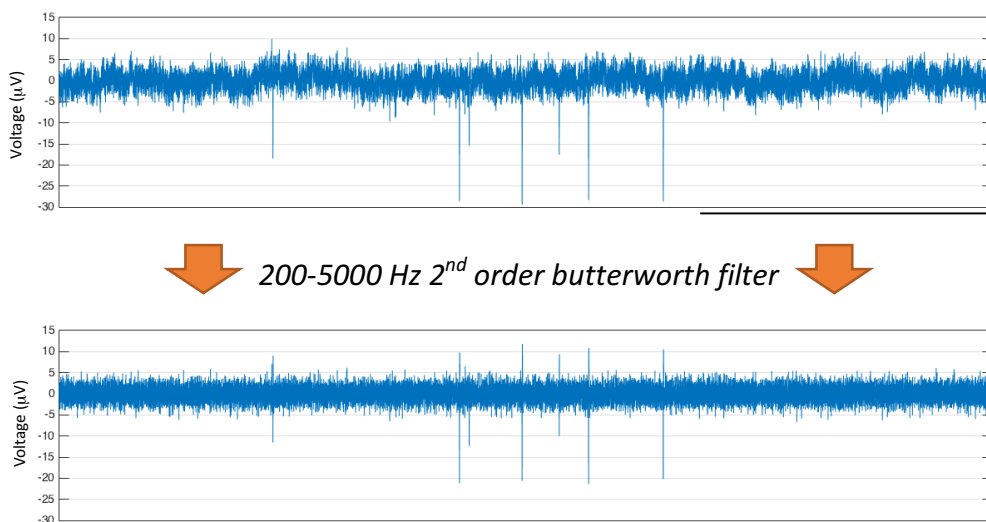
A



B



C



3. Development of MEA analysis pipeline

Figure 3.2 – High/low band pass filtering of raw data from multi electrode arrays (MEAs) is required to perform spike detection and analysis. Raw data recorded from MEAs contains both fast and slow wave components that require filtering before the data can be processed further. Low frequency field potentials cause a consistently fluctuating baseline making reliable detection of extracellular spikes challenging; high frequency noise can influence the shape of detected spikes and produce artefacts. All MEA recordings used in this project were filtered through a 2nd order butterworth high pass filter at 200 Hz (**A**), followed by a 2nd order butterworth filter low pass filter at 5000 Hz (**B**). Top panels in **A** and **B** show the gain response of the filter against the normalised frequency while bottom panels show the phase response against the normalised frequency. **C** shows the raw data from one electrode (top panel) and the same data after filtering (bottom panel). Filter response plots were calculated using a sample rate of 25000 Hz. Scale bars in **C** = 1 second.

3.3.3 Spike detection

The next stage in the pipeline, and the first to be done offline, is the detection of spikes from the filtered data of each electrode to be analysed. The most common method is by using a voltage threshold above (or below in the case of extracellular events) which events are classed as 'spikes'. Of course, the threshold required for each electrode is a balance between one that is high enough to minimise the capturing of false-positives through random changes in baseline noise but not so high as to miss true lower-amplitude spikes. Perhaps the most accurate way to set a threshold for each electrode is to do so manually, such that each threshold best represents the best possible trade off for that particular data trace. However, this clearly introduces a time and user intensive step into the analysis and reduces the scalability of the pipeline. As such, a threshold was determined automatically for each electrode, based upon calculations of the baseline noise.

One of the most commonly used methods for automatic thresholding is based upon taking an overall assessment of the standard deviation of the noise, where noise = background signal + spikes (Vato *et al.*, 2004; Mok *et al.*, 2012; Chiappalone *et al.*, 2006). Indeed, this is also the approach taken by the online spike detection in the MC Rack software. Based upon the number of tools that seemed to have validated this method, together with the relative simplicity of its implementation, it was decided to use this approach for the pipeline developed here.

The automatic threshold was determined as $Thr = k \times \sigma_n$, where k is the multiple to determine the level of threshold and σ_n is the standard deviation of the voltage values for the entire electrode trace. Throughout the project, only negatively deflecting spikes were captured, as these represented the vast majority of events. A threshold multiple of 5.5 was chosen as it provided a level which detected very few recording artefacts. Together this gives a k of -5.5.

Using this method of automatic thresholding (called herein the SD method) seemed to successfully calculate appropriate thresholds for individual electrodes. However, it became clear in certain circumstances, some thresholds may in fact be too high. Figure 3.3A&B show filtered data traces from two different electrodes (not from the same array) which recorded different patterns of neuron firing. In A, the neuron is firing at a consistent rate of around 0.75 Hz. In situations similar to this, the SD method of threshold determination appears to perform well.

3. Development of an MEA analysis pipeline

However, the situation in Figure 3.3B shows bursts of high frequency firing in between quieter periods of low frequency and, importantly, lower amplitude firing. The overall firing rate for this example is 2.59 Hz. It is in these situations where it was noticed that the automatic threshold was perhaps too high, as it appeared that several spikes in the lower frequency firing periods were not being detected. In fact, this is a phenomenon which has been previously studied, with the authors concluding that during high frequency firing, the SD estimation of noise is overrepresented, as the increase in voltage peaks (due to more spikes) disproportionately skews the true baseline (Quian Quiroga *et al.*, 2004). To overcome this issue, the authors proposed another method of estimating signal noise, based upon using the median absolute deviation.

For this method, the threshold is still calculated as $Thr_m = k \times \hat{\sigma}_n$ but in this case, the estimation of noise is given as $\hat{\sigma}_n = \frac{\text{median}(|X|)}{0.6745}$, where $|X|$ is the absolute values of the voltages for the entire electrode trace and 0.6745 is derived from the cumulative distribution function for normally distributed data (which, for the purposes of this equation, the signal data is assumed to be).

The two methods were compared with the two different activity scenarios in Figure 3.3. k for both methods was maintained at -5.5 . In Figure 3.3A&B, the red lines indicate the thresholds calculated using the median absolute deviation (MAD) method and the green lines show the thresholds calculated with the SD method. Figure 3.3C shows the summaries of the calculated noise estimation, threshold and number of spikes detected with each method. In both A and B firing situations, the estimation of noise and therefore the threshold for detection is higher with the SD method. However, while in the the low firing state this difference is around $1 \mu\text{V}$, this increases to a difference of $3.72 \mu\text{V}$ in the high bursting state. This therefore meant that with bursting activity, around 25% of spikes detected by the MAD method were not picked up with the SD method, while this same value was around 10% in the tonic firing state. Finally, the ratio of change in noise to change in spike rate highlights the extent to which the estimation of noise using the SD method increases faster than the for the MAD method, for a given increase in spike rate.

It could be argued that as long as the method for spike detection is kept constant throughout the entirety of the project's experiments, the actual method used is less important. However,

3. Development of an MEA analysis pipeline

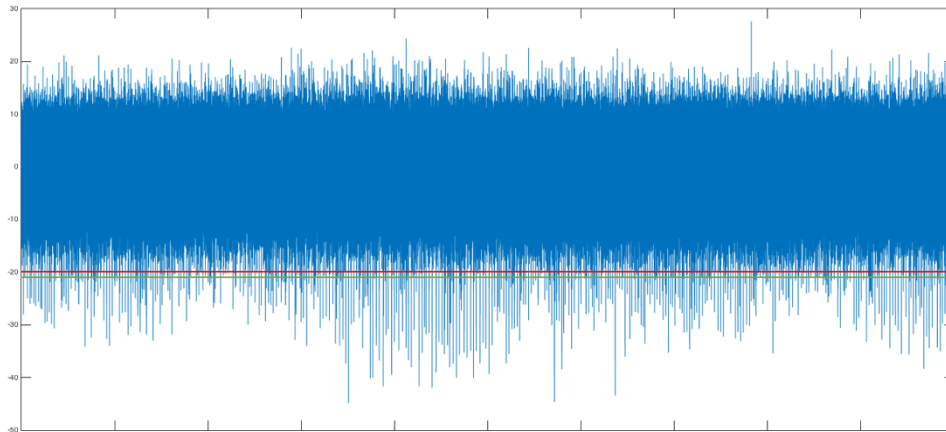
because one of the primary aims of this project is to investigate network function using the MEAs, it was anticipated that changes in spike rate within experiments is likely to be a common occurrence which needs to be addressed. As such, it was decided to use the MAD method for noise estimation, owing to its superior handling of higher rate firing. Therefore, for all experiments analysed in the project, the automatic threshold for each electrode was determined using the following formula:

$$Thr = -5.5 \times \hat{\sigma}_n \text{ where } \hat{\sigma}_n = \frac{\text{median}(|X|)}{0.6745}.$$

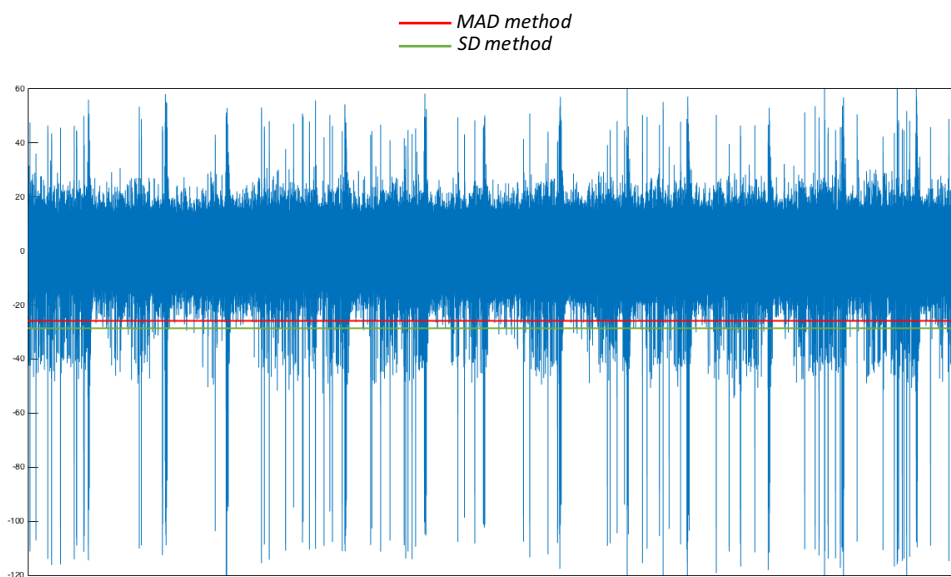
Spikes were then subsequently detected using the *findpeaks* function in Matlab. All parameters were kept as standard, except that the 'minimum peak prominence' option was selected, with a value of 2. This guaranteed that there was a clear vertical drop after the peak to ensure that a small 'shoulder' in the spike was not counted as a separate spike.

3. Development of MEA analysis pipeline

A



B



C

Low rate tonic firing (mean = 0.75 Hz)		
	<i>Standard Deviation</i>	<i>Median absolute deviation</i>
<i>Estimate of Noise (μV)</i>	3.81	3.61
<i>Threshold* (μV)</i>	-20.96	-19.89
<i>Spikes detected</i>	511	565
<i>% difference in spikes</i>	10%	
High rate bursting (mean = 2.59 Hz)		
	<i>Standard Deviation</i>	<i>Median absolute deviation</i>
<i>Estimate of Noise (μV)</i>	5.19	4.69
<i>Threshold* (μV)</i>	-28.56	-24.84
<i>Spikes detected</i>	1557	2052
<i>% difference in spikes</i>	25%	
$\Delta \text{noise}/\Delta \text{rate}$ ($\mu\text{V Hz}^{-1}$)	0.75	0.48
<i>*Threshold = -5.5 x noise estimate</i>		

3. Development of MEA analysis pipeline

Figure 3.3 – Comparison of methods for offline spike detection from MEA data. Two different threshold based methods of spike section were trialed in two different firing situations: one with a low rate of consistent, tonic firing (**A**) and one with periods of low firing in between high-rate burst firing (**B**). Both methods set automatic thresholds for each electrode trace with the formula $Thr = k \times \sigma_n$ where k is the manually determined threshold scale (constant for all electrodes) and σ_n is the estimation of noise (baseline signal + spikes). The standard deviation (SD) method calculates an estimation of noise by taking the standard deviation of the voltage values for the electrode data; the median absolute deviation calculates an estimate of noise by the formula $\hat{\sigma}_n = \frac{\text{median}(|X|)}{0.6745}$, where $|X|$ is the absolute values of the electrode voltage data. Red lines in **A** and **B** show the threshold calculated with the MAD method, green lines show the thresholds calculated with the SD method. **C** shows the details of the values of estimated noise, thresholds and spikes detected with each of the methods. The SD method produced higher thresholds than the MAD method in both firing sates. However, the difference was bigger with high-frequency bursting, meaning that a higher percentage of spikes that were captured with the MAD method were missed by the SD method. This was highlighted by calculating the change in noise: change in rate ratio, which shows that the SD method increases the estimate of noise faster than the MAD method for a given increase in spike rate.

3. Development of an MEA analysis pipeline

3.3.4 Spike waveform extraction

After spike detection, each spike waveform was saved by extracting the 40 samples previous to the peak and the 70 samples after the peak from the continuous filtered electrode trace. This gave a total of 111 samples, corresponding to 2.7 ms of data, with all spikes aligned to their peaks at the 41st sample point. Spike shapes were stored both at the individual electrode level and as a pooled database for the entire array. Plots of spikes shapes included an overlaid trace to show the average shape of the waves in that electrode or array. This was calculated as the median value for each of the 111 samples across each of the spikes being analysed.

In general, the analysis of spike shapes was not used as a key measure in this project. Instead, observation of spikes shapes was primarily used as a quality control method to confirm that detected events were extracellular spikes. Any events that were identified as clearly noise or artefacts (either by shape or by very large amplitude) were then traced back and removed from the analysis.

An exception to this is some of the work presented in Chapter 6, which uses spike shapes as a method of comparing activity between cell lines. For this, the analysis of spike shapes was taken further with feature extraction and clustering and is described in section 3.3.7.

3.3.5 Basic Statistics

After detection of individual spikes from each of the chosen electrodes from an array, the stored time stamps were then used as the basis for the first batch of analysis measures, based upon general culture excitability. This analysis group consisted of six primary measured outcomes: *Total number of spikes, average number of spikes per electrode, average spike rate, max spike rate, average inter spike interval (IsI) and total number of detected bursts*. This section will describe the derivation of each of these analysis measures.

Total number of spikes. The simplest statistic, this is a measure of the total number of spikes detected from all of the analysed electrodes and is a primary determinant of general culture excitability. However, this is not a useful measure for comparing between arrays or experimental repeats etc. as it may be the case that a different number of electrodes were analysed from each array. Instead, the average spikes per electrode was developed as the primary measure of excitability.

Average spikes per electrode. To provide a measure of the number of spikes that could be compared across arrays and experiments, an average for the number of spikes in each electrode was given as $AvgSpikes/electrode = median (Spikes_{E1}, \dots, Spikes_{En})$. The median was chosen as it provided a control for electrodes that were much more or less active than others and gave a more representative overview of the activity of the array as a whole.

Average spike rate. To allow comparisons between arrays and experiments and to provide a measure of the overall activity of a culture, an average spike rate was calculated from across the electrodes. Firstly, the average spike rate for each electrode (E) was calculated as

$$AvgSpkRate_E = \frac{Number\ of\ spikes_E}{t_{max}}, \text{ where } t_{max} \text{ is the total length of the recording in seconds.}$$

Then, to give a spike rate for the entire array (A), $AvgSpkRate_A = median (AvgSpkRate_{E1}, \dots, AvgSpkRate_{En})$. As with average spikes/electrode, the median of the electrode spikes rates was used to control for especially high or low firing rates.

Maximum spike rate. This was simply determined as the highest electrode spike rate ($SpkRate_E$) calculated.

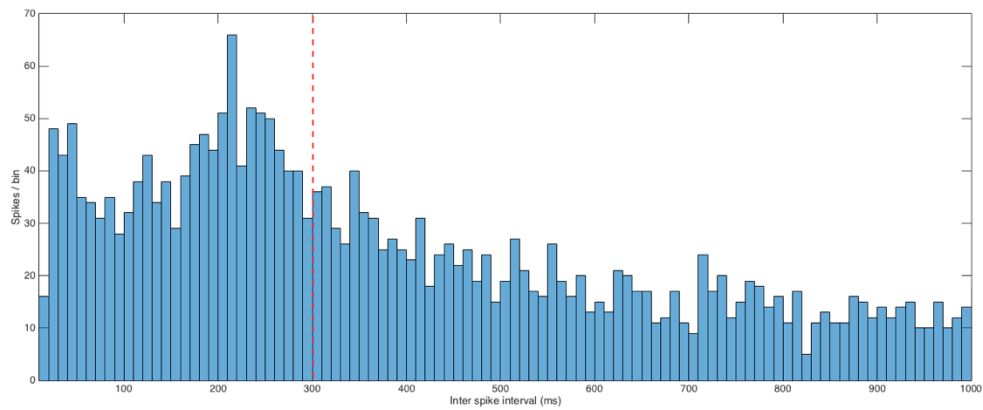
3. Development of an MEA analysis pipeline

Average inter spike interval (IsI). As with spike rate, a single value for IsI was calculated per array to allow comparisons with other cultures. First, the individual IsIs were determined for each electrode by finding the difference between each of the spike time-stamps. Then, the average electrode IsI was determined as $AvgIsI_E = mean(IsI_1, \dots, IsI_n)$. Finally, as with spike rate, the average array IsI was given as $AvgIsI_A = median(AvgIsI_{E1}, \dots, AvgIsI_{En})$.

Number of detected bursts. The detection of bursts in spontaneously activity neural cultures is a topic which has received a large amount of discussion, primarily because there is no standard definition for what counts as neuron burst. Methods for bursts detection include using an IsI threshold (Chiappalone *et al.*, 2005; Wagenaar *et al.*, 2006), a hybrid of parameters based upon IsI and instantaneous spike rate (Bakkum *et al.*, 2013), and methods based upon evaluating a cumulative moving average for IsI distributions {Kapucu 2012 (Kapucu *et al.*, 2016). Despite the appeal of the methods developed by Kapucu *et al.*, especially as they have been adapted for use with developing iPS cell neurons, it was decided to use a more basic approach based upon a maximum IsI threshold. This was primarily down to the difficulty found in adapting the cumulative moving average algorithms for use in Matlab. Two parameters are required for burst detection using an IsI based approach: the number of spikes required in a burst and the maximum IsI between each of those spikes in the burst. The number of spikes required for a burst should be, of course, at least two but is in fact mostly decided at the researcher's discretion. Here, the minimum number of spikes required for a burst was set at 3. Determining the threshold for the maximum IsI interval was achieved by plotting histograms of the total IsIs for each array. Figure 3.4 shows IsI histograms from two different arrays, plotted with bin widths of 10 ms. The threshold for maximum IsI was determined as the nearest 50 ms greater than the major 'short interval' peak + 50 ms (dotted red lines in Figure 3.4; 300 ms in A, 150 ms in B). This threshold was fixed for every set of experiments, not every array and as such was a compromise based on the firing properties of the cohort of arrays being analysed. The maximum IsI interval used was 300 ms.

3. Development of MEA analysis pipeline

A



B

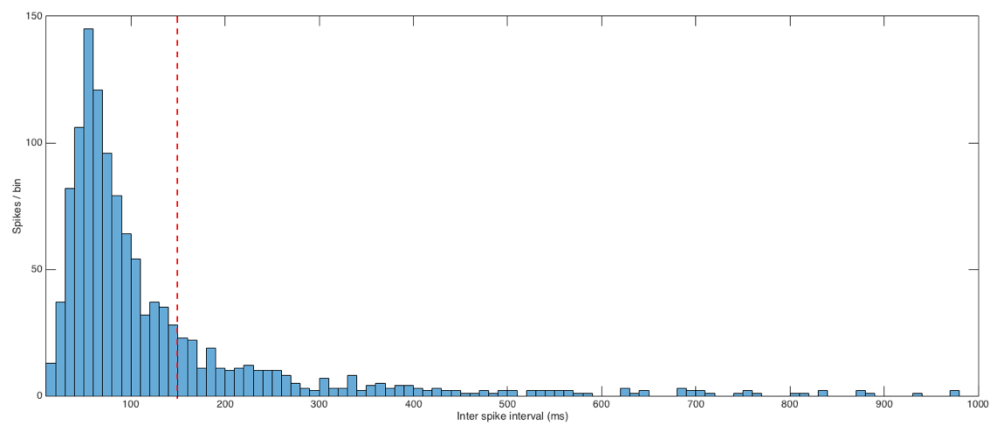


Figure 3.4 - Determination of maximum inter-spike interval (ISI) for the detection of burst firing in MEA cultures. To determine the maximum ISI threshold for burst firing, histograms of ISI from across a single array were created with bin widths of 10 ms. **A** and **B** show the ISI histograms for two different MEA cultures. Thresholds (red dotted lines) were determined manually as the nearest 50 ms greater than the major short interval peak + 50 ms.

3. Development of an MEA analysis pipeline

Figure 3.5A shows a raster plot of spikes for 10 electrodes all which show sustained mid-rate firing. When arrays with consistent culture-wide firing such as this are analysed, the outcome measures as described above performed well. However, Figure 3.5B shows an array of 10 electrodes where 5 of electrodes are either very inactive or silent. In this situation, it was found that the average spike rate and average ISI were being disproportionately reduced, even with the control of medians. While each electrode was manually chosen for analysis as described in section 3.3.3, in some circumstances, electrodes were chosen because of their activity at an earlier or later time point. For example, to maintain the consistency of analysing cultures throughout development, electrodes were chosen based upon their activity across the entire experimental time frame (e.g. 60 days), such that as far as possible, the exact same electrodes were analysed for every time point for each array. This however meant that in some cases, an electrode was silent for a particular time point, therefore introducing error into the calculations of average array wide measurements.

To control for this eventuality, a threshold for electrode analysis was set such that only electrodes with a certain number of spikes would be counted in the measurements. The threshold was calculated as the following:

Electrode analysis threshold = $[a]$, where $a = \frac{Spikes_{Emax}}{100} \times 5$, where $Spikes_{Emax}$ is the number of spikes in the most active electrode. This therefore determines that the threshold is set at the nearest integer corresponding with 5% of the number of spikes seen in the most active electrode in the array.

Figure 3.5C shows the summaries for the statistics calculated using the standard methods, and the adjusted values calculated from only those electrodes which pass the electrode analysis threshold. When the activity in a culture is consistent across the array, as in figure 3.5A, the adjusted analysis is identical to the standard method, as all 10 electrodes pass the activity threshold. However, where array wide activity is inconsistent, as in Figure 3.5B, the adjusted statistics only include the 6 electrodes which contained at least 5% of the number of spikes of the most active electrode (most active electrode had 2321 spikes, $threshold = \frac{2321}{100} \times 5 = 116$). This corrects the measurements involving averages to better represent the activity of the

3. Development of an MEA analysis pipeline

culture, while having little effect on the the total spike count or the number of bursts as the majority of these are already contained in the most active electrodes.

For all MEA experiments in this project, the presented statistics were calculated as described above, with the additional adjustment to control for variable electrode activity.

3. Development of an MEA analysis pipeline

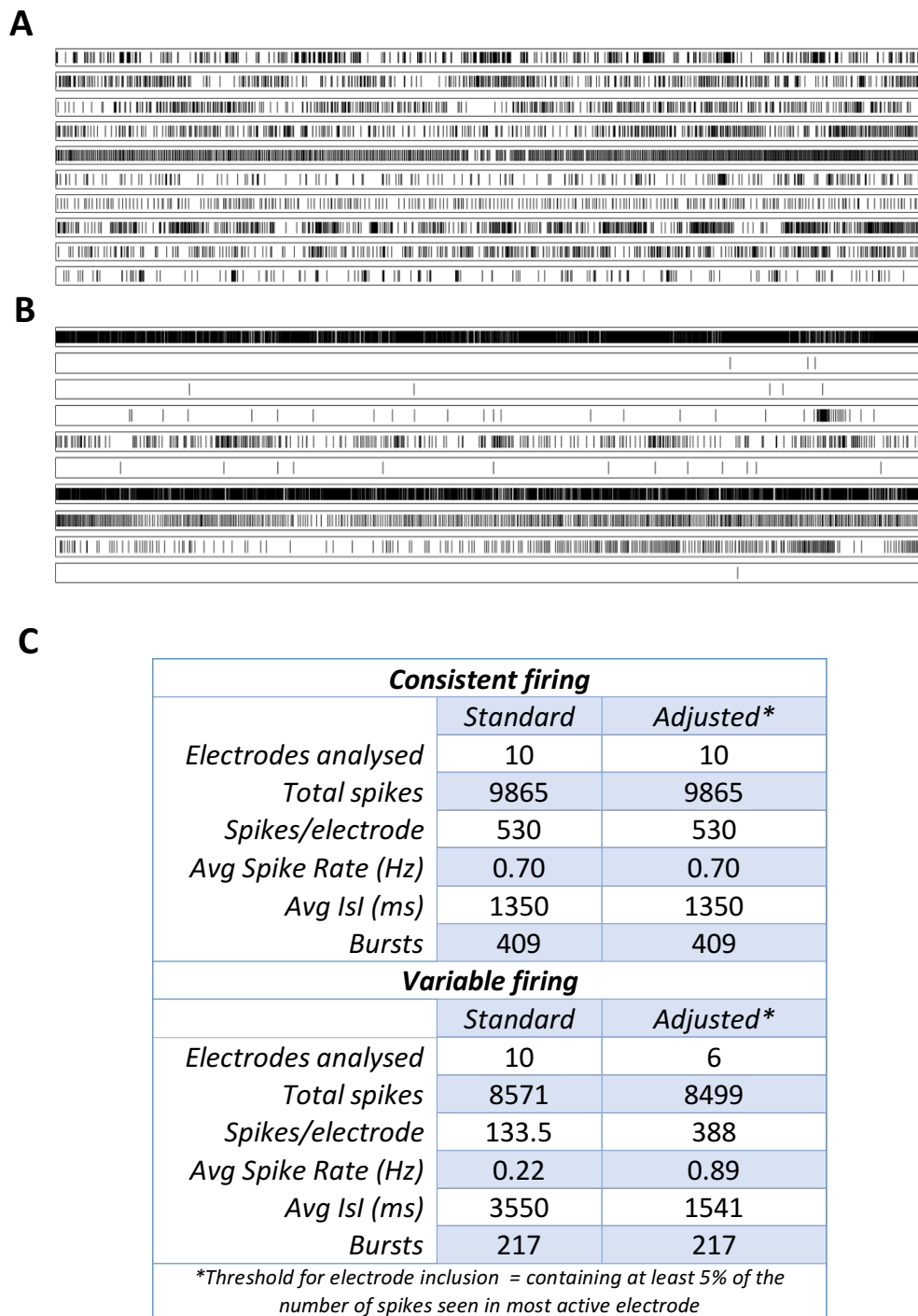


Figure 3.5 - Controlling for variable electrode activity in the calculation of basic MEA statistics. When the majority of analysed electrodes across an array are detecting consistent activity (A), the standard methods for calculating statistics are useful. However, when there is large variability in the amount of firing detected in some electrodes (B), the calculated statistics are often misrepresentative. To account for this variability, an adjusted method of calculation was devised such that only those electrodes showing at least 5% of the number of spikes detected in the most active electrode are included (C). This adjustment provided statistics that better reflected the activity of the culture. Raster plots show activity over 10 minutes.

3.3.6 Network Analysis

The second primary group of analyses used was that concerning the activity of a culture as a whole and in particular the analyses of coordinated network behaviour. These measures were based upon the creation of array wide spike detection rates (ASDR), which have been used by a number of previous studies for the analysis of synchronised behaviour in MEA cultures (Sun *et al.*, 2010; Lu *et al.*, 2016; Mok *et al.*, 2012). ASDRs were calculated by firstly dividing individual electrode data into 200 ms bins and counting the number of detected spikes within that bin. The bin ASDR is then determined by summing the number of spikes seen in each 200 ms bin culture-wide (Figure 3.6A). ASDR plots can then be created by plotting the total number of spikes in each bin serially for the length of the recording (Figure 3.6B). For cultures showing synchronised culture-wide activity, the ASDR plots appear as periods of oscillating peaks (More Active Periods; MAPs) and troughs (Less Active Periods; LAPs). For cultures showing this type of behaviour, two statistics were determined:

Max ASDR. This simply describes the maximum of spikes detected in a single 200 ms bin culture wide i.e. the summed number of spikes seen in each electrode for that bin. This provides a good measure of how synchronised the activity is across the culture as increased synchronicity leads to more spikes being detected in that particular bin.

Average MAP interval. The interval between the MAP peaks of ASDR plots serves as a primary measure of network activity in cultures. As with all outcomes measures, a single value was derived per array. To detect MAP peaks from the remaining ASDR data, threshold was first determined over which peaks had to appear. This ensured any secondary peaks within the same MAP were not counted. The MAP threshold was determined as $MAP\ Thr = \frac{MaxASDR}{100} \times n$, where max ASDR is the measure described above and n determines the threshold level. The threshold level was typically between 40 and 50% but was determined for each individual set of experiments (and kept constant throughout those experiments). The `findpeaks` function of Matlab was then used on the binned spike counts (bin ASDRs) data with a `MinPeakProminence` of 4 and a `MinPeakHeight` corresponding to the MAP threshold. The intervals between each MAP peak (excluding the first detected peak) were then calculated. In some cases, two or more peaks with very similar heights were detected within the same MAP, therefore giving very small

3. Development of an MEA analysis pipeline

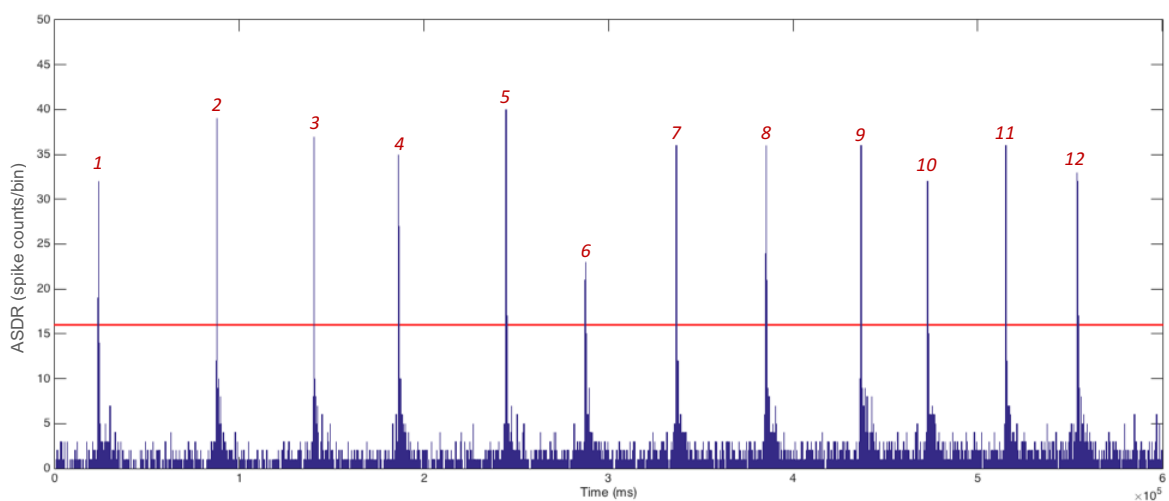
MAP intervals. To ensure that these were not included in analysis, 'true' MAP intervals had to have a value of > 4000 ms. The overall average MAP interval for each array was then calculated as $Avg\ MAP\ interval = median(MAP\ interval_1, \dots, MAP\ interval_n)$, (see figure 3.6C).

3. Development of an MEA analysis pipeline

A

Bin N° (200 ms width)	Spike counts									
	<u>1</u>	<u>2</u>	<u>3</u>	<u>4</u>	<u>5</u>	<u>6</u>	<u>7</u>	<u>8</u>	<u>9</u>	<u>10</u>
Electrode 12	0	0	3	5	6	3	2	0	0	0
Electrode 23	0	0	0	0	0	0	0	0	0	0
Electrode 45	0	0	1	0	0	0	1	1	0	0
Electrode 64	0	0	2	0	1	2	1	0	1	1
Electrode 82	1	0	1	0	1	0	1	2	1	2
Bin total (ASDR)	1	0	7	5	8	5	5	3	2	3

B



C

ASDR Peak	1	2	3	4	5	6	Median MAP Interval = 45800
Interval (ms)	N/A	23800	64000	52600	45800	58200	
ASDR Peak	7	8	9	10	11	12	
Interval (ms)	42600	49200	51000	36000	42400	38600	

Figure 3.6 - Calculation of array wide spike detection rates (ASDRs) for the analysis of network activity in MEA neuronal cultures. ASDRs are calculated by first counting the number of spikes detected in each 200 ms bin in each electrode analysed. The total summed spikes across all electrodes is the ASDR for that bin (**A**). ASDR plots show the total number of culture wide spikes per bin plotted serially across the length of the recording (**B**). Synchronised culture-wide activity is characterised by ASDR peaks (More Active periods; MAPs) and troughs (Less Active Periods; LAPs), which highlights the slow cyclic nature of the firing. The intervals between the peaks (red numbers in **B**) are calculated and the median value represents the average MAP interval for that array (**C**). **A** shows a representative calculation of ASDRs for the first 10 bins (2 seconds in total) across 5 electrodes. **B** shows a complete ASDR plot for a culture of iPS cell derived neurons showing coordinated firing. The red line shows the threshold, above which MAPs are determined and is calculated as 40% of the maximum number of spikes seen in an individual bin. **C** shows the calculation of the average (median) MAP interval for the culture shown in **B**.

3.3.7 Wave feature extraction and clustering

For some of the experiments presented in Chapter 6, spike waveforms were isolated and subsequently compared between different cell lines. To allow the analysis of different sub-populations of spike shapes within a bigger population, features were extracted from spike waveforms and subsequently clustered into distinct groups.

Several approaches are available for the extraction of feature information from spike shapes including using the maximum spike amplitude, spike width, ratio of amplitude:width (Lewicki, 1998) and wavelet transformation of the waveforms (Takekawa *et al.*, 2010; Quian Quiroga *et al.*, 2004). Here, it was decided to use principle component analysis (PCA) which provides both feature extraction and data dimension reduction. This was chosen as it provided a relatively powerful method of feature extraction which was simple enough to integrate into the existing parts of the pipeline and provided output values that could be inputted into clustering algorithms without further manipulation. PCA was performed on the standard voltage (amplitude) data for the spike waveforms. While transformations of this data have also been used in similar approaches (e.g. using the first or second derivatives of the waveform), these data manipulations here did not improve feature separation.

Plotting of the first two principle components from the waveform PCA data provided an idea about the number of groups, if any, that the data could be clustered into. Figure 3.7A shows some representative PCA data of a population of spike shapes containing three clear sub-populations as described by the first two principle components (coloured ovals show manual identification of clusters). Two different algorithms were then tested to compare their ability to cluster such data: k-means clustering is a supervised learning algorithm based upon the clustering of data about defined centre (Kanungo *et al.*, 2002); DBSCAN is a density based clustering tool based upon the grouping of data in terms of the density of nearby neighbourhoods (Schubert *et al.*, 2017).

K-means clustering was performed on the PCA data using the built in function in Matlab. Figure 3.7B shows the results of the 'best' achieved k-means clustering, using cityblock distance calculations, a cluster number of 3 and 10 replications. While cluster 2 (blue) corresponds OK with the leftmost group (red) seen in 3.7A, it was unable to detect the small green cluster in A

3. Development of an MEA analysis pipeline

and instead split the large blue cluster in A between two different groups. Figure 3.7B highlights well some of the limitations of k-means clustering: because the number of clusters into which the data is being grouped is a key part of the algorithm (and therefore needs to be known *a priori*), data is 'forced' into a cluster despite the fact it may not logically belong and furthermore, there is no concept of 'noise' such that *all* data points are clustered one way or another; the algorithm also often struggles, as here, when clusters are of different shapes, sizes and do not have discreet borders.

To help overcome these issues, DBSCAN clustering was performed on the same PCA data. DBSCAN clustering was achieved using a plugin containing an implementation of DBSCAN developed for Matlab (Kalami Heris, 2015). Figure 3.7C shows the results of the 'best' DBSCAN clustering achieved, with an $\epsilon = 40$ and min points = 250. This clustering method performed much better than k-means, identifying well the three manually identified clusters in 3.7A. Furthermore, one of the primary benefits of DBSCAN is its handling of data points which do not fit its clusters, identifying them instead as un-clustered 'noise'.

Based on its superior performance grouping this type of data, clustering was therefore performed in the project (Chapter 6) using DBSCAN. It should be noted however that one of the disadvantages of DBSCAN (and an advantage of k-means) is its high computational workload and processing time, which increases dramatically with larger datasets. Furthermore, unlike k-means clustering, DBSCAN cannot be implemented with parallel processing, again increasing the calculation times.

3. Development of an MEA analysis pipeline

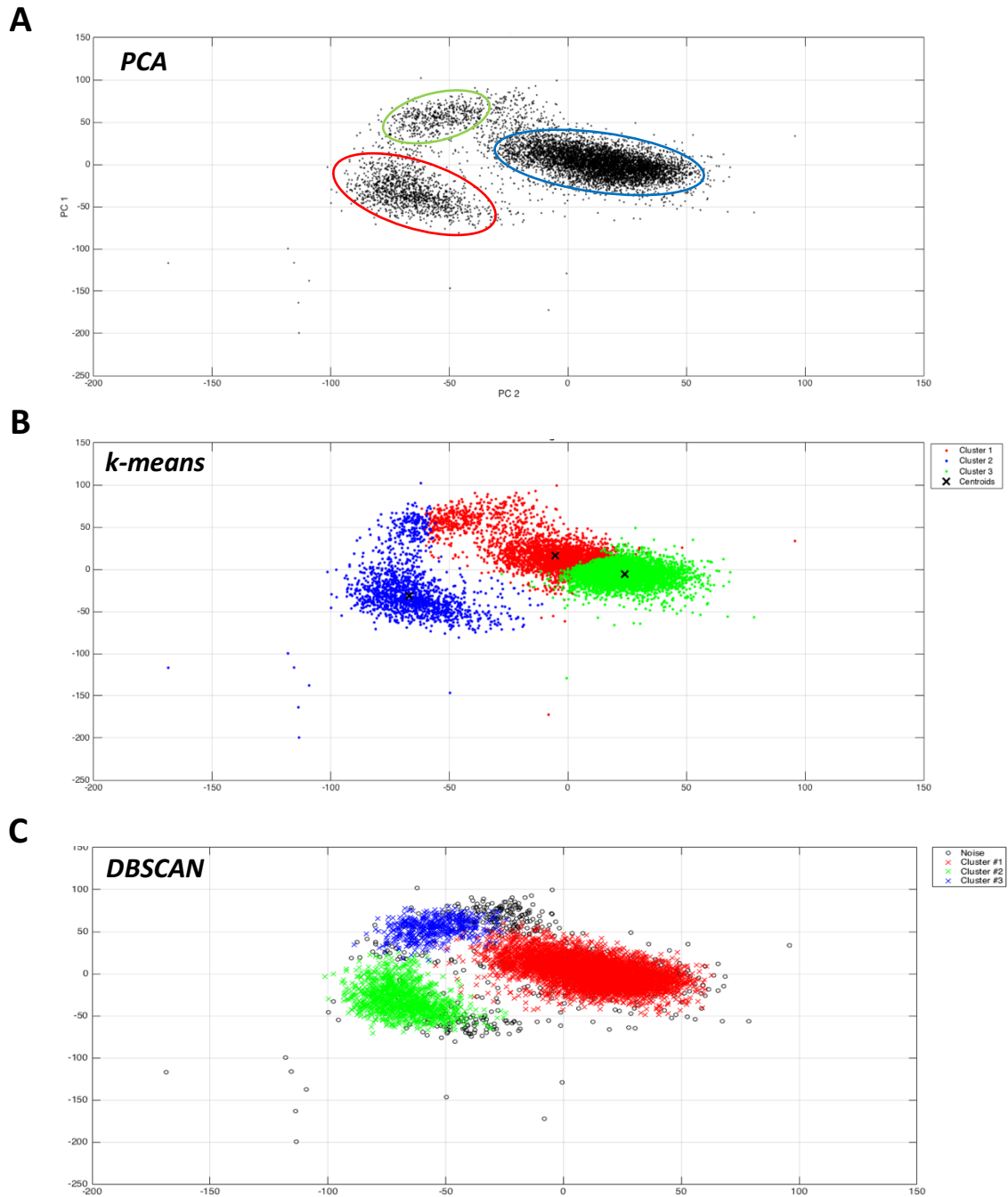


Figure 3.7 - Principle components analysis and clustering of spike waveform data. Feature extraction and dimension reduction was firstly achieved with principle component analysis (PCA). The plotting of the first 2 principle components allowed the visualisation of feature distribution and the manual highlighting of clusters (A). k-means clustering of the PCA data did not successfully identify the three highlighted clusters (B). Clustering was achieved using cityblock distance measurements and 10 replications. DBSCAN clustering performed much more efficiently, clustering the data broadly into the three groups manually identified (C). DBSCAN clustering was achieved with $\epsilon = 40$ and minpoints = 250.

3.4 Summary

This chapter has presented a set of computation tools for the analysis of MEA data which have been specifically designed for use with extracellular recordings of iPS cell derived neurons. While perhaps not as comprehensive as pre-existing packages, this toolset performs a step-by-step analysis of data in a way which is hopefully clear and intuitive for users who are less experienced both with the computational aspects of the procedures and the methodology used at each each step. Moreover, because this toolset has been developed in parallel with MEA culturing and recording of iPS cell derived neurons and has been optimised for the analysis of such cells, it should allow a greater understanding about the nature of these neurons throughout their development. The toolset focuses on the calculation of two key groups of outcome measures, those based upon general excitability at the level of individual units (Avg spike rate, Avg ISI, detected bursts etc.) and those based upon the activity of the cultures when exhibiting network driven behaviours (Max ASDR, Avg MAP interval). While the general excitability measures are relatively standard, the additional controls and adjustments implemented here should provide statistics which are more representative of the activity of cultures and allow reliable comparisons both within and between experiments. Compared to other methods of network analysis (e.g. correlation analyses, coherence etc.) the network statistics produced here are relative simple. However, they should provide a clear and intuitive method of quantifying changes in any such network behaviour, especially when tracking MEA cultures throughout their development.

4. Optimising culturing conditions to improve the physiological maturity of hPS cell - derived neurons

4.1 Introduction

Protocols for the differentiation of human pluripotent stem cells (hPS cells) into neurons have improved immeasurably over the last 10 years, such that reliable and repeatable procedures now exist for the formation of numerous specific neuronal types including glutamatergic (Shi *et al.*, 2012a), GABAergic (Maroof *et al.*, 2013), cholinergic (Hu *et al.*, 2016) and dopaminergic (Kwon *et al.*, 2014) neurons. For understandable reasons, the primary focus of such approaches has been on the homogeneity of cultures and the production of purer populations of neuronal types with increasing efficiency and speed. For example, in general protocols for differentiating neurons from hPS cells are long - often in the order of several months – which may introduce practical limitations in terms of the productivity associated with such experiments. Moreover, the efficiency of early protocols could be relatively poor and variable, especially between different stem cell lines. Consequently, in the years since the first presentation of a standard method of neural differentiation (e.g. Chambers *et al.*, 2009), a number of studies have reported optimised protocols aimed at speeding up the differentiation process and increasing neuron yield (Zhang *et al.*, 2013; Shi *et al.*, 2012b).

Until more recently, the physiological maturity of the neurons produced using such differentiation protocols has perhaps been of lower priority. Although most studies carry out investigations regarding the maturity of neurons, this is often primarily determined by the expression of certain proteins, for example which mark neuron ‘maturity’ (MAP2, NEUN etc.) or the development of functional synapses (PSD-95, Synaptophysin etc.). Assessing the functional maturity of hPS cell derived neurons is important however as these cells have been repeatedly shown to be immature by several physiological measures, including resting membrane potentials (V_{rest}) and the formation of spontaneous action potentials. Moreover, investigating the

4. Optimising culturing conditions of hPS cell derived neurons

function of developing hPS cell derived neurons plays a key part of increasing our understanding about their use as a model system, especially with regards to modelling neurodevelopmental diseases and developing potential therapies.

Recently a number of studies have described differentiation protocols which have produced iPS cell derived neurons with often impressive improvements in a number of physiological measures (Bardy *et al.*, 2015; Telezhkin *et al.*, 2016). However, these protocols either require the use of multiple small molecule supplements or non-standard medium which may not be appropriate in certain circumstances. Over a number of years, a body of evidence has shown that the use of astrocytes either in co-culture with neurons, or to pre-condition differentiation medium can enhance the maturity of neurons, with particular improvements in functional synapse formation (Elmariah *et al.*, 2005; Kucukdereli *et al.*, 2011; Allen *et al.*, 2012; Rushton *et al.*, 2013). Moreover, several studies have also shown that maintaining neuronal cultures in incubators with hypoxic atmospheres improves the survival and growth of rodent and hPS cell derived neural precursors (Bilican *et al.*, 2014; Struder *et al.*, 2000; Liu *et al.*, 2009). Together, these relatively simple physiological modifications provide an opportunity to increase the functional maturity of neurons without large changes to differentiation protocols.

The overall goal of this project is to develop a reliable platform for the analysis of neural network function using extracellular recordings via MEAs. A key prerequisite of the neurons to be studied therefore is that they are sufficiently mature as to form functional synapses and show spontaneous action potentials. Preliminary patch-clamping experiments of iPS cell derived neurons using the dual-SMAD inhibition based protocol described in Chapter 2 showed that even after an extended differentiation period (>80 days), neurons were functionally immature by several measures, including polarised resting membrane potentials (V_m), high input resistance (R_i), low numbers of induced action potentials (current-induced action potentials; iAPs) and, importantly, very few spontaneous action potentials. In light of these preliminary studies and evidence in the recent literature, it was decided to study the optimisation of the differentiation protocol with a primary aim of increasing the functional maturity of iPS cell neurons, with a view to aiding the development of the MEA-based analysis platform. In order to permit minimal changes to the protocol and to allow relatively seamless integration with MEA culturing, it was decided to adapt and develop the current protocol based upon culturing neurons with medium pre-conditioned by human astrocytes and maintaining cells in hypoxic incubator conditions.

4. Optimising culturing conditions of hPS cell derived neurons

4.2 Chapter Aims

This study combines the two physiological conditions described above as experimental variables to the standard differentiation protocol used in the group for the production of glutamatergic forebrain neurons. The aim of the study is to assess the effect of human astrocyte conditioned differentiation media and hypoxic incubator conditions on the functional maturity of hPS cell derived neurons. This will primarily be assessed by single – cell patch clamping of cells at different points throughout development to study intrinsic passive properties and both induced and spontaneous excitability.

4. Optimising culturing conditions of hPS cell derived neurons

4.3 Results

In this chapter, forebrain cortical neurons were produced using the protocol described in chapter 2 within the following experimental groups: For *ACM/2%* conditions, neurons were switched to 1:1 ACM/fresh N2B27 medium and were transferred to an incubator maintained at 37°C with 5% CO₂ and 2% O₂ at D20-22, 2 days after the second passage. They were cultured in these conditions until the end of the experiments. For *standard* conditions, cells were maintained in standard N2B27 and incubated at 37°C in 5% CO₂ and 95% air.

4.3.1 Intrinsic electrophysiological properties of neurons

Neurons cultured in both the standard and *ACM/2%* conditions for these experiments were patched at 30 and 50DPP as described in Chapter 2. Figure 4.1 shows a representative selection of the patched cells, visualised by filling cells with Alexa Flour 594.

Resting membrane potentials. Neuron resting membrane potentials (V_{rest}) provide a good initial measure in determining the relative maturity of developing cells: As neurons mature, V_{rest} becomes more polarised as more channels and transporters are expressed in line with the cells development. Here, it was first determined that there was a clear and significant variation of the V_{rest} of neurons both in terms of experimental conditions and developmental time point (Figure 4.2A&B; see table 3.1 for statistics). In standard culturing conditions there was no change in the median V_{rest} of neurons cultured in standard conditions between 30DPP (-25 mV, CI[-28.8, -20.43]) and 50DPP (-26.65 mV, CI[-30.7, -22.8]). However, there was a significant decrease in V_{rest} between the time points in the *ACM/2%* neurons, from median of -30.62 mV CI[-36.52, -26.55] to -39.5 mV CI[-43, -37]. Looking within the time points, while cells cultured in *ACM/2%* conditions and patched at 30DPP had hyper-polarised V_{rest} compared to control conditions, this difference was not significant. By 50DPP however, the V_{rest} in *ACM/2%* neurons was significantly decreased compared to control conditions (see Table 3.1). The cumulative probability distributions in Figure 4.2B highlight the changes in recorded V_{rest} over both development and between the experimental conditions. It can be seen that at both time points

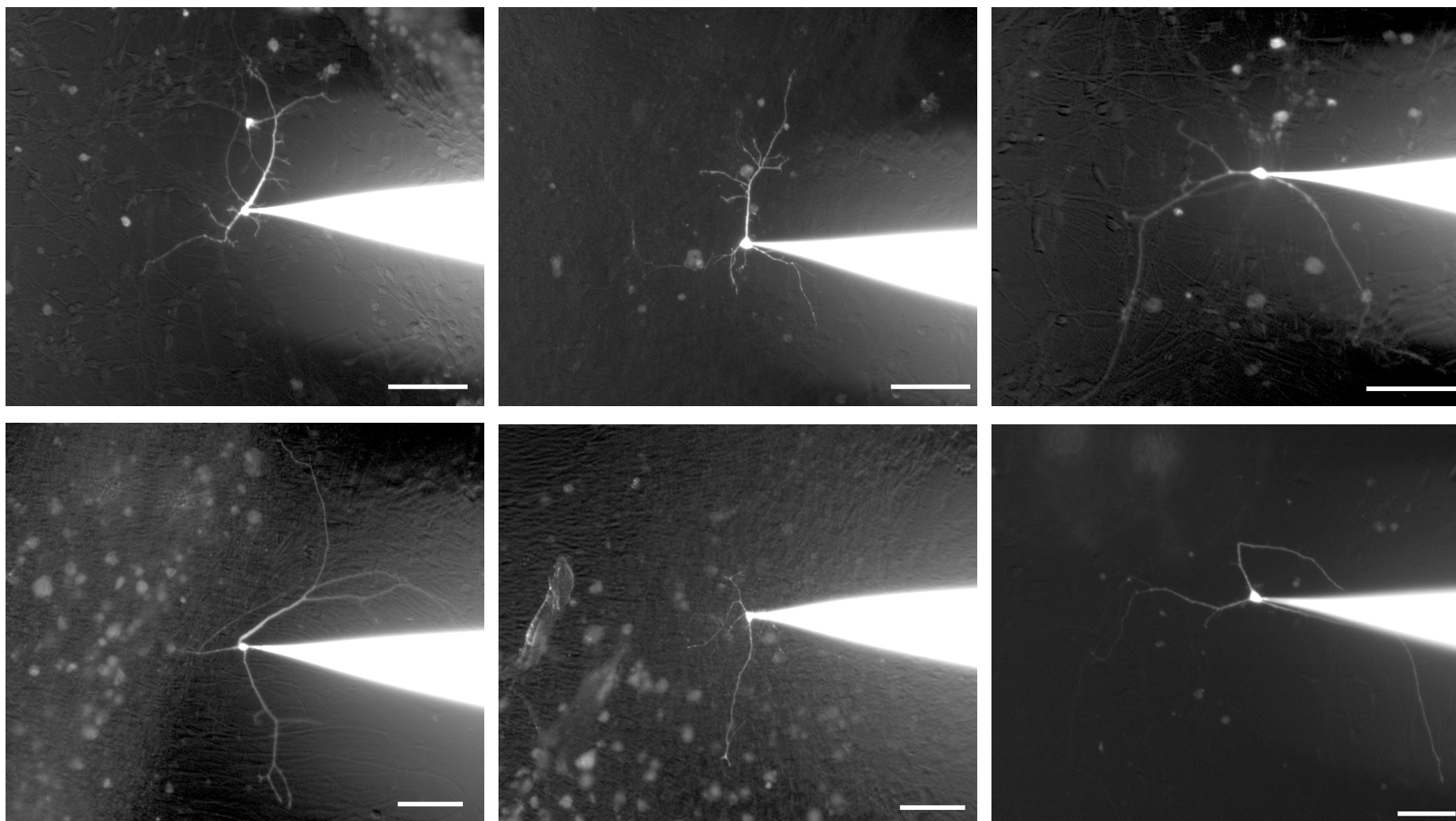


Figure 4.1 – Representative images of iPSC derived cortical neurons patched in this study. Patched neurons were filled with 10mM Alexa Fluor 594 within the internal solution. Fluorescent images were taken using a Q-Imaging Rolera Bolt camera mounted to an Olympus BX51 WI microscope, using an Olympus 10X water immersion objective, with light provided by a CoolLED pE-2 LED system. Captured images were processed with Q-Capture Pro 7 (Q-Imaging) and Fiji. The images presented here are all taken from cultures patched at 50DPP in either Standard or ACM/2% conditions. Scale bars show 100 μ m.

4. Optimising culturing conditions of hPS cell derived neurons

the distribution of V_{rest} in the ACM/2% conditions are shifted towards more hyper-polarised values. In fact this also shows that for the most part, V_{rest} values are lower in the ACM/2% conditions at 30DPP compared to standard conditions at 50DPP. Finally, Figure 4.2B highlights that the neurons recorded at 50DPP in the ACM/2% conditions clearly represent the most functionally mature cells in terms of V_{rest} .

Input Resistance. A second key intrinsic property of neurons, input resistance (R_i) describes the voltage change recorded in a neuron when injected with a known low current-step. A high input resistance implies fewer, closed ion channels while a low input resistance implies more open ion channels and as such, R_i is expected to decrease throughout development as neurons express more functional channels. Here, it was first noticeable that calculated R_i values were highly variable within each's groups population. This was especially the case at 30DPP where the means \pm SD were $2.342 \text{ G}\Omega \pm 1.122$ and $2.524 \text{ G}\Omega \pm 1.34$ for the Std and ACM/2% groups respectively (Figure 4.2C). Perhaps surprisingly given this intra-group variability, a one way ordinary ANOVA of all groups showed that there was significant variation between the population means over time and between the conditions (see Table 3.1). Post-hoc Tukey's multiple comparisons revealed that the only significant difference was between day 30DPP and 50DPP within the ACM/2% group. There were no differences seen between experimental group at either time point. The cumulative probability distributions in Figure 4.2D highlight that only neurons recorded at 50DPP in the ACM/2% conditions had R_i values shifted lower compared to the other three groups.

Membrane time constant. The final passive neuron property analysed here is that of the membrane time constant (τ or τ), which describes the rate at which a neuron returns to a steady resting membrane state after a receiving a current input. It serves as a measure of neuron maturity as, in a similar way to R_i , τ is anticipated to decrease over neuron development due to greater expression of functional channels and transmembrane transporters. In this study, as with R_i , the observed values of τ within each of the four groups were variable. Again this was especially noted at 30DPP where the mean $\tau \pm$ SD was $91.76 \text{ ms} \pm 46.33$ and $95 \text{ ms} \pm 54.15$ for the Std and ACM/2% groups respectively (Figure 4.2E). It was also clear that both in terms of development and between experimental groups that there was little change in the average τ values recorded. Indeed, an ordinary one-way ANOVA of all four groups

4. Optimising culturing conditions of hPS cell derived neurons

confirmed that there was no difference between the distributions (Table 3.1). As with V_{rest} and R_i , it was the neurons recorded at 50DPP in the ACM/2% conditions which showed the most mature phenotype, with an average tau of $74.44 \text{ ms} \pm 37.35$. However, as can be seen in Figure 4.2F, there was no clear separation of the cumulative probability distributions for this group as was observed for the other intrinsic properties.

Finally, to gain further understanding about the nature of the passive properties of these neurons, current-voltage (I-V) curves were calculated for each patched cell. These report the voltage change of the neuron in response to increasing steps of current, beginning with negative current injections and provide a good overview of the cells passive properties with regards to neuron maturity (Figure 4.3A). Here, at both 30 and 50DPP, patched neurons exhibited linear I-V responses, especially with negative current injections (Figure 4.3B&C). At both time points, there is a plateauing of the voltage response with more positive current injections. No differences were observed in the I-V curves between the cells cultured in standard and ACM/2% conditions recorded at either time points, or between the same experimental group at each time point.

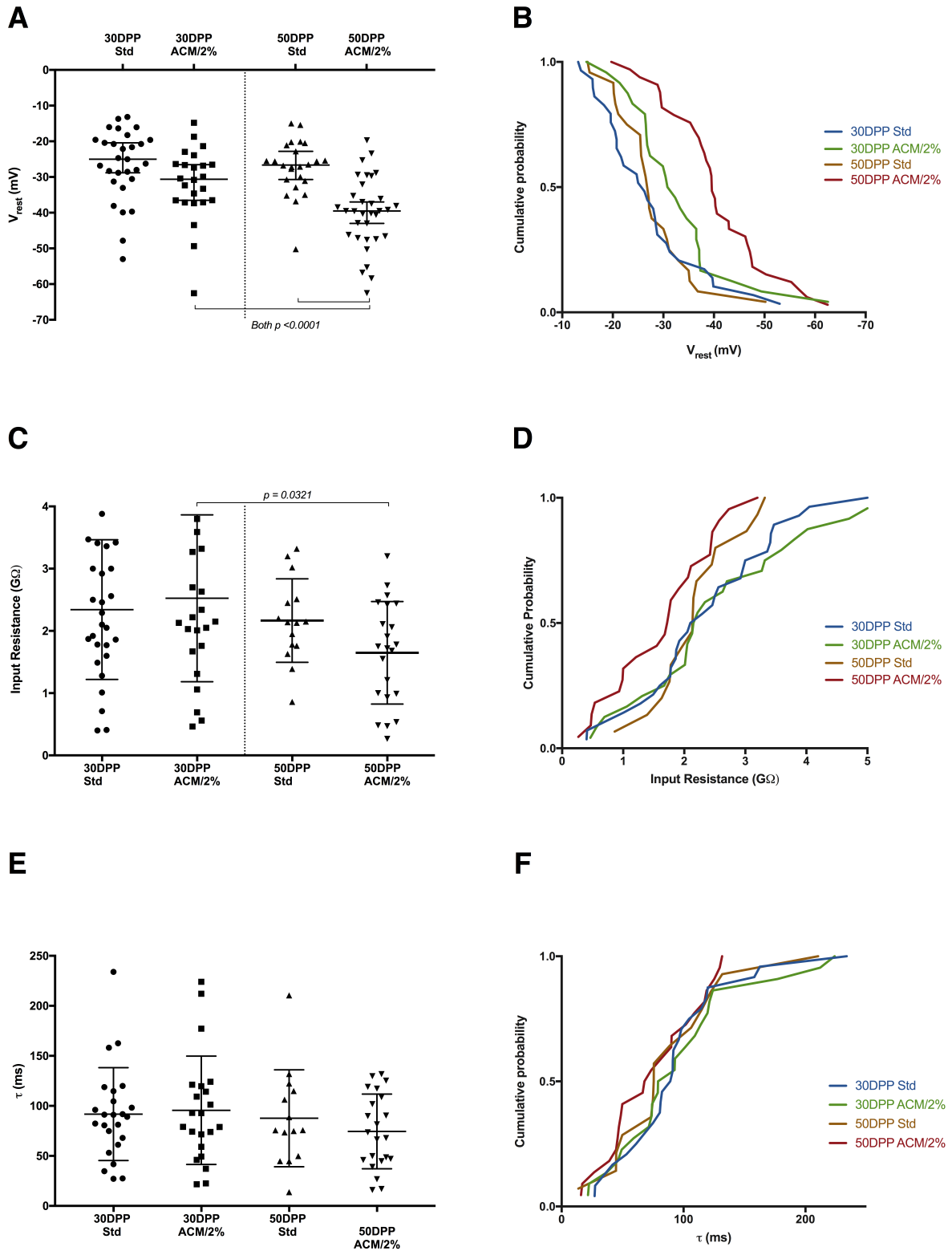
Overall these results show that the ACM/2% conditions generally have a positive effect on the intrinsic properties of iPS cell derived neurons. In particular, the conditions induced a hyperpolarising shift in the V_{rest} of neurons compared to standard conditions at both 30 and 50DPP. Moreover, while there was no change in the V_{rest} over development in the standard conditions, in ACM2% conditions V_{rest} significantly decreased between the time points, suggesting that the conditions aid the functional maturation of the neurons. ACM/2% conditions had more limited effects on R_i and tau, two properties linked strongly to the integrity of the cell membrane and the expression of functional ion channels.

4. Optimising culturing conditions of hPS cell derived neurons

Table 4.1 – Summaries of statistics for the comparisons of intrinsic electrophysiological properties between neurons cultured in standard and ACM/2% conditions.

Resting membrane potential (mV)			
	Kruskal – Wallis test	Dunn’s multiple comparisons	
		Mean rank difference	Adjusted p value
30DPP Std vs 50DPP Std	$H_{(3)} = 31.37$, $p < 0.0001$	2.49	>0.9999
30DPP ACM/2% vs 50DPP ACM/2%		40.69	< 0.0001
30DPP Std vs 30DPP ACM/2%		16.95	0.3251
50DPP Std vs 50DPP ACM/2%		38.2	< 0.0001
Input resistance (GΩ)			
	One-way ANOVA	Tukey’s multiple comparisons	
		Difference in means [CIs]	Adjusted p value
30DPP Std vs 50DPP Std	$F_{(3,85)} = 2.892$, $R^2 = 0.0926$, $p = 0.04$	0.1758 [-0.714 – 1.066]	0.9263
30DPP ACM/2% vs 50DPP ACM/2%		0.8755 [0.054 – 1.697]	0.0321
30DPP Std vs 30DPP ACM/2%		-0.1823 [0.956 – 0.592]	0.9547
50DPP Std vs 50DPP ACM/2%		0.5175 [-0.414 – 1.449]	0.4688
Membrane time constant (ms)			
	One-way ANOVA	Tukey’s multiple comparisons	
		Difference in means [CIs]	Adjusted p value
30DPP Std vs 50DPP Std	$F_{(3,78)} = 0.323$, $R^2 = 0.0318$, $p = 0.809$	No post – hoc comparisons	
30DPP ACM/2% vs 50DPP ACM/2%			
30DPP Std vs 30DPP ACM/2%			
50DPP Std vs 50DPP ACM/2%			

4. Optimising culturing conditions of hPS cell derived neurons



4. Optimising culturing conditions of hPS cell derived neurons

Figure 4.2 - Intrinsic properties of iPS cell derived neurons cultured in standard and ACM/2% conditions recorded at 30 and 50 days post plating (DPP). iPS cell derived neurons were patched at two time points to assess changes in intrinsic cell properties over development and between neurons cultured in standard conditions and those cultured with astrocyte conditioned medium (ACM) and in a hypoxic (2%) incubator environment. **A** shows individual data points together with medians \pm 95% confidence intervals. **C** and **E** show individual data together with means \pm SD. **B**, **D** and **F** show the cumulative probability distributions of the four populations for each property. The resting membrane potential (V_{rest}) of neurons cultured in ACM/2% conditions was significantly lower at 50DPP than neurons in standard conditions. There was no effect on input resistance or membrane time constant (τ or tau) from culturing conditions. p values are result of post-hoc multiple comparison tests following ordinary or nonparametric one way ANOVA. n = 28 (30DPP Std), 25 (30DPP ACM/2%), 19 (50DPP Std) and 23 (50DPP ACM/2%) across 3 differentiations.

4. Optimising culturing conditions of hPS cell derived neurons

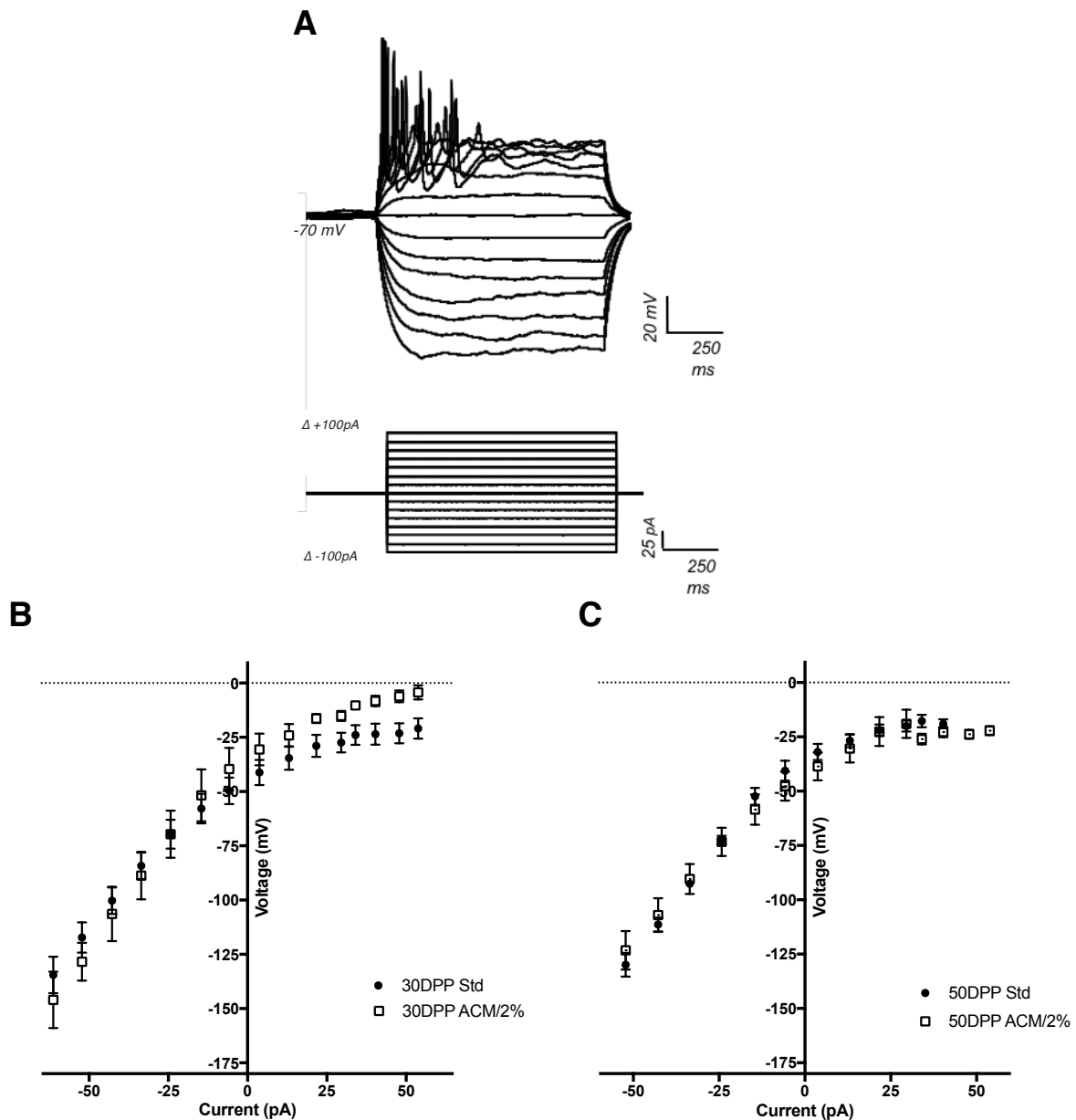


Figure 4.3 – Current-Voltage relationships of iPS cell derived neurons cultured in standard and ACM/2% conditions patched at 30 and 50 Days Post Plating (DPP). 1 second pulses were injected into cells being held at around -70 mV. Initial pulses ranged between -50 and -100 pA with subsequent pulses increases by around 5-20 pA, both depending on the input resistance of the cell. 15 sweeps were performed in total for each cell (A). There was no difference in the shape of the average I-V profile between neurons cultured in standard conditions or those in ACM/2% conditions at either 30DPP (B) or 50DPP (C). Indeed, in all four groups the average profile was generally linear until around +20 pA. Each point in B and C represents the mean voltage response seen across all cells in that group. Bars show ±S.E.M. The average current step for each time point was calculated as the mean of the 15 individual steps for each cell. n = 28 (30DPP Std), 25 (30DPP ACM/2%), 19 (50DPP Std) and 23 (50DPP ACM/2%) across 3 differentiations.

4. Optimising culturing conditions of hPS cell derived neurons

4.3.2 Cell classification by induced action potentials

The intrinsic properties of neurons are closely linked to the function of the cell, in particular to the ability of developing neurons to produce action potentials when injected with increasing steps of current (induced action potentials, iAPs). The classification of neurons based upon their iAP state is a useful measure in determining general cell excitability and is a simple but clear marker of maturity at the time of recording. To compare the iAP state of neurons in standard and ACM/2 conditions, cells were categorised into five groups based on their ability to produce iAPs, ranging from none to trains of APs (Figure 4.4A). Criteria for iAP classification is described in Chapter 2. Due to the fact that the V_{rest} of many of the cells was above the threshold for iAP initiation, all cells were held at ~ -70 mV during these recordings.

55.17% of neurons cultured in standard conditions and patched at 30DPP were classed as active, which included showing single APs (27.59%), single with train attempts (13.79%) and full AP trains (13.79%; Figure 4.4B). At the same time point, ACM/2% neurons were much more excitable, with 79.16% classed as active and a greatly increased 37.50% showing full AP trains. This trend was also seen with cells patched at 50DPP, as 62.96% of cells were active in the standard conditions compared to 83.88% in ACM/2%. At both time points there was a noticeable increase in the number of ACM/2% neurons showing trains of iAPs compared to standard conditions (23.71% and 14.81% increases at 30DPP and 50DPP respectively). Interestingly, changes within the same experimental group between the two time points were less pronounced. Within the standard conditions group, there was a small increase in all three active classes, leading to a 7.79% increase in the number of active cells. Within the ACM/2% group, while there was also a small (4.72%) increase in the total number of active cells (driven by an increase in single AP and single-attempted cells), there was a small decrease in the number of cells showing AP trains and an increase in the number of cells which showed no activity.

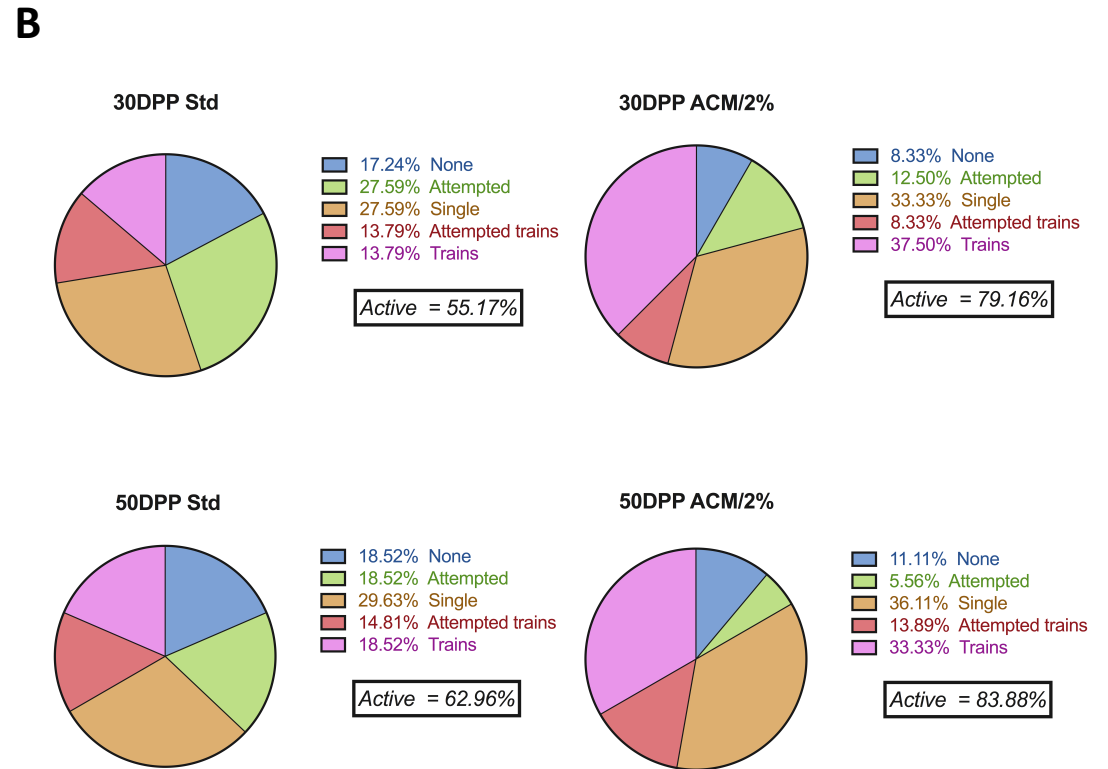
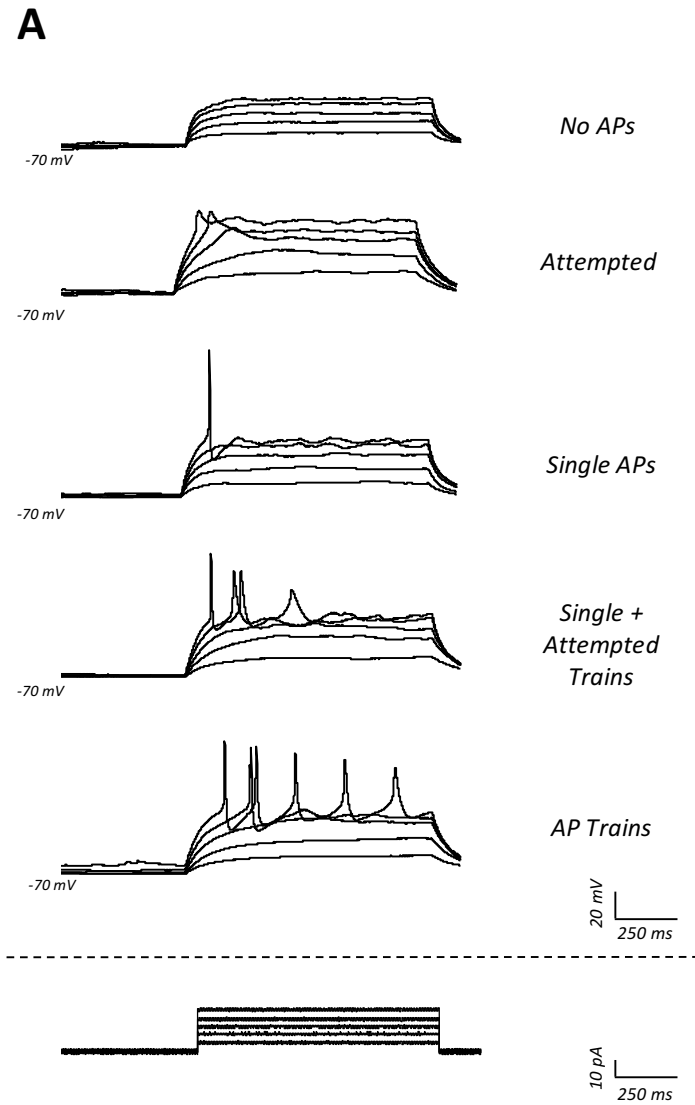


Figure 4.4 – Classification of iPS cell derived neurons in standard and ACM/2% differentiation conditions by induced action potential (iAP) state. Neurons were held at ~ -70 mV and injected with $\Delta+5$ pA current steps. Cells were classified according to five states of iAP observed (A). Full iAPs (including within trains) had to reach 0 mV or were deemed attempted. Neurons cultured in ACM/2% conditions were more active at both 30DPP and 50DPP time points, with more cells showing single iAP, attempted trains or trains of iAP. Neurons were also more active at 50DPP compared to their same-condition counterparts at 30DPP. The boxed 'Active' percentage refers to the total of these three states (B). n = 28 (30DPP Std), 25 (30DPP ACM/2%), 19 (50DPP Std) and 23 (50DPP ACM/2%); across 3 differentiations.

4. Optimising culturing conditions of hPS cell derived neurons

4.3.3 Intrinsic properties grouped by AP classification

The results presented so far in this section provide some evidence that the ACM/2% culturing conditions improve the functional maturity of differentiated neurons. However, they have also shown that a high degree of variability exists within the cell populations, especially with regards to the intrinsic properties R_i and τ . To investigate more fully the relationship between the three intrinsic properties and action potential formation, and to allow a greater understanding about the physiological nature of these neurons, intrinsic property results from both time points and experimental conditions were pooled and subsequently re-grouped according to the iAP classification described in section 4.3.2.

Resting membrane potential. The pooled values for V_{rest} from all recorded cells across each experimental group at both 30DPP and 50DPP were re-categorised according to the iAP classification of the neuron from which they came (Figure 4.5A). This analysis showed clearly that active neurons (i.e. showed at least single iAPs) had hyperpolarised V_{rest} compared to inactive neurons (No iAPs and attempted iAPs), with the mean V_{rest} for inactive cells $-21.85 \text{ mV} \pm 5.75$ compared to -31.57 mV for those grouped in the three active classifications. Following one-way ANOVA, Tukey's post-hoc multiple comparisons revealed that the mean values for each of the active groups were significantly hyperpolarised compared to that of both of the inactive classifications (six significant comparisons in total; see Table 3.2). Interestingly, there was no differences observed between the average V_{rest} of the three active groups, although with a mean of $-35.2 \pm 6.60 \text{ mV}$, neurons producing trains of iAPs had the most 'mature' phenotype of all classification groups.

Input resistance and tau. It was unsurprising that when pooled R_i values were re-grouped according to iAP class, each category showed a large amount of variation, similar to that seen in the time point/condition analysis (Figure 4.5B). Importantly, there were no differences in the mean R_i values of active neurons compared with those classed as inactive ($2.35 \text{ G}\Omega \pm 1.27$ for two inactive classes; $2.16 \text{ G}\Omega \pm 1.01$ for three active classes), which was confirmed by one-way ANOVA. It was interesting to note that unlike V_{rest} , the cell classification with the most mature phenotype was not those producing iAP trains but those showing single iAPs (mean = $1.72 \pm 0.81 \text{ G}\Omega$). A very similar pattern was seen when the pooled observations for τ were re-

4. Optimising culturing conditions of hPS cell derived neurons

grouped according to neuron classification (Figure 4.5C). Again, the intra-group variance was high and there was little change in the mean value of tau between the five cell classifications, confirmed by one-way ANOVA (Table 3.2). However, similarly to R_i , the cell classification group with the most mature phenotype was neurons showing single iAPs, with a mean value of 67.25 ± 35.71 ms).

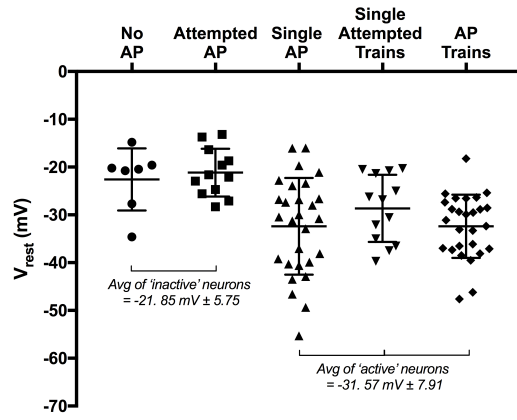
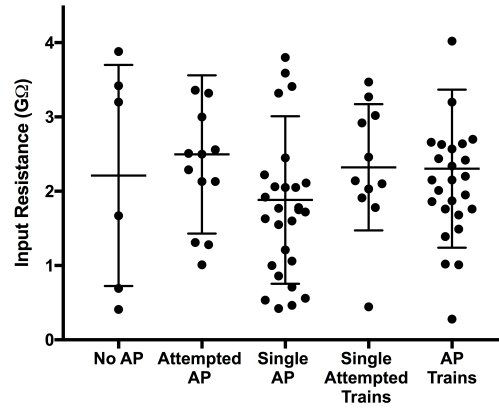
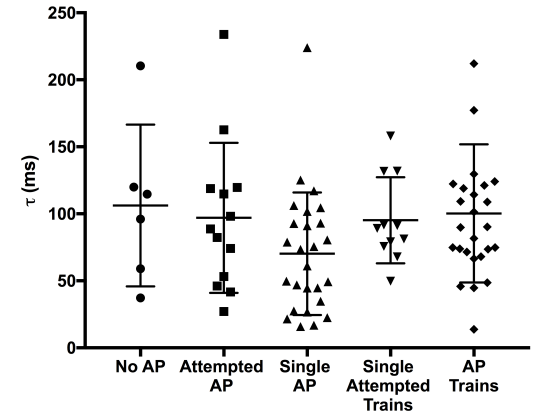
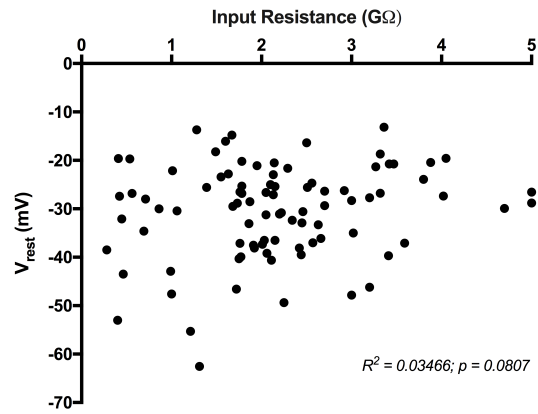
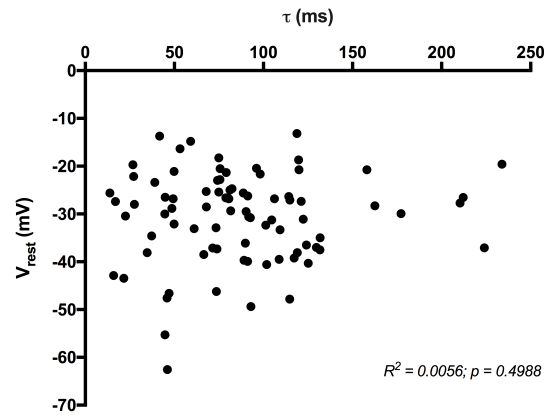
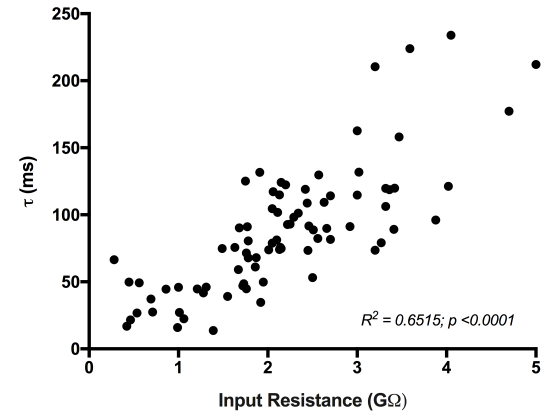
The three intrinsic properties analysed here were chosen partly based on the assumption that they would be good markers of neuron maturity and would therefore show a degree of change either in terms of experimental condition, developmental time point or indeed the iAP ability of a specific neuron. However, the results presented above suggest that, in this study, only V_{rest} is a reliable marker of neuronal function and therefore maturity. Moreover, these results suggest that the three measures do not represent co-ordinated read outs of cell maturity in these neurons – i.e. hyperpolarising V_{rest} is not necessarily linked to a reduction in R_i or increase in tau. To test these associations, each intrinsic property of every patched cell was correlated with its respective other two parameters (Figure 4.5D-E). This analysis, showed that, as was suggested by the results in figure 4.5A-C, values of neuron V_{rest} do not correlate with the R_i (Pearson's correlation; $R^2 = 0.03466$, $p = 0.0807$; figure 4.5D) or tau ($R^2 = 0.0056$, $p = 0.4988$; figure 4.5E). Unsurprisingly given both their reliance on membrane properties, individual neurons R_i and tau values correlated very strongly ($R^2 = 0.6515$, $p < 0.0001$; figure 4.5F).

Overall the results presented so far suggest that the ACM/2% conditions do improve the functional maturity of iPS cell derived neurons as shown in an increase in the number of patched cells showing iAP formation. This appears to be primarily driven by a reduction in V_{rest} , which is the only intrinsic property clearly associated with increased iAP firing. Furthermore, decreased V_{rest} does not appear to be associated with either decreasing R_i or increasing tau, suggesting that these intrinsic measures are not necessarily linked in development and represent different aspects of neuron maturity. To investigate further the role of ACM/2% conditions on neuron maturity, cells were next analysed for any changes to the properties of the action potential produced.

4. Optimising culturing conditions of hPS cell derived neurons

Table 4.2 – Summaries of statistics for the comparisons of intrinsic electrophysiological properties of neurons classified by iAP state.

Resting membrane potential (mV)			
	One way ANOVA	Tukey's multiple comparisons	
		<i>Difference in means [CIs]</i>	<i>Adjusted p value</i>
No AP vs Single AP	$F_{(4,82)} = 6.702$, $R^2 = 0.246$, $p = 0.0001$	9.8 [0.5848 – 19.02]	0.0314
No AP vs Single – attempted		6.06 [-4.166 – 16.28]	0.0460
No AP vs AP trains		9.81 [0.562 – 19.06]	0.0320
Attempted vs Single AP		11.23 [3.701 – 18.75]	0.0007
Attempted vs Single - attempted		7.482 [-1.278 – 16.21]	0.0128
Attempted vs AP trains		11.24 [3.67 – 18.8]	0.0008
Input resistance (GΩ)			
	One-way ANOVA	Tukey's multiple comparisons	
		<i>Difference in means [CIs]</i>	<i>Adjusted p value</i>
No AP vs Single AP	$F_{(4,82)} = 0.923$, $R^2 = 0.0441$, $p = 0.454$	No post – hoc comparisons	
No AP vs Single – attempted			
No AP vs AP trains			
Attempted vs Single AP			
Attempted vs Single - attempted			
Attempted vs AP trains			
Membrane time constant (ms)			
	One-way ANOVA	Tukey's multiple comparisons	
		<i>Difference in means [CIs]</i>	<i>Adjusted p value</i>
No AP vs Single AP	$F_{(4,82)} = 1.605$, $R^2 = 0.0769$, $p = 0.182$	No post – hoc comparisons	
No AP vs Single – attempted			
No AP vs AP trains			
Attempted vs Single AP			
Attempted vs Single - attempted			
Attempted vs AP trains			

A**B****C****D****E****F**

4. Optimising culturing conditions of hPS cell derived neurons

Figure 4.5 – Intrinsic properties of IPS cell derived neurons in relation to cell classification by induced action potential (iAP) formation and the relationships between individual cell properties. Values of three intrinsic properties of neurons were pooled from standard and ACM/2% cultured neurons at both 30 and 50DPP and subsequently re-grouped according to the AP classification of the neurons from which they came (**A** resting membrane potential, **B** input resistance, **C** membrane time constant). Active neurons (those showing at least single iAP) had hyperpolarised resting membrane potentials compared to inactive cells (**A**), while there was no relationship between cell class and either input resistance or membrane time constant (**B** and **C**). In **D,E** and **F**, all values were pooled into one group and correlated with their respective other properties for each cell. There was no relationship seen between V_{rest} and input resistance or tau but a strong correlation between tau and input resistance (**F**). R^2 and p values correspond to Pearson's correlations.

4. Optimising culturing conditions of hPS cell derived neurons

4.3.4 Action potential analysis

Single action potential events from each neuron patched at 30 and 50DPP in both experimental groups were extracted and analysed to study the role of ACM/2% culturing conditions on 4 key action potential properties: iAP threshold, iAP amplitude, iAP half-width and max rise slope. While there are several measures which can be analysed when looking at single events, these four were chosen here to provide a good overview of the action potential features. Figure 4.6A provides a description of the properties of action potentials analysed here.

Action potential threshold. In line with the V_{rest} of developing neurons, the threshold for AP initiation polarises as the cell matures, although it should be noted that this is not necessarily a linear relationship and can be specific to neuron type. The threshold for iAP initiation was calculated for each cell using the first derivative method described in section 2... and shown in figure 4.6A. In this study, there was little effect of developmental time point on neurons in both standard and ACM/2% conditions on the threshold for iAPs (Figure 4.6B). Moreover, there was no difference in AP threshold between standard and ACM/2% cells at both time points. These findings were confirmed with one-way ANOVA (Table 3.3). However, as with V_{rest} , the neurons with the most hyperpolarised iAP thresholds were those cultured in the ACM/2% conditions and patched at 50DPP, presenting with a mean threshold of -26.32 ± 7.154 mV. The cumulative probability plots shown in Figure 4.6C highlights that there was little change in the distributions across the four groups, although the extended tail of the 50DPP ACM/2% trace shows the presence of some hyperpolarised thresholds within that population.

Action potential amplitude. During neuronal development, the profile of an action potential changes as the cell matures. APs begin smaller (in terms of amplitude) and slower (both in terms of width and the time taken to reach peak maxima) and as an increased number of functional ion channels are expressed on the cell membrane through development, APs become larger, thinner and faster. Here, there was little change to the amplitude of detected iAPs both over development and in response to the ACM/2% culturing conditions (Figure 4.6D), which again was confirmed with one-way ANOVA (Table 3.3). ACM/2% neurons patched at 50DPP again presented with the most developed phenotype. (45.09 ± 7.88 mV).

4. Optimising culturing conditions of hPS cell derived neurons

Action potential half-width. The half-width of an action potential describes the width of the event at the voltage which is half that of its maximum amplitude. It provides a standardised way of measuring how wide any action potential is and used often as a key identifier of the nature of the spikes being produced by a particular neuron, especially in relation to physiological maturity. In this study, the half width of recorded action potentials were effected both by the age of the cells and by the culturing conditions (Figure 4.6E). Firstly, in both the standard and ACM/2% conditions, the half-width of iAPs reduced markedly between patching at 30DPP and 50DPP, falling from 6.36 ± 2.84 ms to 5.09 ± 1.51 ms and 7.53 ± 3.16 to 4.29 ± 1.29 respectively. Following one-away ANOVA, Tukey's multiple comparison showed that both of these changes were significant, highlighting that AP half width appears to be strongly linked to neuron development (Table 3.3). Interestingly, the mean AP half-width of cells in the ACM/2% group at 30DPP was actually significantly wider than those in the standard conditions at the same time point (Table 3.3), suggesting that perhaps the ACM/2% conditions counter the maturation of AP width. Conversely, the mean AP half-width of cells in the ACM/2% conditions at 50DPP was significantly narrower than that in the standard culturing conditions (Table 3.3). It's worth noting that as with a number of the other neuron properties discussed above, the ACM/2% cells patched at 50DPP, with a mean AP half width of 4.29 ± 1.29 ms, presented as the most mature of the four populations.

Max rise slope. The speed at which an AP reaches its peak amplitude is another useful measure in profiling neuron maturity, as it relates to the functional expression of voltage gated ion channels, in particular voltage gated sodium channels which are primarily responsible for the rising phase of an AP. As the velocity the upward phase of an AP is dynamic over time, the maximum velocity of the rising phase is often used as a static measure of this property (herein called 'max rise slope' or MRS). Here, the MRS for detected iAPs followed a similar pattern as that seen for AP half width (figure 4.6F). Firstly, the mean AP MRS seen in both standard and ACM/2% groups at 50DPP was significantly increased compared to their respective groups at 30DPP (Table 3.3). As with AP half-width, there was conflicting results in terms of changes to MRS related to ACM/2% conditions. At 30DPP, the mean AP MRS of neurons in the ACM/2% group was similar compared to those in the standard group, while at 50DPP there was a significant increase in the mean MRS between neurons cultured in ACM/2% and standard conditions (Table 3.3). Finally, with a mean AP MRS of 38.02 ± 11.98 mV ms⁻¹, the neurons

4. Optimising culturing conditions of hPS cell derived neurons

patched at 50DPP in the ACM/2% group again presented as the most mature in terms of this analysis measure.

The results from this section present a mixed picture in terms of the effect of ACM/2% culturing conditions on the properties of iAPs. The conditions had little effect on the iAP threshold or the iAP amplitude at either 30 or 50DPP and these properties were also not effected by the neurons development. However, both the AP half-width and MRS were sensitive to time point, with both measures significantly more mature at 50DPP compared to 30DPP. It was these measures that were also effected by culture conditions, as both half-width and MRS were improved further by ACM/2% conditions at 50DPP. This suggests that these conditions may be having a positive effect only on those aspects of neuron maturity which are natively dynamic in these iPS cell neural differentiations.

Table 4.3 – Summaries of statistics for the comparisons of properties of action potentials produced by neurons cultured in standard and ACM/2% conditions.

Action potential threshold (mV)			
	One way ANOVA	Tukey's multiple comparisons	
		<i>Difference in means [CIs]</i>	<i>Adjusted p value</i>
30DPP Std vs 50DPP Std	$F_{(3,84)} = 1.093$, $R^2=0.0572$, $p = 0.36$	No post – hoc comparisons	
30DPP ACM/2% vs 50DPP ACM/2%			
30DPP Std vs 30DPP ACM/2%			
50DPP Std vs 50DPP ACM/2%			
Action potential amplitude (mV)			
	One-way ANOVA	Tukey's multiple comparisons	
		<i>Difference in means [CIs]</i>	<i>Adjusted p value</i>
30DPP Std vs 50DPP Std	$F_{(3,994)} = 1.526$, $R^2=0.0795$, $p = 0.118$	No post – hoc comparisons	
30DPP ACM/2% vs 50DPP ACM/2%			
30DPP Std vs 30DPP ACM/2%			
50DPP Std vs 50DPP ACM/2%			
Action potential half-width (ms)			
	One-way ANOVA	Tukey's multiple comparisons	
		<i>Difference in means [CIs]</i>	<i>Adjusted p value</i>
30DPP Std vs 50DPP Std	$F_{(3,994)} = 110.5$, $R^2=0.25$, $p < 0.0001$	1.27 [0.5287 – 2.011]	< 0.0001
30DPP ACM/2% vs 50DPP ACM/2%		3.24 [2.766 – 3.714]	< 0.0001
30DPP Std vs 30DPP ACM/2%		-1.17 [-1.763 – 0.577]	0.001
50DPP Std vs 50DPP ACM/2%		1.1 [0.149 – 1.45]	0.0086
Max rise slope (mv ms ⁻¹)			
	One-way ANOVA	Tukey's multiple comparisons	
		<i>Difference in means [CIs]</i>	<i>Adjusted p value</i>
30DPP Std vs 50DPP Std	$F_{(3,994)} = 146.3$, $R^2=0.306$, $p < 0.0001$	-8.83 [-12.43 – -5.231]	<0.0001
30DPP ACM/2% vs 50DPP ACM/2%		-17.69 [-20.64 – -15.52]	<0.0001
30DPP Std vs 30DPP ACM/2%		3.13 [0.252 – 6.008]	0.0668
50DPP Std vs 50DPP ACM/2%		-5.86 [-9.017 – -2.703]	0.0004

4. Optimising culturing conditions of hPS cell derived neurons

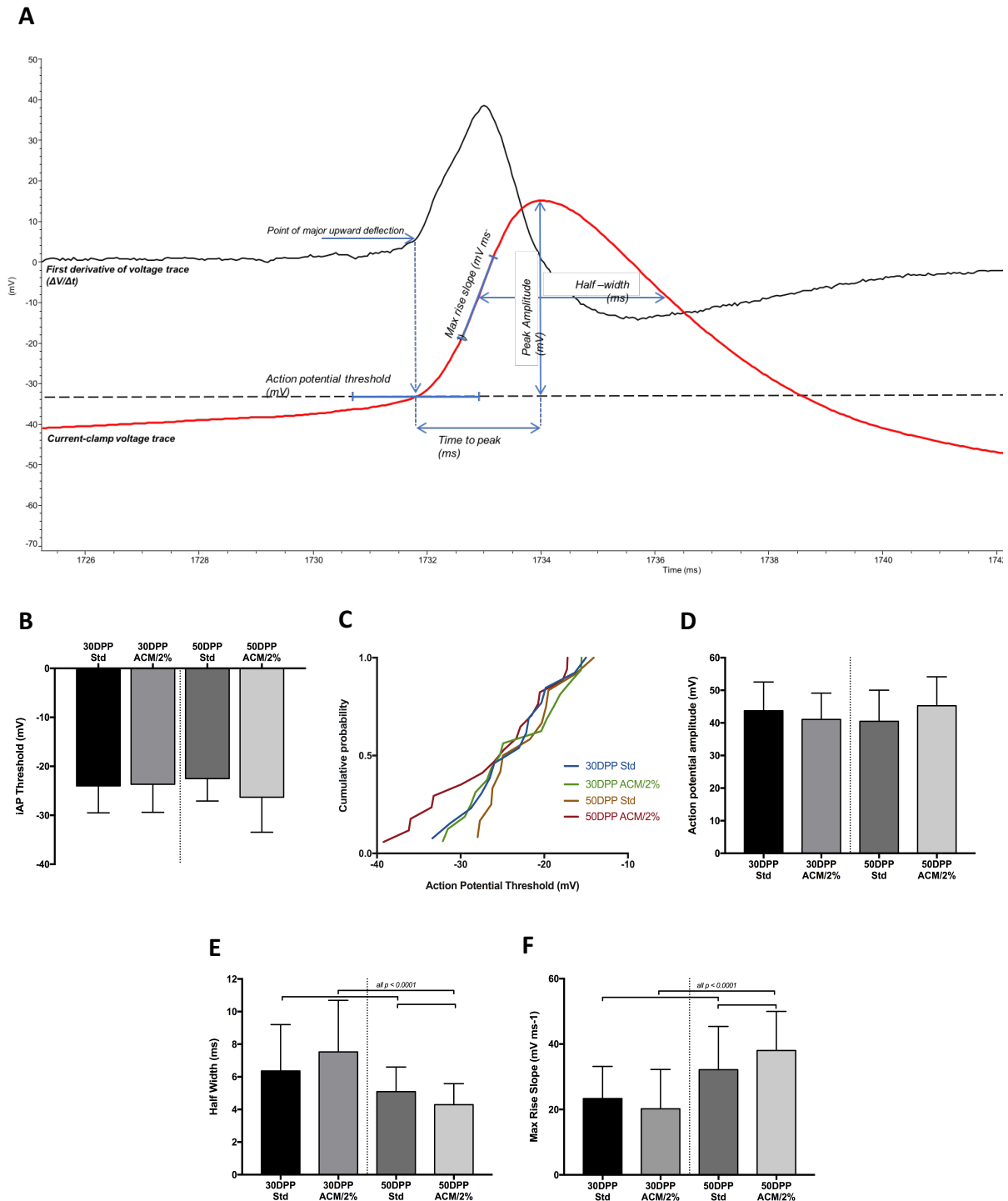


Figure 4.6 – Properties of action potentials recorded from iPS cell derived neurons in standard and ACM/2% culturing conditions. Neurons cultured in standard and ACM/2% conditions were patched at 30 and 50 days post plating (DPP) and iAPs were induced with positive current steps while holding cells at ~70 mV. iAP events were detected and extracted using a threshold based method, where the peak maximum had to reach at least 0 mV. The AP threshold for each cell was determined by the first derivative method, where the point of major upward deflection of the derivative trace of the AP corresponded to AP threshold. Three further properties of detected APs were then analysed (**A**). Neither development or culture conditions had an effect on AP threshold (**B** & **C**) or amplitude (**D**). AP half width (**E**) was decreased and maximum rise slope (MRS; **F**) was increased at 50DPP with the ACM/2% conditions enhancing these changes further. All Bars show means \pm SD. All statistics show results of post-hoc Tukey's multiple comparisons following one-way ANOVA. n values are as follows for each group (number of AP detected; number of neurons patched): 30DPP Std (159; 28), 30DPP ACM/2% (383; 25), 50DPP Std (131, 19) & 50DPP ACM (325; 23). Cells were patched across 3 differentiations.

4. Optimising culturing conditions of hPS cell derived neurons

4.3.5 Spontaneous action potentials

One of the primary reasons for attempting to improve the neuron differentiation protocol in terms of functional maturity was to aid in the development of an MEA platform for the recording and analysis of neuron activity and, in particular, neural network function. As previously described, MEA recordings are based upon the detection of extracellular spikes. This therefore requires neurons that are able to reliably produce spontaneous AP (sAPs), i.e. without the need for depolarising current injections. sAP occurrence in patched neurons was analysed to study the effect of both development and the ACM/2% conditions on the spontaneous activity of iPS cell derived neurons.

The occurrence of sAPs in neurons can be detected while patching cells as they are clearly seen while performing current-clamp gap free recordings with the cell at its V_{rest} ($I = 0$ pA; Figure 4.7A). For both standard and ACM/2% groups at each time point, the total number of cells showing sAPs (pooled across all differentiations) were counted and expressed as a percentage of the total number of cells patched for that group (Figure 4.7B). It should be noted that as counts from each differentiation were pooled, 'n' essentially became 1, meaning that statistics were not possible for this analysis measure. Nevertheless, it can be seen from Figure 4.7 that the percentage of cells showing sAPs was higher at day 50DPP compared to 30DPP in both the standard condition group (3.5% vs 13.5%) and the ACM/2% group (14.6% vs 25.5%).

Furthermore, at both time points, there was a greater number of neurons showing sAPs in the ACM/2% conditions compared to the standard conditions (3.5% vs 14.6% at 30DPP, 13.5% vs 25.5% at 50DPP). Interestingly, the percentage of cells showing sAP at 30DPP in the ACM/2% group was very similar to that in the standard conditions at 50DPP.

Due the practicalities of single-cell electrophysiological recordings, a total of 121 neurons were patched as part of these experiments, meaning that the actual number of cells showing sAPs was low. To establish fuller understanding of whether the ACM/2% conditions improved the spontaneous excitability of a larger population of neurons, a small MEA experiment was performed. Neurons were cultured in standard and ACM/2% conditions as described in Chapter 2 for 10 days, at which point they were re-plated onto MEAs. After 10 days of further culturing on the arrays under the same respective conditions, cells were recorded for 10 minutes and the basic properties of any detected spikes were analysed as described in Chapter 3.

4. Optimising culturing conditions of hPS cell derived neurons

Representative raster plots of detected spikes from MEA-cultures in both standard and ACM/2% conditions are shown in figure 4.8A, while figure 4.8B highlights the results summaries for two basic cell excitation properties: average spike rate and the number of detected bursts. For both of these measures, neurons cultured in ACM/2% conditions had significantly increased average values compared to neurons cultured in standard conditions (Table 4.4).

The results from this section provide good evidence that ACM/2% conditions improve the spontaneous activity of iPS cell derived neurons. Patch clamping experiments showed that the number of cells showing sAPs increased over development and that ACM2% conditions considerably augmented this improvement. However, it should be noted that overall the number of patched cells showing sAPs was low, with even the most active group (50DPP – ACM/2%) having less than 40% of neurons with sAPs. A small MEA experiment using a limited number of array cultures corroborated the patch-clamp findings, with neurons in ACM/2% conditions showing increased spontaneous activity compared to neurons in standard conditions.

Table 4.4 – Statistic summaries of three basic properties of spontaneous activity recorded in from neurons in standard and ACM2% conditions using multi electrode arrays

	Standard		ACM/2%		T-test summaries*
	Mean	SD	Mean	SD	
Average Spike Rate (Hz)	0.73	0.023	2.71	0.612	$t_{(2.004)} = 5.601$; CI[0.462 – 3.489]; $p = 0.0303$
Total detected bursts	24.75	7.182	240.67	66.365	$t_{(2.035)} = 5.611$; CI[53.05 – 378.8]; $p = 0.0292$
* All standard t-tests with Welch's correction for unequal variances. CI represents 95% confidence intervals of the difference between group means. p values are all two-tailed. n = 4 arrays for Std, 3 arrays for ACM/2%.					

4. Optimising culturing conditions of hPS cell derived neurons

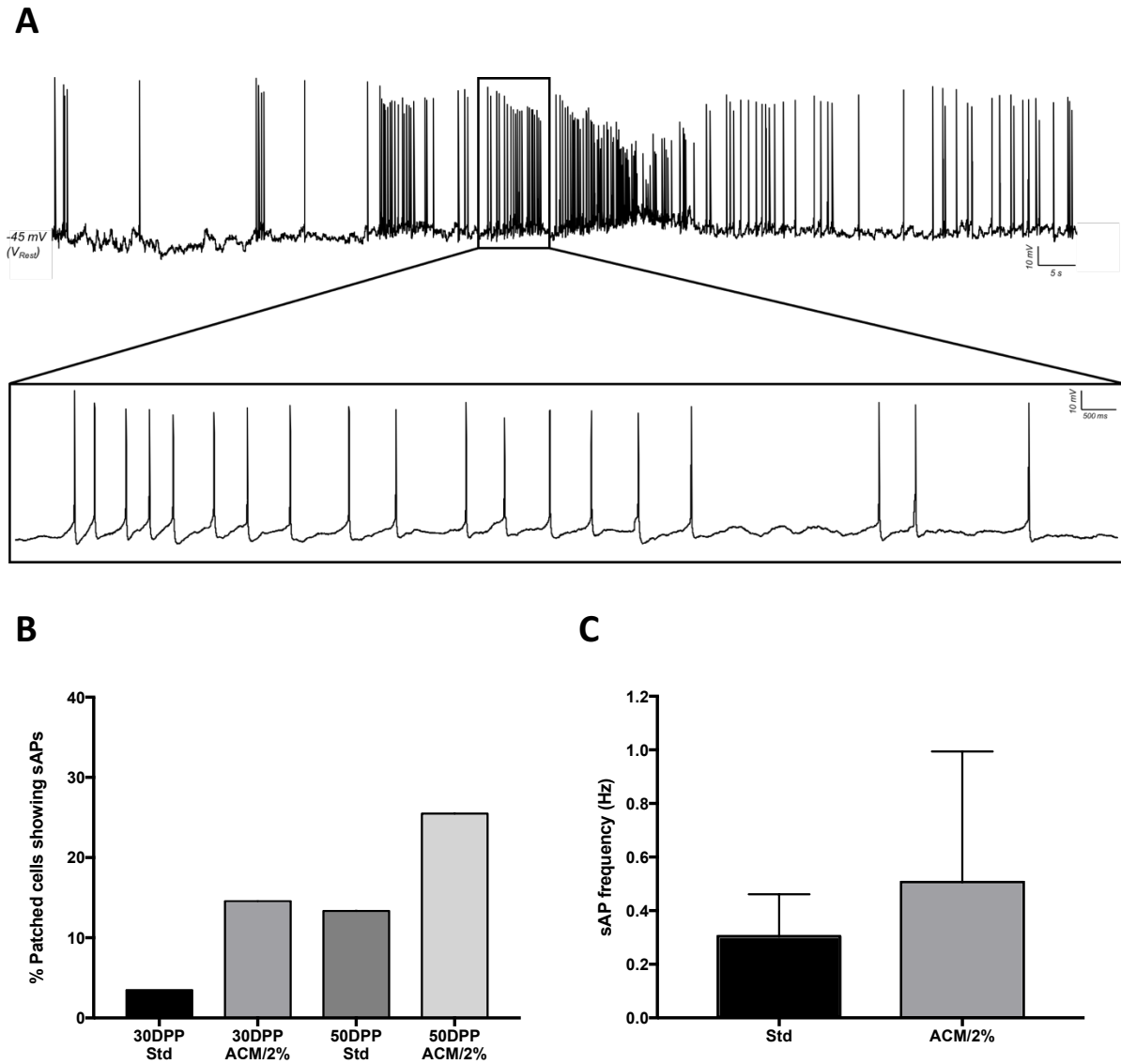
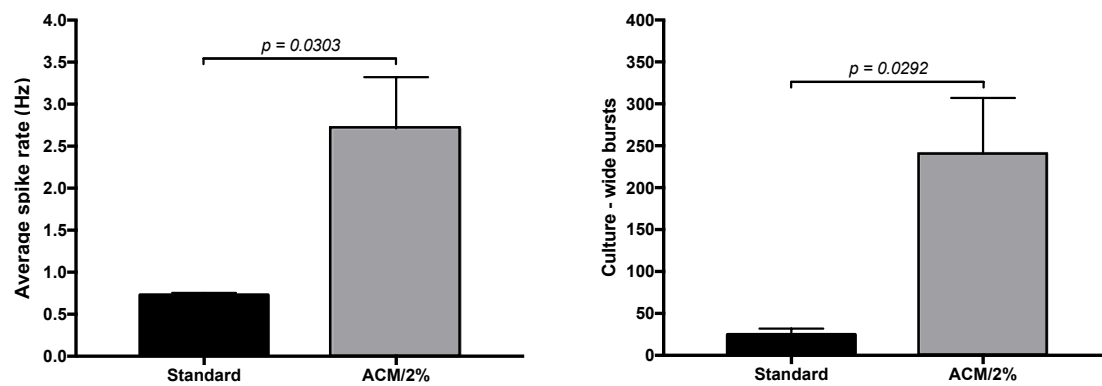


Figure 4.7 – Spontaneous action potentials (sAPs) recorded in iPS cell derived neurons in both standard and ACM/2% culturing conditions. sAPs were detected in 30DPP and 50DPP neurons using gap-free current clamp recording ($I=0$; at V_{rest}) for 4 minutes. Representative trace shown in **A**. The proportion of patched cells showing sAPs increased over development in both conditions and was higher in neurons cultured in ACM/2% conditions at both time points (**B**). The frequency of observed sAPs was also higher in those cells cultured in ACM/2% conditions (pooled neurons from both 30 and 50DPP; **C**). The frequency of sAPs refers to the mean frequency across the 4 minute recordings. $n = 28$ (30DPP Std), 25 (30DPP ACM/2%), 19 (50DPP Std) and 23 (50DPP ACM/2%); Patched across 3 differentiations but data was pooled for **B**. Data in **C** shows means \pm SD.

A**B**

4. Optimising culturing conditions of hPS cell derived neurons

Figure 4.8 – Spontaneous action potentials of iPS cell derived neurons cultured in standard and ACM/2% conditions and recorded with multi electrode arrays. To determine whether astrocyte conditioned medium and hypoxic incubator environments (ACM/2%) had any effect on the spontaneous excitability of neurons cultured on and recorded with multi electrode arrays (MEAs), neurons were plated onto arrays and recorded and analysed after 10 days of culturing in standard and ACM/2% conditions. **A** shows representative raster plots showing the activity of one MEA culture in standard and ACM/2% conditions. These conditions significantly increased the average spike rate and the number of detected bursts compared to standard conditions (**B**). Summary plots in B show means + SD. p values are results of t-tests with Welch's correction. n = 4 arrays for standard and 3 arrays for ACM/2% conditions.

4. Optimising culturing conditions of hPS cell derived neurons

4.4 Discussion

The results presented in this chapter have shown that, overall, culturing iPS cell - derived neurons with astrocyte conditioned medium (ACM) and in a 2% oxygen atmosphere can increase the electrophysiological maturity compared to neurons cultured in standard conditions. Neurons in both conditions were patched at 30 and 50 days post plating (DPP), which revealed variable effects of both development and culturing conditions across a range of intrinsic and active neuron properties. Neurons cultured in ACM/2% conditions had lower resting membrane potentials, had a greater proportion of cells showing iAP activity and, at 50DPP, had faster and thinner action potentials. Importantly, these were measures which generally improved throughout development within each experimental group. Conversely, for other properties including membrane time constant, iAP threshold and iAP amplitude, there was little change over neuron development or effect of the ACM/2% conditions. This suggests that the ACM/2% conditions may specifically enhance those phenotypes which appear to mature natively in these cultures. Importantly, neurons cultured in ACM/2% conditions showed increased spontaneous activity, both at the single-cell level and in MEA cultures recording extracellular activity. Furthermore, these results showed that regardless of age or culture conditions the activity of these iPS cell derived neurons is clearly linked to the V_{rest} of the cells but less so to the passive membrane properties of input resistance and time constant.

It is well established that the V_{rest} of neurons becomes more polarised as the cell develops and as such is a key measure of neuron maturation (Tyzio *et al.*, 2003; Rusu and Borst, 2011; Elston and Fujita, 2014). In this study, the V_{rest} of neurons cultured in standard conditions did not change over development, while it became more negative over the same period in neurons cultured in ACM/2% conditions. Moreover, ACM/2% neurons had significantly lower V_{rest} than standard neurons at 50DPP. The establishment of the negative V_{rest} is down to a combination of the relative concentration gradients of Na^+ and K^+ , due to Na-K-ATPase, and the fact that even at early points in neuron development, the cell membrane is more permeable to potassium than sodium. This leads to the passive efflux of potassium, down its concentration gradient, driving the intracellular potential more negative and towards the potassium reversal potential (around -90 mV). Furthermore, throughout development an increasing number of potassium 'leak' channels are expressed, allowing increased K permeability. While there are several types of

4. Optimising culturing conditions of hPS cell derived neurons

potassium channels, many of which are able to provide a degree of leak, one group is of particular interest regarding the maintenance of membrane potentials. The two-pore domain K channels (TPDKs) are a large group of potassium channels, characterised by the presence of two pores formed by two pairs of two transmembrane domains, high K^+ selectivity, relatively weak conductance (which can be inwardly or outwardly rectifying) and being sensitive to regulation by mechanical stress, pH and endogenous lipids (Goldstein *et al.*, 2001; Lesage, 2003). While TPDK channels are highly expressed in the adult human brain (Medhurst *et al.*, 2001), less is known about their developmental expression or their function in hPS cell derived neurons, although an online database of iPS cell derived neuron expression data suggests that a number of TPDKs are expressed throughout development (van de Leemput *et al.*, 2014). Of most interest for this study is the function of a group of three TDPK channels, TREK-1, TREK-2 and TRAAK, all of which have relatively high conductance, are outwardly rectifying and can be functionally regulated by mechanical deformation and, importantly, cellular lipids (Patel and Honoré, 2001). One of the lipids to which these channels are sensitive is arachidonic acid (AA) which causes reversible opening of the pores and increased potassium efflux (Fink *et al.*, 1998; Lesage *et al.*, 2000). AA is known to be released from astrocytes (Stella *et al.*, 1994; Mishra, 2017; Newman, 2015) and therefore, could potentially be one of the key molecules found in ACM. In this way, AA released from astrocytes and present in the ACM could lead to a potentiation of potassium leak currents via TREK-1, TREK-2 and TRAAK and therefore the hyperpolarisation of V_{rest} seen in neurons cultured in the ACM/2% conditions.

In this study, ACM/2% conditions had limited effect on neuron input resistance (R_i) or membrane time constant (τ). Furthermore, there was little 'maturation' of these measures over development, except in the ACM/2% neurons which did show a small (but statistically significant) decrease in R_i . It is worth noting that even the most mature values for both R_i and τ recorded in these neurons (in ACM/2% neurons at 50DPP) are relatively un-physiological when compared to nature human or rodent neurons. For example, during development, the R_i of post-natal rat hippocampal neurons is around 1 $G\Omega$ at P0 and rapidly decreases to around 0.1 $G\Omega$ by around P5 (Tyzio *et al.*, 2003). In many of the studies involving hPS cell derived neurons, R_i (and to a lesser extent τ) have been reported as high regardless of other factors, including V_{rest} , cell excitability or synaptic maturity (Prè *et al.*, 2014; Bardy *et al.*, 2015; Shi *et al.*, 2012b; Telezhkin *et al.*, 2016). For example, Prè *et al.* differentiated iPS cells into forebrain neurons

4. Optimising culturing conditions of hPS cell derived neurons

which showed average V_{rest} of around -45 to -50 mV, produced trains of iAP, showed spontaneous synaptic currents but had minimum R_i of around 2 G Ω . It is possible that the high R_i reported in this chapter and by other studies could be due to the relative rate of functional neuron development versus morphological development. V_{rest} is generally thought to be primarily product of ion channel function, transporter expression and ionic permeability, particularly at the soma (Ambrogini *et al.*, 2004). However, both R_i and tau are more dependent on the volume of the soma, the extent of proximal dendrites and the integrity of the cell membrane (Esp3sito *et al.*, 2005). If an increase in membrane area, due to increased branching and dendritic arborisation, is not matched by a concomitant increase of functional expression of ion channels in those dendrites, it is possible that R_i and tau remain stable while V_{rest} polarises in response to channel expression at the soma.

At both 30 and 50DPP, neurons cultured in the ACM/2% conditions were more active compared to neurons cultured in standard conditions, as shown by the cell classification analysis in section 4.4.2. The ability to produce action potentials is largely down to the expression of functional voltage gated Na and K channels (Na_v and K_v), especially at the axon hillock and axon initial segment (AIS). A key protein involved in the architectural organisation of channels at the AIS is Ankyrin G. While many studies, including recent high-resolution imaging studies, have shown the importance of Ankyrin-G in correct channel placement and excitability in rodent neurons (Kole and Stuart, 2012; Leterrier *et al.*, 2015; Rasband, 2010), little is known about the expression of Na_v , K_v and ankyrin in hPS cell neurons and their relation to cell maturity. Several studies have reported that hPS cell neurons have measurable Na_v and K_v currents (Pr3 *et al.*, 2014; Bardy *et al.*, 2015; Telezhkin *et al.*, 2016; Zhang *et al.*, 2013), although this has not routinely been viewed as part of a continuous scale of development. A recent study used a similar neuron iAP classification approach as here which was then followed up with single-cell RNA-seq (Bardy *et al.*, 2016). Interestingly, this showed that those neurons showing trains of iAPs had the highest expression of ANK3 (which codes for Ankyrin G) and increased expression of several Na_v (including SCN2A and SCN7A) and K_v channels.

In this chapter, the activity of neurons corresponded well to the V_{rest} of neurons, such that cells producing iAP trains had the most polarised V_{rest} . However, as iAPs were produced in these neurons while holding the cell at -70 mV, it is perhaps difficult to link V_{rest} directly with iAP classification of the cell, although it is clear that in these neurons, V_{rest} is a good marker of

4. Optimising culturing conditions of hPS cell derived neurons

functional development. V_{rest} can more directly be linked to the formation of spontaneous action potentials (sAPs), which are observed in cells without holding of the membrane potential and current injection. In this study, both single cell patching and a small MEA experiment showed that neurons cultured in ACM/2% conditions have a greater number of sAPs than neurons in standard conditions. The V_{rest} of a neuron can be linked to sAP formation as the membrane potential regulates several aspects of AP initiation. Firstly, for sAP to occur, V_{rest} must be more negative than the threshold for action potential initiation. As with V_{rest} , AP threshold has been shown to polarise throughout neuron development but while V_{rest} is more dependent on passive potassium conductance, the AP threshold relies more on Na_v function (Platkiewicz and Brette, 2010). Here, at both time points and in both conditions, the average V_{rest} was at or below the average AP threshold for each group. Secondly, sAP occurrence relies on V_{rest} to be sufficiently polarised as to remove the voltage inactivation of Na_v channels, which, while variable between neuron types, is thought to be around -30 mV for excitatory cortical rat neurons (Platkiewicz and Brette, 2010). Interestingly, there is some evidence that this inactivation is in fact more dependant the value of V_{rest} relative to the threshold potential, as it has been reported that in adult rat hippocampal neurons around 80% of Na_v channels were 'available' at V_{rest} (~ -70 mV), compared to 23% at AP threshold (~ -55 mV; Fricker *et al.*, 1999). As such, in the iPS cell derived neurons in this chapter, it is possible that the ACM/2% conditions promote a polarised V_{rest} , driving it sufficiently below the AP threshold, therefore allowing the subsequent activation of Na_v channels and the occurrence of sAPs. Finally, while sAPs can occur innately (e.g. due to fluctuations in the membrane potential) the appearance of sAPs is increased by functional synapses allowing depolarising excitatory inputs. Although not studied in this chapter, ACM conditions have been shown to increase the number of synaptic events in both rodent primary (Ullian *et al.*, 2004; Hughes *et al.*, 2010) and iPS cell derived neurons (Rushton *et al.*, 2013), while low oxygen culturing environments have been shown to increase synaptogenesis in rodent and human primary cells (Studer *et al.*, 2000; Liu *et al.*, 2009; Brewer and Cotman, 1989).

In general, the action potentials produced by neurons get larger, faster and thinner throughout development, although the timing, extent and exact nature of these changes is highly variable between neuron populations and is especially dependent on the type of firing that the cells produce (Bean, 2007). In this chapter, which studied neurons produced following a protocol to

4. Optimising culturing conditions of hPS cell derived neurons

yield glutamatergic forebrain neurons, there was no change in the iAP amplitude over development or between culturing conditions. However, neurons patched at 50DPP produced faster and thinner AP than neurons at 30DPP, which was potentiated if neurons had been cultured in ACM/2% conditions. The rising phase of an AP is regulated by the action of various Na_v channels and as such are generally thought to be responsible for the speed of this rising phase and the final amplitude of the spike (Bean, 2007; Martina and Jonas, 1997). The expression of Na_v channels increases throughout both human and rodent neuronal development (Mechaly *et al.*, 2005; Miller *et al.*, 2014; Lein *et al.*, 2007) and in hPS cell derived neurons, the expression of several types of Na_v channels increases throughout differentiation (van de Leemput *et al.*, 2014; Shi *et al.*, 2012b). While the increased developmental expression of Na_v channels could explain the increase in max rise slope observed here, it is unclear why this would not also cause an increase in AP amplitude. The falling phase of an AP is driven by the opening of K_v channels, which are also thought to primarily responsible for the width of APs. The family of K_v channels is large and the specific subtypes of channels thought to be responsible for AP width vary between cell type (Nowak *et al.*, 2003). For example, the narrowing and increasing speed of APs from neurons in the superior paraolivary nucleus are thought to be due to increased expression of $\text{K}_v1.1$ channels (Felix *et al.*, 2013), while increased K_v3 currents are known to be responsible for the development of narrow spikes seen in fast spiking interneurons (Du *et al.*, 1996; Rudy and McBain, 2001). In developing hPS cell neurons, both the size of K_v currents and the expression of certain subtypes of K_v1 and K_v3 channels has been shown to increase over time (van de Leemput *et al.*, 2014; Nicholas *et al.*, 2013).

At 50DPP, the neurons cultured in ACM/2% conditions had thinner and faster APs compared to those cultured in the standard conditions, suggesting that the ACM/2% conditions further augmented the maturation of the AP shapes seen over development. However, at 30DPP, the ACM/2% neurons had wider and marginally slower APs than those in the standard conditions, suggesting that at this time point the ACM/2% conditions had a detrimental effect on AP shape. Its not immediately clear why the ACM/2% conditions would have contrasting effects at different time points, especially as the conditions improved the V_{rest} and excitability of neurons at both 30 and 50DPP. One possibility is that the average for this time point was inflated by values observed in neurons from one particular round of differentiation. However, even when excluding these observations, the 30DPP ACM/2% neurons still presented with the slowest and widest APs, suggesting that there is an underlying physiological cause. Another key neuropeptide

4. Optimising culturing conditions of hPS cell derived neurons

released from astrocytes is thyrotropin releasing hormone (TRH), which has been shown to have a number of neurotrophic and pro-maturation roles (Fernández-Agulló, 2001; Kasparov *et al.*, 1994). However, TRH has also been shown to *increase* the half-width and *decrease* the amplitude of APs produced by rat cortical pyramidal neurons via a mechanism involving g-protein mediated signalling (Rodríguez-Molina *et al.*, 2014). As such, it is possible that at 30DPP, the ACM/2% conditions have negative effects on individual APs, through the action of TRH present in the ACM. By 50DPP, it is possible that due to other pro-maturation effects of the ACM/2% conditions described earlier, the detrimental effect of TRH is masked. For example, the action of the ACM/2% conditions on V_{rest} and potassium conductance earlier in development may mean that by 50DPP there is bigger K^+ gradient in these neurons compared to controls (due to increased K_v channel expression) driving a larger K_v current which presents as faster and thinner iAPs. Finally, another of the ways in which ACM is thought to contribute to neuron maturity is via the regulation of available calcium (Ullian *et al.*, 2004; Rushton *et al.*, 2013). Recently, it has been shown that the calcium-activated K_{Ca} channels, which are thought to be expressed later in development, also contribute to AP width (Kimm *et al.*, 2015).

Overall, the results presented in this chapter have shown that culturing differentiations in ACM/2% conditions improve the functional maturation of neurons by a number of measures including V_{rest} and, importantly, both induced and spontaneous AP activity. This is likely to be primarily driven by an earlier increase in potassium permeability and ion channel expression, caused by the action of several neurotrophic molecules present in the ACM and augmented by the pro-maturation and pro-synaptogenesis effects of the 2% O_2 environment. Importantly, the increased maturity and activity of the neurons in ACM/2% conditions should aid in the development of the platform for investigating network activity in iPS cell derived neurons in both development and disease states.

5. Investigating network development in iPS cell derived neurons

5.1 Introduction

While multi-electrode arrays (MEAs) are not a new technology, it has only been in the last few years with the advent of more modern, user-friendly systems that they have begun to be exploited again for the study of neuronal function. In particular, the nature of MEAs allows for the study of neuron function across a population of cells and therefore the study of neural networks. Understanding neural networks, both locally and at the whole brain level, is a key part of investigating brain function throughout development and in models of neurological disease. Indeed, the study of neural networks *in vivo* and intact brain slices has been a key part of the neuroscience field for many years. However, the study of the development and function of dissociated cultures and in particular, neurons derived from human iPS cells, is less understood.

A number of studies have provided good evidence that dissociated primary rodent neurons form functional networks *in vitro* (Maeda *et al.*, 1995; Chiappalone *et al.*, 2006; Hales *et al.*, 2010). This takes the form of spontaneous, self-organising, coordinated bursting behaviour which is detected by multiple electrodes across the culture (Sun *et al.*, 2010; Raichman and Ben-Jacob, 2008). After around a 2-week period of non – synchronous firing, culture wide coordinated behaviour develops and is correlated with an increase in firing rate and neuron burst firing. Recently, it has been shown that this synchronous behaviour may in some cases develop further, such that culture-wide activity can be divided into low and high activity periods lasting for tens of seconds (Lu *et al.*, 2016). Furthermore, this network behaviour is sensitive to pharmacological manipulation and in particular, requires AMPA receptor activity.

Much less is known about the development of networks in hPS cell derived neurons. As described in Chapter 4, the relative immaturity of these neurons might suggest that the formation of functional neural networks is precluded, or at least, sufficiently delayed such that

5. Investigating network development in iPS cell derived neurons

any observation becomes practically limiting. However, a number of studies have shown that hPS cell derived neurons can be cultured on MEAs and do show spontaneous activity which, in general, increases over time (Odawara *et al.*, 2014; Ylä-Outinen *et al.*, 2010; Odawara *et al.*, 2016; Amin *et al.*, 2016). Furthermore, these studies have shown that one of the key applications for MEA – culturing is likely to be for pharmacological profiling and drug screening, as it has been shown that neuronal spiking, at the single unit level, can be manipulated both by ionic changes to extracellular solutions and drug application. To date, only one study has provided good evidence for the development of network behaviour in hPS cell derived neurons, highlighted by the formation of array – wide synchronised burst firing (SBF) after several weeks in culture. However, this behaviour takes an extended period of culturing to appear – at least 20 weeks – and the nature of the SBF seems to change little over development (Odawara *et al.*, 2016).

The work presented in Chapter 4 showed that the optimisation of the differentiation protocol based around ACM/2% culturing conditions produced neurons that were more mature in terms of their physiology. Importantly, neurons produced with this developed protocol exhibited a greater number of spontaneous action potentials, observed with both patch clamping and a small MEA experiment. To extend the work from Chapter 4 and to determine whether these neurons could be cultured on and recorded using MEAs for an extended period of time, this chapter describes a series of experiments to study the development of spontaneous activity.

The creation of a platform for studying network activity in iPS cell derived neurons would provide a useful tool for the investigation of how these cells develop and how they function *in vitro*. Moreover, if successful, it would provide a valuable asset in the study of iPS cell models of neurological disorders, including autism spectrum disorders, for which aberrant network signalling is thought play a key aetiological role. Importantly, such a platform should enable reliable and repeatable detection of spontaneous neural activity and the establishment of coordinated firing, as seen by Odawara *et.al*, to allow the study of network development. Finally, the nature of the arrays allows the simple addition of pharmacological agents to the cultures during recordings. This, therefore, allows both the profiling of any detected activity and opens the possibility for screening potential therapeutic compounds.

5.2 Chapter Aims

The work in this chapter aims to study the formation and development of networked behaviour in iPS cell derived neurons. It will aim to track the spontaneous activity of neurons over long-term culturing of cells on MEAs, will study the establishment of any coordinated activity and monitor this behaviour throughout development. It further aims to profile the observed behaviour in terms of the response of activity to a range of pharmacological agents. In particular, it aims to study the underlying nature of any networked behaviour and how this may lead to a better understanding about the nature of iPS cell neurons. Finally, this chapter aims to establish the use of an MEA system as a reliable and valuable platform for the study of iPS cell neurons in development and disease states.

5.3 Results

5.3.1 Differentiations of IBJ4 iPS cells produce neurons with a cortical projection neuron identity

The work in Chapter 4 described the development of the differentiation protocol to produce the neurons used in this project. The ‘base’ protocol was one initially developed in the institute for the production of forebrain excitatory neurons and has been characterised elsewhere. However, to provide a further understanding about the state of the neurons produced with the optimised protocol (i.e. using astrocyte conditioned medium and a 2% O₂ incubator atmosphere), a selection of cultures parallel to those used for or on MEAs were fixed and stained at two time points. Cells were first stained at day 20-22 (day 0 = iPS cells) to determine the expression of specific proteins at the neural precursor cell (NPC) stage. At this time point, cultures were seen primarily as ‘rosettes’ of polarised cells, a hallmark of NPC generation in 2-dimensional differentiations (Shi *et al.*, 2012; Figure 5.1). The cells expressed the primary marker of NPCs in the intermediate filament protein NESTIN, as well as three key markers of cortical neuron fate: FOXG1, a transcription factor expressed by telencephalic precursors; PAX6, a transcription factor marker of *dorsal* telencephalic progenitor patterning; and TBR2 a key marker of intermediate progenitor cells. These three proteins are frequently used as key determinants of a forebrain projection precursor identity in stem cell models (Muratore *et al.*, 2014).

Coverslips of cells were also stained at 50 days post re-plating (50DPP), corresponding to 50 days after cells were re-plated for MEA experiments. At this time point, cells were stained to determine their identity as more mature neurons with organised synapses. Firstly, all neurons expressed MAP2, the neuron specific microtubule associated protein which, in hPS cell neurons, is expressed from around 30 days (Figure 5.2A). Furthermore, neurons also showed expression of vGLUT1, a transporter involved in the uptake of glutamate into synaptic vesicles, suggesting that neurons had glutamatergic identity. Higher magnification observations of fixed neurons revealed that cells also expressed the key excitatory synaptic markers PSD95 and GluN1. GluN1 is the compulsory glycine-binding subunit of NMDA receptors while PSD95 is a key scaffolding protein involved in the assembly and function of the NMDA receptor complex.

5. Investigating network development in iPS cell derived neurons

Neurons were also stained for a number of proteins that have been identified as markers of cortical layer fate (Figure 5.2B). Many neurons expressed TBR1, a transcription factor subsequently expressed in *post-mitotic* neurons after TBR2 (Englund *et al.*, 2005). TBR1, therefore, is also considered a marker of early-born deep layer neurons, specifically those of layer 6 (Bedogni *et al.*, 2010). Many neurons also expressed CTIP2, a second key marker of deep layer neurons, identifying cells primarily belonging to layers 6 and 5a. Finally, a few neurons also expressed SATB2, a transcription factor involved in the regulation of cell fate in upper layers of the cortex, especially in layers 4 and 3 (Britanova *et al.*, 2008). Overall, these results clearly show that the cells being produced with the developed protocol are, by 50DPP, primarily glutamatergic cortical neurons, most of which express markers of an early, deep cortical layer fate and express proteins required for functional excitatory synapses.

5. Investigating network development in iPS cell derived neurons

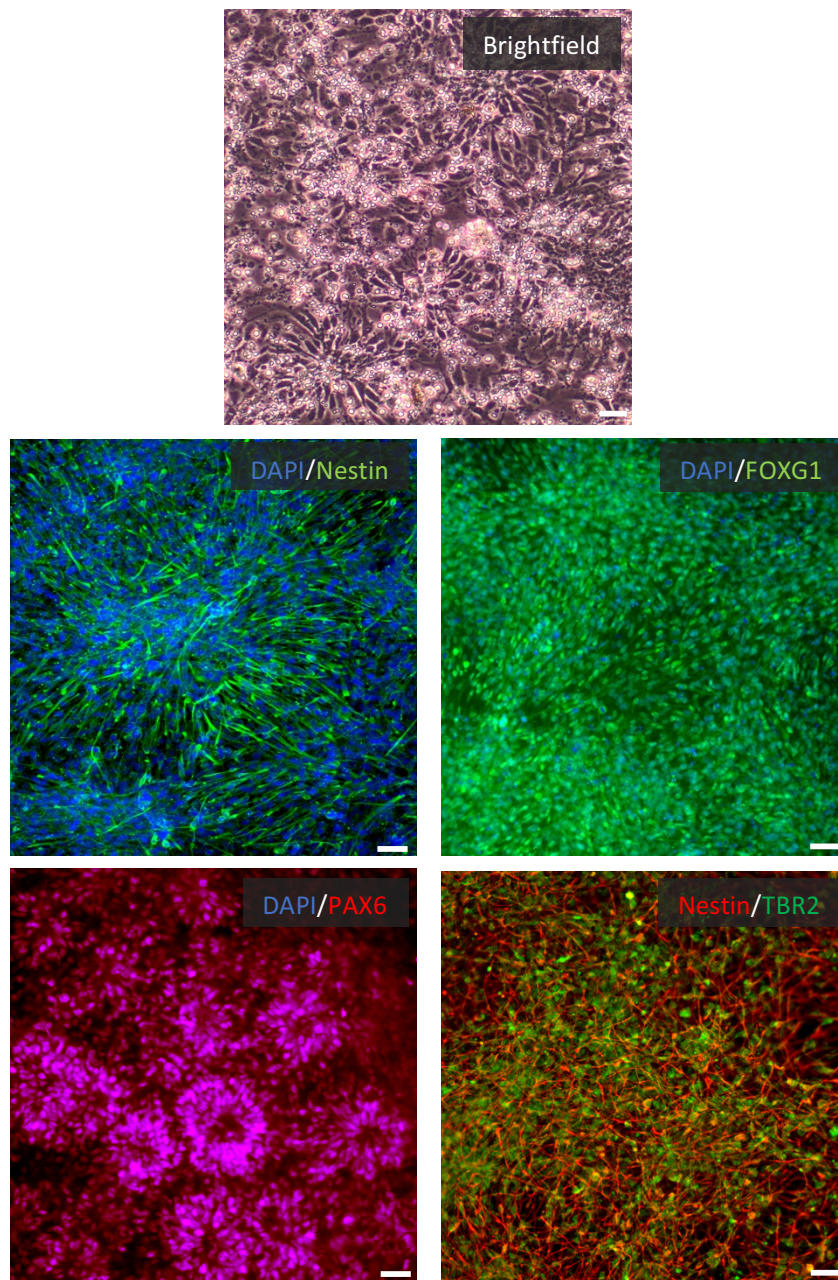


Figure 5.1 – IBJ4 IPS cells differentiate into neural precursors with a forebrain projection neuron identity. IBJ4 cells were differentiated towards neural precursors (NPCs) following a dual SMAD – inhibition protocol. To confirm the identify of these precursors, cells were fixed and stained with markers for progenitors and early neurons 20-22 days after the start of differentiations (as iPS cells). At this point, cells showed expression of nestin, the intermediate filament protein of neural precursors; TBR2 a transcription factor involved in the regulator pathways in radial glial cells; and FOXG1 and PAX6, two key transcription factors expressed by telencephalic and dorsal telencephalic progenitors respectively. Panels show representative images from differentiations of IBJ4 iPS cells. Scale bars show 50 μ m.

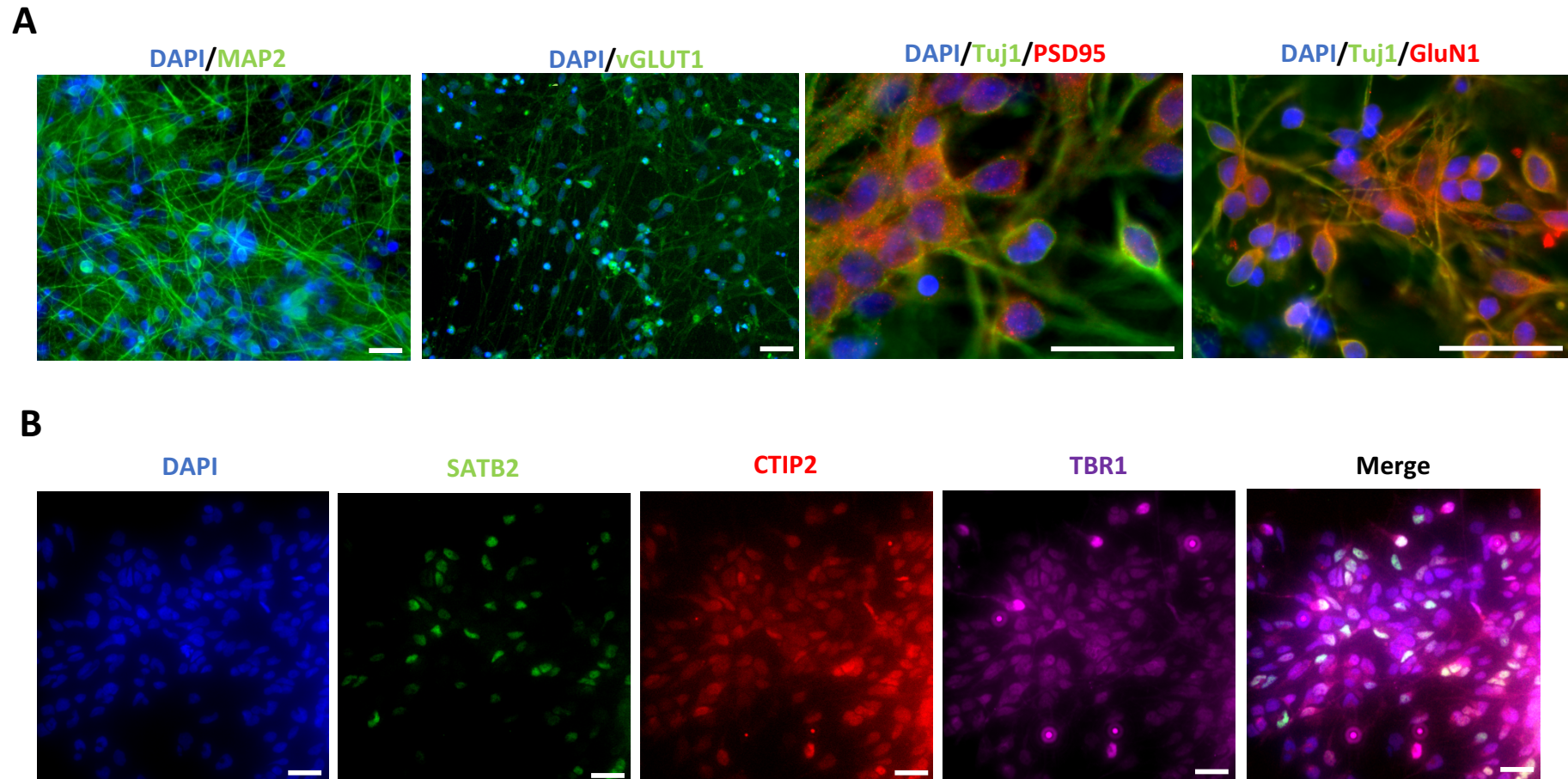


Figure 6.3 – IBJ4 iPS cells differentiate into neurons with a cortical glutamatergic fate. To provide an understanding about the nature of the neurons produced with the differentiation protocols developed in this project later in development, cells were fixed and stained at 50 days post replating (50DPP). Cells showed expression of the neuron marker MAP2, the vesicular glutamate transporter vGLUT1, the excitatory post synaptic density structural protein PSD95 and the universal subunit of NMDA receptors, GluN1 (A). Neurons also expressed the markers of cortical layer fate SATB2, CTIP2 and TBR1. Image show representative images. Scale bars in all images show 50 μm .

5. Investigating network development in iPS cell derived neurons

5.3.2 Development of network behaviour in iPS cell derived neuronal cultures

To study the development of network activity in iPS cell derived neuronal cultures, differentiating cells were replated onto MEAs after around 40 days and subsequently cultured for an extended period (see Chapter 2). Cells were re-plated onto MEAs as drop cultures to provide the required density and to achieve high rates of cell survival. Figure 5.3 shows DIC images of cells re-plated onto MEAs at 5DPP (days post plating) and highlights the rapid recovery of cells to form dense morphologically complex cultures.

Figure 5.4 shows the changes in spontaneous activity seen in one MEA culture, recorded for 10 minutes every 10 days for 50 days post-plating (DPP) and represents recordings from the same 12 electrodes at every time point as shown in the array map inset. Figure 5.5 presents the summary data for five key excitability characteristics as analysed for all developmental experiments (up to 10 arrays across 4 differentiations in total). 10 days after replating, very low level spontaneous firing is seen across the culture with an average firing rate of 0.065 ± 0.021 Hz (Fig 5.5A) and with no bursts detected (Fig 5.5B). By 20DPP, the firing rate had increased to 0.75 ± 0.21 Hz, with 232 ± 103 bursts now observed, indicating that the culture had become much more active over the first 20 days of culturing. However, at both these time points activity is random and uncoordinated across the culture. This is highlighted by the blue ASDR plots in figure 5.4 which shows low-rate firing for the duration of the recording and an absence of any pattern in the rate of firing across the cultures at both 10 and 20 DPP. The lack of synchronicity can also be seen in Figure 5.5C, which shows a low max array-wide spike detection rate (max ASDR; 10 ± 5.23 spikes/bin). This measure presents the maximum number of spikes detected across the culture in a single 200 ms bin and is a useful measure of culture-wide synchronicity (see Chapter 2).

The raster plot for the recording at 30DPP in Figure 5.4 again appears to show that activity in the culture is still largely uncoordinated. However, the corresponding ASDR plot suggests that in fact there is some synchronicity across the array, highlighted most clearly by the first two ASDR peaks, which coordinate with short bursts of firing seen across the culture and visible in the raster plot. The recordings at 30DPP also showed a increase in general neuronal excitability compared to the first two time points, with average spike rate increasing to 2.1 ± 0.8 Hz and 559

5. Investigating network development in iPS cell derived neurons

± 208.1 bursts now detected (Figure 5.5A&B). While there is still a low max ASDR observed (15.67 ± 5.5 ; Figure 5.5C), for the first time a MAP (more active period) interval can be calculated in some of the cultures (Figure 5.5D; 4700 ± 2702 ms). This represents the median time interval between MAP peaks and can therefore only be calculated when cultures show coordinated array-wide activity. It should be noted that about 50% of cultures at 30DPP showed coordinated behaviour and 50% did not.

By 40DPP, a clear pattern had emerged in the activity seen across the culture (Figure 5.4). The raster plot for this time point shows that apart from three electrodes, the array shows short, coordinated bursts of activity across the entire culture. This is highlighted by the ASDR plot which shows regular mid-frequency firing peaks across the culture for the duration of the recording. Furthermore, the MAP interval had increased by 40DPP from 4700 ± 2702 ms at 30DPP to 14700 ± 5730 ms (Figure 5.5D). Note that by 40DPP, 100% of the cultures recorded exhibited coordinated culture-wide behaviour. Interestingly, the general excitability of cultures was broadly similar to that at 30DPP, with a firing rate of 1.78 ± 1.09 Hz and a burst rate of 485 ± 264.1 (Figure 5.5A&B). However, there was an increase in the max ASDR to 51 ± 21.76 , highlighting that many more spikes across the culture appear in the same 200 ms bin, due to the increase in coordinated firing.

50 days after replating the nature of the activity in the culture in Figure 5 had changed markedly. Now, the activity is characterised by periods of very low-level activity (less –active period; LAP), lasting for 10s of seconds, punctuated by periods of higher culture – wide activity (more active period; MAP) again lasting for 10s of seconds. Each of these MAPs begins with a very high frequency burst seen across the culture, before resting at a period of medium frequency firing for around 35 seconds. Both the raster and ASDR plots highlight clearly the extent of the synchronised behaviour at this time point. While it should be noted that not every culture tested at this time point showed such sustained MAPs, the interval between these peaks was consistently higher in all cultures than at 40DPP, giving an average MAP interval of 78333 ± 37845 ms (figure 5.5D). Similarly, the maximum array-wide spike rate increased from 40DPP to 69.67 ± 31.51 further highlighting the increased degree of synchronous firing. There was also a small increase in general firing rate in the cultures at 50DPP back to around the rate seen at 30DPP (2.13 ± 1.44 Hz; Figure 5.5A) while there was a small decrease in the overall number of bursts detected to 421.7 ± 221.2 .

5. Investigating network development in iPS cell derived neurons

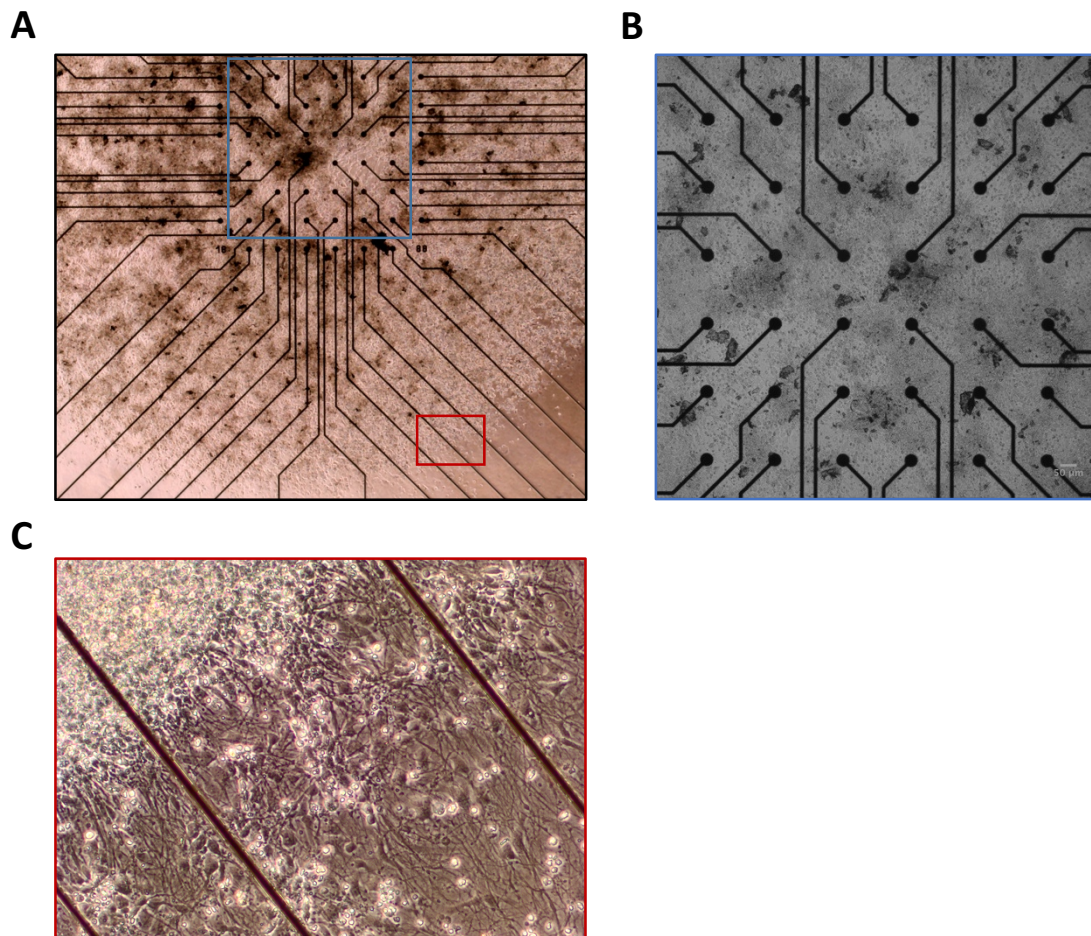
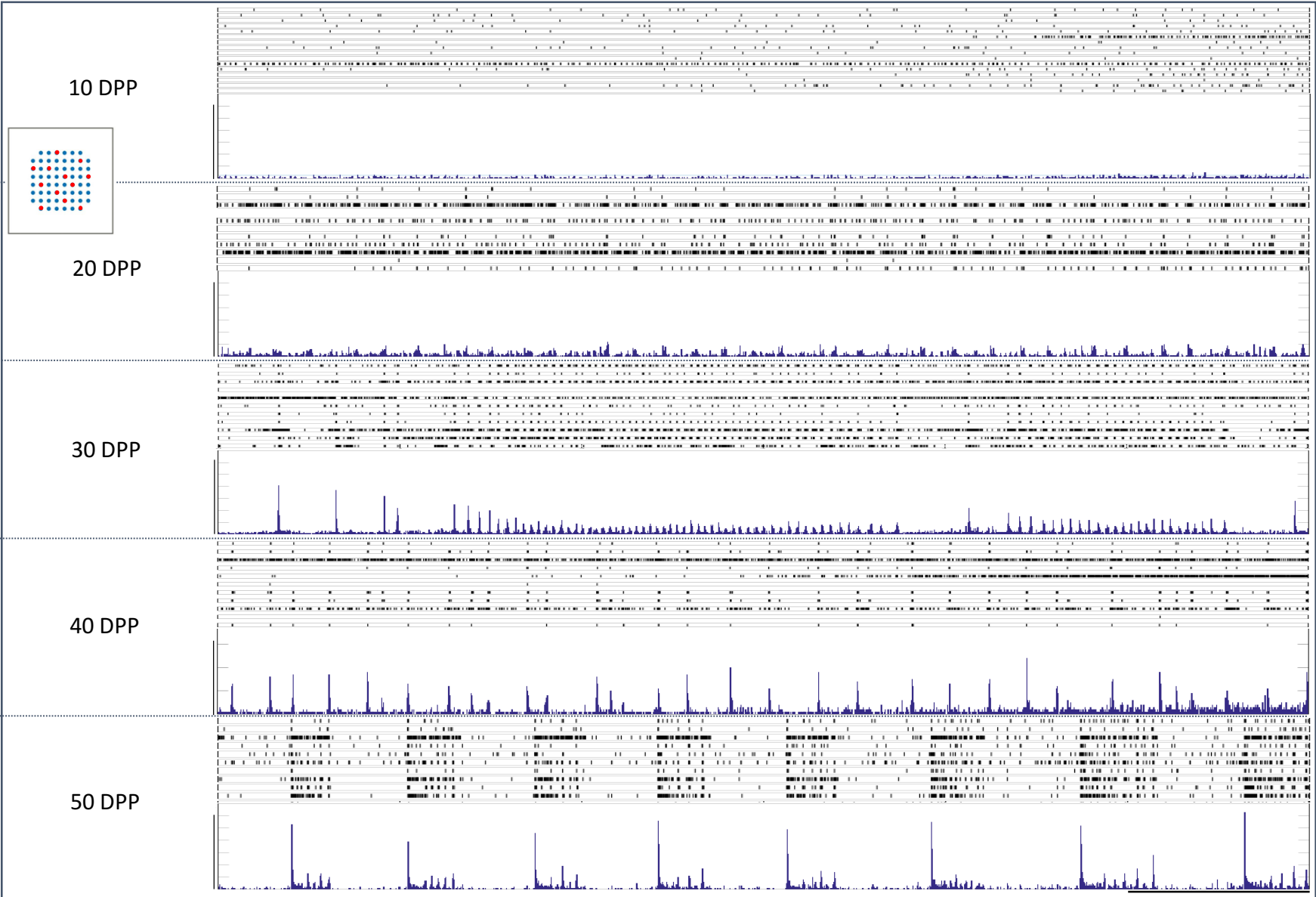


Figure 5.3 – Immature iPS cell derived neurons re-plated onto multi electrode arrays (MEAs) quickly reform dense complex cultures. To record spontaneous extracellular activity, differentiating neurons are re-plated onto MEAs at around day 40. Cells are plated on poly-d-lysine/laminin using drop-cultures of ~40,000 cells, to achieve a dense, localised culture (A; circular nature of plated cells can be seen in the lower half of image). Around 24 hours after re-plating, neurons begin to re-form axons and dendrites and continue to differentiate as normal. The enlarged central area presented in B highlights the density of cultures required for reliable MEA recordings; while the area in C shows the edge of the drop culture where individual neurons can be identified. Images are representative of MEA cultures using neurons derived from IBJ4 iPS cells and show cells 5 days post re-plating. Scale bars show 50 μm.



5. Investigating network development in iPS cell derived neurons

Figure 5.4 The development of network activity in iPS cell derived neurons cultured on and recorded with MEAs. After plating onto MEAs, neurons settle and within 10-20 Days post plating (DPP) begin to fire spontaneous action potentials. Up to around 30DPP, this activity is generally confined to un-coordinated spikes at the single-unit level. Between 30 and 40DPP, spiking across the whole culture becomes coordinated, except for a few electrodes, and is generally characterised by short bursts of spikes. By 50DPP, culture-wide activity can be characterised by 'more active' (MAP) and 'less active periods' (LAP). During LAPs, random, uncoordinated spikes are seen throughout the array. During MAPs, electrodes detect high-frequency synchronised firing across the whole culture, lasting for 10s of seconds. The data shown is the development of network activity seen in the same culture. For each time point, the top panels show raster plots of detected spikes from the same 16 electrodes (highlighted in inset); bottom panels show the array-wide spike detection rate plots (ASDR plots) for each culture, where spike counts for each electrode are parsed into 200ms bins and subsequently summed across the array for each bin. Vertical scale bars in ASDR plots show 80 spikes/bin. Horizontal scale bar represents 100 seconds. The presented behaviour was observed in at least 7 cultures across 4 differentiations.

5. Investigating network development in iPS cell derived neurons

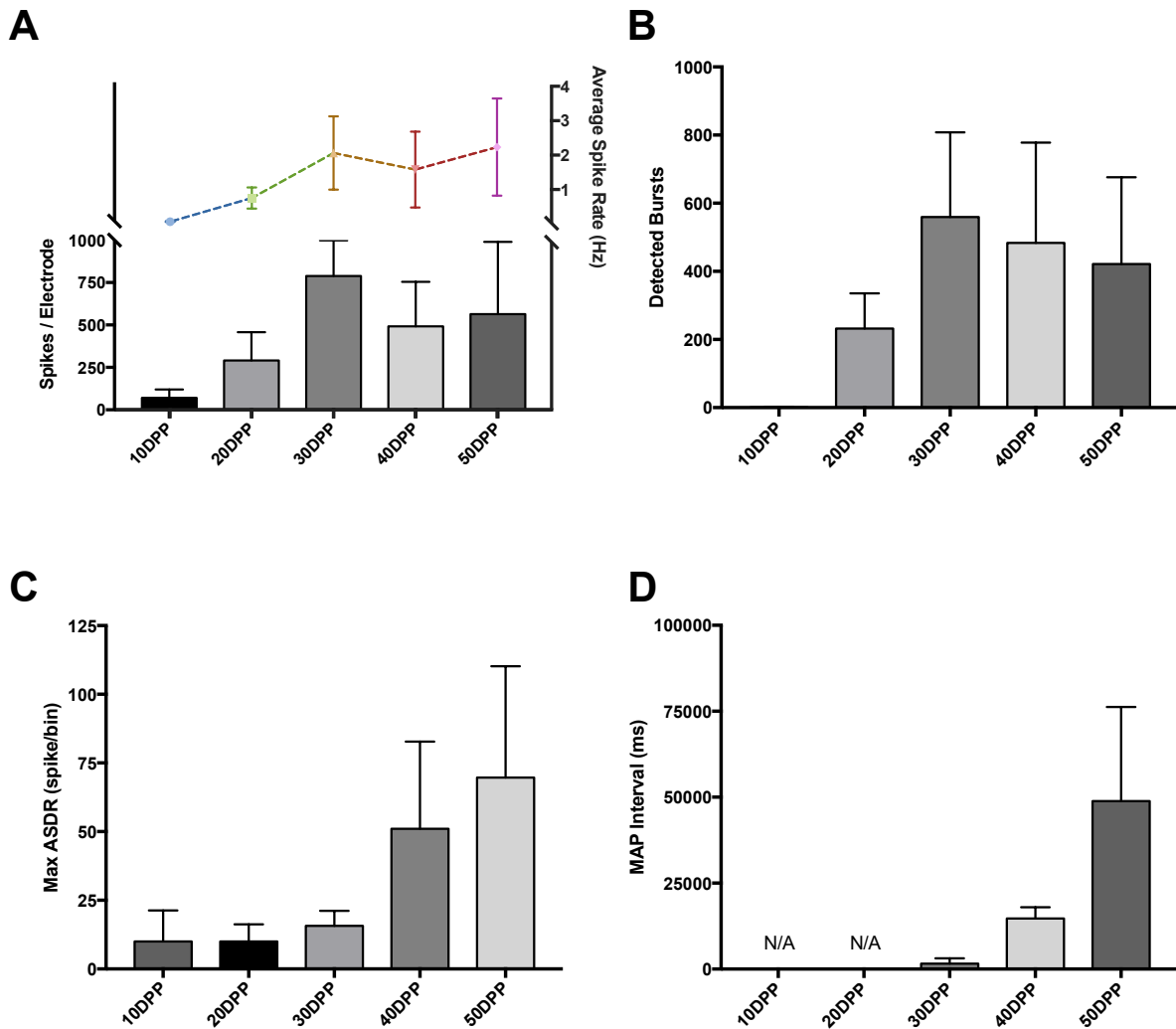


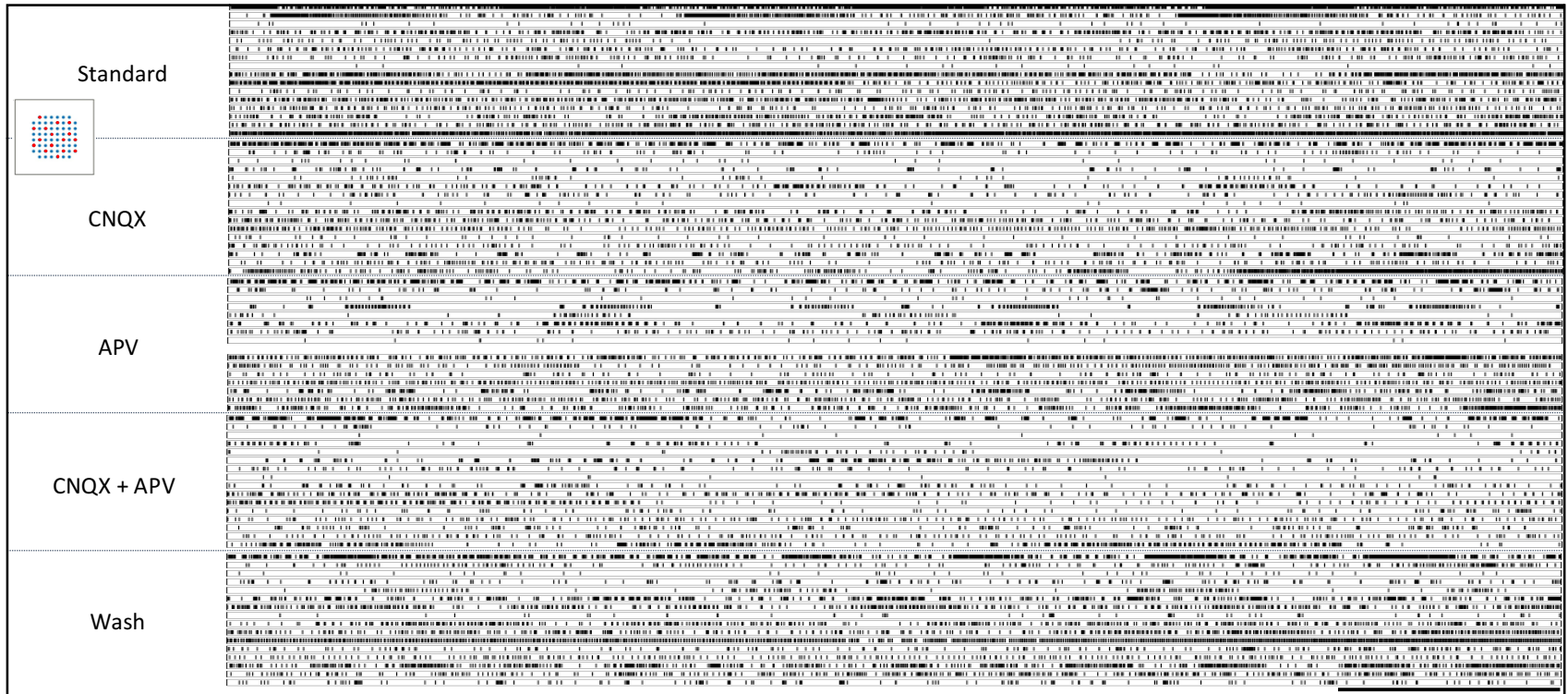
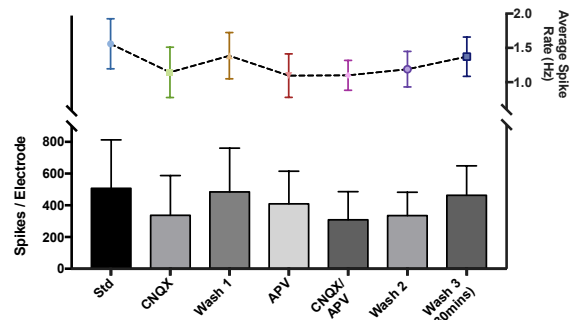
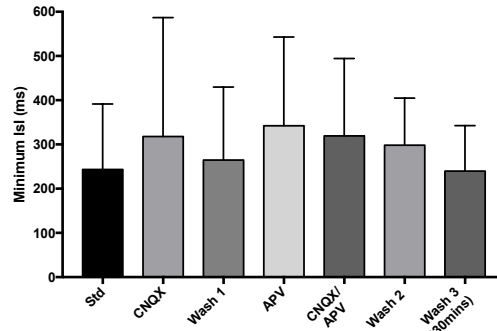
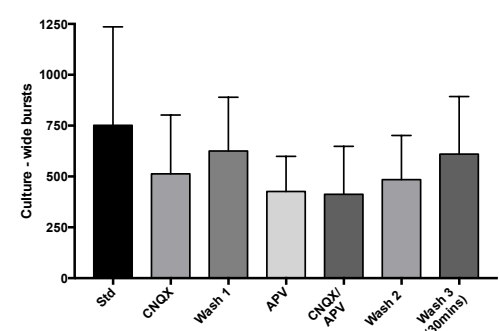
Figure 5.5 – Developmental excitability properties of iPS cell derived neurons cultured on and recorded using MEAs. Differentiating neurons were replated onto MEAs between Day 40 and Day 45 (post iPS cells) and cultured for up to 50 further days. The properties of the firing behaviour of the cultures changed markedly over development. Between 10 and 30 days post plating (DPP) there was large increases in the number of spikes detected (A - bars), the average spike rate (A – coloured line) and the number of bursts detected (B) in the cultures. This trend was partially reversed between 30 and 50DPP. The maximum array wide spike detection rate (ASDR) represents the maximum number of spikes detected across all analysed electrode in a single 200 ms bin. Between 10 and 30DPP, the maximum AWSR was stable but then increased dramatically at 40 and 50 DPP (C), reflecting the increased synchronisation of firing seen at these time points. A similar trend was seen in the MAP interval, which represents the median interval between the more active periods (MAPs) in each culture (D). N/A at 10 and 20DPP represent the fact that no MAP interval could be measured as there was no coordinated activity present at these time points. Between 30 and 50DPP, there was a large increase in the MAP interval, highlighting the changing nature of the network activity at these points. The data presented shows the mean \pm S.D, except spike rate which shows mean \pm SEM. All the data shows the summaries of at least 3 MEAs per differentiation over 3 differentiations.

5. Investigating network development in iPS cell derived neurons

5.3.3 Pharmacological profiling of iPS cell derived neurons during early development

The data presented in the previous section showed that the activity of neurons cultured on and recorded with MEAs changes throughout development, such that initial low-level, uncoordinated activity matures to high-level synchronised behaviour later in the culture. To establish a better understanding about the physiological nature of this activity throughout development, pharmacological agents were applied to cultures at different time points. To investigate the underlying nature of the activity early in development, with cultures showing un-coordinated events, a panel of agents were firstly applied to the cultures at 20DPP. As described in Chapter 2, drugs could not be applied to the cultures during recordings but instead were diluted in recording medium and applied serially along with washes to the cultures to be recorded.

To identify the role of excitatory synaptic communication in driving spontaneous AP activity in these neurons, inhibitors of NMDA and AMPA receptors were applied to the cultures. Figure 5.6A shows raster plots of the response of one culture to the drugs, both individually and simultaneously while Figures 5.6B-D show summary data for four excitability characteristics from all profiling experiments at this time point. Overall, it is noticeable from these experiments that there was no dramatic change in neuron excitability when the cultures are exposed to CNQX, APV or both drugs concurrently, as shown by the representative raster plots in Figure 5.6A. Both CNQX and APV applications alone caused a modest reduction in average spike rate from 1.56 ± 0.81 Hz to 1.14 ± 0.82 Hz and 1.10 ± 0.71 Hz respectively (figure 5.6B), with a correspondingly small increase in average inter-spike interval (ISI; Figure 5.6C). A larger decrease was seen in the number of detected bursts seen over the length of recordings, falling from 751.5 ± 242 in standard conditions to 512.8 ± 132.3 in the presence of CNQX and 426.5 ± 86.2 in the presence of APV (Figure 6.4D). The simultaneous application of both CNQX and APV produced similar changes to excitability as each drug alone and did not seem to produce a summative effect. For example, the average spike rate for cultures with APV+CNQX was 1.10 ± 0.48 Hz compared to 1.14 ± 0.82 Hz and 1.10 ± 0.71 Hz for CNQX and APV alone respectively. All the changes observed here were relatively small and several of the analysis measures were associated with a high degree of variation across the samples. Indeed, one-way ANOVA of each of the variables indicated that there was no significant variation due to application of the drugs (Table 5.1).

A**B****C****D**

5. Investigating network development in iPS cell derived neurons

Figure 5.6 – Early glutamatergic profiling of the activity recorded from iPS cell derived neurons cultured on and recorded with MEAs. 20 days after plating (20DPP), cultures were exposed to 50 μ M CNQX, 50 μ M APV or both simultaneously to study the contribution of glutamate neurotransmission to detected spikes. Serial application of CNQX, APV and both combined on a single array culture shows modest decreases in the number of detected spikes, with very little difference between the drug types (**A**). Basic excitatory analysis of all profiled cultures confirmed that there were no significant changes in the number of spikes detected and spike rate (**B**), the average inter spike interval (ISI, **C**) or in the number of bursts detected culture-wide (**D**) with either drug or both concurrently. **A** shows raster plots of the 16 highlighted electrodes (inset) across the drug applications. Scale bar shows 100 seconds. The data presented in **B**, **C** and **D** show the mean values \pm SD, except average spike rate which presents means \pm SEM. The summary plots represent data from 6 cultures across 3 differentiations.

5. Investigating network development in iPS cell derived neurons

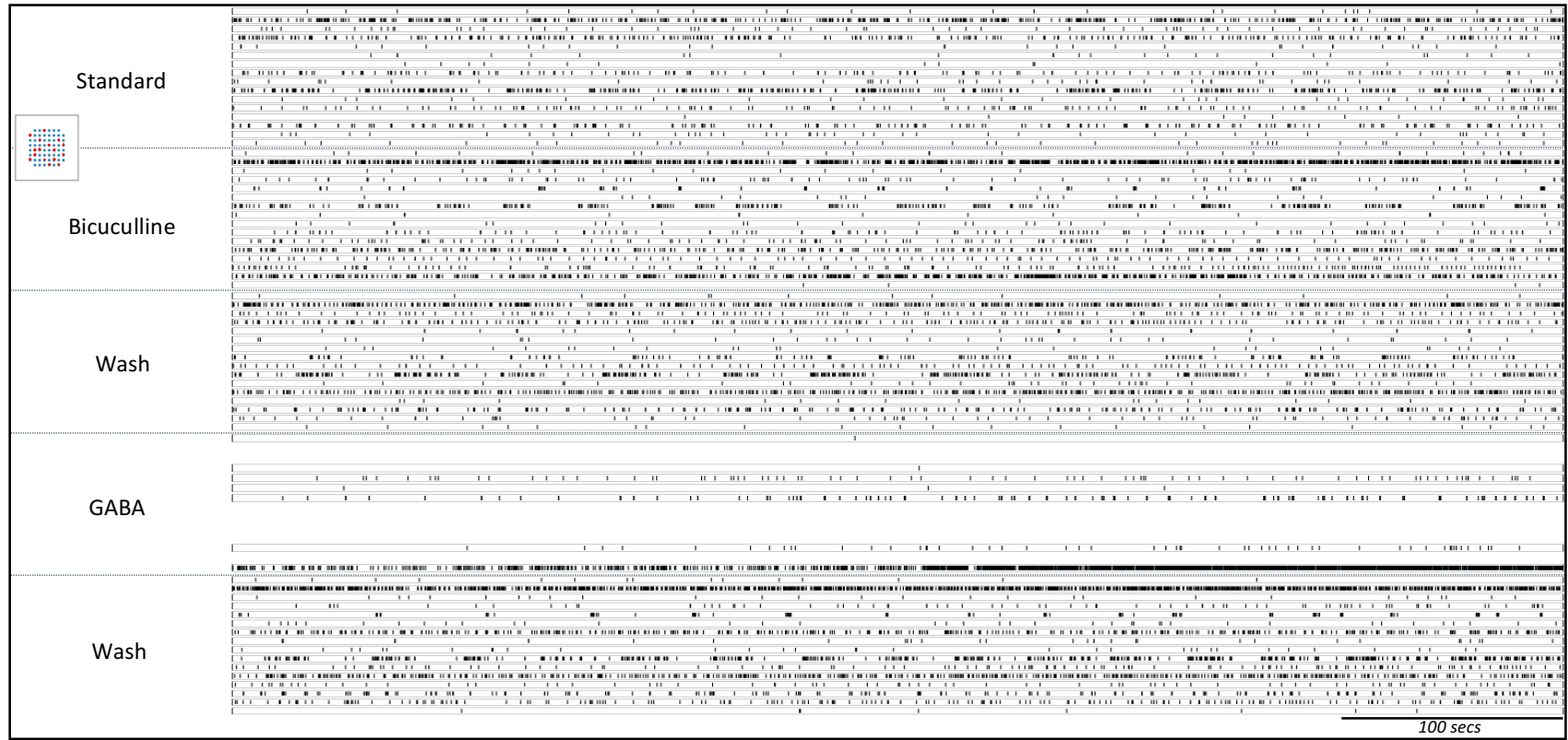
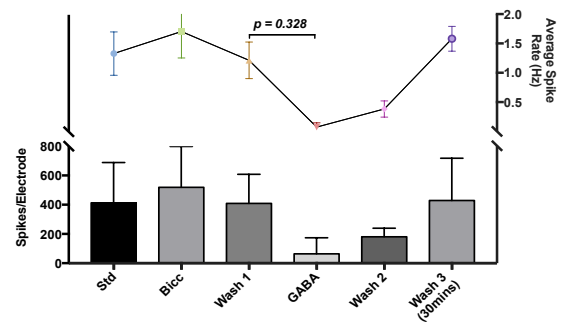
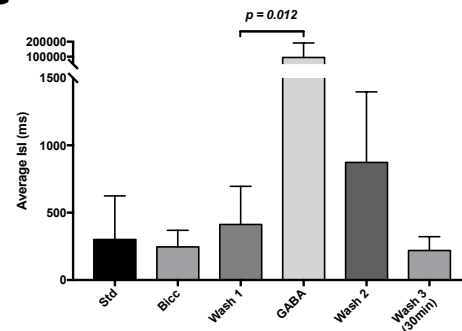
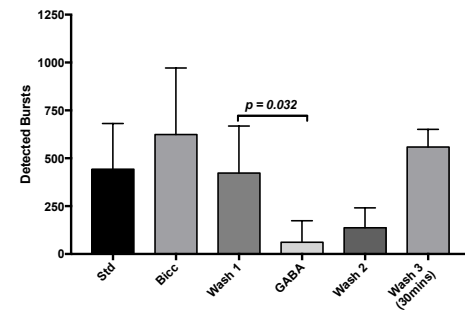
To investigate any role of inhibitory synaptic activity in these cultures at this early time point, a GABA_A receptor antagonist, bicuculline, and GABA itself was applied to cultures at 20DPP. Figure 5.7A shows activity raster plots of a representative culture throughout the experiments while Figure 5.7B-D shows summary data of four analyses measures for all cultures profiled at this time point. The application of bicuculline to the neuronal cultures, induced a small increase the average spike rate increased from 1.33 ± 0.73 Hz to 1.71 ± 0.78 Hz (Figure 5.7B). This was accompanied by a small corresponding decrease in the average ISI (Figure 5.7C) and an increase in the number of detected bursts (5.7D). A one-way ANOVA of these analysis measures showed that while the variation due to inhibitory drug application was significant, Tukey's multiple comparisons showed that the changes associated with bicuculline application were not significant (Table 5.1).

One of the key physiological milestones in neuronal development is the excitatory/inhibitory switch of GABA signalling. In early development, activation of ionotropic GABA_A receptors leads to an efflux of Cl⁻ ions and depolarisation of V_m , while in more mature neurons, activation of the same receptors leads to influx of Cl⁻ ions and membrane hyperpolarisation. This change is due to the shift in the reversal potential of chloride, driven by a developmental change in the relative expression of the K⁺/Cl⁻ co-transporters, NKCC1 and KCC2. To determine the chloride maturity of the neurons being cultured at 20DPP, 10 μ M GABA was applied to arrays and the activity recorded. The application of GABA to the arrays produced a dramatic decrease in the excitability of the cultures. This can be seen clearly for the culture represented by the raster plot in Figure 5.7A, where only around half of the electrodes showed any spike activity and those that did presented with very few. This trend was seen across all the cultures where an average spike rate of 1.21 ± 0.62 Hz (1st wash) decreased dramatically to 0.07 ± 0.12 Hz (Figure 5.7B). Again, this reduction in spike rate corresponded with a large increase in the average ISI (Figure 5.7C) and a decrease in the number of detected bursts from 423 ± 145.6 to 137 ± 107 (Figure 5.7D). Tukey's multiple comparisons following one-way ANOVA showed that these changes were significant compared to the corresponding preceding wash (Table 5.1). Importantly, all three characteristics returned to baseline following washes, although unlike CNQX and APV, this required an extended period of washing. These results strongly suggest that, even at this relatively early time in development, activation of GABA_A receptors leads to inhibitory hyperpolarisation of iPS cell derived neurons.

5. Investigating network development in iPS cell derived neurons

Table 5.1 – Summary of the statistics for the comparisons of general excitability characteristics of iPS cell derived neurons recorded with MEAs in response to pharmacological profiling at 20DPP.

Excitatory profiling			
	One way ANOVA	Tukey's Multiple comparisons	
		Mean difference [95% CI]	Adjusted p value
Average Spike rate (Hz)	F(9, 40) = 0.508; R ² = 0.1026 p = 0.859	No post – hoc comparisons	
Average inter spike interval (ms)	F(9, 40) = 0.321; R ² = 0.063 p = 0.962		
Bursts	F(9, 40) = 1.147; R ² = 0.256 p = 0.3624		
Inhibitory profiling			
	One way ANOVA	Tukey's Multiple comparisons	
		Mean difference [95% CI]	Adjusted p value
Average Spike rate (Hz)	F(5, 15) = 3.770; R ² = 0.557 p = 0.021		
<i>Wash 1 vs GABA</i>		1.139 [-0.384 – 2.662]	0.0328
Average inter spike interval (ms)	F(5, 16) = 3.957; R ² = 0.553 p = 0.0158		
<i>Wash 1 vs GABA</i>		-94505 [-174995 – -14015]	0.0168
Bursts	F(5, 15) = 3.471; R ² = 0.536 p = 0.078		
<i>Wash 1 vs GABA</i>		361.8 [-162.9 – 886.4]	0.0323

A**B****C****D**

5. Investigating network development in iPS cell derived neurons

Figure 5.7 – Early inhibitory profiling of IPS cell derived neurons cultured on and recorded with MEAs. To determine any role of GABAergic activity in the MEA cultures at 20 days post plating (20DPP), neurons were exposed to the GABA_A antagonist bicuculline and GABA itself. 10 μ M bicuculline slightly increased the excitability of cultures, in terms of spike number/rate rate (**B**), inter-spike interval (ISI, **C**) and the number of detected bursts (**D**). 1 μ M GABA almost entirely blocked all spontaneous activity. **A** shows the spontaneous activity as raster plots in response to drug application for one representative MEA culture, showing the same 16 electrodes across the experiment. The selected electrodes are shown in the inset. B-D show summary plots of the four analysis measures from at least 4 arrays across two differentiations. Bars show means + SD, except for average spike rate where they show means \pm SEM.

5. Investigating network development in iPS cell derived neurons

5.3.4 Excitatory pharmacological profiling of iPS cell derived neurons in late development

The experiments in section 5.3.3 highlighted the limited role of glutamatergic synaptic activity on spontaneous action potentials at 20DPP, a time point at which culture-wide activity was uncoordinated. To study the role of glutamatergic function on the network behaviour detected in these cultures later in development, a similar set of experiments with CNQX and APV was performed on MEA cultures at 50DPP. Figure 5.8 presents the raster and ASDR plots for one array culture exposed serially to CNQX and APV (with washes), while Figure 5.9 presents the summary data of five characteristics for all the cultures profiled.

Firstly, it was clear that application of both CNQX and APV had a dramatic effect on the synchronised network behaviour of the culture seen in the standard conditions (Figure 5.8). Indeed, the presence of both drugs (individually) completely attenuated the coordinated activity seen across the culture. This effect was seen across all the profiled cultures, highlighted by the large significant decrease in the max ASDR with the application of both CNQX and APV (Figure 5.9C; Table 5.2) and the lack of calculable MAP intervals for these conditions (Figure 5.9D). Washes following exposure to either compound restored both the synchronised behaviour and the analysis measures back to baseline. This clearly suggests that both AMPA and NMDA receptor mediated neurotransmission is required for the synchronised behaviour seen in these cultures at later time points and that this behaviour is indeed the manifestation of functional neuronal networks.

Although both CNQX and APV caused a loss of the synchronised behaviour, they had differential effects on some more basic excitatory characteristics. Specifically, it was interesting that CNQX application caused a small increase in the average spike rate from 3.13 ± 1.12 Hz to 4.01 ± 0.79 Hz, while treatment with APV caused a decrease in spike rate, from 3.1 ± 1.31 Hz (Wash 1) to 2.65 ± 0.49 Hz (Figure 5.9A), although these comparisons were not significant following one-way ANOVA. However, these contrasting effects can be seen in the example presented in Figure 5.8, with both the raster and ASDR plots highlighting a higher rate of firing in the culture when treated with CNQX over APV. Both CNQX and APV exposure caused a decrease in the number of detected bursts, falling from 881.3 ± 321.6 to 622 ± 420.1 for CNQX and a larger decrease from 1204 ± 402.8 (wash 1) to 490.7 ± 256.3 for APV (Figure 5.9B),

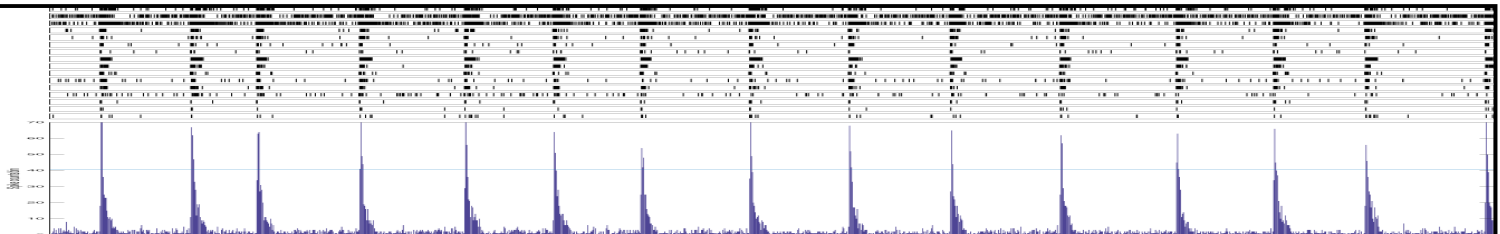
5. Investigating network development in iPS cell derived neurons

although this variation was not significant (Table 5.2). Washes following exposure to either compound rescued both spike rate and detected bursts back to or above baseline.

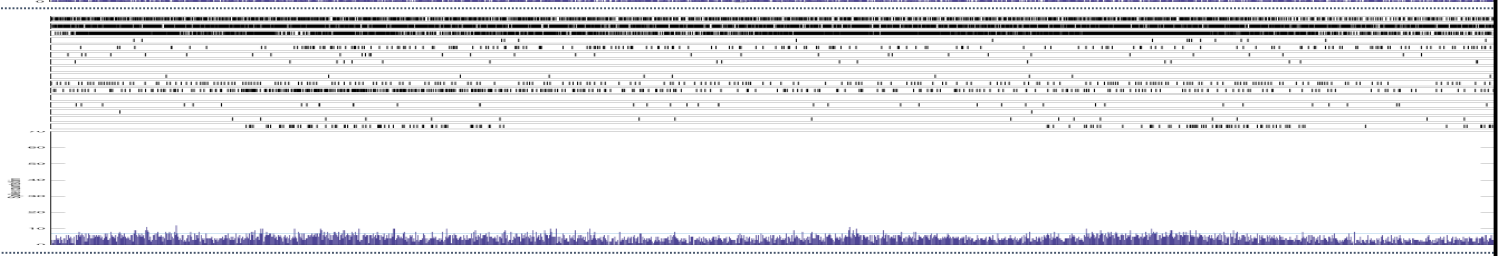
Table 5.2 – Summary of the statistics for the comparisons of excitability and network characteristics of iPS cell derived neurons recorded with MEAs in response to pharmacological profiling at 50DPP.

Excitatory profiling			
	One way ANOVA	Tukey's Multiple comparisons	
		Mean difference [95% CI]	Adjusted p value
Average Spike rate (Hz)	F(11, 10) = 0.453; R ² = 0.1534 p = 0.768	No post – hoc comparisons	
Bursts	F(11, 10) = 1.892; R ² = 0.431 p = 0.188		
Max ASDR (spikes/bin)			
<i>Std vs CNQX</i>	F(11, 10) = 4.466; R ² = 0.545 p = 0.014	53 [-35.86 – 141.9]	0.038
<i>CNQX vs Wash1</i>		-97 [-185.9 – -8.138]	0.023
<i>Wash1 vs APV</i>		98.75 [9.88 – 187.6]	0.026
<i>APV vs Wash2</i>		-67.75 [-156.6 – 21.11]	0.028
MAP interval (ms)		No ANOVA possible	
Inhibitory profiling			
	One way ANOVA	Tukey's Multiple comparisons	
		Mean difference [95% CI]	Adjusted p value
Average Spike rate (Hz)	F(9, 14) = 2.338; R ² = 0.505 p = 0.092	No post – hoc comparisons	
Bursts	F(9, 14) = 3.915; R ² = 0.626 p = 0.0166		
<i>Wash 2 vs GABA</i>	F(9, 14) = 3.915; R ² = 0.626 p = 0.0166	894 [-0.771 – 1789]	0.0203
<i>GABA vs Wash 3</i>		-609.3 [-1504 – 285.4]	0.0497
Max ASDR (spikes/bin)			
<i>Wash 2 vs GABA</i>	F(9, 14) = 2.411; R ² = 0.475 p = 0.0416	192 [-20.49 – 334.5]	0.0377
<i>GABA vs Wash 3</i>		-126.3 [-308.8 – 56.16]	0.0428
MAP interval (ms)			
<i>Std vs Bic</i>	F(9, 18) = 2.411; R ² = 0.553 p = 0.0081	9775 [504.7 – 19045]	0.0345
<i>Bic vs Wash 1</i>		-6725 [-15995 – 2545]	0.0315
<i>Wash 1 vs Picr</i>		5707 [-3564 – 14977]	0.0402
<i>Picr vs Wash2</i>		-6332 [-15602 – 2939]	0.0263

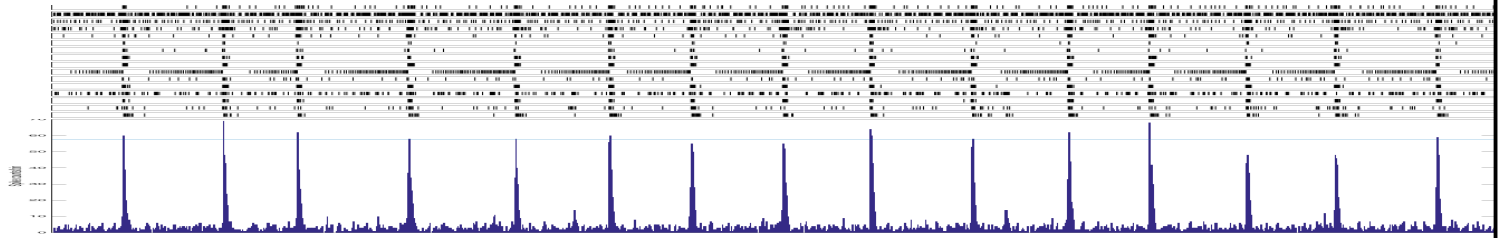
Standard



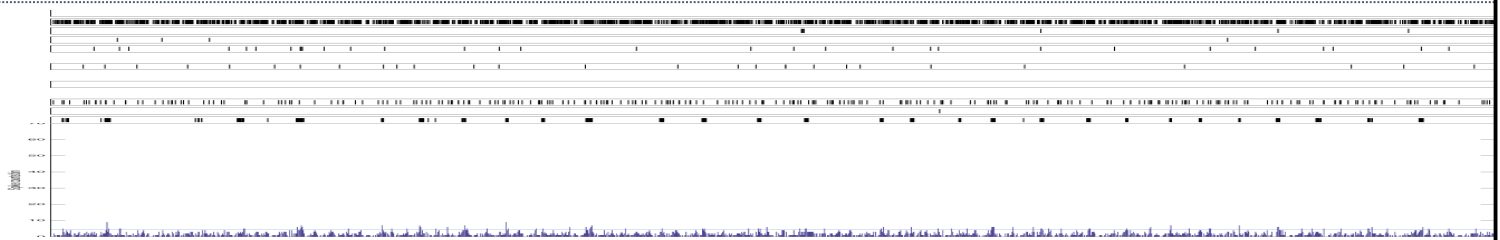
CNQX



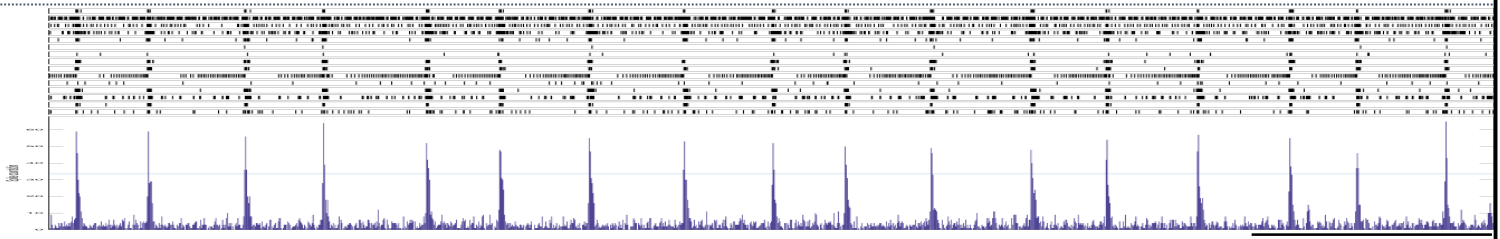
Wash



APV



Wash



5. Investigating network development in iPS cell derived neurons

Figure 5.8 – Neural network behaviour of iPS cell derived neurons requires both AMPA and NMDA receptor mediated synaptic activity. Neurons cultured for 50 days post plating (DPP) form networks which manifest on MEA recordings as cyclic culture-wide synchronised firing. This behaviour is abolished with both application of CNQX and APV (both 50 μ M) and can be recovered with washes. For each condition, top panel shows raster plots of detected spikes from the 16 culture-wide electrodes highlighted in the inset; bottom panel shows ASDR plots which present the summed number of spikes seen across the culture in 200ms bins, y units = spikes/bin. The data presented here is from the same culture, with conditions recorded serially. The same behaviour has been observed in at least 7 cultures across 3 differentiations. Scale bar = 100 seconds.

5. Investigating network development in iPS cell derived neurons

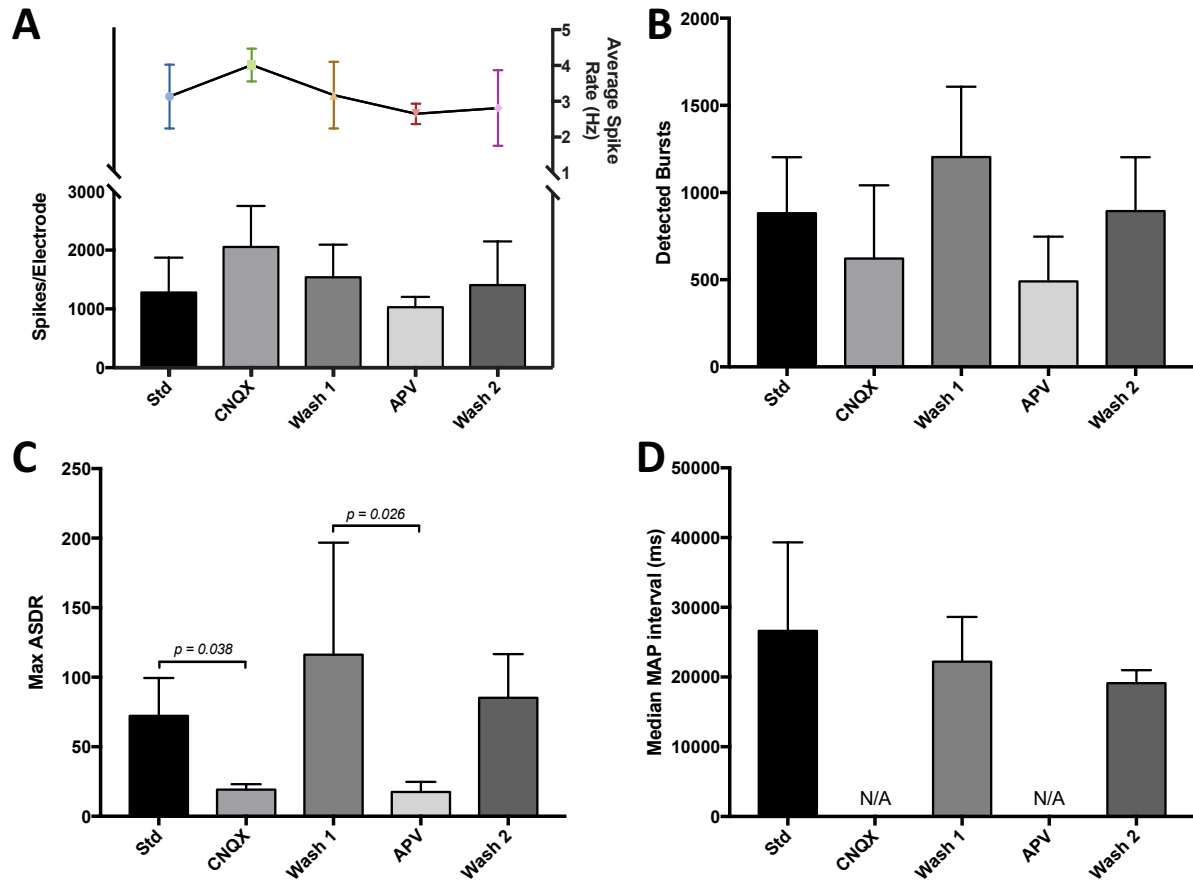


Figure 5.9 – Glutamatergic pharmacological profiling of iPS cell derived neurons cultured on and recorded with MEAs 50 days after plating. After culturing neurons on arrays for 50 days, the activity of cultures was synchronised, such that activity could be divided into less active and more active periods (LAPs and MAPs). To determine whether this coordinated activity was caused by underlying local networks, 50 μ M APV and 50 μ M CNQX were applied to cultures at this developed stage to identify the role of NMDA and AMPA receptors respectively. Application of both drugs completely attenuated the coordinated activity, shown here by the reduction in max array-wide spike rate (C) and median MAP interval (D). Drug application also had small but insignificant effects on the number of detected bursts (B) but generally limited effects on basal excitability of cultures (A). In A-D, data show means + SD, except average spike rate, which shows means \pm SEM. Summary data shows results from at least 3 arrays from three differentiations.

5. Investigating network development in iPS cell derived neurons

5.3.5 Inhibitory pharmacological profiling of iPS cell derived neurons in late development

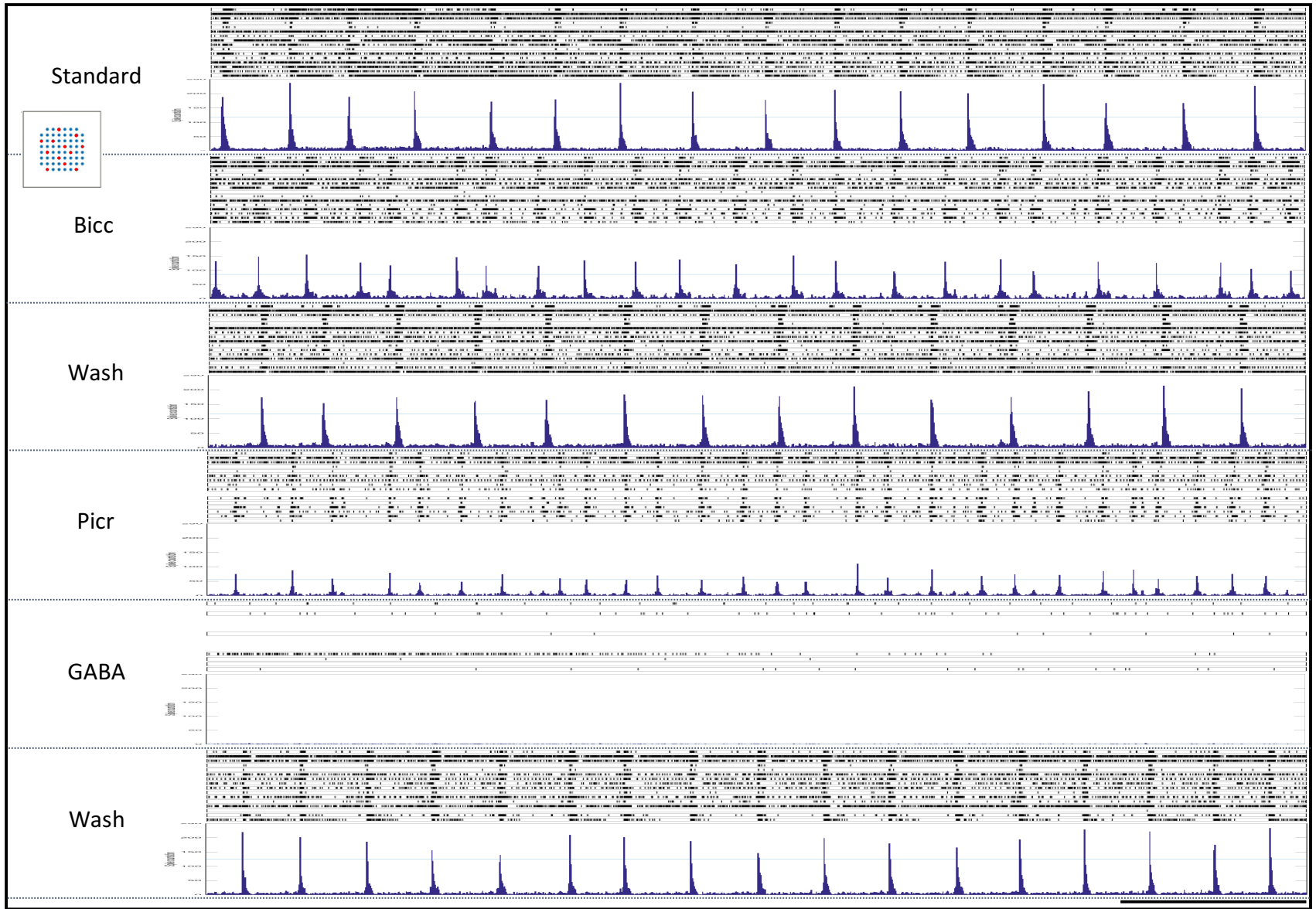
The previous section established that the synchronised activity that develops in these array cultures is mediated by glutamatergic signalling via AMPA and NMDA receptors. However, in intact neural systems, the regulation of functional networks is thought to also involve interneurons and GABAergic signalling. To investigate the role of inhibitory signalling in these iPS cell derived cultures later in development and its contribution to the network function observed here, two GABA_A inhibitors and GABA itself were applied acutely to cultures and recorded. Both bicuculline and picrotoxin were used for these experiments to gain a fuller understanding about the nature of the GABAergic contribution to the network behaviour and to provide confidence that any detected alterations are down to GABA signalling itself. While bicuculline is a classical orthosteric competitive antagonist of GABA_A receptors, picrotoxin is thought to act as non-competitive channel blocker or as an allosteric inhibitor which binds to ligand-bound form of the receptor complex. As before, Figure 5.10 presents raster and ASDR plots of the recorded activity from one culture over the course of the experiment, while Figure 5.11 presents summary data from five analysis measures for all cultures in the experiment.

The application of both bicuculline and picrotoxin to the array culture in figure 5.10 induced a number of interesting changes in the culture's activity. First, the presence of both antagonists caused a reduction in the interval between the the MAPs. This can be seen most clearly on the ASDR plots which show an increase in the number of peaks detected across the 10 minute recordings in both drug conditions. Indeed, this effect was seen in all the profiled cultures with bicuculline causing an average reduction in MAP interval from 25167 ± 6561 ms to 14533 ± 4086 ms, while picrotoxin induced an attenuation from 22300 ± 3236 ms (1st wash) to 16091 ± 5237 ms (figure 5.11D). The variation caused by these drugs to the MAP interval was found to be significant by one-way ANOVA, with the comparisons of bicuculline/picrotoxin to their respective standard conditions also significant (Table 5.2). Second, the ASDR plots in figure 5.10 show clearly that both bicuculline and picrotoxin caused a decrease in the number of spikes seen in each MAP peak, with picrotoxin having a stronger effect than bicuculline. Again, this trend was seen across all cultures, where an average max ASDR reduced from 195.5 ± 77.5 to 101.5 ± 49.5 and from 147.5 ± 84.5 to 84.5 ± 37.48 with bicuculline and picrotoxin respectively (figure 5.11C), although these changes were not found to be significant (Table 6.2).

5. Investigating network development in iPS cell derived neurons

The raster plots of the array shown in figure 5.10 also hint at a change in the general excitability of the culture when treated with both GABA_A antagonists. Overall, bicuculline and picrotoxin exposure appeared to induce a general decrease in the number of spikes detected across the array. However, closer examination of this particular culture shows that the antagonists are having a larger effect on those electrodes which continue to fire continuously throughout the length of the recording, for example, the 2nd 3rd and last electrode trace on the raster plots. Across the cultures as a whole, bicuculline had very little effect on the average spike rate of cultures, while picrotoxin decreased the average spike rate from 3.56 ± 1.34 Hz (1st wash) to 1.93 ± 0.72 Hz (figure 5.11A), although this decrease was not significant.

The early profiling at 20DPP described in section 5.3.3 suggested that even at that early time point, the action of GABA neurotransmission was inhibitory as shown by the widespread loss of activity. To assess the function of GABA signalling at this later time point, 10 μ M GABA was applied to cultures in the same way. Unsurprisingly, exposure to GABA caused almost complete loss of activity in the cultures, as shown by the representative activity plots in figure 5.10 and the almost complete attenuation of average spike rate (figure 5.11A), detected bursts (5.11B), max ASDR (5.11C) and loss of calculable MAP interval (figure 5.11D; see table 5.2 for statistics). All activity characteristics were returned to baseline following media washes.



5. Investigating network development in iPS cell derived neurons

Figure 5.10 – Inhibitory profiling of iPS cell derived neuronal cultures exhibiting synchronised network behaviour. Neurons cultured for 50 days post plating (DPP) form networks which manifest as cyclic culture-wide synchronised firing. This behaviour is characterised by more active periods (MAPs) which present as peaks on array wide spike detection rate (ASDR) plots. The interval between these peaks (MAP interval) is attenuated with the GABA_A competitive antagonist bicuculline (10 μ M) and the allosteric GABA_A channel blocker picrotoxin (2 μ M). This effect is rescued following media washes. Application of 1 μ M GABA to the culture blocked the synchronised behaviour and almost completely blocked all activity. Both spontaneous activity and coordinated culture wide activity returned following media washes. For each condition, top panel shows raster plots of detected spikes from the 16 culture-wide electrodes highlighted in the inset; bottom panel shows ASDR plots which present the summed number of spikes seen across the culture in 200ms bins, y units = spikes/bin. The data presented here is from the same culture and from the same 16 electrodes shown in the inset, with conditions recorded serially. The same behaviour has been observed in at least 4 cultures in 2 differentiations. Scale bar = 100 seconds.

5. Investigating network development in iPS cell derived neurons

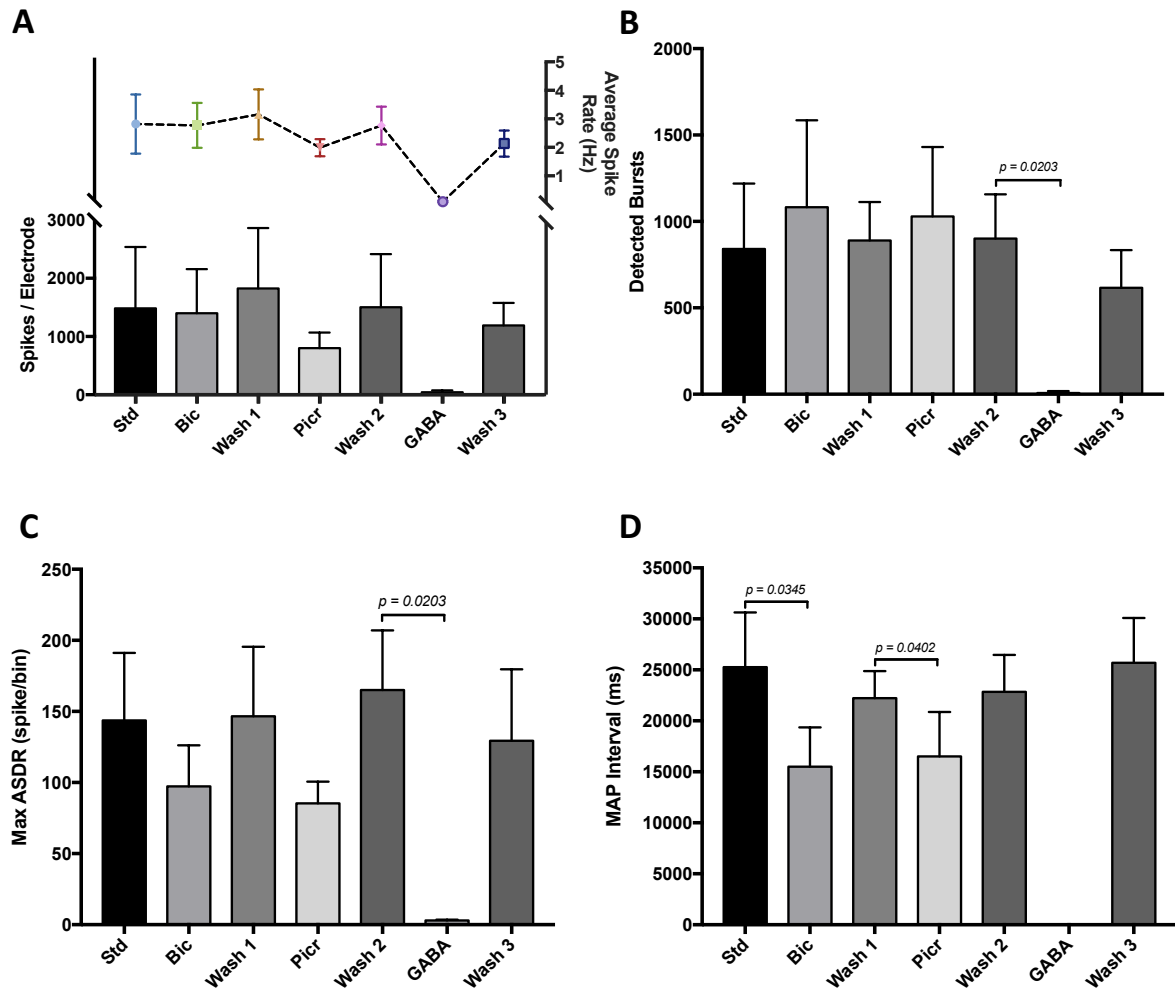


Figure 5.11 – Late inhibitory profiling of iPS cell derived neurons cultured on and recorded with MEAs. 50 days after plating, neuronal cultures showing coordinated network activity were exposed to two GABA_A inhibitors, bicuculline (Bic; 10 μM) and picrotoxin (Picr; 2 μM), and GABA (1 μM) to assess the role of inhibitory signalling in these cultures and to the network behaviour. While bicuculline had very little effect on the average spike number/spike rate, picrotoxin induced small but insignificant reduction in both (A). Both antagonists caused an insignificant increase in the number of detected bursts in the cultures (B). Importantly, both drugs had noticeable effect on the network activity of the cultures: both induced a reduction in the maximum array wide spike rate, indicating that the peaks of the more active periods (MAPs) contained less spikes culture wide than control conditions (C); both drugs also caused a significant reduction in the average MAP interval – the period between the peaks of synchronised cultured wide activity (D). Application of GABA caused a dramatic reduction in basal excitability, number of bursts and Max ASDR. It also blocked all synchronised activity meaning a MAP interval was not calculable. Wash recordings after all applications showed a return to baseline for all measures. The final wash condition represents recordings following two washes over period of 30 mins. All summary plots show means ± SD except average spike rate which shows means ± SEM. p values show results of Tukey's multiple comparisons following one-way ANOVA. The data presents summaries from at least 5 arrays from two differentiations.

5. Investigating network development in iPS cell derived neurons

5.3.6 IBJ4 iPS cells derived neuronal cultures contain GABAergic interneurons

The results presented in section 5.3.3 and 5.3.5 clearly highlighted a role for interneurons in these iPS cells derived cultures, both in terms of general excitability and the regulation of synchronised network activity. However, the differentiation protocols used here are based on those used to produce glutamatergic projection neurons – indeed, the immunocytochemistry results presented in 5.3.1 strongly suggest that this is the identify of the majority of neurons. Furthermore, the differentiation of interneurons from hPS cells generally requires additional morphogens (e.g. sonic hedgehog) in order to ventralise cells, mimicking interneuron development within the medial ganglionic eminence. To determine whether interneurons could be identified in these cultures, as suggested by the pharmacology MEA experiments, cells were fixed and stained at 50DPP for GAD67, one of the primary enzymes involved in the synthesis of GABA.

Fixed cultures from two differentiations only were available for GAD67 staining, however this provided enough cells to permit a limited quantification of stained neurons. In total, 10 images across two coverslips per differentiation were counted. Interestingly, a small number of GAD67 +ve neurons were identified in coverslips from both of the differentiations assessed (Figure 5.12A; neuronal identify confirmed with MAP2 staining). Quantification of the number of GAD67/MAP2 +ve neurons in each imaged region determined that a mean of 4.7 ± 2.0 % and 3.94 ± 2.32 % of MAP2 +ve neurons were also GAD67+ve for the two differentiations respectively (Figure 5.12B). Therefore, based on these results it can be determined that these cultures contain around 4-5% interneurons. It should be noted that all staining is performed on cells parallel to the array cultures – it is possible that the composition of these neuron populations varies compared to that on the MEAs.

5. Investigating network development in iPS cell derived neurons

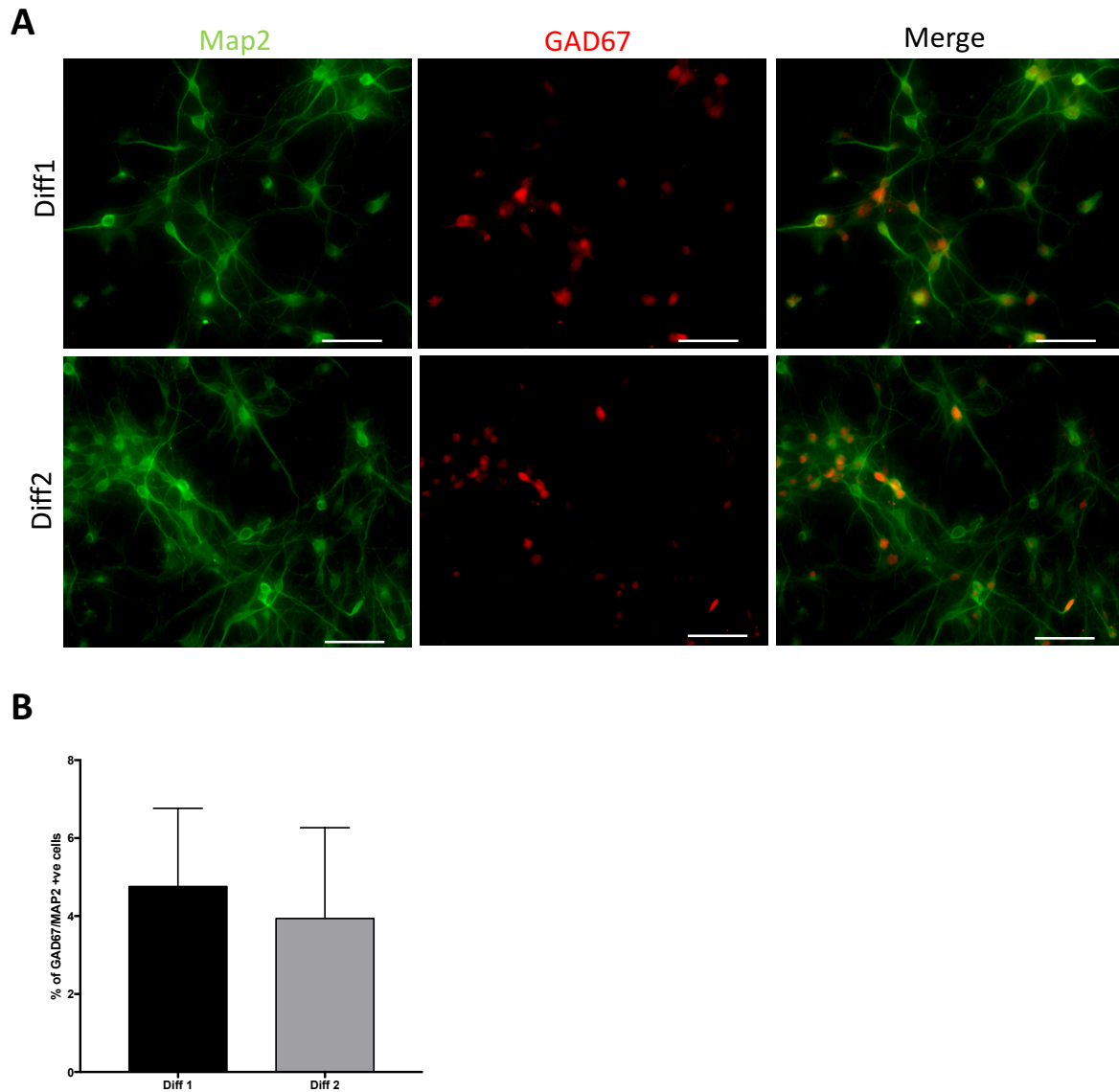


Figure 6.12 – Cultures of IBJ4 iPS cells derived cortical projection neurons contain a small population of interneurons. Pharmacological experiments with multi electrode array (MEA) cultures recording spontaneous network activity provided strong evidence for the presence of GABAergic interneurons in cultures and their role in the regulation of network activity. To determine whether interneurons could be observed in these differentiations, parallel cultures on coverslips were stained for GAD67, a key enzyme responsible for the production of GABA. Assessment of interneuron populations was limited to two differentiations following identical protocols. Panels in **A** show images from each differentiation and represent culture regions with higher than average GAD67 staining to highlight expression. Cells were stained at 50DPP. A limited quantitative assessment of GAD67 +ve neurons in the two differentiations showed that interneurons account for around 4-5% of Map2+ve neurons in the cultures (**B**). Summary plots show means of counts from at least 7 regions across 2 coverslips per differentiation. Error bars show SD.

5. Investigating network development in iPS cell derived neurons

5.3.7 Synchronised network activity in MEA cultures is regulated by L-type calcium channels

To investigate further the physiology of the neuron cultures at the developed time point and to study what other underlying mechanisms could be contributing to the network activity observed in these cultures, an inhibitor of L-type calcium channels, diltiazem, was applied acutely to the cultures during recordings at 50DPP. This target was chosen for a number of reasons. Firstly, calcium signalling via L-type channels has been shown to be involved in the regulation of oscillatory behaviour in some brain regions (He *et al.*, 2005; Przewlocki *et al.*, 1999). Secondly, NMDA mediated network signalling is thought to be regulated via calcium homeostasis mechanism, partly through L-type calcium channels (Wang *et al.*, 2013; Lee and Chung, 2014). Finally, recent genetic studies have implicated L-type calcium channels in increased risk for a range of neurological disorders, including schizophrenia, autism, depression and epilepsies; all pathologies with strong evidence for aberrant network signalling (Schizophrenia Working Group of the Psychiatric Genomics Consortium, 2014; Zamponi *et al.*, 2015).

Very little is known about the action of diltiazem on cell cultures and especially on neurons derived from hPS cells. To determine the range of any action of diltiazem on these neurons, a series of concentrations were applied acutely and serially to cultures. Figure 5.13 presents the results of these experiments from one representative culture in the form of raster and ASDR plots while figure 5.14 presents the summary data from all profiled cultures.

The exposure of four concentrations of diltiazem to the array cultures had several effects on the firing patterns of the neurons. Most strikingly, application of diltiazem induced a reduction in the MAP interval of the synchronised cultures, with the extent of this attenuation dependent upon the dose of the drug (Figure 5.13). This effect was seen across all the cultures, where the average MAP interval decreased from 62650 ± 37309 ms in standard conditions, to 39575 ± 11359 ms (1 μ M), 22900 ± 12709 ms (2 μ M) and to 20525 ± 9412 ms (5 μ M; Figure 5.14D). One-way ANOVA showed that this variation was significant and Tukey's multiple comparisons revealed that the decrease in MAP interval reached significance at 2 μ M (Table 5.3). Exposure to 10 μ M diltiazem ablated the synchronised behaviour of the cultures such that a MAP interval could not be calculated. Media washes restored the network activity and the average MAP interval to 30200 ± 4042 ms. Exposing cultures to diltiazem also had effects on the number of

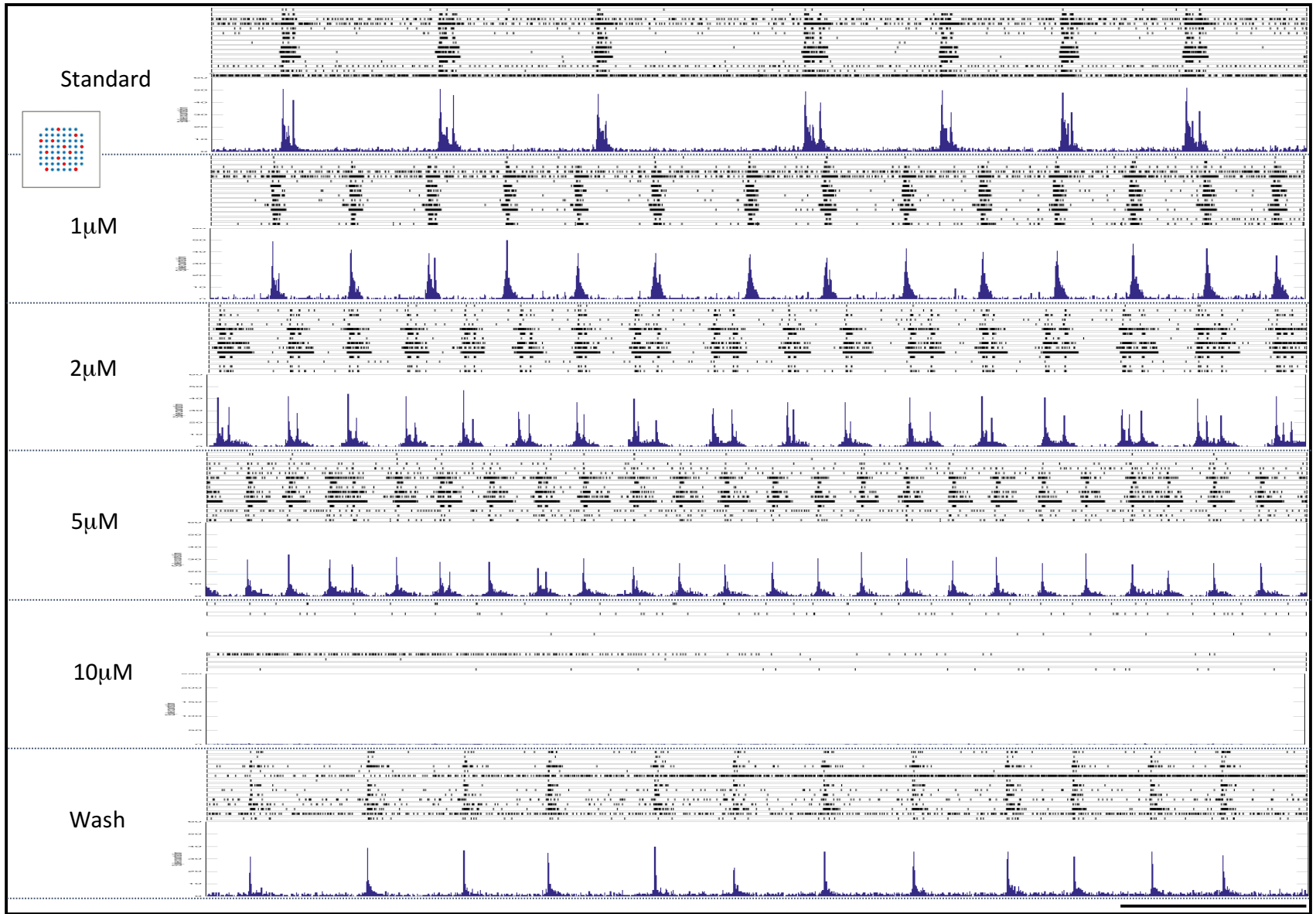
5. Investigating network development in iPS cell derived neurons

spikes seen in the MAP peaks. Up to 2 μM there was little change on the max ASDR however with both 5 and 10 μM treatment there was an attenuation of this rate, falling from 35 ± 15.68 to 15.75 ± 13.52 at 5 μM and to 10.5 ± 12.34 at 10 μM (Figure 5.14C). While the overall variation of max ASDR due to diltiazem was significant, no post-hoc comparisons were (Table 5.3). The max array wide spike rate returned back to baseline following washes.

Concentrations of diltiazem up to 5 μM had mixed effects on the tonic excitation of the cultures. Overall there was little change to the average spike rate (Figure 5.14A) or the number of bursts (Figure 5.14B) up to 2 μM . From 5 μM , there was a decrease observed in both average spike rate and the number of bursts, although this change was not significant (Table 5.3). Indeed, while these changes in basal activity up to and including 5 μM treatment cannot be observed in the representative culture shown in figure 5.13, it is very clear that 10 μM exposure causes a dramatic reduction in activity. This could perhaps represent the threshold at which diltiazem is acting specifically on L-type channels and instead has affinity for calcium channels more broadly.

Table 5.3 – Summary of the statistics for the comparisons of excitability and network characteristics of iPS cell derived neurons recorded with MEAs in response to the L-type calcium channel blocker diltiazem.

L-type calcium channel profiling			
	One way ANOVA	Tukey's Multiple comparisons	
		Mean difference [95% CI]	Adjusted p value
Average Spike rate (Hz)	$F(9, 16) = 2.523; R^2 = 0.440$ $p = 0.724$	<i>No post – hoc comparisons</i>	
Bursts	$F(9, 16) = 1.652; R^2 = 0.341$ $p = 0.203$		
Max ASDR (spikes/bin)	$F(9, 10) = 2.708; R^2 = 0.429$ $p = 0.043$		
MAP interval (ms)			
	$F(9, 16) = 5.281; R^2 = 0.627$ $p = 0.0047$		
Std vs 2 μM		39750 [-1792 – 81292]	0.0378
Std vs 5 μM		42125 [583.2 – 83667]	0.0359



5. Investigating network development in iPS cell derived neurons

Figure 5.13 – The interval between more active periods (MAPs) observed in synchronised iPS cell derived neuronal cultures is attenuated by blocking L-type calcium channels. Neurons cultured for 50 days post plating (DPP) form networks which manifest as cyclic culture-wide synchronised firing. This behaviour is characterised by MAP peaks representing high-frequency firing across the culture. The interval between these peaks (MAP interval) is attenuated by application of the L-type calcium channel blocker diltiazem, in a dose-dependent manner. Application of 10 μ M diltiazem inhibits the majority of culture activity. For each condition, top panel shows raster plots of detected spikes from the 16 electrodes highlighted in the inset; bottom panel shows ASDR plots which present the summed number of spikes seen across the culture in 200ms bins, y units = spikes/bin. The data presented here is from the same culture and the same electrodes, shown in the inset, with conditions recorded serially. The same behaviour has been observed in at least 5 cultures across 2 differentiations. Scale bar = 100 seconds.

5. Investigating network development in iPS cell derived neurons

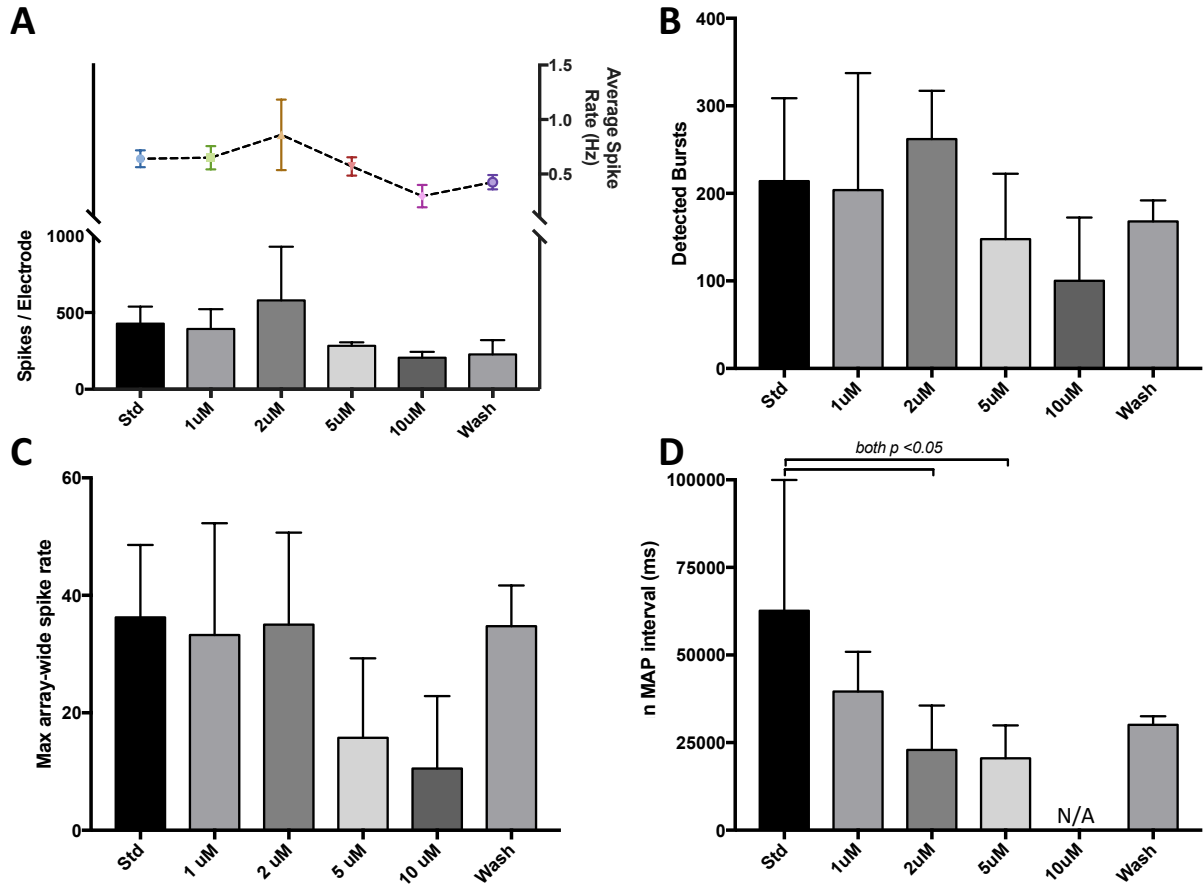


Figure 5.14 – Network activity in iPS cell derived neural cultures is regulated by L-type calcium channels in a dose dependent manner. MEA cultures at 50DPP were exposed to increasing concentrations of diltiazem, a specific L-type calcium channel blocker during recordings. Diltiazem had limited effects on spike number/spike rate (A) and number of detected bursts (B) up to 5 μM; after which activity decreased. This trend was also seen in the maximum array wide spike detection rate (C) which describes the maximum number of spikes seen across the culture in a given 200 ms bin. Diltiazem had a dose dependant attenuation effect on the more active period interval (MAP interval); which describes the interval between coordinated culture wide MAPs (D). 10 μM diltiazem blocked network activity entirely, meaning a MAP interval was not calculable. All summary plots show means + SD, except average spike rate which shows means ± SEM. Plots represent summary data from 5 arrays across two differentiations.

5. Investigating network development in iPS cell derived neurons

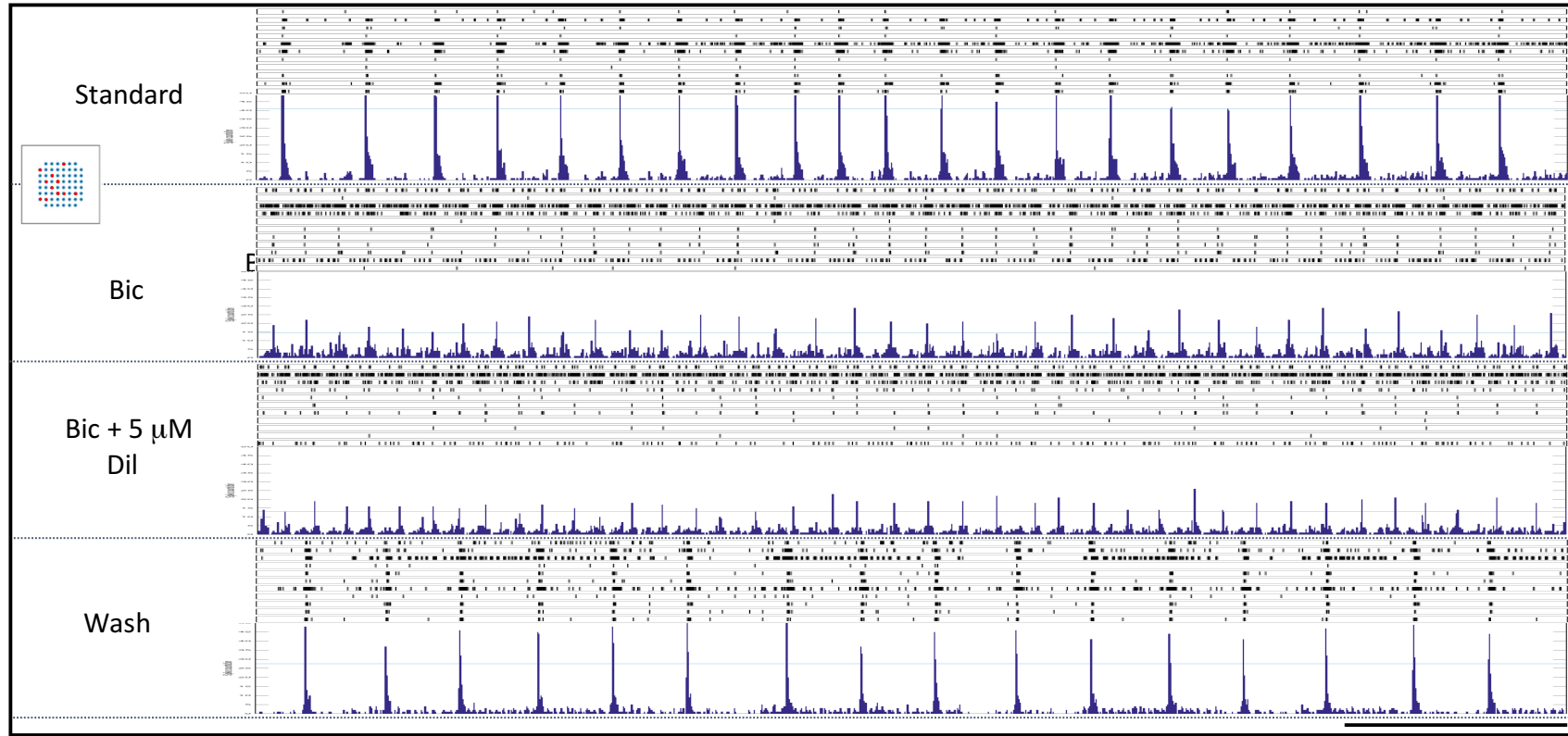
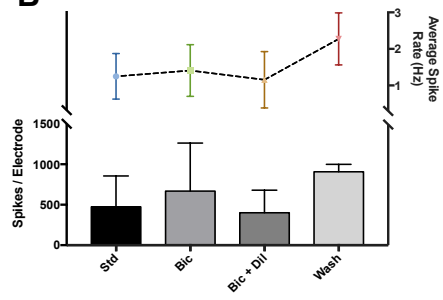
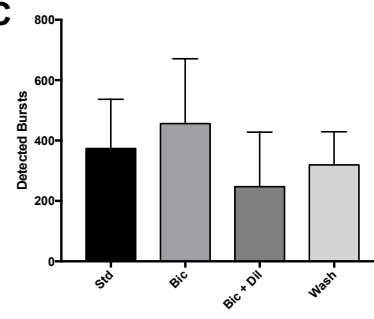
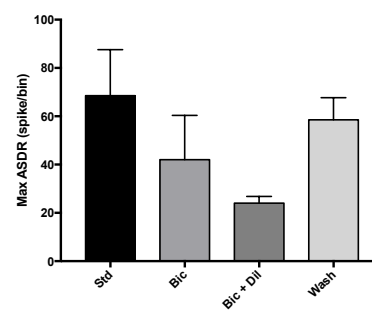
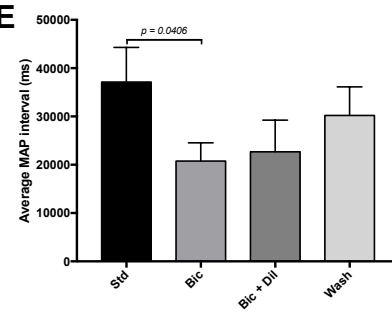
One of the most interesting aspects of the response of the cultures to diltiazem was the similarity to the effects caused by exposure to the GABA_A inhibitors, bicuculline and picrotoxin, although it should be noted that the response to neither bicuculline or picrotoxin was dose dependant in the manner of diltiazem. Specifically, both classes of drug induced a reduction in the MAP interval of coordinated cultures and caused a decrease in the maximum height of the ASDR peaks. To investigate whether the action of these drugs could be acting via a common mechanism, both bicuculline and diltiazem were applied simultaneously to cultures. A concentration of 5 μ M diltiazem was chosen for these experiments as it represented a dose which induced changes in both MAP interval and max array wide spike rate, inline with the GABA_A inhibitors.

Figure 5.15A presents the response of one array culture (61DPP) to the combined exposure of bicuculline and diltiazem. First, the culture responded to bicuculline alone in the same way as seen for the cultures in section 5.3.6, with a reduction in the MAP interval and an attenuation of the number of spikes in the ASDR peaks. Following the addition of 5 μ M diltiazem to the medium, there was no further change in the interval between peaks but there was a further reduction in the maximum number of spikes in the peaks. These trends continued when profiling a small cohort of arrays, where the average MAP interval significantly reduced from 33100 ± 3121 ms in standard conditions to 19400 ± 4243 ms with bicuculline (Tukey's multiple comparison following one-way ANOVA; $p = 0.0406$) and subsequently remained at 19700 ± 5798 ms when in the presence of both bicuculline and diltiazem (Figure 5.15E). After washes, the MAP interval returned to 27100 ± 3567 ms. The average max array wide spike rate of the cultures attenuated to 42 ± 18.4 in the presence of bicuculline from 68.5 ± 19.9 and then further reduced with the addition of diltiazem to 24 ± 5.825 (Figure 5.15D). This deficit was somewhat restored to 58.8 ± 9.78 following washes.

In terms of basal excitability, bicuculline alone induced a modest increase in the average spike rate of the cultures (Figure 5.15B), although the high variation seen across the different arrays perhaps suggest that bicuculline has little effect on basal spike firing, as seen in section 5.3.6. However, similarly to that seen in section 5.3.6, there was a small increase in bursts detected with application of bicuculline (Figure 5.15C). It was more clear that the addition of diltiazem and bicuculline simultaneously caused a decrease in both spike rate and burst number

5. Investigating network development in iPS cell derived neurons

back to around or below baseline (Figure 5.15B&C). This corresponds favourably to the inhibitory effect on tonic excitation caused by 5 μ M diltiazem alone as described earlier in this chapter. The results from this section strongly suggest that both GABA_A and L-type calcium channel signalling play a regulatory role in the network activity of iPS cell derived neurons. Moreover, these final set of results indicate that both of these signalling pathways could be acting via a common underlying mechanism, as the action of diltiazem was precluded by application of bicuculline.

A**B****C****D****E**

5. Investigating network development in iPS cell derived neurons

Figure 5.15 – The attenuation of more active period (MAP) intervals in synchronised iPS cell derived neuronal cultures by inhibitors of L-type calcium channels and GABA_A receptors. The interval between synchronised more active periods (MAP interval) observed in iPS cell derived neuron cultures after 50 days of culturing was attenuated by L-type calcium channel blocker diltiazem and the GABA_A antagonist bicuculline. However, application of both drugs together did not produce a summative effect, suggesting a potential shared mechanism of action. For each condition in **A**, top panel shows raster plots of detected spikes from the same 12 electrodes of one culture highlighted in the inset; bottom panel shows ASDR plots which present the summed number of spikes seen across the culture in 200ms bins, y units = spikes/bin. Limited changes were seen overall in average spike rate (B) or number of bursts (C) but the co-application of drugs caused a large decrease in the max ASDR (D). Bicuculline caused a significant decrease in the MAP interval but remained stable when diltiazem was added (E). Scale bar in **A** = 100 seconds. Summary data in B-E shows means + SD except average spike rate which shows means ± SEM; taken from 4 array cultures across two differentiations.

5.4 Discussion

The work in this chapter has shown that iPS cell derived neurons can be cultured on MEAs for an extended period of time and that the pattern of spontaneous activity recorded in these cultures changes markedly throughout development. Specifically, neurons re-plated onto MEAs take around 10 days to exhibit spontaneous activity; between 10 and 30 DPP activity increases but remains uncoordinated; between 30 and 40 DPP activity becomes more synchronised in the form of short coordinated culture-wide bursts (synchronised burst firing; SBF) and finally by 50 DPP, the majority of culture activity is synchronised into periods of lower activity (LAPs) and more activity (MAPs), which oscillate over a period of 10s of seconds. Importantly, the work here showed that the synchronised behaviour is a manifestation of underlying local excitatory networks, as the coordinated activity required both NMDA and AMPA signalling. Furthermore, the network activity in the cultures is regulated by both GABAergic and L-type calcium channel signalling, as inhibitors of both of these pathways attenuated the period between MAPs seen in synchronised arrays later in development. Importantly, results here suggest that the action of both of these pathways may be acting via a common underlying mechanism. Overall, this chapter has shown that iPS cell derived neurons form mature, complex cultures on MEAs and the recording of their spontaneous activity can be used as a platform for studying network activity throughout development and, importantly, in models of neurological disease.

While MEA technology has been around for many years, it is only in the more recent past with the advent of more user friendly and reliable systems that its use in neurobiology has been more keenly exploited. In particular, the use of planar MEAs onto which neurons can be cultured in a more or less standard way lends itself ideally to the study of network behaviour in developing neurons. Here, iPS cell derived neurons developed a synchronised pattern of firing from around 30 DPP, which progressed further to more fully coordinated behaviour by around 50DPP as described. This behaviour compares well to what has previously been described by a number of groups using very similar MEA systems to study networks in dissociated rodent primary neurons (Wagenaar *et al.*, 2006; Mok *et al.*, 2012; Chiappalone *et al.*, 2006; Sun *et al.*, 2010). In particular, the activity seen here at around 50DPP compares, in general, to what is seen in these studies at around 20DPP. In rodent neurons, this behaviour appears to extend further, such that the oscillations between a MAP and LAP, which here reached a maximum of

5. Investigating network development in iPS cell derived neurons

around 30 seconds, is seen lasting for several minutes (Mok *et al.*, 2012; Lu *et al.*, 2016). The fact that coordinated activity progresses further in rodent neurons is likely to be due to the increased maturity of such cells and their accelerated developmental timeline. Interestingly, a very similar development of slow culture-wide oscillations was also seen by a study which computationally modelled a small network (~1000 cells) of rodent neurons (Compte *et al.*, 2003).

Very few studies have looked at the function of iPS cell derived neurons using MEAs. The work from this project is in agreement with those studies that have, in terms of a general increase in excitability seen throughout culture development (Odawara *et al.*, 2014; Ylä-Outinen *et al.*, 2010; Odawara *et al.*, 2016; Amin *et al.*, 2016), although overall the neurons here present as being more active at corresponding developmental time points. Only one study to date has shown the development of synchronised culture-wide activity in iPS cell neurons (Odawara *et al.*, 2016). However, the coordinated activity observed in this study does not progress further than what was observed here at around 40DPP, namely short burst-firing which is synchronised across the cultures (SBF). The Odawara study does not report the extended periods of oscillatory firing seen here from 50DPP and furthermore, the onset of synchronised behaviour takes around 14 weeks (98 days) to develop compared to between 30-40 days here. It should be noted that the protocols differed greatly between this project and the work by Odawara *et al.*, most noticeably as cells were proprietary 'hiPS cell neurons' and took an extended period of culturing to reach a basic level of physiological maturity (at least 6 weeks). Nevertheless, as far as can be determined, the work from this chapter presents for the first time a model of network behaviour in iPS cell derived neurons which compares favourably to that seen in dissociated rodent neurons and which appears and develops in a practically useful time period.

The pharmacology experiments in this chapter provided useful information about the underlying nature of the activity recorded with the MEAs at particular time points. The experiments at 20 DPP, at point in development where culture activity is uncoordinated, highlighted that a majority of the detected spikes were not sensitive to CNQX or APV, suggesting that they were not dependant on AMPA or NMDA signalling. There was however a reduction in the number of detected bursts, suggesting that synaptic activity is perhaps required more for this type of firing. These results are broadly in line with what has previously been reported with iPS cell derived neurons at around this point in development (Odawara *et al.*, 2016; Odawara *et al.*, 2014); the

5. Investigating network development in iPS cell derived neurons

authors of these papers report a decrease in spikes of around 40% with CNQX application. Overall, this suggests that at this time point neurons are not sufficiently mature to have developed a significant number of functional excitatory synapses. Instead, detected spikes are primarily the result of intrinsic mechanisms within individual neurons, possibly due to their relative immaturity. For example, it is perhaps likely that the resting membrane potential (V_{rest}) of these neurons at this time point is around -25 to -30 mV – indeed, the single cell electrophysiology work in chapter 4 suggests that this would likely be the case. Furthermore, the work in chapter 4 also highlighted that earlier in development, the action potential threshold is fairly close to the V_{rest} of the neuron. As such, it is possible that many of the spikes detected at this time point are due to random fluctuations in membrane potential that, due to the the immaturity of the cell, push the neuron over the threshold for action potential initiation.

Perhaps the more interesting result of the pharmacology at this time point was the response of the neurons to bicuculline and GABA. Application of bicuculline to the cultures induced a small increase in both the number of spikes/average spike rate and the number of detected bursts. This suggests that at least some of the neurons within the cultures express functional GABA_A receptors and more importantly that there is a degree of basal GABAergic tone. Furthermore, the direction of the change in excitability with bicuculline suggests that the action of that basal GABA tone is inhibitory. This was confirmed with application of GABA itself to the cultures which resulted in an almost complete loss of spontaneous activity. This is perhaps a surprising finding based on what is known about the function of GABA throughout neural development. In early development, activation of GABA_A receptors leads to efflux of Cl⁻ ions and depolarisation of V_m , while in more mature neurons, activation of these receptors leads to influx of Cl⁻ ions and membrane hyperpolarisation. The change seen throughout development is due to a shift in the reversal potential of chloride, driven by a change in the relative expression of the NKCC1 and KCC2 K⁺/Cl⁻ co-transporters. In rodents, KCC2 expression, the transporter responsible for the shift to inhibitor action of GABA, only becomes reliably detectable around P0, around when the major shift is also seen (Wang *et al.*, 2002; Rivera *et al.*, 1999). Interestingly, KCC2 mRNA was detected in humans as early as 18-24 PCWs, depending on brain region (Sedmak *et al.*, 2015).

Expression of KCC2 in hPS cell derived neurons is not well understood. A recent study looked at the transcriptome of iPS cell neurons using single-cell RNA-seq and determined that very few neurons expressed detectable levels of KCC2 mRNA, while almost all neurons showed good

5. Investigating network development in iPS cell derived neurons

expression of NKCC1 (Bardy *et al.*, 2016). Conversely, a further study could in fact detect low levels of KCC2 *protein* in iPS cell neurons, which increased gradually over development (Tang *et al.*, 2016). Interestingly, the internal concentration of chloride ions in hPS cell neurons has been shown to decrease over a period of around 7 weeks, which was matched by increase in KCC2 mRNA expression (Livesey *et al.*, 2014). Unfortunately, neither RNA or protein levels were able to be determined in the neurons used in this project. As such, based on the pharmacology, it can only be assumed that there is enough expression of KCC2 in these neurons to provide the switch in chloride reversal potential required for an inhibitory effect of GABA.

The synchronised network activity seen in these cultures was completely eliminated with application of either APV or CNQX. Firstly, this provides compelling evidence that the synchronised behaviour observed is indeed caused by underlying neural network activity and is not an artefact of the culturing conditions. Secondly, it shows that at this time point in development, these neurons are now showing good expression of functional AMPA and NMDA receptors and thirdly, it strongly suggests that the formation and maintenance of this network behaviour requires signalling via both AMPA and NMDA receptors. This finding is in agreement with the only other study to identify a degree of synchronised activity in iPS cell neurons, which found that this behaviour was abolished with CNQX and APV, although the latter only at early time points (Odawara *et al.*, 2016).

It was perhaps somewhat surprising that antagonism of both AMPA and NMDA receptors induced an identical effect on the network activity of these cultures. Indeed, there is evidence to suggest that blockade of NMDA but not AMPA receptors, abolishes slow coordinated activity both *in vivo* and in *in vitro* slices (Harsch and Robinson, 2000; Lazarewicz *et al.*, 2010; Hakami *et al.*, 2009; Molina *et al.*, 2014). Interestingly however, work with dissociated rodent neurons, including some of the earlier generation of MEA studies, has shown that the coordinated burst firing identified is indeed blocked by both AMPA and NMDA receptor inhibition (Maeda *et al.*, 1995; Sanchez-Vives and McCormick, 2000; Chiappalone *et al.*, 2003; Lu *et al.*, 2016). It is possible that the difference seen in dissociated neurons compared to 'intact' models is a function of the more random and heterogeneous nature of such cultures, which lack the intrinsic complexity, highly regulated developmental structure and region specific networking seen in slices and *in vivo*.

5. Investigating network development in iPS cell derived neurons

While inducing the same effect in cultures with regards to the network activity, APV and CNQX caused contrasting changes in terms of more basal excitability, with APV causing a decrease in spike rate and detected bursts, while CNQX application lead to increased in overall average spike rate. In general, AMPA receptors are thought to be responsible for the majority of 'basal' action potentials, due to the fact that their activation requires only the binding of glutamate. NMDA receptors however act as coincidence detectors, requiring binding of both glutamate and glycine as a co-agonist, together with a depolarisation – dependant unblocking of pore-associated Mg^{2+} ions (driven primarily via AMPA receptor currents). Counter-intuitively, functional NMDA receptors are expressed before functional AMPA receptors in mammalian development, suggesting that, in fact, at early time points NMDA receptors are the primary source of excitatory communication (Pickard *et al.*, 2000; Durand *et al.*, 1996). The Mg^{2+} block of NMDA receptors is not 'all or nothing', instead while practically 100% of receptors are blocked at -70 mV, around half are 'empty' at -20 mV (Nowak *et al.*, 1984; Vargas-Caballero and Robinson, 2004). This therefore leads to the suggestion that in the iPS cell derived neurons used here, NMDA activity is perhaps more prominent owing to the relative immaturity of the resting membrane potential compared to adult or rodent primary neurons.

Application of both bicuculline and picrotoxin to the cultures during synchronised network behaviour attenuated the interval between the more active periods (MAP). While bicuculline is a competitive antagonist for $GABA_A$ receptors, picrotoxin is thought to act via an allosteric mechanism, strongly suggesting therefore that the effect of both of these drugs is down to the inhibition of GABAergic signalling. This finding compares well to what has previously been reported with both rodent dissociated primary cultures (Chiappalone *et al.*, 2003; Chiappalone *et al.*, 2006; Lu *et al.*, 2016) and iPS cell derived cultures (Odawara *et al.*, 2014; Odawara *et al.*, 2016). The regulation of coordinated network firing by GABAergic interneurons is well documented. This ranges from coordinating oscillatory activity across brain regions (Blatow *et al.*, 2003; Bruno and Sakmann, 2006; Sanchez-Vives and McCormick, 2000), synchronising networks within structures (e.g. the hippocampus; Mann and Paulsen, 2007; Bartos *et al.*, 2002) to regulating the behaviour of smaller more localised networks (Cobb *et al.*, 1995; Hu *et al.*, 2014). Furthermore, GABAergic activity is thought to be highly important throughout development, where it has been implicated in the correct formation of networks and the regulation of synaptic plasticity (Higley and Contreras, 2006; Tremblay *et al.*, 2016; Takada *et*

5. Investigating network development in iPS cell derived neurons

al., 2014). Importantly, GABAergic malfunction leading to an unphysiological inhibitory/excitatory balance is thought to underlie several neurological disorders including schizophrenia, autism and epilepsies. Therefore, the fact that inhibitory activity can be manipulated pharmacologically in these iPS cell derived MEA cultures allows for the study of inhibitory regulation of networks in disease – relevant models.

The response of the cultures to the GABA antagonists and indeed GABA itself at the later time point corroborates the pharmacology from earlier in development, in suggesting that these cultures must contain a source of GABAergic drive. Indeed, this was further confirmed with the staining for GAD67 +ve cells, which, although a limited quantification study, suggested that around 4-5% of neurons in the cultures were of an GABAergic identity. In terms of the protocols used for the production of neurons in this study, the finding that interneurons are present in cultures, albeit in small numbers, is perhaps surprising. The basic outline of the protocol used here involves the neuralising of iPS cells using dual SMAD inhibition, followed by routine cell culture with a medium containing the neuronal supplements B27 and N2. While several different approaches exist for the differentiation of interneurons, a common step is the addition of morphogens involved in cell patterning across the dorsal-ventral axis, to promote the developmental model of neurons arising from the medial ganglion eminence, in particular, agonism of sonic hedgehog signalling and inhibition of wnt signalling (Kim *et al.*, 2014; Goulburn *et al.*, 2012; Nicholas *et al.*, 2013; Maroof *et al.*, 2013). As such, without the addition of these molecules in the protocol used here, it can only be assumed that there is a low-level intrinsic source of such molecules in these cultures that promotes the formation of a small interneuron population. However, in light of the evidence discussed above for the role of interneurons in network function, the presence of these cells regardless of their origin, is welcome.

Perhaps the most interesting result from this chapter, aside from the development of such complex network behaviour in these neurons, was the response of cultures to the L-type calcium channel (LTCC) blocker diltiazem. Application of diltiazem caused a dose dependant attenuation of the MAP interval of synchronised activity up to 10 μ M, which induced a complete loss of networked behaviour. At low concentrations, diltiazem is a selective pore-blocker of LTCCs (both Ca_v1.2 and Ca_v1.3 channels) however above around 20 μ M, has been shown to act on other voltage gated calcium channels, including P/Q-type (Dobrev *et al.*, 1999), and

5. Investigating network development in iPS cell derived neurons

ionotropic 5-HT₃ receptors (Gunthorpe and Lummis, 1999; Hargreaves *et al.*, 1996). As such, it is perhaps likely that in these cultures, concentrations of diltiazem above around 5 μ M may start to act in a non-specific manner, as this represented the dose which no longer attenuated MAP interval but did begin to cause a decrease in overall excitability.

LTCCs are a class of voltage gated calcium channels characterised by a large single channel conductance, a high threshold of voltage activation and a delayed voltage dependant inactivation (Zamponi *et al.*, 2015). The Ca_v1.2 and Ca_v1.3 subtypes (coded for by CACNA1C and CACNA1D genes respectively) are expressed throughout the mammalian brain and are involved in wide array of calcium regulatory mechanisms (Hell *et al.*, 1993; Schlick *et al.*, 2010). In particular, LTCCs are strongly implicated in NMDA-dependant LTP/LTD, via regulation of local intracellular calcium concentrations (Moosmang *et al.*, 2005; Malenka and Bear, 2004; Zucker, 1999). This regulation of synaptic plasticity is thought to underlie the alterations to hippocampal – dependant learning seen with decreased or absent expression of LTCCs (Moosmang *et al.*, 2005; White *et al.*, 2008; Hofmann *et al.*, 2014). Furthermore, similar rodent KO studies have implicated LTCCs in hippocampal-independent mechanisms of fear learning (Cain *et al.*, 2002; McKinney *et al.*, 2008; Lee *et al.*, 2012; Langwieser *et al.*, 2010), regulation of axon growth (Enes *et al.*, 2010), trafficking of AMPA receptor subunits (Schierberl *et al.*, 2011) and gene expression (Wheeler *et al.*, 2012; Gomez-Ospina *et al.*, 2006).

A role for LTCCs has also been described in a range of oscillatory neural activity in rodent cells. Synchronised calcium transients have been shown to be mediated and controlled by LTCCs in dissociated primary neurons (He *et al.*, 2006; Przewlocki *et al.*, 1999), while further studies have shown that these channels can regulate calcium oscillations in intact systems (Inglefield and Shafer, 2000; Bengtson *et al.*, 2013; Wang *et al.*, 2013). Importantly, it has also been shown that LTCC currents can modulate the network response of neurons during physiological oscillatory behaviour in the hippocampus (Mohajerani *et al.*, 2007; Hansen *et al.*, 2014; Bukalo *et al.*, 2013) and during modelled epileptiform activity (Straub *et al.*, 2000; Empson and Jefferys, 2001). Involvement of LTCCs in these systems is likely to be down to their role in the regulation of the post-burst after-hyperpolarisation (AHP), a period of hyper-polarisation which terminates high frequency firing (Lima and Marrion, 2007). LTCCs have been shown to be a key mediator of the size and duration of the AHP and therefore act as regulators of neuron burst behaviour (Shah and Haylett, 2000; Lima and Marrion, 2007; Gamelli *et al.*, 2011).

5. Investigating network development in iPS cell derived neurons

The evidence reviewed above provides good support for the role of LTCCs in regulating synaptic activity and their possible involvement in the control of neural circuits. Moreover, the majority of this evidence is based upon studies of LTCCs at excitatory synapses and as such, provides a potential mechanism for how these channels may be regulating the NMDA and AMPA dependant synchronised network activity seen here. However, the action of the LTCC blocker diltiazem induced an identical effect on this network behaviour as that caused by inhibition of GABA_A receptors. Furthermore, application of diltiazem and bicuculline concurrently did not produce a summative effect on the interval between culture MAPs, strongly suggesting that the two drugs are acting via a common underlying mechanism. A potential scenario is that diltiazem is acting via presynaptic LTCCs on GABAergic interneurons nerve terminals. Indeed, LTCCs have been shown be expressed in presynaptic terminals in the hippocampus (Tippens *et al.*, 2008) and in interneurons (Westenbroek *et al.*, 1998). While a role for P/Q and N type calcium channels in presynaptic vesicular release is well documented (Evans and Zamponi, 2006), there is less direct evidence for a similar role for LTCCs. However, LTCCs have been shown to interact with aspects of the exocytotic pathways and facilitate neurotransmitter release in certain neuronal populations (Wiser *et al.*, 1996; Wiser *et al.*, 1999). Furthermore, calcium currents via LTCCs have been shown to act through the MAPK ERK1/2 signalling pathway, which its self has been implicated in the regulation of vesicular exocytosis (Ren and Guo, 2012; Dolmetsch *et al.*, 2001). Importantly, this link has been observed directly as inhibition of the ERK1/2 pathway was shown to increase neurotransmitter release via increased calcium influx via LTCCs (Subramanian and Morozov, 2011). This therefore provides a potential mechanism by which LTCCs may be acting to regulate the activity of GABAergic interneurons in these iPS cell derived cultures: Synchronised network activity develops in cultures after maturation of functional synapses and is dependant on both AMPA and NMDA signalling; this activity is regulated by GABAergic innervation, inhibition of which attenuates the period between high frequency culture-wide firing; blocking LTCCs mimics the effect of GABA_A antagonism by reducing vesicular release at the interneuron-projection neuron synapse.

6. Functional phenotyping of autism spectrum disorder patient iPS cell derived neurons

6.1 Introduction

The SHANK3 protein is a key part of the excitatory post-synaptic density (PSD), acting primarily as scaffolding protein involved in the recruitment and assembly of NMDA and AMPA receptors and as link between these receptors, via interactions with other proteins such as PSD95 and HOMERs, and the actin cytoskeleton (Naisbitt *et al.*, 1999; Hayashi *et al.*, 2009). Mutations in *SHANK3* have been implicated in several neurological disorders, including schizophrenia (de Sena Cortabitarte *et al.*, 2017; Guilmatre *et al.*, 2014) and epilepsy (Han *et al.*, 2013). However, by far the most understood implication for *SHANK3* is its role in autism spectrum disorder (ASD). Large scale genetic studies have shown that rare and *de novo* mutations in *SHANK3* are a major risk factor for development of ASD and have suggested that mutations in the gene are present in up to 1% of the ASD population (Gauthier *et al.*, 2009; Boccutto *et al.*, 2013; Leblond *et al.*, 2014). Heterozygous deletions of *SHANK3* are also present in almost all cases of 22q13.3 or Phelan-McDermid syndrome (PMDS), a complex neurological disorder characterised by heterogeneous symptoms including developmental delay, intellectual disability and ASD (Phelan and McDermid, 2012; Wilson *et al.*, 2003). Importantly, *SHANK3* associated PMDS is the genetic implication with the highest penetrance for development of ASD, with around an 80% rate of diagnosis.

Mouse models of PMDS have revealed an array of phenotypes associated with *SHANK3* haploinsufficiency, including reduced spine formation and complexity of dendritic branching (Hung *et al.*, 2008; Durand *et al.*, 2012), decreased excitatory synaptic activity (Wang *et al.*, 2011; Yang *et al.*, 2012) and behavioural deficits (Lee *et al.*, 2015; Bozdagi *et al.*, 2010). However, one of the most consistent findings from mouse studies has been a reduction in LTP associated with *SHANK3* mutations across a range of plasticity protocols (Kouser *et al.*, 2013;

6. Functional phenotyping of ASD patient neurons

Jaramillo *et al.*, 2016; Bozdagi *et al.*, 2010), suggesting that reduced SHANK3 expression may lead to altered signalling within neural networks. A number of these deficits have also been identified in neurons derived from hPS cells with heterozygous expression of SHANK3, including iPS cells from patients with mutations in *SHANK3*. In particular, SHANK3 mutant hPS cell neurons show decreased spontaneous activity, alterations to NMDA/AMPA mediated synaptic currents, aberrant calcium signalling and changes to dendritic morphology (Shcheglovitov *et al.*, 2013; Darville *et al.*, 2016; Yi *et al.*, 2016).

Recently, a study investigated the network behaviour of homozygous Shank3 KO primary mouse neurons using extracellular recordings via an MEA system very similar to that used in this project (Lu *et al.*, 2016). The authors found that Shank3 mutant neurons were less spontaneously excitable than control neurons and, importantly, found that synchronised network activity was altered in mutant cultures. Furthermore, these deficits could only be fully rescued with application of positive allosteric modulators of AMPA and GABA_A receptors, suggesting a role for both excitatory and inhibitory circuit signalling. Although conducted with mouse primary neurons with homozygous mutations, the Lu *et al.* study provides a good comparison for the work in this project, and offers a template to study the network function of heterozygous SHANK3 neurons, which, to date, has not been studied in hPS cell derived neurons.

This chapter therefore focuses on investigating the function of neurons derived from ASD patient iPS cells with heterozygous mutations of *SHANK3*. The cells have been provided for use in this project as part of a collaboration with Jack Price at King's College, London (KCL) and include two ASD patient lines and one control line. All three of the iPS cell lines were derived from keratinocytes and were reprogrammed using a polycistronic lentiviral vector. For use in this project, lines were received as neural precursors (NPCs) which were produced by the group in KCL using the protocol described in Appendix 1. NPCs were subsequently terminally differentiated into neurons for use here following the protocol described in Chapter 2.

6. Functional phenotyping of ASD patient neurons

The two ASD patient lines both contain heterozygous deletions of chromosome 22q13.33 including *SHANK3* and are described below. Figure 6.1A highlights the location of the lesions within 22q13.33.

Shank3_M1 (S3_M1). Derived from a 4-year old male with absent speech, developmental delay and ASD diagnoses. Heterozygous deletion at chromosome 22q13.33 of ~ 50kb extends from the end of the third exon of *SHANK3* to near the start of the neighbouring gene, *ACR*.

Shank3_F1 (S3_F1). Derived from female child, age unknown, with ASD diagnosis. Other diagnoses unknown. Heterozygous deletion at chromosome 22q13.33 of ~ 80kb extends from the end of the third intron of *SHANK3* to near the *end* of the *RABL2B* gene (transcribed from minus strand). S3_F1 cells therefore also have heterozygous deletions of *ACR*, which codes for the spermatozoa-specific protease acrosin.

The control NPC line used in this chapter is **Ctl_M1**. It was derived from a healthy male of unknown age with no diagnoses of ASD or any mental health disorder. It has two full copies of *SHANK3*.

6. Functional phenotyping of ASD patient neurons

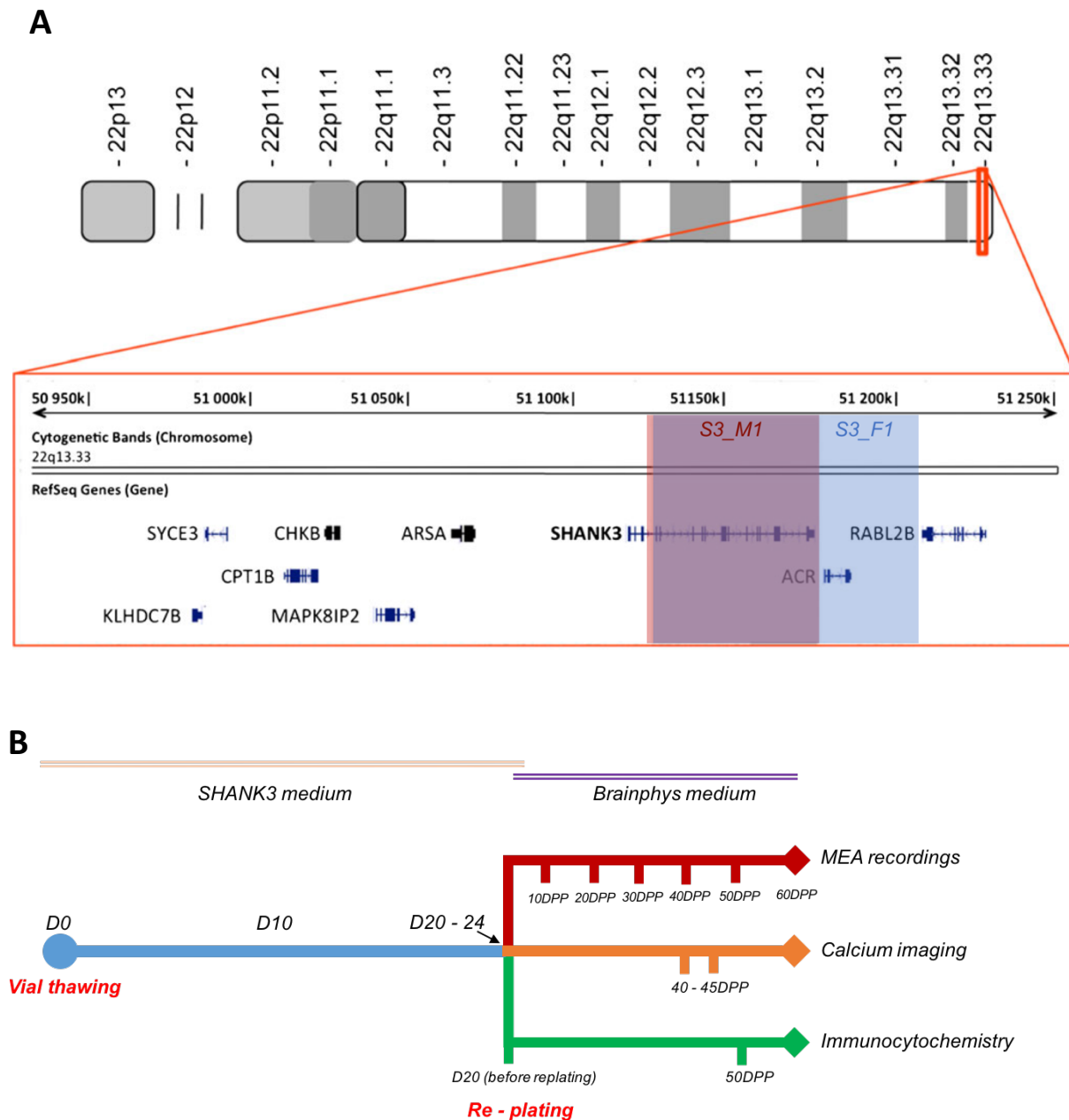


Figure 6.1 – Schematic diagrams of the genetic lesions present in the two neural precursor cell lines derived from patients with autism spectrum disorder (ASD) and the experimental outline used in this study. (A) Both the S3_M1 and S3_F1 lines were derived from _patients with confirmed ASD diagnoses. Comparative genomic hybridisation arrays revealed that both lines had small heterozygous deletions of a distal region of chromosome 22q13.33, including the majority of the *SHANK3* gene. For S3_M1 (red block and text), the deletions spans from the end of the third exon to near the beginning of the neighbouring 3' gene, *ACR*; in the S3_F1 line, the deletion range from the end of the third intron to just before the end of the *RABL2B* gene (on reverse strand) and therefore also includes heterozygous deletion of *ACR*, which codes for acrosin, a protease specific to spermatozoa. This genetic analyses were conducted by Jack Price at KCL, London. **(B)** Overview of the protocol and experimental timeline for the work in Chapter 6. Thawed precursor lines were cultured for 20-24 days in SHANK3 medium. Cells were then re-plated onto either MEAs or coverslips as required for calcium imaging and immunocytochemistry. After re-plating, medium was gradually changed to Brainphys over a period of 4-6 days. DPP = days post (re)plating.

6.2 Chapter Aims

The primary aim of this chapter is to investigate the electrophysiological function of iPS cell derived neurons harbouring heterozygous deletions of *SHANK3*. This will primarily be studied by monitoring the change in spontaneous activity using MEA cultures and recording over an extended period of development, using the platform established in Chapter 5. While general excitability and the response to pharmacological agents will be analysed, the key focus will be on the development and nature of coordinated network driven activity. Additionally, this chapter will also introduce the analysis of extracellular spike shapes, recorded by MEAs, with the aim of investigating changes to spike shape that may be caused by *SHANK3* heterozygosity. Finally, to support the MEA work, the chapter aims to study the nature of single-cell calcium events from *SHANK3* mutant neurons, with a view to investigating potential underlying physiological phenotypes.

6.3 Results

6.3.1 Identification of neural precursor and determined neuron fate

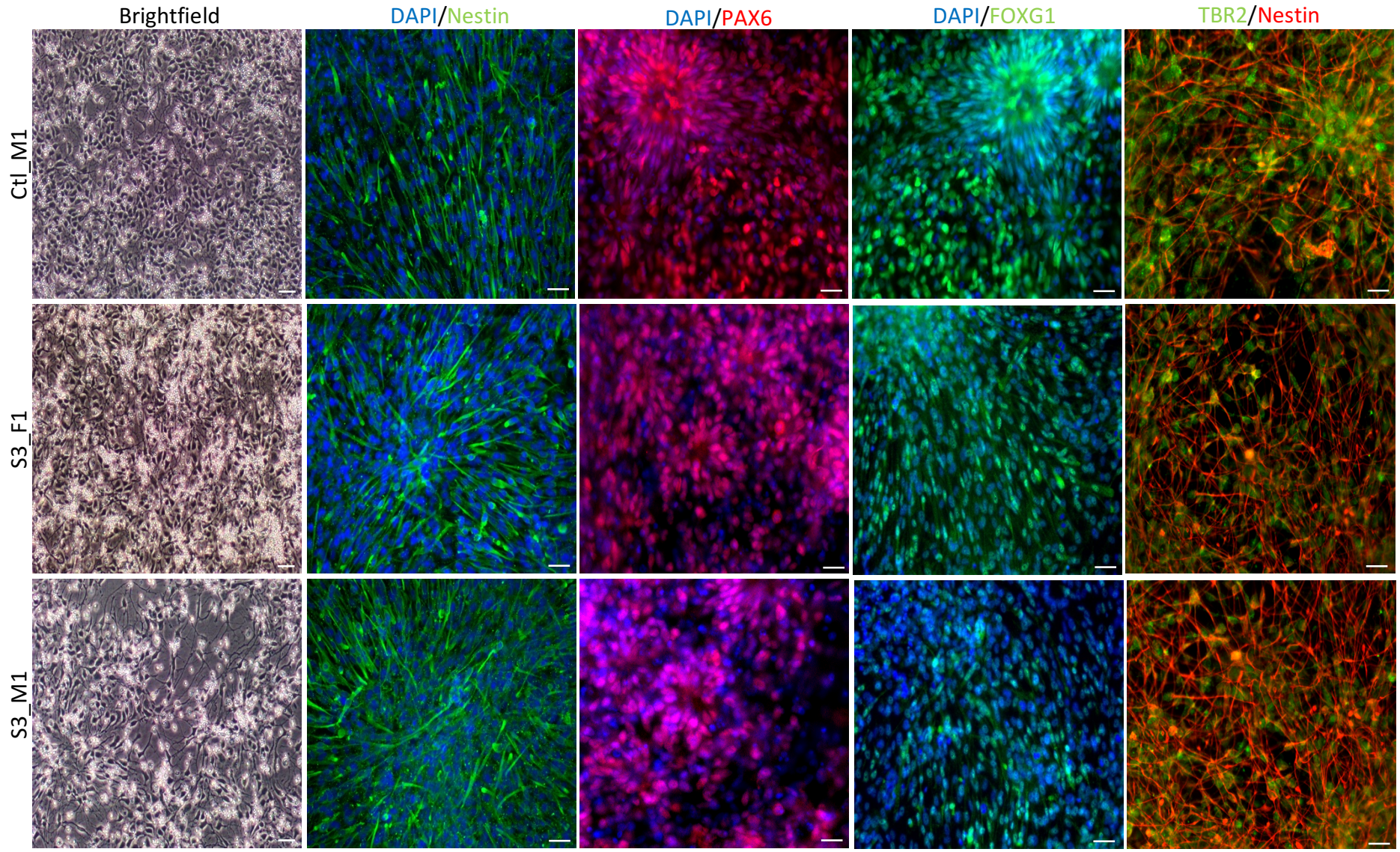
While the primary focus of this chapter was on the electrophysiological function of SHANK3 mutant neurons and not the developmental biology of such lines, it was important to establish the differentiation state of the neurons being tested. This was especially important as the protocol used was a hybrid of that developed in KCL and that used for the differentiations in Chapters 4 and 5. To gauge the identity of the cells replated onto MEAs, neurons from Ctl_M1, S3_F1 and S3_M1 lines were fixed for immunocytochemistry at two time points: 20-24 days after NPC thawing (24 hours before replating onto MEAs/coverslips) and 50 days after replating (50 DPP). Note, a quantitative comparative analysis between the cell lines was outside the scope of this study. Figure 6.1B presents a schematic of the protocol and timetable for the experiments conducted in this chapter.

Figure 6.2 shows representative images from each of the cell lines showing stained early neurons. First, brightfield images showed that, morphologically, the early neurons from each of the cell lines were virtually identical just before replating. While the brightfield image of the S3_M1 line shows noticeably fewer cells than the other lines, this was because NPCs were plated at vial density which varied between the cell lines. Cell numbers were then normalised when replated onto MEAs/coverslips. Cells at 20-24 days post thawing from all three lines showed expression of several key markers of early projection neurons including nestin, an intermediate filament protein and primary marker of neural progenitor cells, and TBR2, a marker of intermediated progenitor cells. Importantly, neurons from all three cell lines also expressed PAX6 and FOXG1, two key proteins involved in the patterning of forebrain glutamatergic neurons. While FOXG1 is expressed by telencephalic precursors, PAX6 is a marker of the more specific *dorsal* telencephalic NPCs. This staining therefore suggests that cells at this early time point from both SHANK3 mutant lines and the control line are (*dorsal*) telencephalic neural precursors with the potential to develop into populations of glutamatergic forebrain neurons.

To attempt to provide an identify for the cells at a more developed time point, coverslips of neurons were stained at 50 days after replating (50DPP). This was to provide an indication about the state of the neurons and in particular the formation of synapses at a time point where,

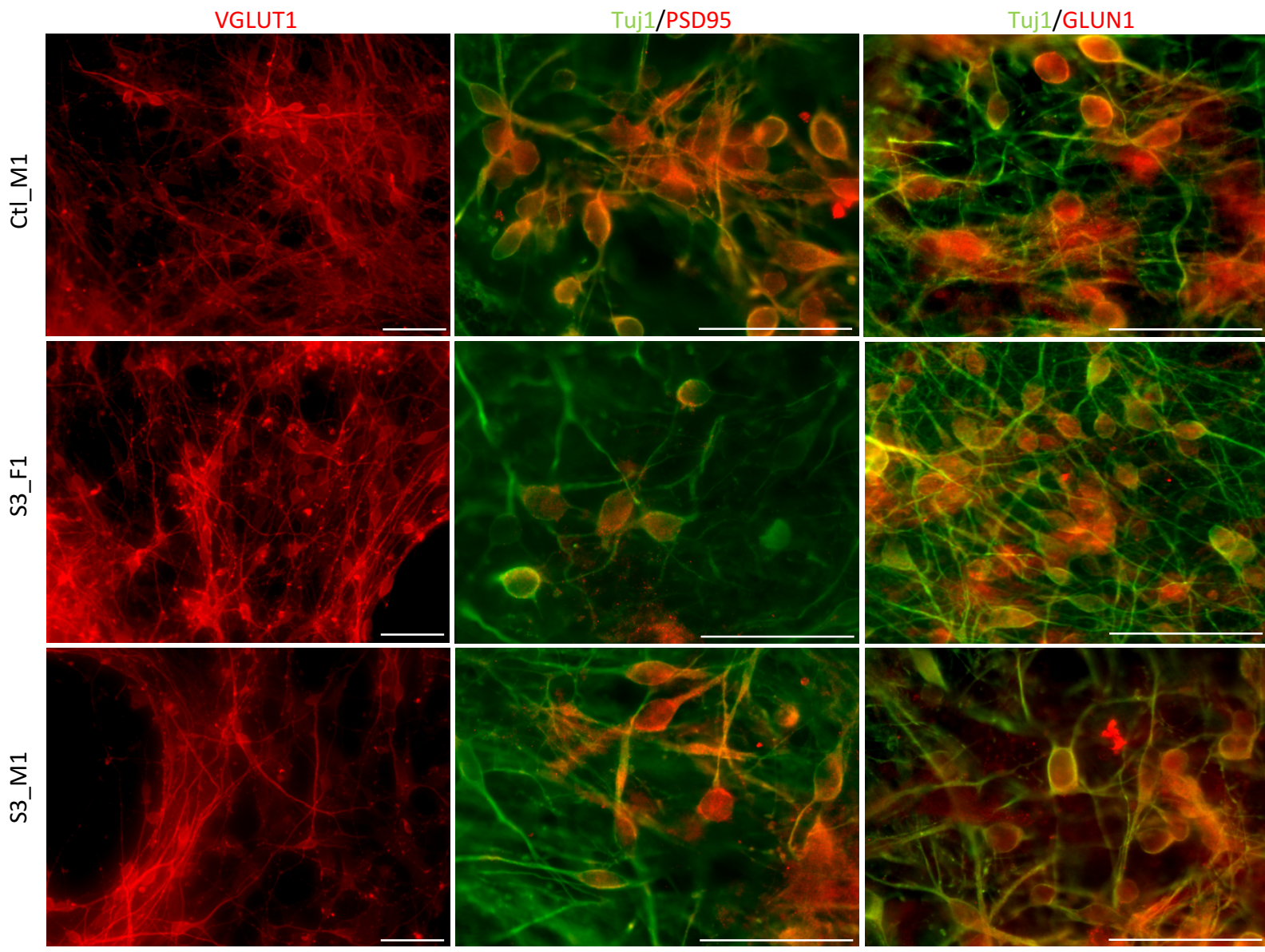
6. Functional phenotyping of ASD patient neurons

as shown in Chapter 5, functional networks may exist in the culture. As with the previous chapter, it was not possible to stain the neurons on the arrays themselves; instead, coverslips of parallel cultures were used (see Figure 6.1B). Along with ubiquitous expression of the neuron marker class III β -tubulin (Tuj1), 50DPP cells from all three cell lines expressed VGLUT1, one of primary vesicular transporters of glutamate that is thought to be universally expressed in cortical neurons (Figure 6.3). Neurons from all lines also expressed two key markers of mature glutamatergic synapses: PSD95 and GLUN1. While GLUN1 is the required universal subunit of NMDA receptors (coded for by *GRIN1*), PSD95 is a key protein involved in the assembly and the scaffolding of the NMDA/PSD complex at excitatory synapses. The pattern of staining seen on all of these neurons is worth noting. For both PSD95 and GLUN1, a 'punta' type staining was seen, in line with what would be expected for synaptic proteins. However, in both cases, this appeared mostly on the cell bodies rather than within dendrites, although it is possible that dendritic staining would be better observed with higher resolution imaging. Overall, the staining at 50DPP confirms that the neurons produced from all three cell lines are primarily excitatory glutamatergic neurons and show evidence of functional synapse formation.



6. Functional phenotyping of ASD patient neurons

Figure 6.2 - iPS cell derived neural progenitors from *SHANK3* mutant patient cells show a telencephalic progenitor phenotype. Neural progenitors from a control (Ctl_M1) and two *SHANK3* mutant (S3_F1, S3_M1) cell lines were stained at day 20-24, prior to replating onto multi electrode arrays. Coverslips of cells were fixed and stained with markers to determine the identity of the early neurons. Cells from all three lines expressed nestin, a key marker of neural progenitors, TBR2, a marker of mitotic precursor cells and FOXG1 and PAX6, markers of telencephalic and dorsal telencephalic progenitors respectively. Panels show representative images from each cell line. Scale bar in each panel = 50 μ m.



6. Functional phenotyping of ASD patient neurons

Figure 6.3 - iPS cell derived neurons at 50DPP from patients with heterozygous deletions of SHANK3 show a glutamatergic excitatory neuron phenotype. Immunohistochemistry of Ctl_M1 and S3_F1, S3_M1 neurons was performed at 50 days post replating (50 DPP) on parallel cultures to those replated onto MEAs. The control line, Ctl_M1 and both SHANK3 mutant lines, S3_F1, S3_M1 showed expression of the neuron marker TUJ1, the vesicular glutamate transport vGLUT1, the post synaptic density protein PSD95 and the universal subunit of NMDA receptors, GluN1. Together the staining suggests that these neurons are of a glutamatergic projection neuron fate and form excitatory NMDA receptor containing synapses. Panels show representative images from each cell line. Scale bars in all images show 50 μm .

6.3.2 Investigating the development of spontaneous activity in SHANK3 mutant neurons

The work presented in chapter 5 showed how the spontaneous activity of iPS cell derived neurons changes over development, such that maturing networks within the cultures drive a synchronised firing behaviour at later time points. To study both the general excitability of neurons derived from SHANK3 patient iPS cells and any change in activity over a prolonged period of neural development, two SHANK3 mutant lines and one control were plated as immature neurons onto MEAs and cultured and recorded for 60 days. It should be noted that although there were differences in the initial culturing protocols for the Shank3 (and control) lines prior to MEA-replating, after replating the procedures remained identical to those used for the work in Chapter 5 (see Chapter 2 and Figure 6.1B).

Figure 6.4 presents raster plots showing representative spontaneous activity of neurons derived from Ctl_M1, S3_F1 and S3_M1 lines over a period of 60 days culturing. First, the clearest observation was the absence of the development of synchronised activity after 30DPP in either SHANK3 line or the control line, in contrast to what was observed in Chapter 5. Note, it is for this reason that the raster plots in Figure 6.4 are presented without their corresponding ASDR plots as these offer little further insight about the nature of firing in the absence of coordinated behaviour. In fact, across a total of around 60 cultures across 4 differentiations of all three cell lines, no synchronised behaviour was detected even after 70+ days of culturing. The fact that this activity was not cell-line specific clearly signals that this was not an effect of genotype and instead, despite efforts to overcome the issue, was likely due to technical differences in the way that these neurons have been cultured compared to the cells in Chapter 5.

Despite the absence of coordinated behaviour, the plots in Figure 6.4 provided interesting insights into the general excitability of the SHANK3 mutant neurons. In both mutant lines, it appears that, in terms of the number of visible spikes, the neurons are less spontaneously active compared to the control cells. This is especially noticeable in recordings 30DPP, where several of the S3_F1 and S3_M1 plots show a number of 'silent' electrode traces, indicating that no spikes could be detected. This observation was confirmed when looking across the experimental cultures as a whole. Figure 6.5A shows the average spike rate of cultures recorded across 60 days for all three cell lines. The summary bar plots highlight that

	Ctl_M1	S3_F1	S3_M1
10 DPP			
20 DPP			
30 DPP			
40 DPP			
50 DPP			
60 DPP			

6. Functional phenotyping of ASD patient neurons

Figure 6.4 – The development of spontaneous activity in neurons derived from iPS cells from patients with heterozygous *SHANK3* deletions, cultured on and recorded with MEAs. Immature neurons from two *SHANK3* mutant lines, S3_F1 and S3_M1, and a control line, Ctl_M1, were plated onto MEAs after a 20 days period of standard culturing. Within 10 days post (re)plating (DPP), neurons from all three lines begin to fire spontaneous action potentials, however there is noticeably less firing observed in both mutant lines compared to control line at this time point. Overall, the activity of all three lines increases over development up to 60DPP. In both S3_F1 and S3_M1 lines, the increase in activity up to around 30DPP is clearly less than that in the control line. After 30DPP, there is a noticeable increase in both mutant lines, suggesting that perhaps the development of these cells is delayed compared to the control line. Furthermore, in these selected cultures, at 60DPP the spontaneous activity in mutant lines is still observably less than the control line. The data shown is the development of activity seen in the same three cultures, representing one cell line each. For each time point, the raster plots show detected spontaneous spikes from the same 16 electrodes within each cell line. Scale bar represents 100 seconds.

6. Functional phenotyping of ASD patient neurons

Table 6.1. Summary of the significant variation observed in measurements of basic excitability properties in control and SHANK3 mutant iPS cell derived neurons

2 Way ANOVA (Genotype variation)		Tukey's Multiple comparisons		
		Mean difference [95% CI]	Adjusted p value	
Average Spike rate				
10DPP				
<i>Ctl_M1 vs S3_F1</i>	F(2, 86) = 9.438; p = 0.0002	0.816 [-.0149 – 1.782]	0.034	
<i>Ctl_M1 vs S3_M1</i>		1.138 [0.173 – 2.104]	0.0166	
30DPP				
<i>Ctl_M1 vs S3_F1</i>		0.968 [0.0378 – 1.898]	0.0395	
<i>Ctl_M1 vs S3_M1</i>		0.934 [0.004 – 1.865]	0.0486	
50DPP				
<i>Ctl_M1 vs S3_M1</i>		0.888 [-0.045 – 1.812]	0.0445	
Bursts				
10DPP				
<i>Ctl_M1 vs S3_F1</i>	F(2, 82) = 0.741; p = 0.4798	429.8 [37.17 – 822.3]	0.0285	
<i>Ctl_M1 vs S3_M1</i>		455.7 [97.29 – 814]	0.0089	
Max ASDR				
10DPP				
<i>Ctl_M1 vs S3_F1</i>	F(2, 83) = 1.343; p = 0.2666	8.75 [1.51 – 15.99]	0.0285	
<i>Ctl_M1 vs S3_M1</i>		7.667 [1.058 – 14.28]	0.0089	

throughout the duration of the experiment, the firing rate of both S3_F1 and S3_M1 neurons was generally lower than Ctl_M1 neurons. These differences reached significance at certain time points, most noticeably at 10 and 30DPP, with Table 6.1 presenting a summary of the statistics for the significant variation seen across the culturing period. The firing behaviour of both S3_F1 and S3_M1 neurons developed in a similar manner to Ctl_M1 neurons, such that spontaneous activity increased over the 60-day period. This was also in line with the pattern of change reported in Chapter 5. However, from 40DPP, the rate of firing in both SHANK3 mutant lines is around the level seen at the previous time point for the control neurons, suggesting that the development of activity in the mutant lines is delayed by around 10 days.

A high degree of variation was observed in the average spike rate, especially in the Ctl_M1 neurons, highlighting the variability of MEA cultures in general and contributing to the large errors associated with certain time points here. To try to gain a broader overall picture of the excitability of the SHANK3 mutant neurons, average firing rate data from all time points were pooled for each of the cell lines and plotted as cumulative probability distributions (Figure 6.5B). This highlighted that, across the full length of the experiment, the spontaneous excitability of both SHANK3 mutant lines was lower than control cells, as shown by shifting of the SHANK3 distributions towards lower firing rates. Kolmogorov – Smirnov tests of the distributions showed

6. Functional phenotyping of ASD patient neurons

however that only the firing rate of S3_M1 neurons was significantly lower compared to Ctl_M1 ($D = 0.2571$, $p = 0.0172$).

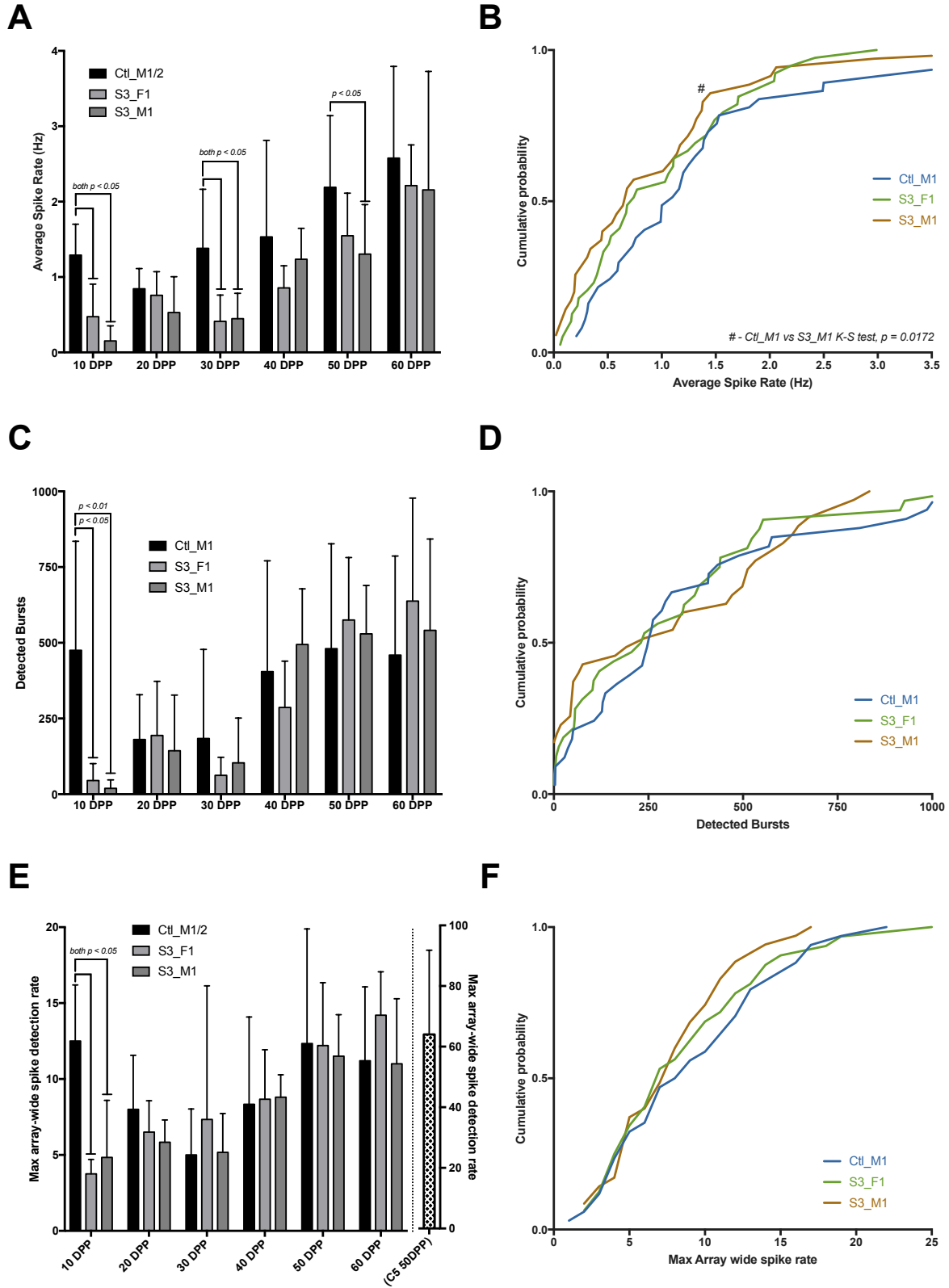
Neuron bursting is a second key measure of neuronal maturity and excitability, with an increase in bursts anticipated as the cell develops, owing to an increase in expression of synaptic ligand- and voltage- gated ion channels. In this study, the number of detected bursts increased throughout the experiment in both SHANK3 mutant lines and the control line (Figure 6.5C). A notable exception to this trend was the number of bursts detected at 10DPP in the Ctl_M1 neurons, which presented with an average of 475 ± 306.22 bursts, over double the number detected at 20DPP (180.6 ± 148.11) and 30DPP (183.6 ± 294.40). Indeed, due to this exception, 10DPP was also the only time point to show a significant difference between the control and both SHANK3 lines (see table 6.1 for statistics). Across the remaining time points there was no difference observed in the number of bursts detected between the SHANK3 lines and the control line. As with average spike rate, to gain an overall picture of the number of bursts detected across the experiment, pooled data over all time points for each cell line was processed as cumulative probability distributions (Figure 6.5D). This shows clearly across the experiment as a whole that there was no difference in the number of bursts detected in the S3 lines compared to the Ctl_M1 line.

Finally, as discussed and shown in Figure 6.4, there was no development of synchronised network behaviour in any of the cultures across all three cell lines. As described in Chapters 3 and 5, one of the most useful measures for analysing the synchronicity of cultures is the maximum array-wide spike detection rate (max ASDR), which represents the average maximum number of spikes detected across the whole culture in a single 200 ms bin. Figure 6.5E shows the development of the max ASDR for both SHANK3 lines and the control line across the 60 days of the experiment. Throughout the cultures development, there is an overall increase in the number of spikes counted in 200 ms bins across all three cell lines, which corresponds to the increase in general excitability already reported. Again, there is an exception at 10 DPP, where the max ASDR in Ctl_M1 neurons was higher than observed at 20DPP to 40DPP and there was significant difference between control neurons and both SHANK3 lines. As with detected bursts, at all other time points there was no difference between the control and SHANK3 lines. However, the most important aspect of this analysis was that it highlighted how low the max ASDR was even at the most developed time point compared to what was observed for a

6. Functional phenotyping of ASD patient neurons

corresponding time point in Chapter 5 (Figure 6.5E; 'C5 50DPP'). At every time point in this study, the max ASDR is below 20 for all three cell lines, which compares to around that reported for the neurons up to 30 DPP in Chapter 5, before the development of synchronised behaviour. This strongly suggests that the cultures in this chapter are not approaching a state of network-driven coordination. Finally, Figure 6.5F presents the cumulative probability distributions of the pooled max ASDR data from all six time points for both SHANK3 cell lines and the control line. While this showed a slight shift in the distributions of both SHANK3 lines, especially in S3_M1 neurons, towards fewer spikes per bin, this is essentially a correlate for the general excitability described in Figure 6.5A&B. K-S tests of the distributions showed that neither the S3_F1 or S3_M1 populations were significantly different to the control population.

6. Functional phenotyping of ASD patient neurons



6. Functional phenotyping of ASD patient neurons

Figure 6.5 – Analysis of spontaneous excitatory behaviour in developing iPS cell derived neurons from patients with heterozygous deletions in *SHANK3* cultured on and recorded with MEAs. Two NPC cell lines harbouring mutations in *SHANK3*, S3_F1 and S3_M1, and one control line, Ctl_M1, were differentiated into forebrain projection neurons and re-plated onto MEAs after 2 weeks of standard culturing. On arrays, neurons were cultured for 60 days and 10 minute recordings of spontaneous action potentials were taken every 10 days. **A, C and E** show the summary plots of the data recorded at each time point for each cell line; **B, D and F** represent cumulative probability distributions for the pooled data of all time points for each cell line. General spontaneous activity, in the form of average spike rate, increased over development in both *SHANK3* and control cell lines, however mutant lines were less active overall than control lines with differences reaching significance at 10, 30 and 50 DPP (**A**). This trend was seen when looking at the spike rate across the whole experiment time course (**B**). The number of bursts detected in cultures generally increased in all three cell lines over development, however there were no differences between the mutant and control neurons except at 10DPP (**C**). Across the entire population time course, there was no difference in the number of burst detected between the cell lines (**D**). **E** shows the maximum array wide spike detection rate (max ASDR) which represent the maximum number of spikes detected across the cultures in a single 200 ms bin. For all cell lines, this increased throughout the experiment (with a notable exception at 10 DPP for Ctl_M1 neurons) however it remained very low for all time points, indicating that neuronal activity from all three lines did not develop to become coordinated later in development. This is highlighted by the C5 50DPP bar which shows the extent of the max ASDR from the work in Chapter 5, where cultures did become synchronised. Summary plots **A, C and E** show means + S.D and statistics represent Tukey's multiple comparisons following 2-way ANOVA. All data represents recordings from at least 10 arrays/time point/cell line across 3 differentiations.

6. Functional phenotyping of ASD patient neurons

6.3.3 Interneuron populations in SHANK3 mutant and control cultures

The work in Chapter 5 suggested an important role for GABAergic interneurons in the regulation of synchronised network activity in iPS cell derived cultures. It also showed that, despite differentiation protocols tailored for the production of forebrain projection neurons, around 5% of the neurons expressed GAD67, a key marker of GABAergic interneuron fate. The previous section highlighted that, despite repeated attempts, coordinated network-driven activity was not observed in cultures from all three of the cell lines used in this chapter. To determine whether the neurons produced in this study, with different protocols, also contained a population of interneurons, a quantitative assessment of GAD67 +ve cells was performed. Neurons at 50 DPP from both SHANK3 mutant lines and the control line did show some limited expression of GAD67 (Figure 6.6). The images in Figure 6.6A show the regions imaged which represented the highest number of observed GAD67 +ve neurons for each line. Quantification of this staining showed that an average of fewer than 1% of MAP2 +ve neurons also expressed GAD67 across all three cell lines (Ctl_M1: $0.905 \pm 0.36\%$; S3_F1: $0.8 \pm 0.29\%$; S3_M1: $0.73 \pm 0.21\%$; Figure 6.6B). There were no differences between the number of GAD67 +ve cells between SHANK3 mutant and control neurons. Importantly, the number of interneurons present in these cultures here are considerably below what was observed in the cultures used in Chapter 5 (around 5%), suggesting that a lack of inhibitory tone in these cultures here could be responsible for the absence of observed network activity.

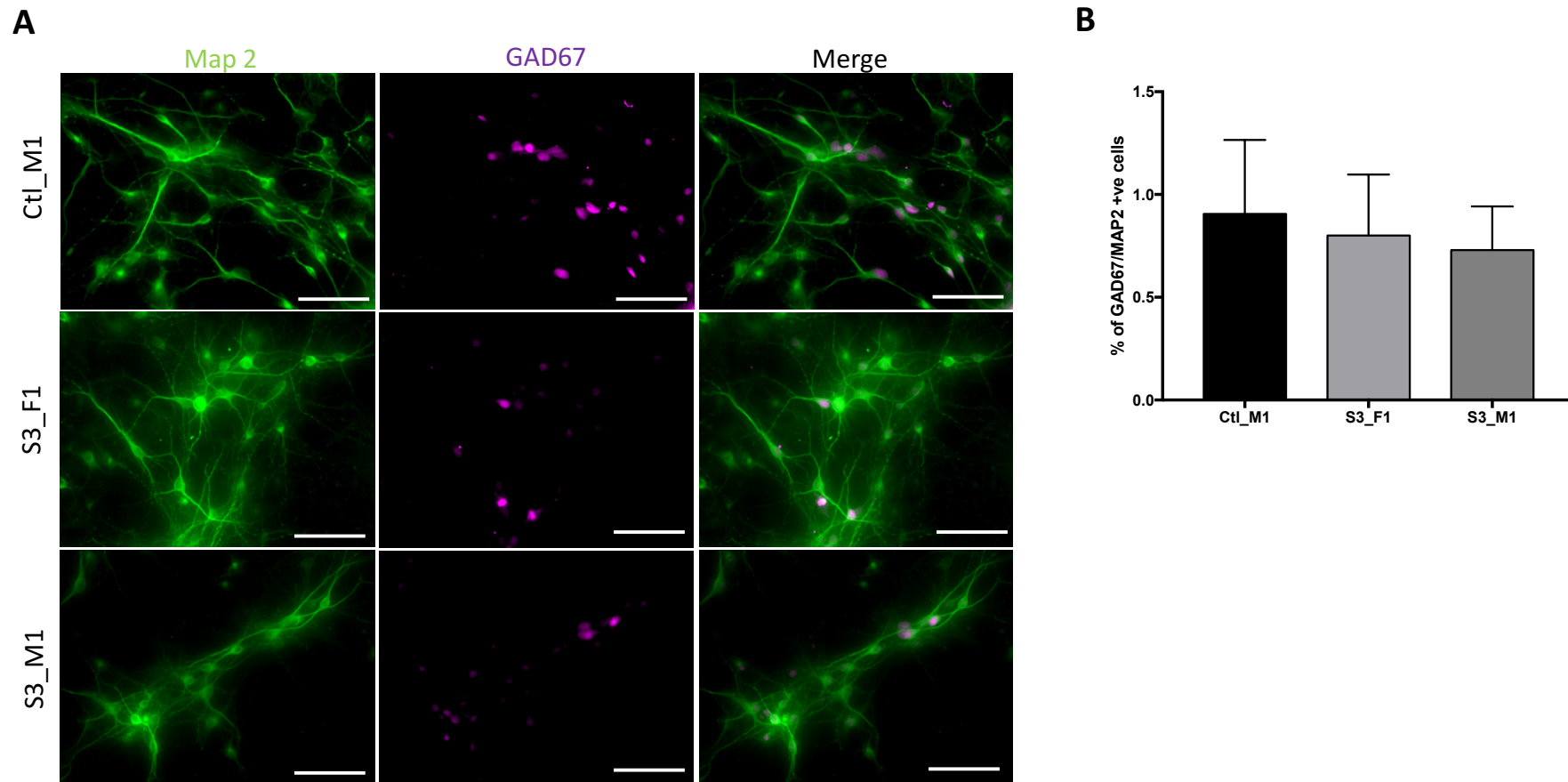


Figure 6.6 – Neuronal cultures derived from both patient *SHANK3* mutant and control iPS cells contain very few interneurons. To determine whether interneurons in neuronal cultures could be the cause of unsynchronised activity detected with MEA recordings, parallel cultures of Ctl_M1, S3_F1 and S3_M1 neurons were stained for GAD67 and MAP2 at 50 days for plating (50DPP). Due to technical limitations, 2 coverslips was available for staining for each cell line across 2 differentiations. Very few GAD67 +ve neurons were seen in any of the regions imaged across any of the cell lines. The images shown in **A** are the regions from each of the cell lines that represented the highest number of GAD67 +ve neurons seen in each. **B** shows the number of GAD67 and MAP2 +ve neurons as a proportion of the total MAP2 cells, in the limited quantification available. Bars show means + SD. Scale bars in **A** = 50 μ m.

6. Functional phenotyping of ASD patient neurons

6.3.4 Pharmacological profiling of SHANK3 mutant and control neurons

Section 6.3.2 presented results which suggested that, in general, neurons derived from iPS cells with heterozygous SHANK3 deletions are less spontaneously excitable than those from control neurons. To establish an understanding about the physiological nature of the spikes being produced by neurons from both SHANK3 and control lines, pharmacological profiling was performed on a sub-set of arrays at 41DPP, exposing neurons to APV, CNQX and bicuculline. As in Chapter 5, this was performed serially on cultures, in between washes where required, with a 10 minute period of equilibration in an incubator.

Figure 6.7A shows raster plots of one array culture (S3_F1 cell line) throughout the profiling experiment, excluding intermediate washes. Although difficult to determine accurately by eye, the raster plots suggest that there is very little effect of any four drug combinations used for the experiment – indeed, it is for this reason that representative raster plots for one cell line only is presented as there was little observable difference between any of the corresponding plots. It should be noted that due to the high degree of both inter- and intra- cell line variation observed when assessing average spike rate and bursts, the summary plots of actual means for each condition were difficult to visually resolve. As such, it was decided to present summary data as the ratio of change, relative to a baseline determined as the first recordings in standard medium for each cell line ('Std' on graphs; e.g. mean Ctl_M1 APV spike rate / mean Ctl_M1 Std spike rate). Figure 6.7B and C therefore present the normalised change in average spike rate and detected bursts respectively, for Ctl_M1, S3_F1 and S3_M1 neurons in the presence of APV, CNQX and bicuculline.

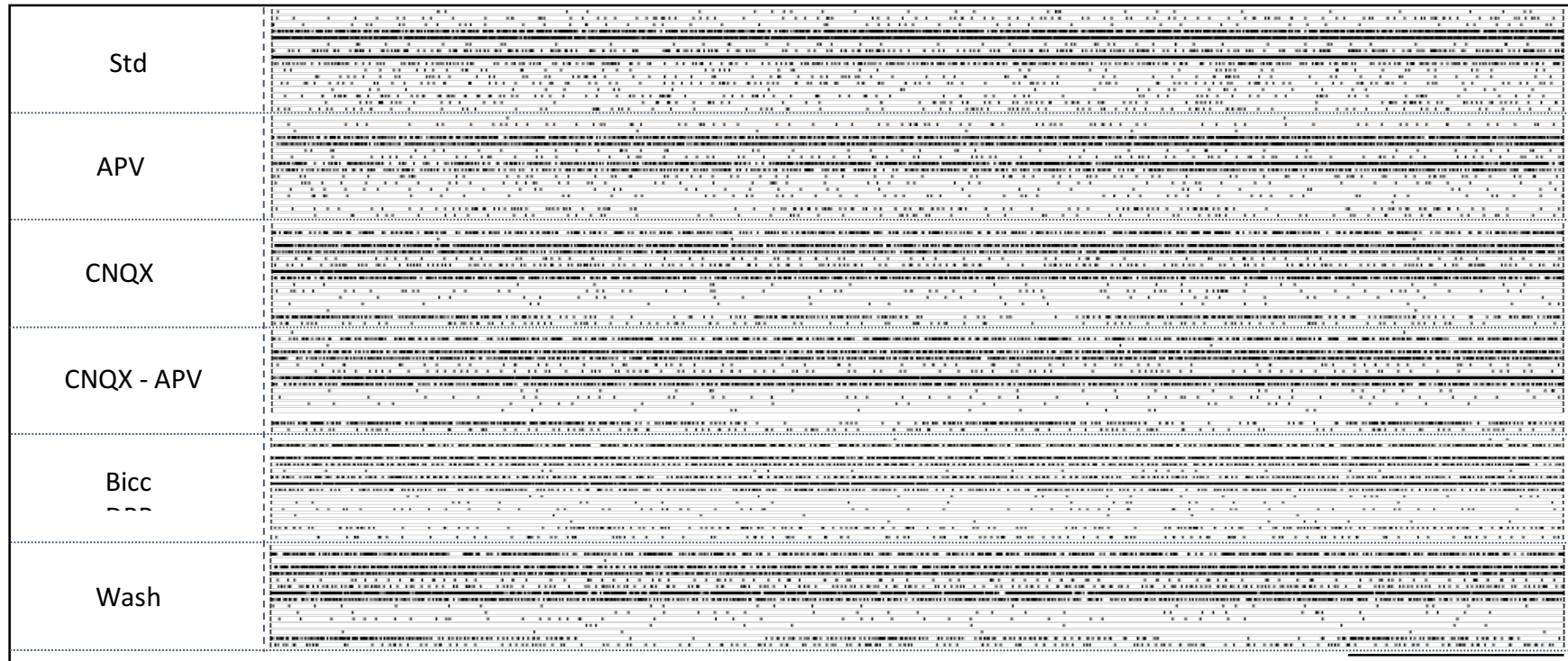
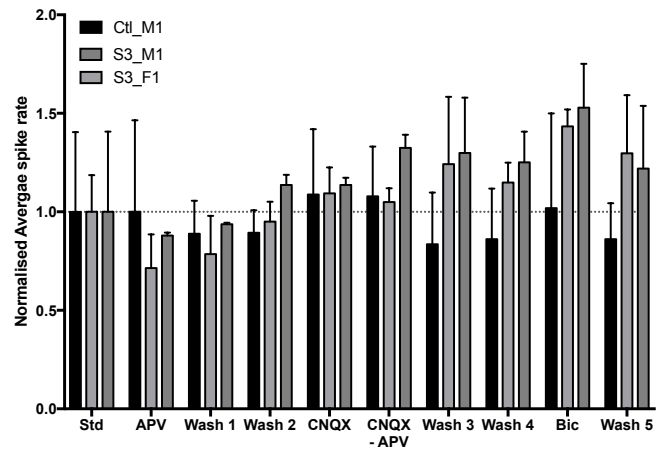
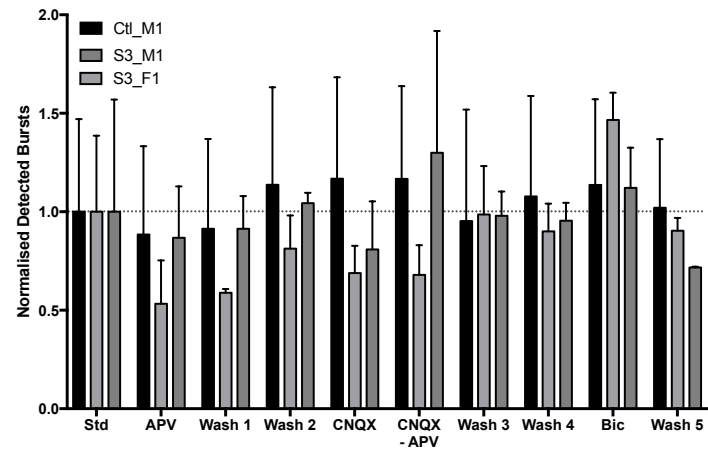
Overall, these results present a very variable picture of the response of these neurons to the drugs. For example, it appears that exposing S3_F1 and S3_M1 neurons, but not Ctl_M1 neurons, to APV causes a reduction in the average spike rate. However, while subsequent washes do rescue the reduction seen in the SHANK3 neurons, these washes actually reduce the average spike rate of the control neurons. Furthermore, the application of CNQX together with APV does not produce the same effect on SHANK3 neurons as APV alone, strongly suggesting that the observed changes seen are a result of variation within the experiment. Indeed, although 2-way ANOVA detected that there was a contribution of drug condition to the variation seen across the recordings ($F_{(9,45)} = 5.422$, $p < 0.0001$), no intra-cell line post-hoc

6. Functional phenotyping of ASD patient neurons

multiple comparisons were significant for normalised average spike rate. Similarly, application of bicuculline induced an increase in average spike rate in SHANK3 mutant neurons only, however this increase was not significantly different to either the standard conditions or the control cells with bicuculline.

As similarly variable pattern was seen with the number of bursts detected in response to drug application (Figure 6.7C). As with average spike rate, it appears that with application of certain drugs there is a differential response of neurons between the SHANK3 and control cell lines. However, as before, these changes are not consistent and suffer from a high degree of variation. For example, application of CNQX seems to reduce the number of bursts detected in both SHANK3 lines, while application of both CNQX and APV actually causes an increase in the number of bursts detected in the S3_M1 line compared to baseline. A 2 way ANOVA of the results showed that the contribution of drug condition to the variation in detected bursts was significant ($F_{(10,45)} = 4.196$, $p = 0.006$) but again no intra-cell line post-hoc multiple comparisons were significant.

The results from this section overall indicate that neurons from both SHANK3 lines and control lines are, at 41 DPP, largely insensitive to pharmacological manipulation. This in turn suggests that the spikes being produced by these neurons are primarily not driven by synaptic communication and are instead caused by intrinsic membrane potential fluctuations.

A**B****C**

6. Functional phenotyping of ASD patient neurons

Figure 6.7 – Pharmacological profiling of spontaneous activity in neurons derived from patients with heterozygous SHANK3 deletions and control iPS cells. MEA cultures of two SHANK3 mutant lines, S3_F1 and S3_M1, and a control line, Ctl_M1, were exposed to 50 μ M APV, 50 μ M CNQX and 10 μ M bicuculline during recordings at 41 days post plating (DPP). Drug application was applied serially to cultures, with 10 minute incubation periods between media changes and array recordings. **A** shows raster plots from one culture (S3_F1 line), excluding intermediate washes. Across the experiment as a whole, the application of these inhibitors had very variable effects on the spontaneous firing of the neurons from all cell lines, in terms of average spike rate (**B**) and Number of bursts (**C**). There were no differences between the response of the SHANK3 mutant neurons compared to the control neurons. The plots in **B** and **C** show the mean values, normalised to the first Std condition for each of the cell lines (e.g. Ctl_M1 APV / Ctl_M1 Std). Error bars show the SD of the normalised change. Total analysed cultures were at least 4 arrays in 3 differentiations. Scale bar in **A** shows 100 seconds.

6.3.5 Investigating the shape of extracellular spikes produced by SHANK3 mutant neurons

Throughout this project, the analysis of the shape of the spikes being produced by neurons has largely been limited to quality control measures: confirming that the detected events are extracellular spikes, isolating noise and the dissociation of groups of waveform traces in the event that a single electrode is detecting the activity of multiple units. The analysis of the waveforms themselves has not been a focus of this project, partly because similar data can be obtained more accurately using single cell electrophysiology and partly because the informatic protocols required for the analysis of such data has been more difficult to develop. However, routine inspection of the spike shapes being produced by neurons from both SHANK3 patient lines revealed the presence of shapes previously unobserved throughout all this projects experiments. Figure 6.8A&B shows the waveforms of extracellular spikes for 16 electrodes recording the activity of a Ctl_M1 and S3_F1 culture at 40DPP. The S3_F1 traces highlighted in red and expanded in Figure 6.8C show the electrodes recording noticeably different spike shapes. These spikes appear markedly wider than other shapes across either culture and surprisingly, some appear to have a 'double-peak' shape, which manifests as a shoulder when the waveforms from that electrode trace, including more standard spike shapes, are averaged (Figure 6.8C; E31 - thick black trace shows median waveform for the electrode). Importantly, it should be noted that the majority of the spike shapes produced by this SHANK3 mutant culture appear identical to the range of shapes that are seen in the Ctl_M1 neurons and are also in line with the waveforms seen throughout the work in Chapter 5. However, visual inspection of waveforms from all of the recordings done as part of the experiments for this chapter, suggested that these wider 'double-peak' spikes only appeared in neurons derived from SHANK3 mutant lines. Moreover, examples of these waveforms were identified in every time point examined and in every round of neuron differentiation.

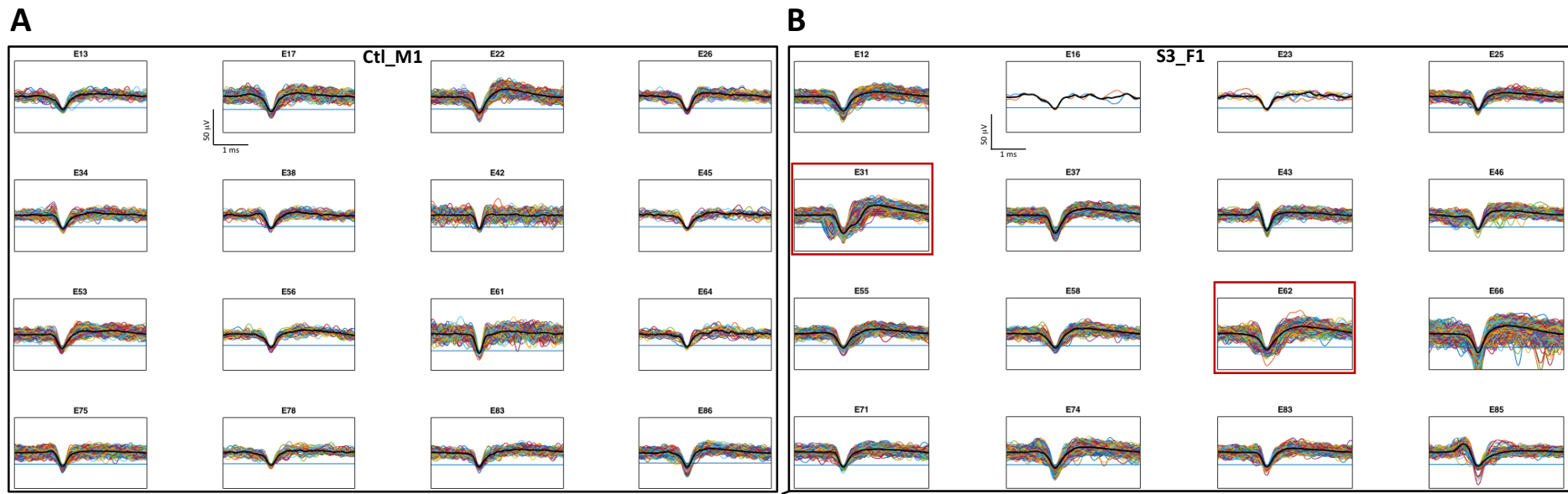
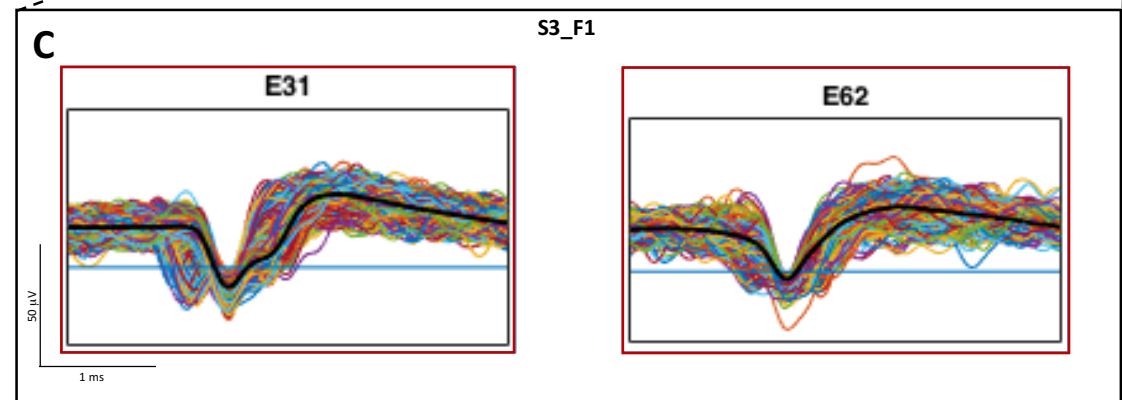


Figure 6.8 – iPS cell derived neurons with deletions in SHANK3 produce extracellular spikes with novel shapes. The analysis of the shape of the spikes being produced by neurons is primarily used as a ‘quality control’ measure for more general analysis or to identify multi-unit activity. However, visual observations of several of the electrode traces from SHANK3 mutant neurons revealed the presence of markedly different spike shaped that appeared unique to these cell lines. **A** shows the spike shapes for the 16 analysed electrodes for a recording of Ctl_M1 neurons at 40DPP, **B** shows the shapes for the 16 electrodes analysed for a recording of S3_F1 neurons at 40DPP. The traces highlighted in red and enlarged in **C** show the electrodes which contained spike shapes which appeared broader and in some cases, with a ‘double-peak’. Black waveforms show the median trace shape for each electrode.



6. Functional phenotyping of ASD patient neurons

To try to determine objectively whether these new spike shapes were unique to SHANK3 mutant neurons, waveform feature extraction followed by unsupervised clustering was performed. In order to achieve the most complete analysis possible of the waveforms, the spike shapes from 3 arrays per cell line (control: Ctl_M1, two SHANK3: S3_F1 and S3_M1) for 6 time points (10DPP to 60DPP) across 2 differentiations were pooled together to create a comprehensive database of spike shapes throughout development of these neurons. The resulting data pool was a total of 401394 spikes, which ultimately proved too large for effectual handling. However, feature extraction could be performed on the dataset in the form of principle component analysis (PCA) of the waveform amplitude. This was chosen over using transformed data, such as the first or second derivative of the waveform, as this did not provide any benefit in terms of separation of shapes but added another step in analysis. Figure 6.9A shows the distribution of the first two principle components of the wave forms for all 401349 spikes. This showed that the vast majority of waveforms cluster together in a central region, with 4 or 5 satellite clusters presumably representing spikes with different shapes. As mentioned, the use of the full pooled data set was logistically prohibitive. Instead, a random sample of 20000 waveforms from the full dataset was extracted to provide a set which, as far as possible, represented the total dataset in terms of the variety and respective ratios of spike shapes, while allowing a comprehensive analysis of the data. The distribution of the first two principle components for the waveforms in this random sample is presented in Figure 6.9A, along with the stacked traces for each of the 20000 waveforms. PCA profiling of the sample dataset (referred to herein as the '20k set') produced a data spread similar to that of the full set, with a central cluster surrounded by smaller, less dense clusters. In order to objectively cluster the 20k set and to allow identification of the spikes within each cluster, the density-based clustering algorithm DBSCAN was used. DBSCAN was chosen over other methods such as k-means clustering as it does not require the pre-determination of the number of clusters in the sample, can sort data with a variety of cluster shapes and sizes and allows the concept of unclustered noise (see Chapter 2 and 3 for clustering details).

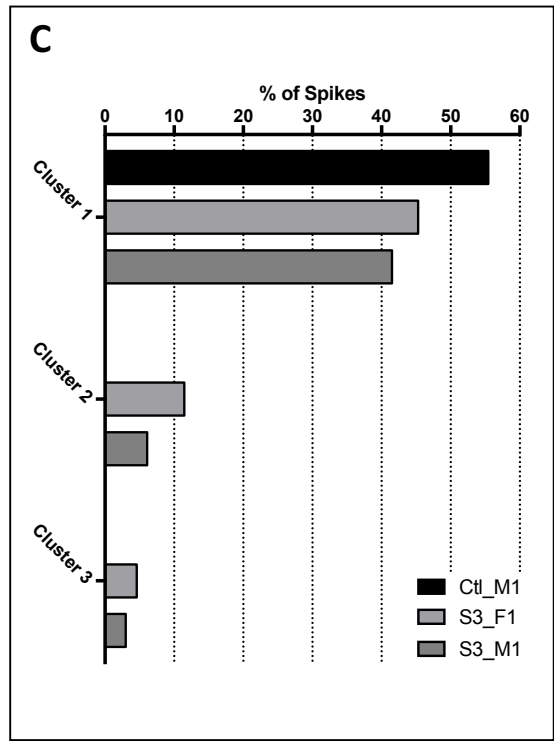
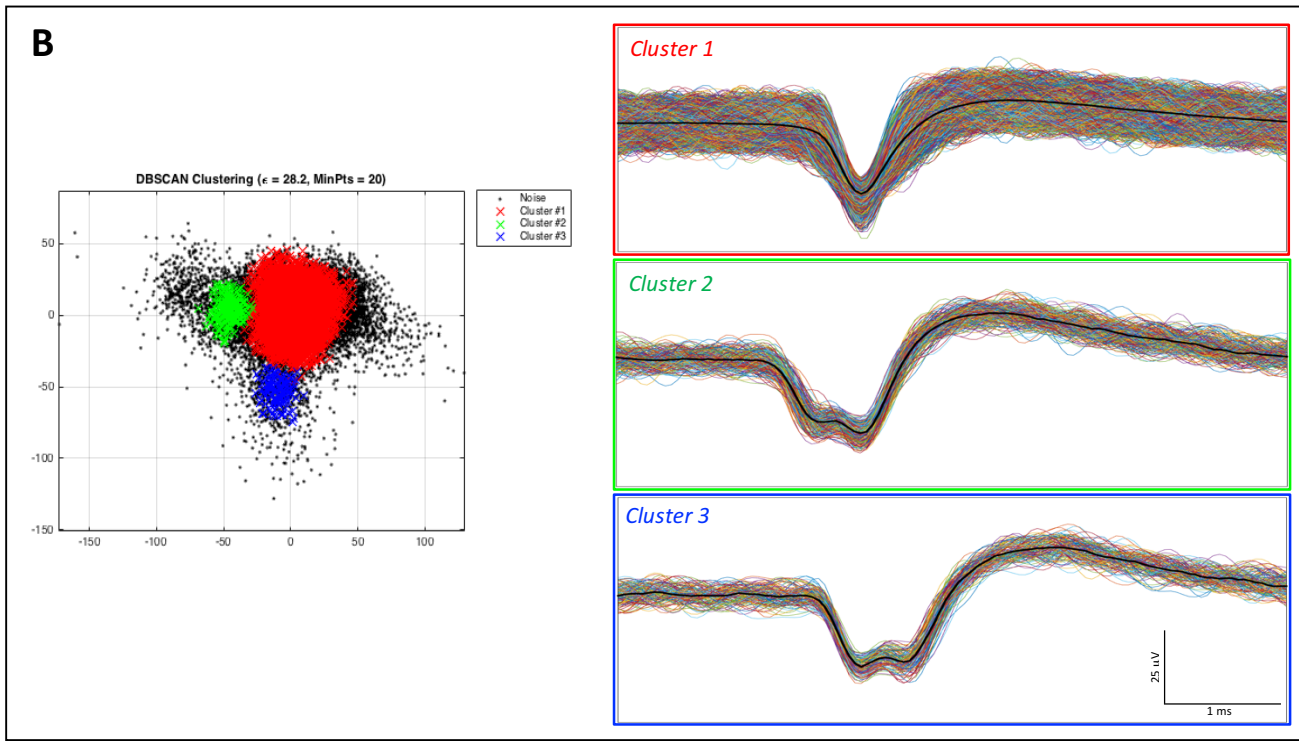
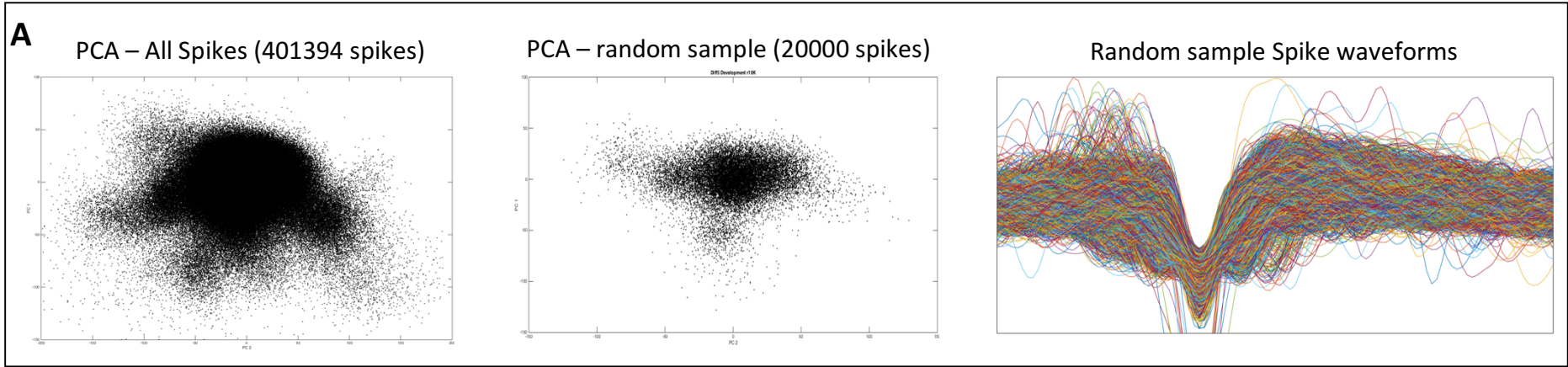
The PCA data of the 20k set was put through DBSCAN with the optimised parameters $\epsilon = 28.2$, min points = 20. This analysis produced three distinct clusters in the data: a large central cluster comprising the majority of data points, and two smaller surrounding clusters (Figure 6.9B). It should be noted that around 50% of the spikes were not successfully clustered and were excluded as noise. The spike shapes from each cluster were then extracted and are presented

6. Functional phenotyping of ASD patient neurons

in Figure 6.9B. This showed clearly the differences in the spike waveforms of the three clusters and, importantly, identified that clusters 2 and 3 were comprised entirely of the wide double-peak waveforms that were observed initially in SHANK3 mutant cultures. Furthermore, this also highlighted that the double - peak nature of these spikes are the cause of the markedly increased width. It is interesting that two spatially distinct clusters are identified which represent spike shapes that appear visually to be very similar – or, at least, as dissimilar as many of the spike shapes that appear in the albeit larger central cluster 1.

Finally, to determine whether these wider spikes were unique to SHANK3 mutant neurons, individual waveforms from each of the clusters was traced back to the array from which it was recorded. Strikingly, this corroborated the initial observations that these wider double-peak spikes were only produced by neurons with SHANK3 mutations (Figure 6.9C). In fact, the majority of clustered spike shapes from both S3_F1 and S3_M1 neurons appeared in cluster 1 (45.29% and 41.5% respectively) along with 55.43% of Ctl_M1 spikes (representing 100% of the clustered control spikes). However, both S3_F1 and S3_M1 neurons had a small percentage of spikes which appeared in clusters 2 (11.46% and 6.11%) and 3 (4.58% and 2.99% respectively). No Ctl_M1 spikes appeared in Clusters 2 or 3.

The results from this section have revealed the presence of a small population of spike shapes that are unique to neurons derived from SHANK3 mutant iPS cells. These spikes are dramatically wider than any other observed waveform, due to the presence of notable double 'peak'. Importantly, the majority of spikes produced by SHANK3 mutant neurons have standard shapes in line with that observed from control neurons. Moreover, these unique shapes are not detected by every analysed electrode of a particular array, suggesting that these shapes are not produced by all SHANK3 mutant neurons. Instead, the double-peak waveforms appear in a small number of electrode traces, often together with more standard spike shapes, possibly implying that they are produced by a small number of SHANK3 mutant neurons which are also capable of producing standard spikes. Importantly, the waveforms were observed in arrays from all developmental time points and across multiple differentiation repeats.



6. Functional phenotyping of ASD patient neurons

Figure 6.9 – Clustering of spike shapes from patient SHANK3 mutant iPS cell derived neurons reveals a unique population of waveforms. Spike wave forms were extracted from array recordings comprising 3 arrays per cell line across 6 developmental time points and over two differentiations of a control line (Ctl_M1) and two SHANK3 mutant lines (S3_F1 and S3_M1) and pooled together. This comprehensive developmental database of spike shapes totalled 401394 spikes – too large for effectual handling and analysis. However, plotting of the first two principle components following principle components analysis (PCA) was possible and showed the presence of a main central cluster surrounded by several satellite clusters (**A**). To provide a representation of waveforms from across development which could be processed, a random sample of 20000 spike shapes was taken from the complete pool (first 2 PCs and waveforms shown in **A**). To objectively cluster the dataset, DBSCAN clustering was performed on the PCA data from the sample data set with the parameters $\epsilon = 28.2$, min points = 20 (**B**). This identified 1 central cluster surrounded by 2 smaller clusters, which contained the spikes shapes shown in the wave plots. Importantly, the analysis pulled out unique ‘double-peak’ spike shapes present in the smaller clusters 2 and 3. Each spike waveform was traced back to to the array and cell line from which it came and the proportion of each clustered waveform present in each cell line was calculated (**C**). Strikingly, the double-peak wave forms were only present in SHANK3 mutant cell lines. Bars in **C** show the percentage of clustered waveforms that appeared in each cluster from each cell line. Note that roughly half of the spike shape from each line could not be successfully clustered.

6. Functional phenotyping of ASD patient neurons

6.3.6 Pharmacological profiling of spike shapes in SHANK3 mutant neurons

The previous section showed that in a sample dataset of spikes recorded across neural development, a minority of spikes produced only by SHANK3 mutant neurons present with a markedly different shape. As described in Chapter 1, many of the key interactions of SHANK3 at the synapse are as part of the extended NMDA receptor complex. To determine whether the double-peak spikes produced by SHANK3 mutant neurons could be caused by an underlying alteration in the NMDA receptor complex, the spikes shapes from the pharmacology experiments described in 6.3.3 were analysed. For this, the data from two arrays of both S3_F1 and S3_M1 cultures that underwent the pharmacological profiling was pooled and processed using PCA followed by DBSCAN clustering of the waveforms, as described in the previous section. To maintain consistency of the analysis, the same parameters were used for the clustering of each condition ($\epsilon = 30$, min points = 20).

Figure 6.10A shows the results of DBSCAN clustering of the spike wave forms of SHANK3 neurons in standard conditions and in the presence of APV and CNQX, which was used as a control for the APV application. Each plot shows the distribution of first two principle components together with the clustered spikes as determined by DBSCAN. The blue and green insets show the waveforms of clusters 2 and 3 for each condition, which only contain spikes showing the double peaks. Firstly, its noticeable that there is not a clear visible difference between the distributions and the clustering results when the cells are exposed to APV or CNQX. All four conditions show, as in the previous section, a central main cluster surrounded by two satellite clusters containing the two similar but spatially distinct groups of double-peak spikes. Its worth noting that, due to the more focused data set on which this analysis was performed (i.e. a total of 4 cultures, serially recorded four times each, all at 41 DPP) a more efficient clustering of the data was achieved, with fewer data points excluded as noise than those in section 6.3.5. Quantification of the number of cluster 2 and 3 spikes detected across drug applications confirmed that there was no difference in the proportion of each cluster representation with APV or CNQX treatment compared to standard conditions (Figure 6.10B). These results therefore suggest that the double-peak spike shapes identified from SHANK3 mutant neurons are not driven by NMDA (or AMPA) receptor mediated synaptic activity.

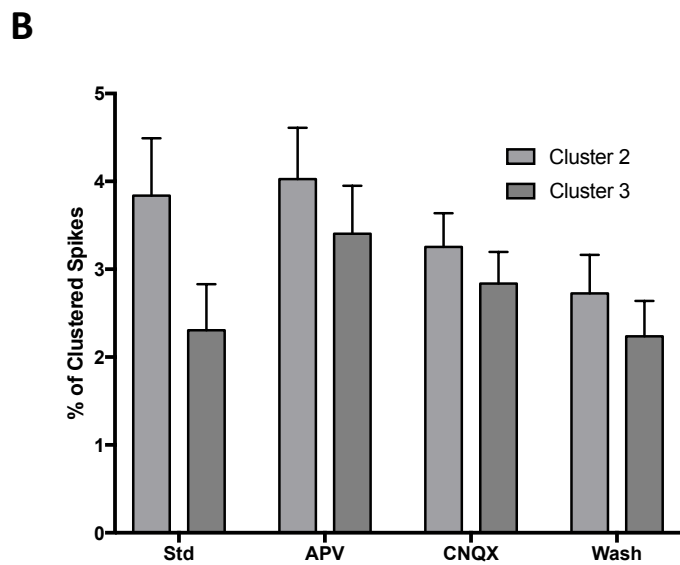
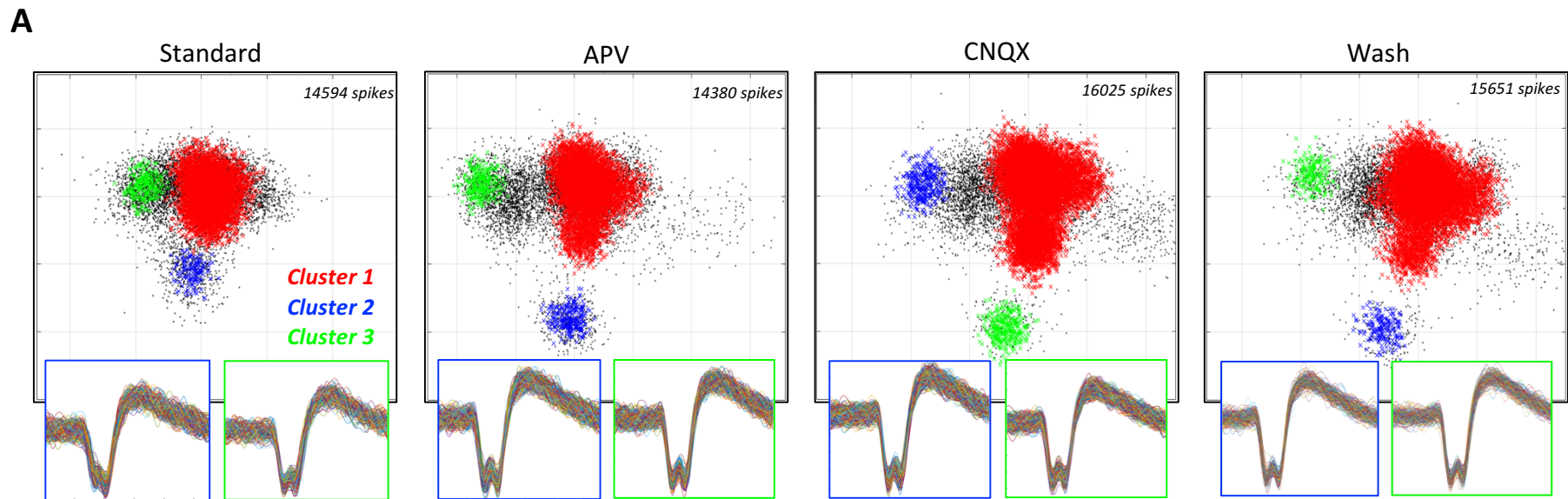


Figure 6.10 – Extracellular spike shapes from iPS cell derived neurons with mutations in SHANK3 are not sensitive to NMDA and AMPA receptor inhibition. A minority of the spikes produced by SHANK3 mutant neurons have a unique waveform shape, with a ‘double-peak’ and, subsequently, a wider profile. To determine whether these spikes may be driven by NMDA receptor activity, of which SHANK3 is part of the wider NDMA protein complex, the spike shapes of a sample of MEA array cultures with SHANK3 mutant neurons (both S3_F1 and S3_M1 lines) were analysed over the course of a pharmacological profiling experiment. **A** shows the results of DBSCAN clustering of the principle components of the pooled waveform data from two arrays each of S3_F1 and S3_M1 neurons during exposure to APV (50 μ M) and CNQX (50 μ M). DBSCAN parameters were set at $\epsilon = 30$, min points = 20 for each analysis. Coloured insets for each show the resulting waveforms for the corresponding green or blue clusters. The analysis showed that there was no change in the number of these double-peak spikes with APV or CNQX exposure, as a percentage of the total clustered spikes (**B**). In each treatment, the majority of clustered spikes all appear in cluster 1. The number of spikes analysed for each treatment is noted in each plot. Bars show % of clustered spikes + Wilson/Brown proportion confidence intervals.

6.3.7 Investigating spontaneous calcium events in SHANK3 mutant iPS cell derived neurons

Section 6.3.2 highlighted that neurons derived from patient iPS cells with heterozygous SHANK3 deletions showed decreased excitability, in terms of spontaneous action potentials, compared to control neurons. As part of its scaffolding function at excitatory synapses, SHANK3 is associated with several aspects of intercellular calcium levels, including entry via NMDA and AMPA receptors, activity of post-synaptic L-type calcium channels and regulation of mGluR5 receptor – linked intracellular calcium storage. To investigate whether reduced spontaneous neuronal activity could be driven by underlying alterations to cellular calcium transients, neurons from both SHANK3 mutant lines and the control line were subjected to calcium imaging.

As described in Chapter 2, calcium imaging was achieved with acute exposure of the cells to the labelled calcium indicator Fluo-4, allowing visualisation of the cells and calcium movements with a 488 nm wavelength filter set (Figure 6.11A). Images of chosen regions were captured at 10 Hz for 5 mins for all experiments. Following image processing, regions of interest (ROIs) were selected using a semi-automated segmentation algorithm based in the Matlab based package NeuroCa. For all of these experiments, calcium transients were only analysed in somas, therefore all ROIs were confined to individual cell bodies (Figure 6.11B). Analysis of fluorescence traces from each ROI and the detection and analysis of individual calcium events was performed using the Matlab based FluoroSNNAP (Figure 6.11C), where four key characteristics were chosen for comparisons: inter-spike interval (ISI), event amplitude, rise-time and fall-time (Figure 6.11D).

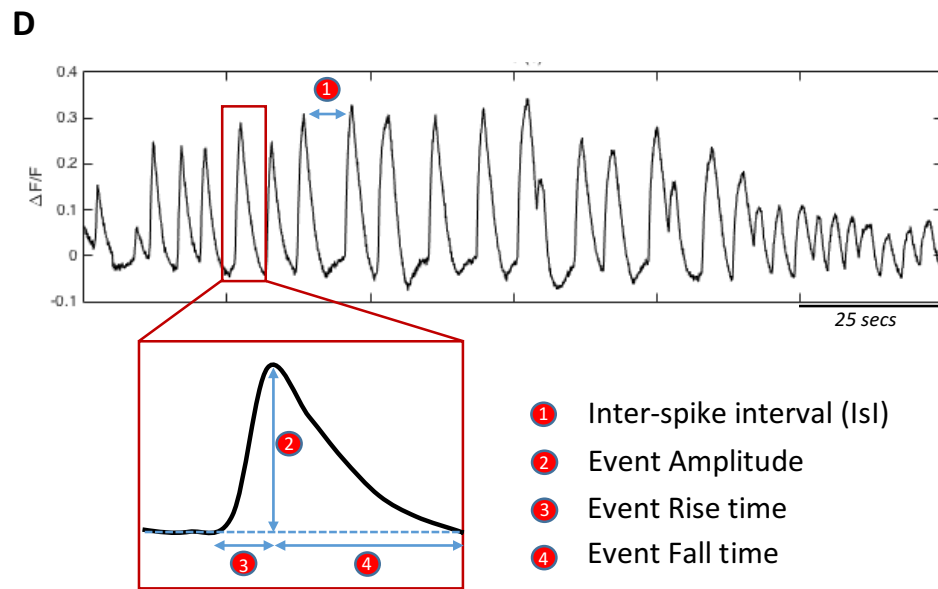
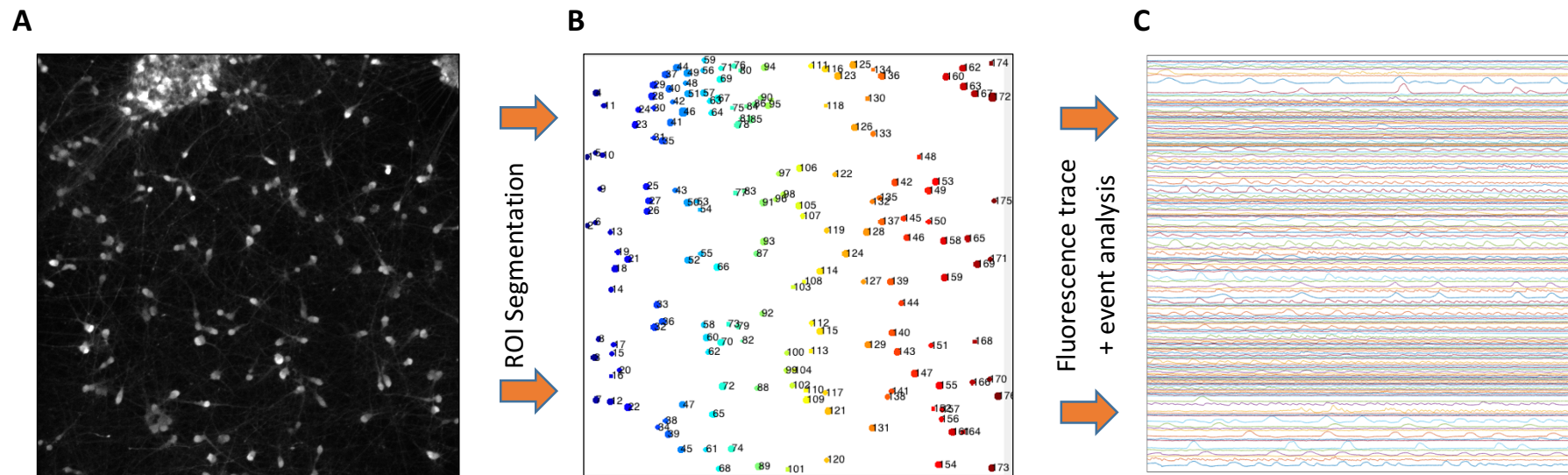


Figure 6.11 – Calcium imaging of iPS cell derived neurons. Differentiating neurons were analysed for spontaneous calcium events using Fura 4 dye at 40 – 45DPP. After exposing neurons to the dye and accessory agents, neurons were imaged using epifluorescence with a 488 nm excitation filter set. Images were captured at 10 Hz for 5 minutes (**A**). Individual ROIs (cell bodies) were found using a circular Hough transform - based method via NeuroCa software (**B**). The analysis of single cell fluorescence traces and detection and analysis of calcium events was performed using FluoroSNNAP, where events were selected based upon a combination of threshold and template matching (**C**). Analysis of calcium events was limited to the level of single cells – no network or cluster analysis was completed. Along with inter-spike interval (ISI) as a proxy for general cell excitability, three key event characteristics were selected as analysis measures: event amplitude, event rise time and event fall time (**D**).

6. Functional phenotyping of ASD patient neurons

The use of dye-based calcium imaging in iPS cell derived neurons can often lead to confusion over the nature of any detected activity, particularly because of the potential for poor signal-to-noise ratios and the often-slow nature of calcium events compared to those recorded from rodent neurons. To first establish an understanding about the events being recorded here and to determine any role of synaptic function in the calcium transients, coverslips of neurons from the control line Ctl_M1, and both SHANK3 mutant lines, S3_F1 and S3_M1, lines exposed to APV and CNQX during imaging at 40DPP. Figure 6.12A shows representative normalised fluorescence traces ($\Delta F/F$) from the Ctl_M1 line of the same 10 ROIs (using the same segmentation mask) over the period of the experiment. Strikingly, application of APV induced an almost total loss of calcium events in all ROIs, which was rescued following drug washout. Application of CNQX attenuated the activity less, with some traces showing a reduction of events while others remaining broadly similar. These trends were mirrored in the full experimental analysis, where APV exposure caused a dramatic and significant reduction in the average number of events detected per ROI in the control line and both SHANK3 lines (Figure 6.12B, change compared to respective Std values; Tukey's multiple comparisons following 2-Way ANOVA, see Table 6.2). Application of CNQX to the neurons caused a smaller but still significant reduction in the number of calcium events compared to standard conditions, with an average decrease of 38% across the three lines (see Table 6.2 for statistics). Calcium transient activity returned to baseline after washout following application of both drugs. Note, the average number of events was presented in this initial analysis rather than average inter spike interval (as presented in the following section) due to the low number of events in the APV conditions and the subsequent difficulty of calculating a representative average inter spike interval for each ROI.

These results show that the events being detected by these calcium imaging experiments on control and SHANK3 mutant neurons are, for the most part, calcium transients being driven by glutamatergic synaptic activity. Moreover, the results strongly suggest that the majority of the calcium events require NMDA receptor function, while around 40% require AMPA receptor function. This is notable as these results are in contrast with those reported with the MEA experiments in section 6.3.4, where extracellular – recorded action potential activity was largely unaffected by AMPA or NMDA receptor inhibition. Never the less, these results provide confidence that any genotype effects that may be observed in subsequent calcium imaging experiments can be analysed in the context of functional synaptic activity.

6. Functional phenotyping of ASD patient neurons

Table 6.2. Summaries of statistics of the calcium imaging experiments profiling SHANK3 mutant and control iPS cell derived neurons in the presence of APV and CNQX.

2-Way ANOVA, within genotype effects only - $F_{(10, 2352)} = 4.459, p < 0.0001$		
Tukey's Multiple Comparisons		
	Mean Difference (\pm S.E.)	p value
Std Vs APV		
<i>Ctl_M1</i>	43.34 \pm 1.908	p < 0.0001
<i>S3_F1</i>	35.63 \pm 1.458	p < 0.0001
<i>S3_M1</i>	36.74 \pm 1.573	p < 0.0001
Std Vs CNQX		
<i>Ctl_M1</i>	16.95 \pm 1.75	p = 0.0016
<i>S3_F1</i>	18.18 \pm 2.048	p < 0.0001
<i>S3_M1</i>	7.99 \pm 1.961	p = 0.0002

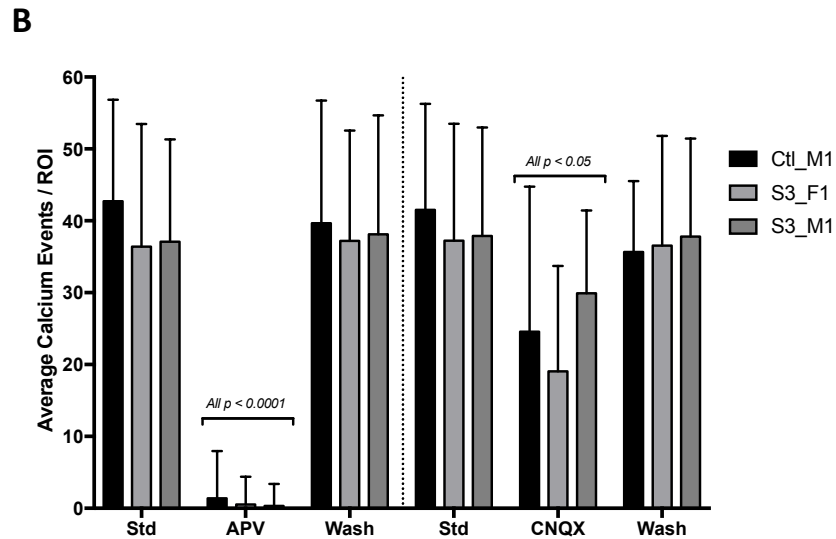
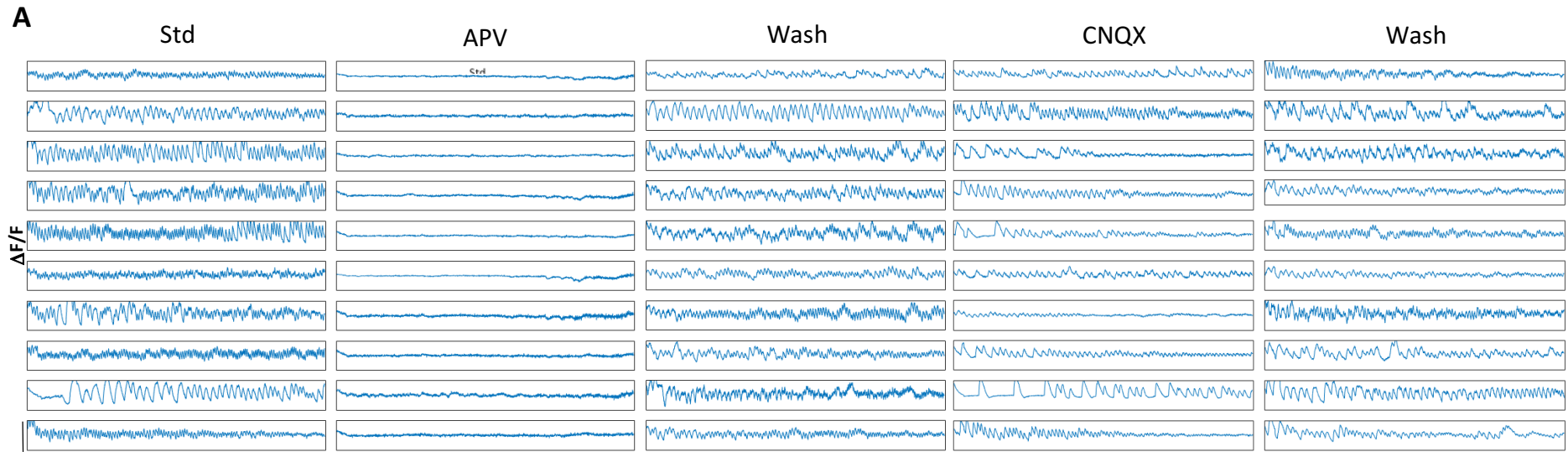


Figure 6.12 – Detected single-cell calcium transients from iPS cell derived neurons are sensitive to both NMDA and AMPA receptor antagonism. Two neural precursor lines derived from patients harbouring heterozygous deletions of SHANK3 (S3_F1 and S3_M1) and one control line (Ctl_M1) were differentiated into forebrain neurons. 40 days after replating, coverslips of neurons were exposed to fluo-4 calcium sensitive dye and somatic spontaneous calcium transients were recorded and analysed. To assess whether the events being recorded were mediated via synaptic communication, 50 μ M APV and 50 μ M CNQX were perfused into the recording chamber during imaging. **A** shows the fluorescence traces ($\Delta F/F$) for the same 10 neurons (Ctl_M1 cell line) during the drug profiling experiments. Exposure of the neurons to APV blocked most calcium activity in all 10 ROIs, while CNQX application inhibited some activity in some neurons. This trend was seen more generally across all three cell lines, where APV exposure caused an almost complete block of calcium events while CNQX caused around a 50% decrease in activity (**B**). Note, for each condition the same segmentation mask was used for each ROI. Vertical scale bar in **A** shows 0.4 ($\Delta F/F$); horizontal bar shows 100 s. Data in **B** shows means \pm SD. All statistics are Tukey's multiple comparisons following 2-way ANOVA. $n = 150$ ROIs for all cell lines across 4 imaging regions over 2 coverslips/line.

6. Functional phenotyping of ASD patient neurons

To investigate the effect of heterozygous SHANK3 deletions on the spontaneous calcium activity of iPS cell derived neurons, the full cohort of cells across three differentiations were imaged and analysed, focussing on the four characteristics described in figure 6.11B. For all experiments, neurons were imaged at between 40 and 45 DPP. Neurons derived from both SHANK3 mutant lines were less excitable in terms of calcium events compared to the control neurons, as shown by a significant increase in average inter spike interval (ISI), from a median of 3.25 s CI[3.85 – 4.37] in Ctl_M1 cells to 3.91 s CI[4.68 – 5.62] and 3.85 s CI[4.67 – 5.64] for S3_F1 and S3_M1 respectively (Figure 6.13A, Dunn's multiple comparisons following Kruskal-Wallis test, see Table 6.3 for statistics). Figure 6.13A also presents the corresponding cumulative probability plot, which clearly highlights the shift in distributions towards increased ISIs in both SHANK3 mutant lines.

Calcium transients from SHANK3 mutant neurons also exhibited changes in event shapes compared to those from control neurons. Most noticeably, calcium events from both S3_F1 and S3_M1 cells had significantly larger amplitudes ($\Delta F/F$) compared to Ctl_M1 neurons (Figure 6.13B; Table 6.3 for statistics), where transients from control neurons had a median amplitude of 0.08 CI[0.09 – 0.09] compared to 0.1 CI [0.09 – 0.11] and 0.11 CI[0.09 – 0.12]. Again, these changes were highlighted with the corresponding cumulative frequency plot (Figure 6.13B). There was also changes to the timing of the calcium events from SHANK3 mutant neurons. While there were no differences in the rise time of events between mutant and control neurons (Figure 6.13C), there was a small decrease in the fall time of events in both mutant lines compared to controls, falling from 0.94 CI[0.89 – 0.98] to 0.85 CI[0.79 – 0.90] and 0.85 CI[0.77 – 0.91] for S3_F1 and S3_M1 respectively (Figure 6.13D). However, only the decrease observed in S3_M1 neurons reached statistical significance (Table 6.3).

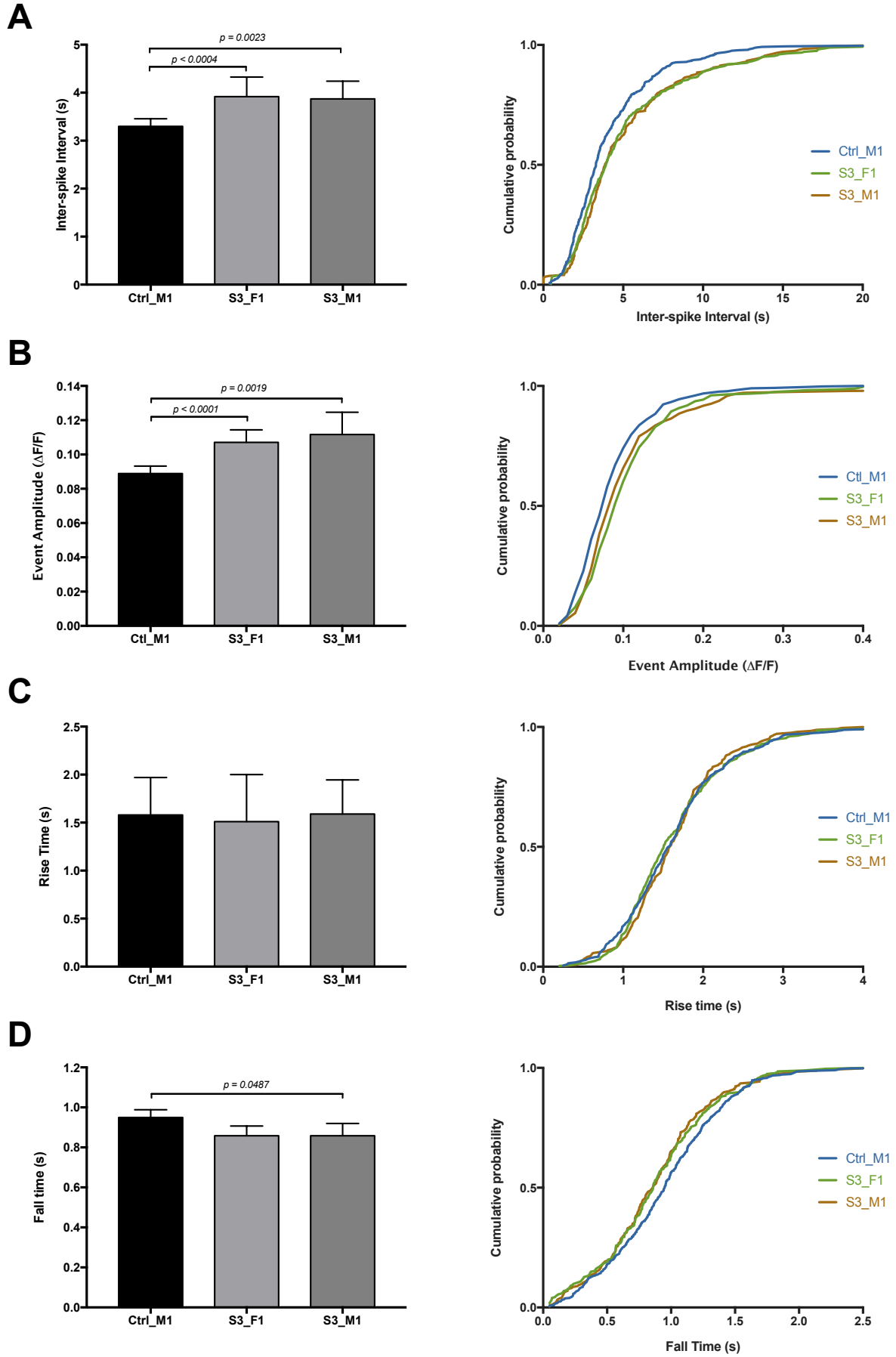
Together, these results suggest that heterozygous deletions of SHANK3 causes aberrant changes in the synaptically driven spontaneous calcium events observed in iPS cell derived neurons. The results corroborated the findings from the MEA experiments showing decreased neuronal excitability in SHANK3 mutant cells and also showed that these neurons had small but significant alterations in the shape of calcium events.

6. Functional phenotyping of ASD patient neurons

Table 6.3. Summary of the statistics calculated for the calcium imaging experiments on neurons derived from control iPS cells and iPS cells from patients harbouring heterozygous mutations in SHANK3.

	Kruskal wallis test	Dunn's multiple comparisons	
		Mean rank diff	Adjusted p value
Inter Spike interval	H = 19.51; p < 0.0001		
Ctl_M1 vs S3_F1		-73.98	0.0023
Ctl_M1 vs S3_M1		-88.83	0.0004
S3_F1 vs S3_M1		-14.85	> 0.9999
Event Amplitude	H = 28.47; p < 0.0001		
Ctl_M1 vs S3_F1		-110.8	< 0.0001
Ctl_M1 vs S3_M1		-79.08	0.0019
S3_F1 vs S3_M1		31.67	0.6696
Event Rise time	H = 0.42; p = 0.812		
Ctl_M1 vs S3_F1		No post-hoc comparisons	
Ctl_M1 vs S3_M1		No post-hoc comparisons	
S3_F1 vs S3_M1		No post-hoc comparisons	
Event Fall time	H = 7.86; p = 0.0197		
Ctl_M1 vs S3_F1		48.23	0.088
Ctl_M1 vs S3_M1		55.28	0.0487
S3_F1 vs S3_M1		7.044	> 0.9999

6. Functional phenotyping of ASD patient neurons



6. Functional phenotyping of ASD patient neurons

Figure 6.13 – iPS cell derived neurons from patients with heterozygous SHANK3 deletions show changes in single cell calcium events. Two neural precursor lines from iPS cells derived from two patients harbouring heterozygous deletions of SHANK3 (S3_F1 and S3_M1) and one control line (Ctrl_M1) were differentiated into forebrain neurons. After 40 days, coverslips of neurons were exposed to fura-4 calcium sensitive dye and somatic spontaneous calcium transients were recorded and analysed. Neurons from both S3_F1 and S3_M1 were less excitable than those from control cells, as shown by a significant increase in the inter-spike interval (**A**). Both mutant lines also showed changes in the shape of calcium events, with a significant increase in event amplitude seen in both (**B**) and a decrease in the fall time of events, although only the events from S3_M1 reached significance (**D**). There was no change in the rise time of events (**C**). For each group, the left panel summary plots show the median value + 95% confidence intervals; right panels show cumulative probability plots of all the grouped data. All statistics show results of Dunn's multiple comparisons following Kruskal-Wallis tests. n = 507 (CtI_M1), 482 (S3_F1) & 443 (S3_M1) ROIs across at least 5 image regions on at least 2 coverslips repeated over 3 differentiations.

6.4 Discussion

The results from this chapter have highlighted several functional phenotypes in neurons derived from ASD patient iPS cells harbouring heterozygous deletions of *SHANK3*. Firstly, throughout development, *SHANK3* mutant neurons were less spontaneously active than control neurons, as determined with extracellular recording of spikes with MEAs. As well as showing a reduced average spike rate, *SHANK3* mutant neurons also produced fewer action potential bursts than control neurons. This reduced excitability was also seen when recording single cell calcium transients, with both S3_F1 and S3_M1 neurons having increased inter spike intervals (ISIs) between spontaneous calcium events compared to control cells. Single cell calcium imaging also highlighted a subtle but significant difference in the shape of the events produced by *SHANK3* mutant neurons, where calcium events had increased average amplitudes and decreased fall times compared to control neurons. Finally, analysis of the shape of the extracellular spikes recorded across development using MEAs revealed a small population of novel spike shapes that were produced only by *SHANK3* mutant neurons. These spikes were wider than standard due the presence of a double peak and were observed at all points across development.

The primary aim of this chapter was to investigate the electrophysiological function of heterozygous *SHANK3* iPS cell derived neurons across an extended period of development. More specifically, it was to utilise the platform for analysing network function, developed in Chapter 5, to study the effect of *SHANK3* mutations in the development of coordinated network driven behaviour. However, one of the most striking results from this chapter was that the synchronised culture-wide activity, observed in cultures in Chapter 5 after around 30 days of MEA culturing, did not develop at any point in these cultures in either *SHANK3* mutant or control neurons. This was despite repeated differentiations and optimisation of the culturing protocol to bring it in line with, as much as possible, the protocol used with the cells in Chapters 4 and 5, including the use of astrocyte conditioned medium (ACM) and a 2% O₂ incubator. However, a key difference between the protocols still remained: while the IBJ4 neurons used in Chapters 4 and 5 were differentiated from iPS cells following the protocols used in the institute and developed as part of this project, the cells used for this Chapter (both the *SHANK3* lines and the Ctl_M1 line) were differentiated from iPS cells to NPCs by the group in KCL, following a different

6. Functional phenotyping of ASD patient neurons

protocol, and subsequently cultured from precursors to neurons following the optimised protocol developed in this project.

Overall, the neurons produced by the two different protocols were similar. Both protocols produced mostly glutamatergic forebrain neurons, as is their design, and showed similar levels of baseline excitation early in development with MEA experiments. However, a key difference was the percentage of GAD67 +ve neurons identified in the cultures, a key marker of GABAergic interneurons. While around 5% of the neurons present in the cultures at 50 DPP in Chapter 5 were identified as interneurons, under 1% of the neurons from all three lines used in this chapter at the same time point were GAD67 +ve. While the work in Chapter 5 highlighted the possibility of a role of interneurons in the regulation of network activity in iPS cell cultures, the results presented here strongly suggest that a certain level of interneuron innervation is required for the formation and development of synchronised network behaviour.

The role of interneurons in the development and function of networks *in vivo* and in intact (slice) networks *in vitro* is well understood. Interneurons are required for the generation of synchronised oscillations in the hippocampus (Xu *et al.*, 2016; Amilhon *et al.*, 2015) and cortex (Chen *et al.*, 2012; Kuki *et al.*, 2015). Moreover, during development, selective inhibition of interneuron populations causes a deficit in the synchronisation of cortical networks in adulthood (Takada *et al.*, 2014). These studies implicate, primarily, a role for phasic interneuron activity in network function, however there is also evidence to suggest that tonic GABAergic tone is also important in the development of coordinated networks. While phasic inhibition is driven by interneuron innervation, tonic inhibition consists of activity caused by basal levels of extracellular GABA, mediated via alpha 4/5/6 (Caraiscos *et al.*, 2004; Chandra *et al.*, 2006) and delta (Marowsky and Vogt, 2014) subunit containing GABA_A receptors. Tonic GABA conductance has been shown to be required for oscillatory activity in the hippocampus and cortex (Pavlov *et al.*, 2014; Mann and Mody, 2010).

The contribution of interneurons in hPS cell derived cultures is less understood. A number of studies have identified a role for a required level of GABAergic activity in the maturation of individual neurons. Specifically, this involves the activation of GABA_A receptors early in development, which is thought to act via regulation of calcium and an augmentation the ratio of KCC2/KCC1 in an activity dependant manner, which in turn increases the maturity of neurons

6. Functional phenotyping of ASD patient neurons

(Rushton *et al.*, 2013; Kirmse *et al.*, 2017; Kemp *et al.*, 2016). Furthermore, a recently study mapping the development of interneurons in hPS cell cultures highlights the importance of these cells in the development of functional excitatory synapses (Close *et al.*, 2017). In the few studies which have looked at culture wide activity of hPS cell neurons using MEAs, the numbers of interneurons in cultures has not been assessed. However, in the most recent study of this kind, cultures responded to both GABA_A agonists and antagonists after around 20 weeks in culture (Odawara *et al.*, 2016). Taken together, this provides good evidence for an important role of interneurons in hPS cell cultures, both in neural development and in the formation and regulation of networked behaviour. Therefore, it is likely that the lack of such activity in the cultures used in this chapter can be attributed to limited numbers of GABAergic neurons, across both SHANK3 lines and the control line.

This study showed that the spontaneous activity of SHANK3 mutant iPS cell derived neurons was, in general, lower than that of control neurons. This finding is in line with previous studies which have investigated SHANK3 mutations in neurons in a range of models. Firstly, mouse SHANK3 mutant primary neurons were less spontaneously active than control neurons in a study using using MEAs (Lu *et al.*, 2016), the study which also identified altered network activity in the SHANK3 mutant primary cultures. Several studies involving patching of hippocampal slices have also shown decreased excitability in SHANK3 mutant mice (Jaramillo *et al.*, 2016; Lee *et al.*, 2015; Zhou *et al.*, 2016). Importantly, in almost all of these studies, the reduction in baseline excitation was attributed to attenuated excitatory synaptic transmission and in some cases this was linked more specifically to a reduction in the NMDA/AMPA current ratio (Kouser *et al.*, 2013; Jaramillo *et al.*, 2016). It is worth noting that one of the most consistent findings among rodent electrophysiological studies is a reduction in NMDA receptor mediated long term potentiation (LTP) (Yang *et al.*, 2012; Kouser *et al.*, 2013; Wang *et al.*, 2011; Bozdagi *et al.*, 2010). Indeed, it is this evidence which informed the work of Lu. *et al* who studied the activity of networks at the population level and provided the primary focus of this chapter.

Reduced spontaneous activity, determined by single cell electrophysiology, was also seen in iPS cell derived neurons from patients with mutations in SHANK3 (Shcheglovitov *et al.*, 2013). Importantly, this reduction in activity was attributed to impaired excitatory synaptic transmission, including reduced NMDA-EPSP amplitude and frequency, which could be rescued by viral expression of SHANK3. Reduced spontaneous activity was also seen in a SHANK3 conditional

6. Functional phenotyping of ASD patient neurons

heterozygous KO of hES cells (Yi *et al.*, 2016). Interestingly, both of these studies (which are, to date, the only two to study the electrophysiology of SHANK3 mutant hPS cells) also showed that SHANK3 mutant neurons have a higher input resistance than control cells. This actually manifested in *increased* induced action potentials when neurons are held at -70 mV, due to the more resistive nature of the cell membrane (Yi *et al.*, 2016).

Single cell calcium imaging experiments in this study corroborated the work using the MEAs, with neurons from S3_F1 and S3_M1 cell lines producing significantly fewer calcium events than control neurons. This was in line with a similar study which showed that neurons derived from two different patient SHANK3 mutant iPS cell lines, produced fewer calcium events compared to control neurons, which then could be rescued with VPA and lithium treatment (Darville *et al.*, 2016). Here, SHANK3 mutant neurons produced calcium transients that had larger amplitudes and slightly reduced fall times compared to controls. As far as can be determined, this is a novel finding in terms of both human and rodent SHANK3 mutant neurons, although a number of studies have also shown alterations to spontaneous calcium transients in other mutant models (Zhang *et al.*, 2014; Lee *et al.*, 2017) and in iPS cells from idiopathic ASD patients (Schmunk *et al.*, 2017).

While reduced excitation appears to be a common phenotype in both rodent and human SHANK3 mutant neurons, the underlying mechanism for how these mutations may confer aberrant signalling is less well understood. The prominent role of SHANK3 as part of the NMDA receptor complex suggests that mutations in SHANK3 will primarily affect signalling via this receptor and its associated proteins. Indeed, several rodent studies have shown altered NMDA mediated conductance in SHANK3 mutant neurons, although the mechanism by which this occurs is unclear (Kouser *et al.*, 2013; Bozdagi *et al.*, 2010). One of the primary roles of SHANK3 is thought to be in the trafficking and assembly of NMDA receptors, with rodent studies showing that the functional expression of several NMDA receptor subunits is reduced in SHANK3 mutant neurons (Peça *et al.*, 2011; Mei *et al.*, 2016). While all NMDA receptors possess two GluN1 subunits, the remaining subunits can be a combination of GluN2/3, of which there are several isoforms. GluN2 A and B are the most highly expressed subunits in the majority of the brain and importantly, possess different channel kinetics and unique developmental expression patterns. In general, the majority of immature NMDA receptors contain primarily GluN2B subunits, which switches to predominantly GluN2A subunits later in

6. Functional phenotyping of ASD patient neurons

development (Cull-Candy *et al.*, 2001; Monyer *et al.*, 1994). Importantly, the correct assembly of NMDA subunits requires the involvement of several PSD proteins, including SHANK3 (Sans *et al.*, 2000; Horak *et al.*, 2014), deficiency of which has been shown to lead to incorrect subunit assembly (Duffney *et al.*, 2013). Additionally, the expression of other PSD proteins such as HOMER1 and PSD-95 have also been shown to be reduced in SHANK3 mutants (Peça *et al.*, 2011; Wang *et al.*, 2016), suggesting that loss of SHANK3 protein has implications for the correct assembly and function of the wider PSD.

One of the most consistent findings in studies of SHANK3 haploinsufficiency are the morphological changes to neurons, in particular a reduction in the complexity of the dendritic arbor and a reduction in the number of spines (Zhou *et al.*, 2016; Hung *et al.*, 2008; Peça *et al.*, 2011; Mei *et al.*, 2016). Together with the evidence for the altered synaptic function, this perhaps provides a template for reduced spontaneous excitation in SHANK3 mutant neuronal cultures: heterozygous SHANK3 neurons produce fewer connections with other neurons, and those connections contain excitatory synapses with misassembled NMDA complexes, including, perhaps, miss-trafficked NMDA subunits. However, more recent evidence implicates an additional mechanism involving the metabotropic glutamate receptor mGluR5 and Homer1, a PSD protein involved in the synaptic assembly of mGluR5. Mice with heterozygous KO of SHANK3 showed aberrant synaptic localisation of both mGluR5 and Homer1 (Wang *et al.*, 2016; Vicidomini *et al.*, 2017), which lead to altered synaptic activity, changes to glutamate mediated calcium activity and increased *induced* action potentials (in line with the work by Yi *et al.*, 2016 attributing increased induced excitability to increased neuron input resistance). Importantly, both these studies reported the rescue of functional deficits to control levels by application of positive modulators of mGluR5 receptors, strongly suggesting that reduced excitation in SHANK3 mutant neurons can partly be attributed to the miss-assembly and function of mGluR5 receptors.

An interesting aspect of the work in this chapter was the response of cells of all genotypes to pharmacological profiling, both in terms of the extracellular spike recording and the single cell calcium imaging. Individual application of APV and CNQX had limited but variable effects on the rate of spontaneous firing recorded with MEAs at 41 DPP, such that no response could clearly be attributed to the action of either of the drugs. However, application of APV to neurons during calcium imaging dramatically reduced the number of spontaneous calcium transients observed

6. Functional phenotyping of ASD patient neurons

at 40 DPP to below 10% of standard conditions, while CNQX application reduced the number of events by around 50%. This clearly suggests that the majority of the recorded calcium events were driven by synaptic activity, whereas the sAPs recorded with MEAs were caused primarily by intrinsic fluctuations in membrane potentials. In fact, the MEA profiling results at 40 DPP from this chapter are more inline with the results from Chapter 5, where spontaneous activity in iPS cell derived neurons at 20 DPP were largely insensitive to both CNQX and APV application. When profiled at a later time point (50DPP), the neurons in Chapter 5 responded dramatically to application of both drugs, more in line with the calcium imaging experiments in this chapter. This therefore suggests that the neurons produced in this chapter could be developmentally delayed, in terms of physiological function, compared to those produced in Chapter 5. As discussed earlier, it is possible that the lack of GABAergic tone in these neurons contributes to a more immature phenotype at the level of individual cells, including lower expression of mature PSD complexes. However, there is clearly a degree of NMDA and CNQX function present, as shown by the response of the neurons during calcium imaging. It is therefore possible that the calcium transients recorded in these cells, while clearly mediated by NMDA and AMPA receptors, do not represent events that underlie action potential activity, perhaps because of delayed cell wide maturity.

Finally, perhaps the most interesting result of this chapter was the finding that neurons derived from SHANK3 heterozygous patient iPS cells produce a small population of unique spike waveforms that are not present in control neurons. Moreover, the nature of these waveforms, being larger, wider and most noticeably possessing a double-peak, is a shape that has not been seen in any MEA experiments throughout this project, or indeed, anything broadly similar, except for those involving S3_F1 or S3_M1 neurons. While these spike shapes represented a small minority of total recorded waveforms from these cell lines, they were repeatedly observed at all time points across multiple rounds of neuron differentiation. It should be noted however that these spikes were not seen in all neurons as most electrode traces presented with normal spike shapes. Instead, a small number of electrodes (on average around 3 per 16 analysed electrodes) recorded activity which included these double-peak spikes. In the majority of cases these were the only spikes present in the electrode trace but in rare cases they were seen as part of a complex of spike shapes, which probably represented multi-unit activity. These unique spikes did not appear to be caused specifically by NMDA or AMPA driven synaptic activity, as there was no change in the proportion of these spikes when neurons were recorded in the

6. Functional phenotyping of ASD patient neurons

presence of APV or CNQX. However, this is perhaps not a surprise given the insensitivity of neurons in general to these compounds that was observed here.

The underlying identify and cause of these spikes unique to the SHANK3 neurons is not clear. Is it possible that these spikes represent an artefact of the extracellular recording process and the subsequent analysis pipeline? Several aspects of the experiments suggest however that this is unlikely. Firstly, these spikes were routinely and objectively only observed in either S3_F1 or S3_F1 neurons. After initially identifying the spikes by visual observations during experiment analysis, they were objectively identified as unique in a random sample of spikes drawn from a pool of control and SHANK3 mutant spikes taken across neuronal development. Furthermore, as previously mentioned, these spike shapes have not been seen in any other experiments throughout this wider project. Secondly, an artefact with a shape as seen here would suggest a downsampling effect, perhaps masking a very short burst of two spikes. However, all MEA recordings were taken with a sample rate of 40,000/second, which was filtered below 200 Hz and above 6000 Hz. This low-pass rate is still well above the firing rate for even the fastest spiking interneurons (~120 Hz; Hu *et al.*, 2014) and as such should be more than able to reliably record all of the activity from these stem cell derived neurons, which in this project, have achieved a maximum single unit firing rate of around 10 Hz.

A theoretical underlying cause for the appearance of these double spikes could involve hyperpolarisation-activated cyclic nucleotide-gated channels (HCN channels). These are ligand gated non-selective cation channels, coded for by four genes (*HCN1-4*) and mediate an I_h -current, which depolarises membrane potentials towards action potential threshold (Postea and Biel, 2011). As such, these channels are involved in the regulation of resting membrane potentials, integration of synaptic inputs and basal excitability (Benarroch, 2013; Nolan *et al.*, 2004). Changes in the activity of HCN channels have been shown to lead to alterations in the way that certain populations of mouse neurons produce bursts of action potentials, primarily driven by regulation of the currents following membrane depolarisation (Kodirov *et al.*, 2016). Furthermore, increased seizure like activity, including spontaneous bursting, is associated with both reduced HCH channel expression and channel malfunction (Chen *et al.*, 2001; Dibbens *et al.*, 2010; Huang *et al.*, 2009). Most interestingly, a recent study investigating the role of SHANK3 haploinsufficiency on neuronal activity in hPS cells found that changes in excitability were caused by an impairment of I_h – currents (Yi *et al.*, 2016). The authors found that in ES

6. Functional phenotyping of ASD patient neurons

cells with conditional heterozygous KO of SHANK3, increased induced excitability, reduced spontaneous excitability and reduced synaptic events was mediated via altered currents through HCN channels. Importantly, they also found that SHANK3 directly binds to HCN channels (although this was achieved using heterologous expression of the proteins in HEK293 cells) and that heterozygous SHANK3 neurons had decreased levels of endogenous HCN protein.

While the studies described above do not provide direct evidence for a role of HCN channels in action potential shape, they do provide good insight into their role in neuronal excitability and, importantly, an interaction with SHANK3. It is therefore possible that in this study, the spike shapes unique to SHANK3 mutant neurons are the result of aberrant HCN currents. Furthermore, because these spikes have been recorded with extracellular electrodes, it is possible that shapes observed are an extracellular manifestation of these complex transmembrane currents when temporally couple to spontaneous burst firing. However, it is clear that further investigations surrounding the biological nature of these spikes are required before an understanding of their link to SHANK3 function is determined.

7. General Discussion

7.1 Results chapter summaries

7.1.1 Chapter 3 – Development of a pipeline for the analysis of MEA data

At the onset of this project, a number of analysis packages were trialled for use with the data collected from initial MEA experiments with hPS cell derived neurons. However, it was decided to create a new package of tools, based in Matlab, to allow a tailored approach to the analysis of such neurons and to aid in the understanding about the nature of firing seen in these cells. Chapter 3 described the development of the tools and measures used for the analysis of MEA data throughout the remainder of the project.

Key aspects of the developed analysis pipeline:

- Raw data sampled at 25 kHz; filtered online between 200 Hz and 5000 Hz.
- Spikes detected using an automatic thresholding method where an estimate of noise is determined by the median absolute deviation of the filtered signal.
- Key basic excitability statistics included average spikes per electrode, average spike rate and number of bursts. Variable array-wide activity was controlled for by the use of an electrode activity threshold to eliminate 'quiet' electrodes from analysis.
- Bursts were detected using a maximum inter-spike interval method determined by histogram analysis. Max interval used was 300 ms.
- Network statistics were determined by the creation of array wide spike detection (ASDR) plots comprising the total number of array-wide spikes detected in serial 200 ms bins. This included the the average MAP interval, which reports the interval between the more active periods of coordinated firing cultures.
- For spike waveform analysis, feature extraction was achieved with principle component analysis of the spike amplitude and was followed by a DBSCAN algorithm for the objective clustering of spike shapes.

7.1.2 Chapter 4 – Optimising culturing conditions to improve the physiological maturity of hPS cell derived neurons

While many protocols exist for the differentiation of hPS cells into neurons, several physiological characteristics of the cells are immature, even after extended culture periods. Chapter 4 described the extension of a dual – SMAD inhibition differentiation protocol to include two physiological adaptations which have previously been shown to increase the functional maturity of neurons: astrocyte condition medium (ACM) and hypoxic (2%) oxygen incubator environments. The Chapter focused on the intrinsic and excitability characteristics of iPS cell derived neurons using primarily single-cell patch clamping at two points in development and aimed to study the effect of ACM/2% conditions on the physiological maturity of neurons a view of aiding the formation of the MEA – based platform discussed in Chapter 5.

Key findings of Chapter 4:

- Neurons cultured in ACM/2% conditions had hyperpolarised resting membrane potentials compared to neurons in standard conditions. The resting membrane potential of neurons became more negative over development in ACM/2% cells but not in standard conditions.
- The input resistance and membrane time constant of neurons was largely unaffected by either developmental stage or ACM/2% conditions, although a small reduction of input resistance was observed in ACM/2% conditions over the two time points.
- Neurons cultured in ACM/2% conditions had increased excitability compared to standard condition neurons, with a increase in the number of cells showing at least single induced action potentials
- The induced activity state of a neuron was strongly related to the resting membrane of the cell, but not to either input resistance or membrane time constant.
- Neurons cultured in ACM/2% conditions displayed significant higher levels of spontaneous action potentials, as shown by patch-clamping and a small MEA experiment

7.1.3 Chapter 5 – Investigating network development in iPS cell derived neurons

The advent of more accessible multi electrode array (MEA) systems has ignited opportunities for studying neural networks in dissociated cultures. While several studies have shown that rodent neurons form networks with complex activity patterns *in vitro*, evidence for similar behaviour in hPS cell derived neuron cultures has been limited. The work in Chapter 5 used the analysis measures described in Chapter 3 and the protocol adaptations described in Chapter 4 to study the development of spontaneous network driven activity in iPS cell derived neurons using an MEA system.

Key findings of Chapter 5:

- The spontaneous activity of iPS cell derived neurons cultured on and recorded with MEAs changed markedly over development. Up to 30 days post plating (30DPP), spontaneous activity increased but remained uncoordinated across the culture. Between 30 and 40DPP, array – wide activity began to coordinate in the form of culture wide synchronised burst firing. After 50 days of culture, array-wide activity was highly organised into high/mid frequency periods (more active periods; MAPs) and low frequency firing periods (low activity periods) each lasting for a number of seconds.
- Early in development, the observed spontaneous activity was largely insensitive to NMDA, AMPA or GABA_A receptor inhibition. However, application of GABA to the cultures dramatically reduced excitability, showing that even at this early point of development, GABA currents are inhibitory.
- The network driven synchronised activity observed later in development was dependant on both NMDA and AMPA mediated synaptic activity.
- The interval between more active periods (MAP interval) of synchronised cultures was attenuated with GABA_A antagonists and a blocker of L type calcium channels in a dose dependant manner. The application of these two drugs together did not produce a summative effect suggesting that they may be working via a common pathway

7.1.4 Chapter 6 – Functional phenotyping of autism spectrum disorder patient iPS cell derived neurons

Autism spectrum disorder (ASD) is a heterogeneous neurodevelopmental disorder for which converging genetic and modelling evidence implicates aberrant synapse and network function as a key aetiological factor. iPS cell technologies together with MEA systems provide a unique opportunity for studying the network function of neurons derived from ASD patients. Chapter 6 focused on investigating the development of spontaneous activity in neurons derived from patient iPS cells with heterozygous deletions of *SHANK3*, a synaptic scaffolding protein mutations of which are strongly associated with ASD.

Key findings of Chapter 6:

- iPS cell derived neurons with heterozygous deletions of *SHANK3* were less spontaneously excitable than control neurons. While activity increased over development in *SHANK3* cells, it appeared to be delayed by ~10 days compared to control cells
- Neurons derived from neither *SHANK3* mutant or control lines showed development of the network-driven behaviour described in Chapter 5. Immunocytochemistry revealed that the cells produced with the protocol used in this chapter had noticeably fewer interneurons than the cultures in Chapter 5, suggesting that the absence of synchronised activity could be due to lack of inhibitory tone.
- Analysis of the spike shapes produced by neurons revealed the presence of a small population of waveforms that were unique to *SHANK3* mutant cells. These spikes were much wider than others due to the presence of a 'double-peak' and their occurrence was not sensitive to NMDA or AMPA receptor inhibition.
- Single cell calcium imaging corroborated the findings from the MEA experiments that neurons with heterozygous *SHANK3* deletions were less excitable than control neurons. Calcium events from mutant neurons also had larger amplitudes and shorter fall times than those from control neurons.
- Pharmacology experiments showed that calcium transients were dependent on NMDA and AMPA receptor signalling but spontaneous action potentials detected by MEAs were not.

7.2 Context and points of discussion

7.2.1 Modelling network behaviour with hPS cells derived neurons

The study of neural networks and circuits has been a key part of neurobiological research for many years. Studies with both wild type and genetic rodent *in vitro* slice models, together with *in vivo* work, has provided a wealth of information surrounding the nature of circuit formation and function throughout development and in disease states. However, until more recently the study of networks in human neurons has been limited to that at the level of the whole-brain or regions, for example with EEG or imaging studies. The development of iPS cell technologies and neuron differentiations protocols together with the advent of modern multi-electrode array (MEA) systems has provided exciting opportunities to study the the network function of human neurons during development and in disease – relevant models. The work in Chapter 4 and 5 of this study presented the formation of an MEA – based platform to study the development of network behaviour in iPS cell neurons. This is not the first study to have combined hPS cells and MEAs to investigate the firing patterns in such neurons, with the first reports appearing in 2009 (Heikkilä *et al.*, 2009). However, while a number of subsequent studies showed that the complexity of spontaneous firing increases over development and that synchronised behaviour may appear at latter stages (Ylä-Outinen *et al.*, 2010; Kapucu *et al.*, 2012; Odawara *et al.*, 2014), it was only in 2016 that consistent network driven coordination was reported in hPS cell derived neuron cultures (Odawara *et al.*, 2016). Importantly though, the behaviour reported by Odawara *et al.* was limited to short synchronised burst firing (lasting around 2 seconds) and developed over a period of > 20 weeks. The work presented here in Chapter 5 showed the extension of SBF in cultures to a more complex pattern of synchronised firing, characterised by periods of high and low activity each lasting >10 seconds. Moreover, equivalent SBF was seen in neurons here at between 30 – 40 days post plating, with the extended synchronicity seen 50+ DPP, a vastly increased time scale to that previously reported. The nature of the behaviour reported here is in fact much closer to that reported by MEA studies involving dissociated rodent neurons (Wagenaar *et al.*, 2006; Mok *et al.*, 2012; Lu *et al.*, 2016). While the timeline for the development of spontaneous activity is shorter in these rodent studies, the slow oscillatory firing observed is remarkably similar to that reported here in Chapter 5. Therefore, as far as can be determined, the platform developed in this project presents the most complex pattern of coordinated network driven behaviour observed in hPS cell derived neurons.

It is perhaps likely that one of the reasons that the behaviour reported in this project was closer to dissociated rodent neurons was the fact that the differentiations used in Chapter 5 produced a small population of GABAergic interneurons within primarily glutamatergic cortical projection neurons. Indeed, the absence of any detectable synchronised activity in the experiments in Chapter 6 together with the very low number of interneurons identified in those cultures strongly suggests a key role for interneurons in the development of network behaviour in these cells. This should perhaps not be surprising based upon the strong body of evidence that implicates interneurons in the formation of functional networks throughout development (Takada *et al.*, 2014; Zecevic *et al.*, 2011) and the maintenance of synchronised behaviour in adulthood (Mann and Mody, 2010; Kuki *et al.*, 2015). Nevertheless, it is important that the role of interneurons is not forgotten when utilising iPS cell neuron models. Indeed, although the presence of interneurons in the cultures in Chapter 5 was not specifically designed, it has highlighted that their presence is probably necessary for these cells to be thought of as a robust physiological model. This is especially important when modelling neurodevelopmental disorders with iPS cell neurons, such as ASD, for which a good body of evidence exists implicating interneuron dysfunction as a key aetiological factor.

Overall, the platform and protocols presented here should provide a reliable technique for the investigation of spontaneous network development function in a human neuron context. The use of the platform described here could be used in conjunction with traditional single – cell patch clamping methods to provide a comprehensive package of techniques for the analysis of hPS cell derived neuron function. A primary limitation of the MEA recordings is the resolution of amplitudes and the inability to determine the nature of underlying sub-threshold currents – some of the key strengths of single cell patch clamping. However, MEAs allow the recording and analysis of the same small population of neurons over the period of development typical for hPS cell neuron differentiations, while the relative simplicity of introducing pharmacological agents onto cultures during recordings allows a comprehensive profiling of activity at various stages of development. Furthermore, while single-cell electrophysiological techniques can provide detailed information surrounding the nature of interactions between two or possibly three neurons, MEA techniques, especially as developed and described here in Chapter 5, can reveal the varied and complex array of both coordinated and uncoordinated firing present in hPS cell neuron cultures. Finally, perhaps one of the biggest applications for the methods developed here is that, unlike other electrophysiological techniques, the use of MEAs can be adapted with

relative simplicity for high-throughput screening of hPS cell derived neuron function. For example, this could take the form of a large cohort of the 60 electrode arrays as used in this study or the protocols and analysis measures could be adapted for use with multi-well MEA systems, comprising 24/48 well plates each with 12 electrodes. Such methods could be exploited to provide large-scale pharmacology/toxicology studies in developing neurons and, importantly, can be routinely used for the high-throughput screening of novel pharmaceuticals aimed at rescuing functional phenotypes identified in human neuron models of neurological disease. As such, the work presented here forms the basis for a unique and valuable method for investigating the function of hPS cell models of disease and the development of novel therapies.

7.2.2 Functional differences in cell lines

As previously discussed, the results presented in Chapter 6 were in contrast to those in Chapter 5, in terms of the development of coordinated network behaviour in iPS cell derived neuron cultures. While, as suggested in Chapter 6, this could be due to the lower numbers of GAD67 +ve neurons identified in the cultures, it is worth considering whether, in fact, the variable observations were due to differences in the methods used to differentiate the iPS cells to neurons. All the cell lines used in Chapter 6 (one control and two Shank3 mutant lines) were received as neural progenitors and were subsequently cultured identically to the IBJ4 cells used in Chapters 4 and 5. However, the protocols used to derive the precursors differed in several key ways to those used to create the IBJ4 NPCs. In the 18-20 days between the start of differentiations and the formation of NPCs, cells are passaged twice following the 'Cardiff' protocol as used for IBJ4 cells: at D8-10 onto fibronectin at a ratio of 1:1.5 and at D18-20 onto PDL/laminin at various ratios (typically around 1:3-1:5). Following the 'King's' protocol, used to derive all the NPC lines used in chapter 6, cells are passaged four times during the same time period: at D7 (1:1), D12 (1:1), D15/16 (2:3) and D18/19 (1:2). After each passage, cells are replated back onto geltrex (a matrigel analogue). These passages were also each performed with accutase and while cells were kept as clusters until D15/16, were passaged as single cells from then on. IBJ4 cells were passaged firstly with EDTA (as clusters) and then with EDTA/acutase as clusters or single cells depending on the application. Finally, in the King's protocol, N2B27 medium is changed fully every 24 hours; for IBJ4 cells, half the medium is changed every 48 hours.

While it is difficult to acutely identify what could be the defining difference in the two procedures, it is clear that enough differences are present as to potentially alter the functional outcome of the mature neurons, especially perhaps in the variation of the frequency and methods used to passage cells. In fact, information that has come to light since the work on this project from collaborators working with these exact cell lines (starting from the same NPC stocks) who have determined that although the cells show functional expression of Na_v and K_v channels, form action potentials and show expression of proteins of the excitatory synapse, no synaptic activity could be detected with voltage clamping experiments. This, together from the work in this project, therefore suggests that there is something in the protocols used to create the NPCs which is precluding the development of functional excitatory synapses in these neurons. This lack of synaptic tone would suitably explain the absence of network behaviour observed with all of the cell lines used in Chapter 6.

7.2.3 L-type calcium channels, network function and mental health disorders

One of the most interesting findings from this project was the dose-dependent attenuation of MAP intervals observed in synchronised cultures by the L-type voltage gated calcium channel blocker (LTCC) diltiazem, reported in Chapter 5. Ca_v1.2 and Ca_v1.3 (coded for by CACNA1C and CANCA1D genes respectively) LTCCs are expressed throughout the brain and are involved in a range of calcium homeostatic functions, including regulating NMDA receptor – dependant LTP (Moosmang *et al.*, 2005), hippocampal dependant learning (Hofmann *et al.*, 2014), trafficking of AMPA receptors (Schierberl *et al.*, 2011) and regulation of gene expression (Wheeler *et al.*, 2012). Importantly, LTCCs have also been implicated in the modulation and control of oscillatory and circuit behaviour (Bengtson *et al.*, 2013; Hansen *et al.*, 2014; Bukalo *et al.*, 2013). Mutations in genes coding for subunits of LTCCs, in particular CACNA1C, are some of the most strongly associated with psychiatric disorders. Genome wide association studies (GWAS) have identified a number of common single nucleotide variations (SNVs) present in CACNA1C which are enriched in patients diagnosed with bipolar (Ferreira *et al.*, 2008), major depressive disorder (Green *et al.*, 2010) schizophrenia (Schizophrenia Working Group of the Psychiatric Genomics Consortium, 2014) and ASD (Cross-disorder group of Psychiatric Genomic Consortium, 2013). Moreover, rare exonic mutations in CACNA1C have also been identified in schizophrenia patients (Purcell *et al.*, 2014) and *de novo* SNVs in both CACNA1C

and *CACNA1D* have been identified in ASD patients (De Rubeis *et al.*, 2014; Jiang *et al.*, 2013). Finally, specific gain of function mutations of *CACNA1C* are known to cause Timothy syndrome, a rare neurodevelopmental disorder characterised by cardiac arrhythmia (Long Q-T), facial dysmorphologies and ASD in around 80% of patients for whom assessment is possible (Splawski *et al.*, 2004).

The results presented here in Chapter 5 represent the response of iPS cell derived neuron cultures to increasing doses of a LTCC blocker, effectively modelling variable loss of function. It should be noted however that genetic lesions resulting in effective haploinsufficiency have not been reported for any LTCC. Moreover, it is not clear whether and to what extent the intronic common SNVs in *CACNA1C* effect functional gene expression, with reports of both increased (Bigos *et al.*, 2010) and decreased (Gershon *et al.*, 2014) brain mRNA levels detected post-mortem in individuals carrying the risk allele. Interestingly though, brain imaging studies involving healthy carriers of the same common SNVs have shown altered regional activity and connectivity involving circuits implicated in schizophrenia and ASD (Bigos *et al.*, 2010; Paulus *et al.*, 2014). However, due to the difficulty in modelling common variation and the gain of function mutations in Timothy syndrome, heterozygous mice models of *CACNA1C* have been more routinely studied. These reports have shown that decreased *CACNA1C* expression is associated with a reduction in hippocampal neurogenesis (Volkening *et al.*, 2017), aberrant regional activity patterns (Kabir *et al.*, 2017) and reduction of NMDA independent LTP (Moosmang *et al.*, 2005). Ongoing work in the institute where this project was completed has also shown reduced regional connectivity and alterations to NMDA – independent LTP in heterozygous *CACNA1C* rats.

The finding in Chapter 5 that the regulation of LTCC activity can modulate network driven activity therefore provides an interesting insight into the function of these channels both throughout development and in disease relevant contexts. Of course, without single-cell voltage – clamping experiments it is not possible to determine an IC_{50} for diltiazem and it is also not clear at what concentrations the drug remains specific for LTCC in these neurons. Nevertheless, the fact that the response observed was dose-dependant strongly suggests that it was caused by modulation to LTCC activity. The fact that this response was very similar to that observed with two inhibitors of GABA_A receptors was also interesting and was discussed in detail in Chapter 5. These results suggested that the action of these drugs could have a common

underlying mechanism involving regulation of interneuron activity. Together, these results provide an interesting and potentially revealing set of preliminary findings which implicate LTCC function in the regulation of network activity in iPS cell derived neurons.

7.2.4 Network function and iPS cell modelling in ASD

The advent of large scale human genetic studies has provided a wealth of information about the genetic component of autism spectrum disorder (ASD) and has identified a number of genes in which rare and *de novo* protein deleterious mutations are thought to be highly penetrative for development of the disorder (Sanders *et al.*, 2012; O'Roak *et al.*, 2012; lossifov *et al.*, 2014). Similarly to other mental health disorders, such as depression and schizophrenia, many of these genes code for proteins with functions at the synapse (Kenny *et al.*, 2014; De Rubeis *et al.*, 2014; Gilman *et al.*, 2011). Together with human imaging studies (Belger *et al.*, 2011; Hernandez *et al.*, 2015), neuropathological studies (Courchesne *et al.*, 2011; Wegiel *et al.*, 2010), and single gene transgenic rodent models (e.g. Schmeisser *et al.*, 2012; Auerbach *et al.*, 2011; Molosh *et al.*, 2014) this evidence points for a strong aetiological role of aberrant synapse and network function in ASD. The work here in Chapter 6 focused on *SHANK3*, a key post-synaptic density scaffolding protein, heterozygous deletions of which cause Phelan McDermid syndrome (PMDS) and are one of the most highly penetrative genetic lesions in the formation of ASD.

A primary aim of Chapter 6 was to extend the work in Chapter 5 to utilise the MEA platform to investigate the development of network function of iPS cell neurons derived from patients with heterozygous deletions of *SHANK3*. Unfortunately, as previously described, synchronised network-driven behaviour was not observed in either the *SHANK3* mutant or the control lines and therefore this aim was not achieved. Nevertheless, a key finding of Chapter 6 was the reduction of spontaneous neuron activity, detected with both MEA experiments and calcium imaging, which corroborated with that reported by studies investigating hPS cell derived neuron function from PMDS patient cells (Shcheglovitov *et al.*, 2013) and with isogenic hES cells with heterozygous deletions of *SHANK3* (Yi *et al.*, 2016). Reduced spontaneous excitability was also a feature of dissociated cortical neurons from mice with homozygous deletions of *Shank3*, detected using a very similar MEA approach as here (Lu *et al.*, 2016).

It is likely that the deficit in spontaneous firing seen with both human and rodent SHANK3 mutant neurons is a product of aberrant synaptic signalling. Indeed, altered excitatory synaptic activity has been reported in both Shank3 transgenic rodent studies (Bozdagi *et al.*, 2010; Yang *et al.*, 2012) and with hPS cell derived neurons (Shcheglovitov *et al.*, 2013). While the formation of an action potential, especially in hPS cell derived neurons, does not definitively require depolarising synaptic inputs, they are generally regarded as the key determinate of basal neuron excitability. As such, the extent of spontaneous excitability can be seen as a correlate of basic culture maturity and connectivity, albeit at the level of single-cell communication.

The physiological function of SHANK3 as a key part of the excitatory post synaptic density clearly implicates aberrant protein function in altered synaptic signalling and connectivity. For example, the PZD domain of SHANK3 is known to interact with NMDA receptors via PSD95 (Naisbitt *et al.*, 1999) and directly to GluR1 subunits of AMPA receptors (Uchino *et al.*, 2006), which provide the key associations required in its role in the correct recruitment and assembly of NMDA and AMPA receptors at the excitatory synapse. As such, it is not a surprise that alterations to synaptic signalling is also a key feature of Shank3 rodent models (e.g. Wang *et al.*, 2011; Yang *et al.*, 2012). However, as previously mentioned, an increasing body of evidence from a range of sources implicates aberrant circuit function and connectivity in ASD more generally. At the level of the synapse, genetic studies have identified a number of other ASD associated genes with key synaptic functions, including cell adhesion molecules (e.g. neuroligins, Vaags *et al.*, 2012; and neuroligins, Jamain *et al.*, 2003), GABA_A receptor subunits (Piton *et al.*, 2013) and the scaffolding protein gephyrin (Lionel *et al.*, 2013). Allied with human post-mortem pathology studies and rodent transgenic models involving these genes, this represents a strong set of cellular and molecular evidence for altered signalling. Importantly, the involvement of both excitatory and inhibitory synaptic architectures strongly point to potential abnormalities in the general excitatory /inhibitory balance. More globally, patient studies using EEG techniques and MRI imaging have described a range of network and connectivity deficits in ASD patients, most of whom have no identifiable genetic lesions (Belger *et al.*, 2011; Hernandez *et al.*, 2015).

While altered synaptic function is clearly a key trait associated with SHANK3 haploinsufficiency and is thought to be involved in ASD pathology more generally, it is worth considering the suitability of SHANK3 as a model of ASD. Indeed, while mutations in SHANK3 are some of the

most strongly genetic factors associated with ASD, they account for only a very small percentage of ASD cases. Moreover, identifiable rare and *de novo* mutations in any gene overall appear in probably no more than 4-5% of ASD cases (de la Torre-Ubieta *et al.*, 2016; Vorstman *et al.*, 2017) meaning the majority of ASD cases are regarded as idiopathic. Is studying the phenotypes associated with *SHANK3* mutations therefore useful in progressing our understanding about the neurobiology of ASD more generally?

Firstly, studies with Shank3 mutant mice recapitulate several of the specific findings seen with other transgenic models harbouring mutations in ASD – associated genes. For example, the reduced social interaction and increased repetitive behaviours seen in *SHANK3* mutant mice (e.g. Bozdagi *et al.*, 2010; Zhou *et al.*, 2016) has also been reported in mice with deletions of *Fmr1* (Auerbach *et al.*, 2011), *Tsc1* (Tsai *et al.*, 2012), *Ngl3* (Etherton *et al.*, 2011), *Nrxn1* (Born *et al.*, 2015), *Scn1a* (Han *et al.*, 2012) and *Cntnap2* (Peñagarikano *et al.*, 2011). Furthermore, Shank3 mutant mice have been repeatedly shown to have altered excitatory synaptic signalling, a deficit also identified in *Fmr1* (Auerbach *et al.*, 2011), *Tbr1* (Huang *et al.*, 2014) and *Nrxn1* (Born *et al.*, 2015) knock out mice. Finally, the impaired LTP routinely reported in *SHANK3* mutant mice is also seen in mice with mutations in *Nf1* (Molosh *et al.*, 2014), *Tsc2* (Young *et al.*, 2010) and *Fmr1* (Auerbach *et al.*, 2011). It should be noted that in many of these studies mice have homozygous deletions of the associated gene.

Secondly, as described above, the finding in Chapter 6 of reduced spontaneous excitability is in line with the two previous *SHANK3* heterozygous hPS cell neuron studies. Importantly this is a finding which has also been reported in iPS cell derived neurons from patient with deletions of *MECP2* (Kim *et al.*, 2011) and *FMR1* (Sheridan *et al.*, 2011). Unfortunately, a recent study investigating neurons derived from idiopathic ASD patient iPS cells did not report on the state of spontaneous excitability, although it did find increased production of GABAergic progenitors and an increase in the number of inhibitors PSDs (Mariani *et al.*, 2015).

Finally, despite their rarity, mutations of *SHANK3* are clearly and directly associated with ASD. A diagnosis of ASD is thought to occur in around 80% of PMDS patients, although this could potential be even higher as an autism diagnosis can be precluded by the appearance of more ‘conspicuous’ neurological symptoms (Phelan *et al.*, 2015). Moreover, while up to 90 genes have been implicated in PMDS, the majority of cases involve at least partial deletions of

SHANK3 and a diagnosis of PMDS has been given in cases where only SHANK3 is affected (Leblond *et al.*, 2014).

Together with the growing evidence that implicates the synapse and network dysfunction in ASD, the points addressed above provide good substantiation for the use of heterozygous SHANK3 deletions as model for ASD. In terms of providing opportunities to study the disease in a range of systems (e.g. patients, iPS cells and rodent models) it is only possible to focus on individual genes (or CNVs) for which strong associations are known but which are rare in the ASD population. In this way, using mutations of SHANK3 is a strong candidate for ASD modelling. In terms of iPS cell research alone, there is the potential to study the function of human neurons from patients with idiopathic ASD, which, together with neurons with known mutations, represents a unique possibility to link the two aspects of disease research.

Although the work in this project was not able to directly investigate the network function of iPS cell derived neurons from ASD patients with deletions of SHANK3, it has provided the basis for studying such behaviour and, with further optimisation of culturing procedures, should still provide a unique and valuable tool in linking patient studies with rodent models of ASD.

7.2.5 hPS cell derived neuron maturity

The results presented in Chapter 4 showed that culturing differentiations in ACM/2% conditions improved the functional maturity of iPS cell derived neurons, specifically with regards to resting membrane potential and both induced and spontaneous AP activity. For the purposes of this project overall, the physiology of the neurons produced with this adapted protocol was satisfactory, as they exhibited the complex network driven behaviours described in Chapter 5. However, it should be noted that by several measures the neurons remained immature, not least in the observed values of input resistance and membrane time constant as discussed in Chapter 4. A number of recent studies have reported the production of hPS cell derived neurons with more mature phenotypes than observed here, although they would still be considered foetal in terms of normal human development (Bardy *et al.*, 2016; Telezhkin *et al.*, 2016) Gunhanlar *et al.*, 2017). This issue of hPS cell neuron maturity is important to consider when attempting to model neurological disease and especially in the case of neurodevelopmental disorders such as ASD. In some ways, the immaturity of neurons is perhaps a benefit as it allows insights into the way in which neurons mature, synapses establish and connections form. However, the highly plastic nature of the brain during early development means that the function of fully mature neurons may not represent their early physiology, due to various molecular and cellular compensation mechanisms. As such, it is important to view all findings with hPS cell derived neurons in the context of their immature state, especially with regards to modelling neurodevelopmental disorders. The fact also remains that regardless of what protocol improvements might be able to achieve, hPS cell neurons are unlikely to achieve physiological maturity comparable to that of post-natal cells. Overall, the extent to which neuron maturity becomes a limiting factor is therefore primarily down to the experimental questions being addressed and the knowledge that these cells will remain a model of true neuron function.

7.3 Study limitations

7.3.1 Neuron maturity and patch-clamping

For the work in Chapter 4, iPS cell derived neurons were patched at two time points, 30 and 50DPP, which corresponded to a period of 4 days from that time point (e.g. 30 – 34DPP). This was to allow the collection of enough data from each condition at each time point. If around 8-10 cells were patched per day, allowing 2 days for each condition meant that around 20 cells were patched per condition per time point for each differentiation. While over a total of three differentiations this should around 60 cells per time point per condition, various technical issues meant that in fact the highest total number of cells patched in one group was 41. While this is not too dissimilar to the reported number of cell patched in similar studies (Telezhkin *et al.*, 2016; Prè *et al.*, 2014; Gunhanlar *et al.*, 2017), the high degree of variation seen here in some of the measures suggests that the neuron cultures were fairly heterogeneous. Increasing the number of patched cells over a greater number of differentiations may aid in the understanding about the nature of the intrinsic properties of the neurons produced.

The adaptations to the differentiation protocol in Chapter 4 consisted of ACM together with a 2% oxygen incubator environment. Based upon the reports of previous studies, it was decided to to combine these measures and compare cells cultured in these conditions to those in standard conditions. This therefore meant that any changes observed in the ACM/2% conditions could only be directly attributed to these conditions together and therefore the individual actions of each component was unknown. While individual actions could be suggested based upon the existing literature, to provide a full understanding about the contributions of any effects to each component of the conditions, a larger experiment with 4 experimental groups should be performed.

The physiological maturity characteristics described in Chapter 4 were based around intrinsic neuron properties and formation of action potentials. However, a prerequisite of functional networks is the formation and maturation of synapses. While the work in Chapter 5 highlighted the role of both NMDA and AMPA receptor mediated synaptic activity in synchronised spontaneous activity, synaptic activity at the level of individual cells was not successfully determined. Spontaneous synaptic potentials can, in theory, routinely be recorded while

patching cells using a gap-free current clamp protocol. However, while individual events were observed, the membrane potential could not be routinely adequately stabilised to detect enough events for a quantitative comparison.

Finally, all patch-clamp experiments were achieved in current-clamp mode, recording the change in voltages throughout the cell. As discussed in Chapter 4, a key factor regulating the physiological maturity of neurons is the functional expression of voltage gated sodium and potassium channels. Voltage-clamping experiments showing the ionic currents associated with individual neurons would establish a fuller understanding about the functional maturity of the iPS cell derived neurons used in chapter 4 and 5 and could provide additional insight into the action of the ACM/2% culturing conditions.

7.3.2 Variability in MEA recordings

The development of network driven activity in iPS cell derived neurons described in Chapter 5 was, overall, observed consistently in number of array cultures and over at least 4 differentiations. However, activity was, in some cases, highly variable between individual arrays, both at the level of basal excitability and during coordinated firing. For example, while many cultures did show the extended synchronised behaviour which cycled over a number of seconds, some cultures did not progress beyond short synchronised burst firing. This variability was also seen in the cultures in Chapter 6, albeit in non-coordinated cultures, highlighting that it is likely a feature of this technique. This variability can be somewhat reduced by increasing the number of array-cultures per experiment but this is limited by the availability of arrays for a given experiment.

7.3.3 SHANK3 expression in ASD patient derived neurons

A number of limitations were associated with the work with the ASD patient lines in Chapter 6. Firstly, although the two patient lines used were presented with their respective genetic lesions showing, more or less, full heterozygous deletions of *SHANK3*, no data surrounding the expression levels of the gene transcripts or the protein were shown. Investigating the expression of *SHANK3* protein was precluded by the unavailability of an antibody which could reliably give results either with western blots, including with adult human brain tissue, or

immunocytochemistry. This is an issue not specific to this project as the group in King's College, London from where these cell lines came have also been unable to identify a useful antibody. Instead, that group has relied on determining the levels of *SHANK3* mRNA in neurons derived from the patient iPS cells, which in their hands is routinely reduced by around 50% compared to control neurons (Personal communication, April 2017). A similar approach was attempted here, however consistent levels of *SHANK3* mRNA were not detected, prohibiting any meaningful conclusions about the levels of *SHANK3* expression in the patient neurons. While any indication surrounding mRNA levels would be beneficial, it is worth considering that the relationship between mRNA levels and protein expression of individual is not necessarily linear, and in some cases, poorly correlated (Gong *et al.*, 2017; Koussounadis *et al.*, 2015). As such, the ideal outcome would be the identification of a reliable antibody that could determine *SHANK3* protein expression.

The experiments looking at the extracellular spike shapes produced by the neurons in Chapter 6 revealed the presence of a population of shapes unique to *SHANK3* mutant cells. These experiments however were limited by the number of spikes shapes that could be effectively processed: the total number of spikes shapes that were available for analyses was >400000 but handling was limited to a random sample of 20000 spikes. While this sample was, as far as possible, a good representation of the entire population, ideally a larger, if not the full, dataset would have been used. With increased computing power, the full data set could be analysed in exactly the same way. However, an alternative method would be to use a second machine learning algorithm which uses a random sample of the dataset as training data, and then subsequently takes further random samples to test any conclusions against the data set as a whole. This would allow analysis of the entire dataset without a necessary increase in handling capability and at the same time provide a computational method of making many objective and statistically verifiable comparisons of the spike waveform data.

7.4 Future directions

7.4.1 L-type calcium channels

An interesting finding from this project was the modulation of network activity in iPS cell neurons by the L-type calcium channel blocker diltiazem. As discussed earlier, mutations in LTCCs and in particular $Ca_v 1.2$, coded for by *CACNA1C*, are associated with several MHDs, including ASD. It would be very interesting to therefore investigate the network function of iPS cell neurons with mutations in *CACNA1C*. This could involve patient cells with common intronic SNVs or modelling haploinsufficiency by introducing deletions into WT iPS cells. This would therefore allow the comparison of function between neurons with a general reduction of LTCC function (i.e. with diltiazem) and specific loss of the disease associated $Ca_v 1.2$.

Another interesting finding from was the suggestion that the action of GABA_A antagonists and diltiazem may be acting via a common underlying mechanism to attenuate the interval between more active periods of synchronised cultures. While Chapter 5 discussed some of the possible pathways by which these two drugs may be acting, it would be highly attractive to study this shared action further. These studies would likely be focussed on the role of interneurons within the cultures and the functional expression of L-type calcium channels within these cells. Targeted patch-clamping of interneurons allied with voltage-clamping experiments could initially determine whether these channels are expressed while extended pharmacology experiments with MEAs could help determined whether interneuron function is required for the action of the L-type calcium channels.

7.4.2 Observing network behaviour in *SHANK3* mutant (and control) neurons

A curious result in this project was the absence of observed network driven behaviour in the neurons produced in Chapter 6, regardless of genotype. Analysis of the number of interneurons present in these cultures suggested that this was perhaps due to a lack of inhibitory tone, as it appeared that there was fewer than half the GABAergic neurons present in these neurons compared to those in Chapter 5. An initial solution to this could be as simple as treating the *SHANK3* mutant cells (+ controls) identically to the in chapter 5, rather than using the hybrid protocol which began with neural precursors. In theory, by using the protocols developed in

chapters 4 and 5, sufficient interneurons would be produced to drive network driven behaviour. However, there is also the opportunity to study the role of interneurons in the development of hPS cell derived cultures more generally. This could take the form of exploring the effect of known numbers of interneurons within spontaneously activity excitatory neuron cultures or by harnessing targeted optogenetics to control the action of interneurons during activity experiments. This could also then open up the possibility to study the role of interneurons in neurons with heterozygous deletions of SHANK3 and hPS cell models of ASD models more generally.

7.4.3 Unique spike shapes of SHANK3 mutant neurons

One of the most interesting findings in this project was the appearance of small population of extracellular spikes, unique to SHANK3 mutant neurons, which were wider than other spikes observed due to the presence of a 'double-peak'. It would initially be interesting to study these spike shapes in the context of more complex spontaneous behaviour – i.e. in coordinated firing. The previous section described how an initial approach to observe network behaviour in the SHANK3 cells would be to adopt the protocols used in Chapters 4 and 5. This would hopefully allow observation of these unique spike shapes during synapse-dependant synchronised activity and would also provide an additional control for the appearance of the shapes as, while the genotype of the cells would remain constant, the protocols to produce the neurons would be different.

The appearance of these unique spike shapes with extracellular recordings strongly suggests that a spike phenotype would be also observed with single cell patch-clamping, although it is perhaps likely that the manifestation of the aberrant firing would be different inside the cell. Moreover, while the double-peak spikes were only seen in SHANK3 mutant cells, they contributed to a small minority (< 10%) of the overall spikes detected from these neurons. As such, it may be difficult to routinely detect any changes to intracellular spike shape without patching a large number of neurons. Nevertheless, it is important to pursue single cell electrophysiology with the SHANK3 mutant neurons to better understand some of the more basic function properties of the cells and to investigate any potential underlying causes for the shapes seen with the MEA experiments here.

7.4.4 Extending the analysis of networks

The quantitative analysis of network behaviour in this project was focused on two measures: Max ASR and MAP interval. While these measures are useful and will remain a key part of the analysis process, it would be beneficial to develop further methods of describing the observed activity. In a number of the experiments in this project, it was noticeable that the length of the more active period (MAP) of synchronised cultures may also be dynamic both over development and in response to synaptic agents. As such, it would be useful to devise a method for quantifying the length of MAPs to complement the MAP interval, provide a more detailed description about the nature of the coordinated firing. Indeed, a measure of MAP length was in development in this project but could not be suitably optimised to provide a reliable and objective statistic across a range of firing. Furthermore, it would also be interesting to develop tools to look at the pattern of firing *within* the MAPs, which also appears to vary depending on development state or conditions and in particular it would be useful to demine the firing rate within both the more and less active states.

7.4.5 Conclusions

The work in the project has presented a platform for the observation and analysis of network driven activity in iPS cell derived neurons. This platform, based upon MEA recordings, provides an effective method of investigating such behaviour in human neurons, which, until recently has been limited. Moreover, the adaptations to the neuron differentiation protocols described here, based upon the physiological adaptations of astrocyte conditioned medium and hypoxic environments, has allowed, as far as can be determined, the development of complex network driven activity which has not previously been reported in iPS cell neurons. This project then studied the function of neurons derived from ASD patient iPS cells with heterozygous deletions of SHANK3, a mutation strongly associated with development of the disorder. Although the network function of these neurons was not successfully analysed, the work did provide interesting insights into their spontaneous activity and revealed a interesting phenotype in the shape of the spikes recorded by MEAs, thereby highlighting further possible application of the platform. Overall, the work of this project has shown that the techniques, protocols and analysis measures developed here can provide a valuable tool for investigating the function of hPS cell derived neurons in both development and disease modelling. The platform can be simply adapted and used as part of studies into hPS cell models of many neurological diseases and, importantly, provides a unique opportunity for the screening of compounds in the development of novel therapeutics.

References

- Aasen T, Raya A, Barrero MJ, Garreta E, Consiglio A, Gonzalez F, *et al.* (2008) Efficient and rapid generation of induced pluripotent stem cells from human keratinocytes. *Nat Biotechnol* 26:1276-1284.
- Abrahams BS, Arking DE, Campbell DB, Mefford HC, Morrow EM, Weiss LA, *et al.* (2013) SFARI Gene 2.0: a community-driven knowledgebase for the autism spectrum disorders (ASDs). *Mol Autism* 4:36.
- Akechi H, Senju A, Kikuchi Y, Tojo Y, Osanai H, Hasegawa T (2010) The effect of gaze direction on the processing of facial expressions in children with autism spectrum disorder: an ERP study. *Neuropsychologia* 48:2841-2851.
- Allen NJ, Bennett ML, Foo LC, Wang GX, Chakraborty C, Smith SJ, Barres BA (2012) Astrocyte glypicans 4 and 6 promote formation of excitatory synapses via GluA1 AMPA receptors. *Nature* 486:410-414.
- Ambrogini P, Lattanzi D, Ciuffoli S, Agostini D, Bertini L, Stocchi V, *et al.* (2004) Morpho-functional characterization of neuronal cells at different stages of maturation in granule cell layer of adult rat dentate gyrus. *Brain Res* 1017:21-31.
- Amilhon B, Huh CY, Manseau F, Ducharme G, Nichol H, Adamantidis A, Williams S (2015) Parvalbumin Interneurons of Hippocampus Tune Population Activity at Theta Frequency. *Neuron* 86:1277-1289.
- Amin H, Maccione A, Marinaro F, Zordan S, Nieuws T, Berdondini L (2016) Electrical Responses and Spontaneous Activity of Human iPSC-Derived Neuronal Networks Characterized for 3-month Culture with 4096-Electrode Arrays. *Front Neurosci* 10:121.
- Androutsellis-Theotokis A, Leker RR, Soldner F, Hoepfner DJ, Ravin R, Poser SW, *et al.* (2006) Notch signalling regulates stem cell numbers in vitro and in vivo. *Nature* 442:823-826.
- Arber C, Precious SV, Cambrey S, Risner-Janiczek JR, Kelly C, Noakes Z, *et al.* (2015) Activin A directs striatal projection neuron differentiation of human pluripotent stem cells. *Development* 142:1375-1386.
- Arenas E, Denham M, Villaescusa JC (2015) How to make a midbrain dopaminergic neuron. *Development* 142:1918-1936.
- Attwell D, Buchan AM, Charpak S, Lauritzen M, Macvicar BA, Newman EA (2010) Glial and neuronal control of brain blood flow. *Nature* 468:232-243.
- Auerbach BD, Osterweil EK, Bear MF (2011) Mutations causing syndromic autism define an axis of synaptic pathophysiology. *Nature* 480:63-68.
- Bachevalier J, Loveland KA (2006) The orbitofrontal-amygdala circuit and self-regulation of social-emotional behavior in autism. *Neurosci Biobehav Rev* 30:97-117.
- Baird G, Simonoff E, Pickles A, Chandler S, Loucas T, Meldrum D, Charman T (2006) Prevalence of disorders of the autism spectrum in a population cohort of children in South Thames: the Special Needs and Autism Project (SNAP). *The Lancet* 368:210-215.
- Bakkum DJ, Radivojevic M, Frey U, Franke F, Hierlemann A, Takahashi H (2013) Parameters for burst detection. *Front Comput Neurosci* 7:193.
- Barberi T, Klivenyi P, Calingasan NY, Lee H, Kawamata H, Loonam K, *et al.* (2003) Neural subtype specification of fertilization and nuclear transfer embryonic stem cells and application in parkinsonian mice. *Nat Biotechnol* 21:1200-1207.
- Bardy C, van den Hurk M, Eames T, Marchand C, Hernandez RV, Kellogg M, *et al.* (2015) Neuronal medium that supports basic synaptic functions and activity of human neurons in vitro. *Proc Natl Acad Sci U S A* 112:E2725-E2734.
- Bardy C, van den Hurk M, Kakaradov B, Erwin JA, Jaeger BN, Hernandez RV, *et al.* (2016) Predicting the functional states of human iPSC-derived neurons with single-cell RNA-seq and electrophysiology. *Mol Psychiatry* 21:1573-1588.
- Barnard RA, Pomaville MB, O'Roak BJ (2015) Mutations and Modeling of the Chromatin Remodeler CHD8 Define an Emerging Autism Etiology. *Front Neurosci* 9:477.
- Baron MK, Boeckers TM, Vaida B, Faham S, Gingery M, Sawaya MR, *et al.* (2006) An architectural framework that may lie at the core of the postsynaptic density. *Science* 311:531-535.
- Bartos M, Vida I, Frotscher M, Meyer A, Monyer H, Geiger JR, Jonas P (2002) Fast synaptic inhibition promotes synchronized gamma oscillations in hippocampal interneuron networks. *Proc Natl Acad Sci U S A* 99:13222-13227.
- Bateup HS, Johnson CA, Denefrio CL, Saulnier JL, Kornacker K, Sabatini BL (2013) Excitatory/inhibitory synaptic imbalance leads to hippocampal hyperexcitability in mouse models of tuberous sclerosis. *Neuron* 78:510-522.
- Bauman M, Kemper TL (1985) Histoanatomic observations of the brain in early infantile autism. *Neurology* 35:866-874.
- Bean BP (2007) The action potential in mammalian central neurons. *Nature Reviews Neuroscience* 8:451-465.
- Bedogni F, Hodge RD, Elsen GE, Nelson BR, Daza RA, Beyer RP, *et al.* (2010) Tbr1 regulates regional and laminar identity of postmitotic neurons in developing neocortex. *Proc Natl Acad Sci U S A* 107:13129-13134.
- Belger A, Carpenter KL, Yucel GH, Cleary KM, Donkers FC (2011) The neural circuitry of autism. *Neurotoxicity research* 20:201-214.
- Benarroch EE (2013) HCN channels: function and clinical implications. *Neurology* 80:304-310.
- Bengtson CP, Kaiser M, Obermayer J, Bading H (2013) Calcium responses to synaptically activated bursts of action potentials and their synapse-independent replay in cultured networks of hippocampal neurons. *Biochim Biophys Acta* 1833:1672-1679.
- Bernier R, Golzio C, Xiong B, Stessman HA, Coe BP, Penn O, *et al.* (2014) Disruptive CHD8 mutations define a subtype of autism early in development. *Cell* 158:263-276.

- Blatow M, Rozov A, Katona I, Hormuzdi SG, Meyer AH, Whittington MA, *et al.* (2003) A novel network of multipolar bursting interneurons generates theta frequency oscillations in neocortex. *Neuron* 38:805-817.
- Boccutto L, Lauri M, Sarasua SM, Skinner CD, Buccella D, Dwivedi A, *et al.* (2013) Prevalence of SHANK3 variants in patients with different subtypes of autism spectrum disorders. *Eur J Hum Genet* 21:310-316.
- Born G, Grayton HM, Langhorst H, Dudanova I, Rohlmann A, Woodward BW, *et al.* (2015) Genetic targeting of NRXN2 in mice unveils role in excitatory cortical synapse function and social behaviors. *Front Synaptic Neurosci* 7:3.
- Bozdagi O, Sakurai T, Papapetrou D, Wang X, Dickstein DL, Takahashi N, *et al.* (2010) Haploinsufficiency of the autism-associated Shank3 gene leads to deficits in synaptic function, social interaction, and social communication. *Mol Autism* 1:15.
- Böckers TM, Mameza MG, Kreutz MR, Bockmann J, Weise C, Buck F, *et al.* (2001) Synaptic scaffolding proteins in rat brain. Ankyrin repeats of the multidomain Shank protein family interact with the cytoskeletal protein alpha-fodrin. *J Biol Chem* 276:40104-40112.
- Brennan K, Savas JN, Kim Y, Tran N, Simone A, Hashimoto-Torii K, *et al.* (2014) Phenotypic differences in hiPSC NPCs derived from patients with schizophrenia. *Mol Psychiatry*.
- Brewer GJ, Cotman CW (1989) Survival and growth of hippocampal neurons in defined medium at low density: advantages of a sandwich culture technique or low oxygen. *Brain Res* 494:65-74.
- Britanova O, de Juan Romero C, Cheung A, Kwan KY, Schwark M, Gyorgy A, *et al.* (2008) Satb2 is a postmitotic determinant for upper-layer neuron specification in the neocortex. *Neuron* 57:378-392.
- Brugha T, McManus S, Meltzer H, Smith J, Scott FJ, Purdon S, *et al.* (2009) Autism spectrum disorders in adults living in households throughout England: Report from the adult psychiatric morbidity survey 2007. *Leeds: The NHS Information Centre for Health and Social Care.*
- Bruno RM, Sakmann B (2006) Cortex is driven by weak but synchronously active thalamocortical synapses. *Science* 312:1622-1627.
- Bucan M, Abrahams BS, Wang K, Glessner JT, Herman EI, Sonnenblick LI, *et al.* (2009) Genome-wide analyses of exonic copy number variants in a family-based study point to novel autism susceptibility genes. *PLoS genetics* 5:e1000536.
- Bukalo O, Campanac E, Hoffman DA, Fields RD (2013) Synaptic plasticity by antidromic firing during hippocampal network oscillations. *Proc Natl Acad Sci U S A* 110:5175-5180.
- Buxhoeveden DP, Semendeferi K, Buckwalter J, Schenker N, Switzer R, Courchesne E (2006) Reduced minicolumns in the frontal cortex of patients with autism. *Neuropathol Appl Neurobiol* 32:483-491.
- Cain CK, Blouin AM, Barad M (2002) L-type voltage-gated calcium channels are required for extinction, but not for acquisition or expression, of conditional fear in mice. *Journal of Neuroscience* 22:9113-9121.
- Cao Z, Hulsizer S, Tassone F, Tang HT, Hagerman RJ, Rogawski MA, *et al.* (2012) Clustered burst firing in FMR1 premutation hippocampal neurons: amelioration with allopregnanolone. *Hum Mol Genet* 21:2923-2935.
- Caraiscos VB, Elliott EM, You-Ten KE, Cheng VY, Belelli D, Newell JG, *et al.* (2004) Tonic inhibition in mouse hippocampal CA1 pyramidal neurons is mediated by alpha5 subunit-containing gamma-aminobutyric acid type A receptors. *Proc Natl Acad Sci U S A* 101:3662-3667.
- Casanova MF, Buxhoeveden DP, Switala AE, Roy E (2002) Minicolumnar pathology in autism. *Neurology* 58:428-432.
- Celik M, Gökmen N, Erbayraktar S, Akhisaroglu M, Konak S, Ulukus C, *et al.* (2002) Erythropoietin prevents motor neuron apoptosis and neurologic disability in experimental spinal cord ischemic injury. *Proc Natl Acad Sci U S A* 99:2258-2263.
- Chambers SM, Fasano CA, Papapetrou EP, Tomishima M, Sadelain M, Studer L (2009) Highly efficient neural conversion of human ES and iPS cells by dual inhibition of SMAD signaling. *Nat Biotechnol* 27:275-280.
- Chang MY, Son H, Lee YS, Lee SH (2003) Neurons and astrocytes secrete factors that cause stem cells to differentiate into neurons and astrocytes, respectively. *Mol Cell Neurosci* 23:414-426.
- Cheng L, Hu W, Qiu B, Zhao J, Yu Y, Guan W, *et al.* (2014) Generation of neural progenitor cells by chemical cocktails and hypoxia. *Cell Res* 24:665-679.
- Chen JY, Chauvette S, Skorheim S, Timofeev I, Bazhenov M (2012) Interneuron-mediated inhibition synchronizes neuronal activity during slow oscillation. *J Physiol* 590:3987-4010.
- Chen K, Aradi I, Thon N, Eghbal-Ahmadi M, Baram TZ, Soltesz I (2001) Persistently modified h-channels after complex febrile seizures convert the seizure-induced enhancement of inhibition to hyperexcitability. *Nat Med* 7:331-337.
- Chen X, Dzakpasu R (2010) Observed network dynamics from altering the balance between excitatory and inhibitory neurons in cultured networks. *Phys Rev E Stat Nonlin Soft Matter Phys* 82:031907.
- Chiappalone M, Bove M, Vato A, Tedesco M, Martinoia S (2006) Dissociated cortical networks show spontaneously correlated activity patterns during in vitro development. *Brain Res* 1093:41-53.
- Chiappalone M, Novellino A, Vajda I, Vato A, Martinoia S, van Pelt J (2005) Burst detection algorithms for the analysis of spatio-temporal patterns in cortical networks of neurons. *Neurocomputing* 65:653-662.
- Chiappalone M, Vato A, Tedesco MB, Marcoli M, Davide F, Martinoia S (2003) Networks of neurons coupled to microelectrode arrays: a neuronal sensory system for pharmacological applications. *Biosens Bioelectron* 18:627-634.
- Chin MH, Mason MJ, Xie W, Volinia S, Singer M, Peterson C, *et al.* (2009) Induced pluripotent stem cells and embryonic stem cells are distinguished by gene expression signatures. *Cell Stem Cell* 5:111-123.
- Chong ZZ, Kang JQ, Maiese K (2002) Hematopoietic factor erythropoietin fosters neuroprotection through novel signal transduction cascades. *J Cereb Blood Flow Metab* 22:503-514.

Chuang HC, Huang TN, Hsueh YP (2015) T-Brain-1--A Potential Master Regulator in Autism Spectrum Disorders. *Autism Res* 8:412-426.

Chung W-S, Allen NJ, Eroglu C (2015) Astrocytes control synapse formation, function, and elimination. *Cold Spring Harbor perspectives in biology* 7:a020370.

Clarke LE, Barres BA (2013) Emerging roles of astrocytes in neural circuit development. *Nat Rev Neurosci* 14:311-321.

Close JL, Yao Z, Levi BP, Miller JA, Bakken TE, Menon V, *et al.* (2017) Single-Cell Profiling of an In Vitro Model of Human Interneuron Development Reveals Temporal Dynamics of Cell Type Production and Maturation. *Neuron* 93:1035-1048.e5.

Cobb SR, Buhl EH, Halasy K, Paulsen O, Somogyi P (1995) Synchronization of neuronal activity in hippocampus by individual GABAergic interneurons. *Nature* 378:75-78.

Compte A, Sanchez-Vives MV, McCormick DA, Wang X-J (2003) Cellular and network mechanisms of slow oscillatory activity (< 1 Hz) and wave propagations in a cortical network model. *J Neurophysiol* 89:2707-2725.

Conturo TE, Williams DL, Smith CD, Gultepe E, Akbudak E, Minshew NJ (2008) Neuronal fiber pathway abnormalities in autism: an initial MRI diffusion tensor tracking study of hippocampo-fusiform and amygdalo-fusiform pathways. *J Int Neuropsychol Soc* 14:933-946.

Courchesne E, Mouton PR, Calhoun ME, Semendeferi K, Ahrens-Barbeau C, Hallet MJ, *et al.* (2011) Neuron number and size in prefrontal cortex of children with autism. *JAMA* 306:2001-2010.

Crawford TQ, Roelink H (2007) The notch response inhibitor DAPT enhances neuronal differentiation in embryonic stem cell-derived embryoid bodies independently of sonic hedgehog signaling. *Dev Dyn* 236:886-892.

Cull-Candy S, Brickley S, Farrant M (2001) NMDA receptor subunits: diversity, development and disease. *Curr Opin Neurobiol* 11:327-335.

Dalton KM, Nacewicz BM, Johnstone T, Schaefer HS, Gernsbacher MA, Goldsmith HH, *et al.* (2005) Gaze fixation and the neural circuitry of face processing in autism. *Nat Neurosci* 8:519-526.

Darville H, Poulet A, Rodet-Amsellem F, Chatrousse L, Pernelle J, Boissart C, *et al.* (2016) Human Pluripotent Stem Cell-derived Cortical Neurons for High Throughput Medication Screening in Autism: A Proof of Concept Study in SHANK3 Haploinsufficiency Syndrome. *EBioMedicine* 9:293-305.

Dawson G, Carver L, Meltzoff AN, Panagiotides H, McPartland J, Webb SJ (2002) Neural correlates of face and object recognition in young children with autism spectrum disorder, developmental delay, and typical development. *Child Dev* 73:700-717.

Debanne D, Boudkazi S, Campanac E, Cudmore RH, Giraud P, Fronzaroli-Molinieres L, *et al.* (2008) Paired-recordings from synaptically coupled cortical and hippocampal neurons in acute and cultured brain slices. *Nat Protoc* 3:1559-1568.

Dibbens LM, Reid CA, Hodgson B, Thomas EA, Phillips AM, Gazina E, *et al.* (2010) Augmented currents of an HCN2 variant in patients with febrile seizure syndromes. *Ann Neurol* 67:542-546.

Disciglio V, Rizzo CL, Mencarelli MA, Mucciolo M, Marozza A, Di Marco C, *et al.* (2014) Interstitial 22q13 deletions not involving SHANK3 gene: a new contiguous gene syndrome. *American journal of medical genetics Part A* 164:1666-1676.

Dobrev D, Milde AS, Andreas K, Ravens U (1999) The effects of verapamil and diltiazem on N-, P- and Q-type calcium channels mediating dopamine release in rat striatum. *Br J Pharmacol* 127:576-582.

Doi A, Park I-H, Wen B, Murakami P, Aryee MJ, Irizarry R, *et al.* (2009) Differential methylation of tissue- and cancer-specific CpG island shores distinguishes human induced pluripotent stem cells, embryonic stem cells and fibroblasts. *Nat Genet* 41:1350-1353.

Dolmetsch RE, Pajvani U, Fife K, Spotts JM, Greenberg ME (2001) Signaling to the nucleus by an L-type calcium channel-calmodulin complex through the MAP kinase pathway. *Science* 294:333-339.

Dolphin AC (2012) Calcium channel auxiliary $\alpha 2\delta$ and β subunits: trafficking and one step beyond. *Nat Rev Neurosci* 13:542-555.

Duan X, Gao R, Xie P, Cohen-Karni T, Qing Q, Choe HS, *et al.* (2011) Intracellular recordings of action potentials by an extracellular nanoscale field-effect transistor. *Nat Nanotechnol* 7:174-179.

Duffney LJ, Wei J, Cheng J, Liu W, Smith KR, Kittler JT, Yan Z (2013) Shank3 deficiency induces NMDA receptor hypofunction via an actin-dependent mechanism. *J Neurosci* 33:15767-15778.

Du J, Zhang L, Weiser M, Rudy B, McBain CJ (1996) Developmental expression and functional characterization of the potassium-channel subunit Kv3.1b in parvalbumin-containing interneurons of the rat hippocampus. *J Neurosci* 16:506-518.

Durand CM, Betancur C, Boeckers TM, Bockmann J, Chaste P, Fauchereau F, *et al.* (2007) Mutations in the gene encoding the synaptic scaffolding protein SHANK3 are associated with autism spectrum disorders. *Nat Genet* 39:25-27.

Durand CM, Perroy J, Loll F, Perrais D, Fagni L, Bourgeron T, *et al.* (2012) SHANK3 mutations identified in autism lead to modification of dendritic spine morphology via an actin-dependent mechanism. *Mol Psychiatry* 17:71-84.

Durand GM, Kovalchuk Y, Konnerth A (1996) Long-term potentiation and functional synapse induction in developing hippocampus. *Nature* 381:71-75.

Egert U, Knott T, Schwarz C, Nawrot M, Brandt A, Rotter S, Diesmann M (2002) MEA-Tools: an open source toolbox for the analysis of multi-electrode data with MATLAB. *J Neurosci Methods* 117:33-42.

Elkabetz Y, Panagiotakos G, Al Shamy G, Socci ND, Tabar V, Studer L (2008) Human ES cell-derived neural rosettes reveal a functionally distinct early neural stem cell stage. *Genes Dev* 22:152-165.

Elmariah SB, Oh EJ, Hughes EG, Balice-Gordon RJ (2005) Astrocytes regulate inhibitory synapse formation via Trk-mediated modulation of postsynaptic GABAA receptors. *J Neurosci* 25:3638-3650.

- Elston GN, Fujita I (2014) Pyramidal cell development: postnatal spinogenesis, dendritic growth, axon growth, and electrophysiology. *Front Neuroanat* 8:78.
- Emerson E, Baines S (2010) The estimated prevalence of autism among adults with learning disabilities in England. *Improving Health and Lives: Learning Disabilities Observatory, Durham*.
- Empson RM, Jefferys JG (2001) Ca(2+) entry through L-type Ca(2+) channels helps terminate epileptiform activity by activation of a Ca(2+) dependent afterhyperpolarisation in hippocampal CA3. *Neuroscience* 102:297-306.
- Enes J, Langwieser N, Ruschel J, Carballosa-Gonzalez MM, Klug A, Traut MH, *et al.* (2010) Electrical activity suppresses axon growth through Ca(v)1.2 channels in adult primary sensory neurons. *Curr Biol* 20:1154-1164.
- Englund C, Fink A, Lau C, Pham D, Daza RA, Bulfone A, *et al.* (2005) Pax6, Tbr2, and Tbr1 are expressed sequentially by radial glia, intermediate progenitor cells, and postmitotic neurons in developing neocortex. *J Neurosci* 25:247-251.
- Erecińska M, Silver IA (2001) Tissue oxygen tension and brain sensitivity to hypoxia. *Respiration physiology* 128:263-276.
- Eroglu C, Allen NJ, Susman MW, O'Rourke NA, Park CY, Ozkan E, *et al.* (2009) Gabapentin receptor alpha2delta-1 is a neuronal thrombospondin receptor responsible for excitatory CNS synaptogenesis. *Cell* 139:380-392.
- Espósito MS, Piatti VC, Laplagne DA, Morgenstern NA, Ferrari CC, Pitossi FJ, Schinder AF (2005) Neuronal differentiation in the adult hippocampus recapitulates embryonic development. *J Neurosci* 25:10074-10086.
- Espuny-Camacho I, Michelsen KA, Gall D, Linaro D, Hasche A, Bonnefont J, *et al.* (2013) Pyramidal neurons derived from human pluripotent stem cells integrate efficiently into mouse brain circuits in vivo. *Neuron* 77:440-456.
- Etherton M, Földy C, Sharma M, Tabuchi K, Liu X, Shamloo M, *et al.* (2011) Autism-linked neuroligin-3 R451C mutation differentially alters hippocampal and cortical synaptic function. *Proc Natl Acad Sci U S A* 108:13764-13769.
- Etherton MR, Blaiss CA, Powell CM, Südhof TC (2009) Mouse neurexin-1alpha deletion causes correlated electrophysiological and behavioral changes consistent with cognitive impairments. *Proc Natl Acad Sci U S A* 106:17998-18003.
- Evans RM, Zamponi GW (2006) Presynaptic Ca2+ channels--integration centers for neuronal signaling pathways. *Trends Neurosci* 29:617-624.
- Felix RA, Vonderschen K, Berrebi AS, Magnusson AK (2013) Development of on-off spiking in superior paraolivary nucleus neurons of the mouse. *J Neurophysiol* 109:2691-2704.
- Fernández-Agulló T (2001) Thyrotropin-releasing hormone and its receptor in glia. *Glia* 33:267-276.
- Fink M, Lesage F, Duprat F, Heurteaux C, Reyes R, Fosset M, Lazdunski M (1998) A neuronal two P domain K+ channel stimulated by arachidonic acid and polyunsaturated fatty acids. *EMBO J* 17:3297-3308.
- Fricker D, Verheugen JA, Miles R (1999) Cell-attached measurements of the firing threshold of rat hippocampal neurones. *J Physiol* 517 (Pt 3):791-804.
- Gamelli AE, McKinney BC, White JA, Murphy GG (2011) Deletion of the L-type calcium channel Ca(V) 1.3 but not Ca(V) 1.2 results in a diminished sAHP in mouse CA1 pyramidal neurons. *Hippocampus* 21:133-141.
- Gaugler T, Klei L, Sanders SJ, Bodea CA, Goldberg AP, Lee AB, *et al.* (2014) Most genetic risk for autism resides with common variation. *Nat Genet* 46:881-885.
- Gauthier J, Spiegelman D, Piton A, Lafrenière RG, Laurent S, St-Onge J, *et al.* (2009) Novel de novo SHANK3 mutation in autistic patients. *Am J Med Genet B Neuropsychiatr Genet* 150B:421-424.
- Georgiadis V, Stephanou A, Townsend PA, Jackson TR (2015) MultiElec: A MATLAB Based Application for MEA Data Analysis. *PLoS One* 10:e0129389.
- Geschwind DH, Levitt P (2007) Autism spectrum disorders: developmental disconnection syndromes. *Curr Opin Neurobiol* 17:103-111.
- Ghosh Z, Wilson KD, Wu Y, Hu S, Quertermous T, Wu JC (2010) Persistent donor cell gene expression among human induced pluripotent stem cells contributes to differences with human embryonic stem cells. *PLoS One* 5:e8975.
- Gilman SR, Iossifov I, Levy D, Ronemus M, Wigler M, Vitkup D (2011) Rare de novo variants associated with autism implicate a large functional network of genes involved in formation and function of synapses. *Neuron* 70:898-907.
- Goda F, O'Hara JA, Liu KJ, Rhodes ES, Dunn JF, Swartz HM (1997) Comparisons of measurements of pO2 in tissue in vivo by EPR oximetry and microelectrodes. *Adv Exp Med Biol* 411:543-549.
- Goldstein SA, Bockenhauer D, O'Kelly I, Zilberberg N (2001) Potassium leak channels and the KCNK family of two-P-domain subunits. *Nat Rev Neurosci* 2:175-184.
- Gomez-Ospina N, Tsuruta F, Barreto-Chang O, Hu L, Dolmetsch R (2006) The C terminus of the L-type voltage-gated calcium channel Ca V 1.2 encodes a transcription factor. *Cell* 127:591-606.
- Gomot M, Giard MH, Adrien JL, Barthelemy C, Bruneau N (2002) Hypersensitivity to acoustic change in children with autism: electrophysiological evidence of left frontal cortex dysfunctioning. *Psychophysiology* 39:577-584.
- Gong H, Wang X, Liu B, Boutet S, Holcomb I, Dakshinamoorthy G, *et al.* (2017) Single-cell protein-mRNA correlation analysis enabled by multiplexed dual-analyte co-detection. *Sci Rep* 7:2776.
- Goulburn AL, Stanley EG, Elefanty AG, Anderson SA (2012) Generating GABAergic cerebral cortical interneurons from mouse and human embryonic stem cells. *Stem Cell Res* 8:416-426.
- Grosser S, Queenan BN, Lalchandani RR, Vicini S (2014) Hilar somatostatin interneurons contribute to synchronized GABA activity in an in vitro epilepsy model. *PLoS One* 9:e86250.
- Gross GW, Williams AN, Lucas JH (1982) Recording of spontaneous activity with photoetched microelectrode surfaces from mouse spinal neurons in culture. *J Neurosci Methods* 5:13-22.

Grove EA, Fukuchi-Shimogori T (2003) Generating the cerebral cortical area map. *Annual review of neuroscience* 26:355-380.

Guilmatre A, Huguet G, Delorme R, Bourgeron T (2014) The emerging role of SHANK genes in neuropsychiatric disorders. *Dev Neurobiol* 74:113-122.

Gunhanlar N, Shpak G, van der Kroeg M, Gouty-Colomer LA, Munshi ST, Lendemeijer B, *et al.* (2017) A simplified protocol for differentiation of electrophysiologically mature neuronal networks from human induced pluripotent stem cells. *Mol Psychiatry*.

Gunthorpe MJ, Lummis SC (1999) Diltiazem causes open channel block of recombinant 5-HT₃ receptors. *J Physiol* 519 Pt 3:713-722.

Hai A, Dormann A, Shappir J, Yitzchaik S, Bartic C, Borghs G, *et al.* (2009) Spine-shaped gold protrusions improve the adherence and electrical coupling of neurons with the surface of micro-electronic devices. *J R Soc Interface* 6:1153-1165.

Hakami T, Jones NC, Tolmacheva EA, Gaudias J, Chaumont J, Salzberg M, *et al.* (2009) NMDA receptor hypofunction leads to generalized and persistent aberrant γ oscillations independent of hyperlocomotion and the state of consciousness. *PLoS One* 4:e6755.

Hales CM, Rolston JD, Potter SM (2010) How to culture, record and stimulate neuronal networks on micro-electrode arrays (MEAs). *J Vis Exp*.

Hallmayer J, Cleveland S, Torres A, Phillips J, Cohen B, Torigoe T, *et al.* (2011) Genetic heritability and shared environmental factors among twin pairs with autism. *Archives of general psychiatry* 68:1095-1102.

Hama H, Hara C, Yamaguchi K, Miyawaki A (2004) PKC signaling mediates global enhancement of excitatory synaptogenesis in neurons triggered by local contact with astrocytes. *Neuron* 41:405-415.

Han K, Holder JL, Schaaf CP, Lu H, Chen H, Kang H, *et al.* (2013) SHANK3 overexpression causes manic-like behaviour with unique pharmacogenetic properties. *Nature* 503:72-77.

Han S, Tai C, Westenbroek RE, Yu FH, Cheah CS, Potter GB, *et al.* (2012) Autistic-like behaviour in Scn1a^{+/-} mice and rescue by enhanced GABA-mediated neurotransmission. *Nature* 489:385-390.

Hansen AK, Nedergaard S, Andreassen M (2014) Intrinsic Ca²⁺-dependent theta oscillations in apical dendrites of hippocampal CA1 pyramidal cells in vitro. *J Neurophysiol* 112:631-643.

Hargreaves AC, Gunthorpe MJ, Taylor CW, Lummis SC (1996) Direct inhibition of 5-hydroxytryptamine₃ receptors by antagonists of L-type Ca²⁺ channels. *Mol Pharmacol* 50:1284-1294.

Harsch A, Robinson HP (2000) Postsynaptic variability of firing in rat cortical neurons: the roles of input synchronization and synaptic NMDA receptor conductance. *J Neurosci* 20:6181-6192.

Hayashi K, Hashimoto M, Koda M, Naito AT, Murata A, Okawa A, *et al.* (2011) Increase of sensitivity to mechanical stimulus after transplantation of murine induced pluripotent stem cell--derived astrocytes in a rat spinal cord injury model. *Journal of Neurosurgery: Spine* 15:582-593.

Hayashi MK, Tang C, Verpelli C, Narayanan R, Stearns MH, Xu R-M, *et al.* (2009) The postsynaptic density proteins Homer and Shank form a polymeric network structure. *Cell* 137:159-171.

Hazan L, Zugaro M, Buzsáki G (2006) Klusters, NeuroScope, NDManager: a free software suite for neurophysiological data processing and visualization. *J Neurosci Methods* 155:207-216.

Heikkilä TJ, Ylä-Outinen L, Tanskanen JM, Lappalainen RS, Skottman H, Suuronen R, *et al.* (2009) Human embryonic stem cell-derived neuronal cells form spontaneously active neuronal networks in vitro. *Exp Neurol* 218:109-116.

He J, Zhou W, Zeng S, Luo Q (2005) L-type calcium channels mediate synchronized spontaneous Ca²⁺ spikes in cultured cortical networks. *Conf Proc IEEE Eng Med Biol Soc* 2:1783-1785.

Hell JW, Westenbroek RE, Warner C, Ahljianian MK, Prystay W, Gilbert MM, *et al.* (1993) Identification and differential subcellular localization of the neuronal class C and class D L-type calcium channel alpha 1 subunits. *The Journal of cell biology* 123:949-962.

Hernandez LM, Rudie JD, Green SA, Bookheimer S, Dapretto M (2015) Neural signatures of autism spectrum disorders: insights into brain network dynamics. *Neuropsychopharmacology* 40:171-189.

Higley MJ, Contreras D (2006) Balanced excitation and inhibition determine spike timing during frequency adaptation. *J Neurosci* 26:448-457.

Hill EL (2004) Executive dysfunction in autism. *Trends in cognitive sciences* 8:26-32.

Hjelmeland MD, Hjelmeland AB, Sathornsumetee S, Reese ED, Herbstreith MH, Laping NJ, *et al.* (2004) SB-431542, a small molecule transforming growth factor-beta-receptor antagonist, inhibits human glioma cell line proliferation and motility. *Mol Cancer Ther* 3:737-745.

Hofmann F, Flockerzi V, Kahl S, Wegener JW (2014) L-type CaV1.2 calcium channels: from in vitro findings to in vivo function. *Physiol Rev* 94:303-326.

Horak M, Petralia RS, Kaniakova M, Sans N (2014) ER to synapse trafficking of NMDA receptors. *Front Cell Neurosci* 8:394.

Hsiao MC, Yu PN, Song D, Liu CY, Heck CN, Millett D, Berger TW (2014) An in vitro seizure model from human hippocampal slices using multi-electrode arrays. *J Neurosci Methods*.

Huangfu D, Maehr R, Guo W, Eijkelenboom A, Snitow M, Chen AE, Melton DA (2008) Induction of pluripotent stem cells by defined factors is greatly improved by small-molecule compounds. *Nat Biotechnol* 26:795-797.

Huang TN, Chuang HC, Chou WH, Chen CY, Wang HF, Chou SJ, Hsueh YP (2014) Tbr1 haploinsufficiency impairs amygdalar axonal projections and results in cognitive abnormality. *Nat Neurosci* 17:240-247.

Huang Z, Walker MC, Shah MM (2009) Loss of dendritic HCN1 subunits enhances cortical excitability and epileptogenesis. *J Neurosci* 29:10979-10988.

Hughes EG, Elmariah SB, Balice-Gordon RJ (2010) Astrocyte secreted proteins selectively increase hippocampal GABAergic axon length, branching, and synaptogenesis. *Mol Cell Neurosci* 43:136-145.

Hu H, Gan J, Jonas P (2014) Fast-spiking, parvalbumin+ GABAergic interneurons: From cellular design to microcircuit function. *Science* 345:1255-1263.

Hung AY, Futai K, Sala C, Valtschanoff JG, Ryu J, Woodworth MA, et al. (2008) Smaller dendritic spines, weaker synaptic transmission, but enhanced spatial learning in mice lacking Shank1. *J Neurosci* 28:1697-1708.

Hussein SM, Batada NN, Vuoristo S, Ching RW, Autio R, Närvä E, et al. (2011) Copy number variation and selection during reprogramming to pluripotency. *Nature* 471:58-62.

Hutsler JJ, Zhang H (2010) Increased dendritic spine densities on cortical projection neurons in autism spectrum disorders. *Brain Res* 1309:83-94.

Hu Y, Qu ZY, Cao SY, Li Q, Ma L, Krencik R, et al. (2016) Directed differentiation of basal forebrain cholinergic neurons from human pluripotent stem cells. *J Neurosci Methods* 266:42-49.

Inglefield JR, Shafer TJ (2000) Polychlorinated biphenyl-stimulation of Ca(2+) oscillations in developing neocortical cells: a role for excitatory transmitters and L-type voltage-sensitive Ca(2+) channels. *J Pharmacol Exp Ther* 295:105-113.

Iossifov I, O'Roak BJ, Sanders SJ, Ronemus M, Krumm N, Levy D, et al. (2014a) The contribution of de novo coding mutations to autism spectrum disorder. *Nature* 515:216-221.

Iossifov I, O'Roak BJ, Sanders SJ, Ronemus M, Krumm N, Levy D, et al. (2014b) The contribution of de novo coding mutations to autism spectrum disorder. *Nature* 515:216-221.

Irie F, Badie-Mahdavi H, Yamaguchi Y (2012) Autism-like socio-communicative deficits and stereotypies in mice lacking heparan sulfate. *Proc Natl Acad Sci U S A* 109:5052-5056.

Irwin SA, Galvez R, Greenough WT (2000) Dendritic spine structural anomalies in fragile-X mental retardation syndrome. *Cerebral cortex* 10:1038-1044.

Itsykson P, Ilouz N, Turetsky T, Goldstein RS, Pera MF, Fishbein I, et al. (2005) Derivation of neural precursors from human embryonic stem cells in the presence of noggin. *Mol Cell Neurosci* 30:24-36.

Jamain S, Quach H, Betancur C, Råstam M, Colineaux C, Gillberg IC, et al. (2003) Mutations of the X-linked genes encoding neuroligins NLGN3 and NLGN4 are associated with autism. *Nat Genet* 34:27-29.

Jang MJ, Nam Y (2015) NeuroCa: integrated framework for systematic analysis of spatiotemporal neuronal activity patterns from large-scale optical recording data. *Neurophotonics* 2:035003.

Jaramillo TC, Speed HE, Xuan Z, Reimers JM, Liu S, Powell CM (2016) Altered Striatal Synaptic Function and Abnormal Behaviour in Shank3 Exon4-9 Deletion Mouse Model of Autism. *Autism Res* 9:350-375.

Jiang M, Ash RT, Baker SA, Suter B, Ferguson A, Park J, et al. (2013) Dendritic arborization and spine dynamics are abnormal in the mouse model of MECP2 duplication syndrome. *J Neurosci* 33:19518-19533.

Jiang YH, Ehlers MD (2013) Modeling autism by SHANK gene mutations in mice. *Neuron* 78:8-27.

Just MA, Cherkassky VL, Keller TA, Minshew NJ (2004) Cortical activation and synchronization during sentence comprehension in high-functioning autism: evidence of underconnectivity. *Brain* 127:1811-1821.

Juul SE, Anderson DK, Li Y, Christensen RD (1998) Erythropoietin and erythropoietin receptor in the developing human central nervous system. *Pediatric research* 43:40-49.

Kaczor P, Rakus D, Mozrzymas JW (2015) Neuron-astrocyte interaction enhance GABAergic synaptic transmission in a manner dependent on key metabolic enzymes. *Front Cell Neurosci* 9.

Kana RK, Keller TA, Cherkassky VL, Minshew NJ, Just MA (2006) Sentence comprehension in autism: thinking in pictures with decreased functional connectivity. *Brain* 129:2484-2493.

Kandel ER (2013) Principles of neural science. New York: McGraw-Hill.

Kanungo T, Mount DM, Netanyahu NS, Piatko CD, Silverman R, Wu AY (2002) An efficient k-means clustering algorithm: Analysis and implementation. *IEEE transactions on pattern analysis and machine intelligence* 24:881-892.

Kapucu FE, Mäkinen ME, Tanskanen JMA, Ylä-Outinen L, Narkilahti S, Hyttinen JAK (2016) Joint analysis of extracellular spike waveforms and neuronal network bursts. *J Neurosci Methods* 259:143-155.

Kapucu FE, Tanskanen JM, Mikkonen JE, Ylä-Outinen L, Narkilahti S, Hyttinen JA (2012) Burst analysis tool for developing neuronal networks exhibiting highly varying action potential dynamics. *Front Comput Neurosci* 6:38.

Kasparov S, Pawelzik H, Zieglgänsberger W (1994) Thyrotropin-releasing hormone enhances excitatory postsynaptic potentials in neocortical neurons of the rat in vitro. *Brain Res* 656:229-235.

Kazerounian S, Yee KO, Lawler J (2008) Thrombospondins in cancer. *Cell Mol Life Sci* 65:700-712.

Kemp PJ, Rushton DJ, Yarova PL, Schnell C, Geater C, Hancock JM, et al. (2016) Improving and accelerating the differentiation and functional maturation of human stem cell-derived neurons: role of extracellular calcium and GABA. *J Physiol* 594:6583-6594.

Kenny EM, Cormican P, Furlong S, Heron E, Kenny G, Fahey C, et al. (2014) Excess of rare novel loss-of-function variants in synaptic genes in schizophrenia and autism spectrum disorders. *Mol Psychiatry* 19:872-879.

Kim K, Doi A, Wen B, Ng K, Zhao R, Cahan P, et al. (2010) Epigenetic memory in induced pluripotent stem cells. *Nature* 467:285-290.

Kim KY, Hysolli E, Park IH (2011) Neuronal maturation defect in induced pluripotent stem cells from patients with Rett syndrome. *Proc Natl Acad Sci U S A* 108:14169-14174.

Kimm T, Khaliq ZM, Bean BP (2015) Differential Regulation of Action Potential Shape and Burst-Frequency Firing by BK and Kv2 Channels in Substantia Nigra Dopaminergic Neurons. *J Neurosci* 35:16404-16417.

Kim TG, Yao R, Monnell T, Cho JH, Vasudevan A, Koh A, *et al.* (2014) Efficient specification of interneurons from human pluripotent stem cells by dorsoventral and rostrocaudal modulation. *Stem Cells* 32:1789-1804.

Kirmse K, Hübner CA, Isbrandt D, Witte OW, Holthoff K (2017) GABAergic Transmission during Brain Development: Multiple Effects at Multiple Stages. *Neuroscientist*:1073858417701382.

Klei L, Sanders SJ, Murtha MT, Hus V, Lowe JK, Willsey AJ, *et al.* (2012) Common genetic variants, acting additively, are a major source of risk for autism. *Mol Autism* 3:9.

Kleinhans NM, Richards T, Johnson LC, Weaver KE, Greenson J, Dawson G, Aylward E (2011) fMRI evidence of neural abnormalities in the subcortical face processing system in ASD. *Neuroimage* 54:697-704.

Kodirov SA, Wehrmeister M, Colom L (2016) Nicotine-Mediated ADP to Spike Transition: Double Spiking in Septal Neurons. *J Membr Biol* 249:107-118.

Kole MH, Stuart GJ (2012) Signal processing in the axon initial segment. *Neuron* 73:235-247.

Kouser M, Speed HE, Dewey CM, Reimers JM, Widman AJ, Gupta N, *et al.* (2013) Loss of predominant Shank3 isoforms results in hippocampus-dependent impairments in behavior and synaptic transmission. *J Neurosci* 33:18448-18468.

Koussounadis A, Langdon SP, Um IH, Harrison DJ, Smith VA (2015) Relationship between differentially expressed mRNA and mRNA-protein correlations in a xenograft model system. *Sci Rep* 5.

Krencik R, Zhang SC (2011) Directed differentiation of functional astroglial subtypes from human pluripotent stem cells. *Nat Protoc* 6:1710-1717.

Krey JF, Paşca SP, Shcheglovitov A, Yazawa M, Schwemberger R, Rasmusson R, Dolmetsch RE (2013) Timothy syndrome is associated with activity-dependent dendritic retraction in rodent and human neurons. *Nat Neurosci* 16:201-209.

Kucukdereli H, Allen NJ, Lee AT, Feng A, Ozlu MI, Conatser LM, *et al.* (2011) Control of excitatory CNS synaptogenesis by astrocyte-secreted proteins Hevin and SPARC. *Proc Natl Acad Sci U S A* 108:E440-E449.

Kuki T, Fujihara K, Miwa H, Tamamaki N, Yanagawa Y, Mushiaki H (2015) Contribution of parvalbumin and somatostatin-expressing GABAergic neurons to slow oscillations and the balance in beta-gamma oscillations across cortical layers. *Front Neural Circuits* 9:6.

Kwon CH, Luikart BW, Powell CM, Zhou J, Matheny SA, Zhang W, *et al.* (2006) Pten regulates neuronal arborization and social interaction in mice. *Neuron* 50:377-388.

Kwon YW, Chung YJ, Kim J, Lee HJ, Park J, Roh TY, *et al.* (2014) Comparative study of efficacy of dopaminergic neuron differentiation between embryonic stem cell and protein-based induced pluripotent stem cell. *PLoS One* 9:e85736.

Langwieser N, Christel CJ, Kleppisch T, Hofmann F, Wotjak CT, Moosmann S (2010) Homeostatic switch in hebbian plasticity and fear learning after sustained loss of Cav1.2 calcium channels. *J Neurosci* 30:8367-8375.

de la Torre-Ubieta L, Won H, Stein JL, Geschwind DH (2016) Advancing the understanding of autism disease mechanisms through genetics. *Nat Med* 22:345-361.

Laurent LC, Ulitsky I, Slavin I, Tran H, Schork A, Morey R, *et al.* (2011) Dynamic changes in the copy number of pluripotency and cell proliferation genes in human ESCs and iPSCs during reprogramming and time in culture. *Cell Stem Cell* 8:106-118.

Lawrence YA, Kemper TL, Bauman ML, Blatt GJ (2010) Parvalbumin-, calbindin-, and calretinin-immunoreactive hippocampal interneuron density in autism. *Acta Neurol Scand* 121:99-108.

Lazarewicz MT, Ehrlichman RS, Maxwell CR, Gandal MJ, Finkel LH, Siegel SJ (2010) Ketamine modulates theta and gamma oscillations. *J Cogn Neurosci* 22:1452-1464.

Leblond CS, Nava C, Polge A, Gauthier J, Huguet G, Lumbroso S, *et al.* (2014) Meta-analysis of SHANK Mutations in Autism Spectrum Disorders: a gradient of severity in cognitive impairments. *PLoS Genet* 10:e1004580.

Lee E, Lee J, Kim E (2017) Excitation/Inhibition Imbalance in Animal Models of Autism Spectrum Disorders. *Biol Psychiatry* 81:838-847.

Lee H, Shamy GA, Elkabetz Y, Schofield CM, Harrision NL, Panagiotakos G, *et al.* (2007) Directed differentiation and transplantation of human embryonic stem cell-derived motoneurons. *Stem Cells* 25:1931-1939.

Lee J, Chung C, Ha S, Lee D, Kim DY, Kim H, Kim E (2015) Shank3-mutant mice lacking exon 9 show altered excitation/inhibition balance, enhanced rearing, and spatial memory deficit. *Front Cell Neurosci* 9:94.

Lee KY, Chung HJ (2014) NMDA receptors and L-type voltage-gated Ca²⁺ channels mediate the expression of bidirectional homeostatic intrinsic plasticity in cultured hippocampal neurons. *Neuroscience* 277:610-623.

Lee SH, Ripke S, Neale BM, Faraone SV, Purcell SM, Perlis RH, *et al.* (2013) Genetic relationship between five psychiatric disorders estimated from genome-wide SNPs. *Nat Genet* 45:984-994.

Lein ES, Hawrylycz MJ, Ao N, Ayres M, Bensinger A, Bernard A, *et al.* (2007) Genome-wide atlas of gene expression in the adult mouse brain. *Nature* 445:168-176.

Lesage F (2003) Pharmacology of neuronal background potassium channels. *Neuropharmacology* 44:1-7.

Lesage F, Terrenoire C, Romey G, Lazdunski M (2000) Human TREK2, a 2P domain mechano-sensitive K⁺ channel with multiple regulations by polyunsaturated fatty acids, lysophospholipids, and Gs, Gi, and Gq protein-coupled receptors. *J Biol Chem* 275:28398-28405.

- Letierrier C, Potier J, Caillol G, Debarnot C, Rueda Boroni F, Dargent B (2015) Nanoscale Architecture of the Axon Initial Segment Reveals an Organized and Robust Scaffold. *Cell Rep* 13:2781-2793.
- Levy D, Ronemus M, Yamrom B, Lee YH, Leotta A, Kendall J, *et al.* (2011) Rare de novo and transmitted copy-number variation in autistic spectrum disorders. *Neuron* 70:886-897.
- Lewicki MS (1998) A review of methods for spike sorting: the detection and classification of neural action potentials. *Network* 9:R53-R78.
- Lima PA, Marrion NV (2007) Mechanisms underlying activation of the slow AHP in rat hippocampal neurons. *Brain Res* 1150:74-82.
- Lim MS, Lee SY, Park CH (2015) FGF8 is Essential for Functionality of Induced Neural Precursor Cell-derived Dopaminergic Neurons. *Int J Stem Cells* 8:228-234.
- Lim S, Naisbitt S, Yoon J, Hwang JI, Suh PG, Sheng M, Kim E (1999) Characterization of the Shank family of synaptic proteins. Multiple genes, alternative splicing, and differential expression in brain and development. *J Biol Chem* 274:29510-29518.
- Lin Y, Chen C, Chen L, Zeng S, Luo Q (2005) The analysis of electrode-recording-horizon in multi-electrode array(MEA). *Conf Proc IEEE Eng Med Biol Soc* 7:7345-7348.
- Lionel AC, Vaags AK, Sato D, Gazzellone MJ, Mitchell EB, Chen HY, *et al.* (2013) Rare exonic deletions implicate the synaptic organizer Gephyrin (GPHN) in risk for autism, schizophrenia and seizures. *Hum Mol Genet* 22:2055-2066.
- Liu S, Tian Z, Yin F, Zhao Q, Fan M (2009) Generation of dopaminergic neurons from human fetal mesencephalic progenitors after co-culture with striatal-conditioned media and exposure to lowered oxygen. *Brain Res Bull* 80:62-68.
- Li W, Sun W, Zhang Y, Wei W, Ambasadhan R, Xia P, *et al.* (2011) Rapid induction and long-term self-renewal of primitive neural precursors from human embryonic stem cells by small molecule inhibitors. *Proc Natl Acad Sci U S A* 108:8299-8304.
- Li X, Krawetz R, Liu S, Meng G, Rancourt DE (2009) ROCK inhibitor improves survival of cryopreserved serum/feeder-free single human embryonic stem cells. *Hum Reprod* 24:580-589.
- Loh YH, Hartung O, Li H, Guo C, Sahalie JM, Manos PD, *et al.* (2010) Reprogramming of T cells from human peripheral blood. *Cell Stem Cell* 7:15-19.
- Lu C, Chen Q, Zhou T, Bozic D, Fu Z, Pan JQ, Feng G (2016a) Micro-electrode array recordings reveal reductions in both excitation and inhibition in cultured cortical neuron networks lacking Shank3. *Mol Psychiatry* 21:159-168.
- Lu J, Zhong X, Liu H, Hao L, Huang CT, Sherafat MA, *et al.* (2016b) Generation of serotonin neurons from human pluripotent stem cells. *Nat Biotechnol* 34:89-94.
- Luo M, Ling T, Xie W, Sun H, Zhou Y, Zhu Q, *et al.* (2013) NuRD blocks reprogramming of mouse somatic cells into pluripotent stem cells. *Stem Cells* 31:1278-1286.
- Lykissas MG, Korompilias AV, Vekris MD, Mitsionis GI, Sakellariou E, Beris AE (2007) The role of erythropoietin in central and peripheral nerve injury. *Clin Neurol Neurosurg* 109:639-644.
- MacLean JE, Teshima IE, Szatmari P, Nowaczyk MJ (2000) Ring chromosome 22 and autism: report and review. *Am J Med Genet* 90:382-385.
- Maeda E, Robinson HP, Kawana A (1995) The mechanisms of generation and propagation of synchronized bursting in developing networks of cortical neurons. *J Neurosci* 15:6834-6845.
- Malenka RC, Bear MF (2004) LTP and LTD: an embarrassment of riches. *Neuron* 44:5-21.
- Malow BA, Byars K, Johnson K, Weiss S, Bernal P, Goldman SE, *et al.* (2012) A practice pathway for the identification, evaluation, and management of insomnia in children and adolescents with autism spectrum disorders. *Pediatrics* 130 Suppl 2:S106-S124.
- Mann EO, Mody I (2010) Control of hippocampal gamma oscillation frequency by tonic inhibition and excitation of interneurons. *Nat Neurosci* 13:205-212.
- Mann EO, Paulsen O (2007) Role of GABAergic inhibition in hippocampal network oscillations. *Trends Neurosci* 30:343-349.
- Marchetto MC, Carromeu C, Acab A, Yu D, Yeo GW, Mu Y, *et al.* (2010) A model for neural development and treatment of Rett syndrome using human induced pluripotent stem cells. *Cell* 143:527-539.
- Mariani J, Coppola G, Zhang P, Abyzov A, Provini L, Tomasini L, *et al.* (2015) FOXP1-Dependent Dysregulation of GABA/Glutamate Neuron Differentiation in Autism Spectrum Disorders. *Cell* 162:375-390.
- Maroof AM, Keros S, Tyson JA, Ying SW, Ganat YM, Merkle FT, *et al.* (2013) Directed differentiation and functional maturation of cortical interneurons from human embryonic stem cells. *Cell Stem Cell* 12:559-572.
- Marowsky A, Vogt KE (2014) Delta-subunit-containing GABAA-receptors mediate tonic inhibition in paracapsular cells of the mouse amygdala. *Front Neural Circuits* 8:27.
- Martina M, Jonas P (1997) Functional differences in Na⁺ channel gating between fast-spiking interneurons and principal neurons of rat hippocampus. *J Physiol* 505 (Pt 3):593-603.
- Massagué J, Seoane J, Wotton D (2005) Smad transcription factors. *Genes & development* 19:2783-2810.
- McKinney BC, Sze W, White JA, Murphy GG (2008) L-type voltage-gated calcium channels in conditioned fear: a genetic and pharmacological analysis. *Learn Mem* 15:326-334.
- McPartland J, Klin A (2006) Asperger's syndrome. *Adolesc Med Clin* 17:771-88; abstract xiii.
- Mechaly I, Scamps F, Chabbert C, Sans A, Valmier J (2005) Molecular diversity of voltage-gated sodium channel alpha subunits expressed in neuronal and non-neuronal excitable cells. *Neuroscience* 130:389-396.

Medhurst AD, Rennie G, Chapman CG, Meadows H, Duckworth MD, Kellsell RE, *et al.* (2001) Distribution analysis of human two pore domain potassium channels in tissues of the central nervous system and periphery. *Brain Res Mol Brain Res* 86:101-114.

Mei Y, Monteiro P, Zhou Y, Kim JA, Gao X, Fu Z, Feng G (2016) Adult restoration of Shank3 expression rescues selective autistic-like phenotypes. *Nature* 530:481-484.

Miller JA, Ding S-L, Sunkin SM, Smith KA, Ng L, Szafer A, *et al.* (2014) Transcriptional landscape of the prenatal human brain. *Nature* 508:199-206.

Mishra A (2017) Binaural blood flow control by astrocytes: listening to synapses and the vasculature. *J Physiol* 595:1885-1902.

Moessner R, Marshall CR, Sutcliffe JS, Skaug J, Pinto D, Vincent J, *et al.* (2007) Contribution of SHANK3 mutations to autism spectrum disorder. *Am J Hum Genet* 81:1289-1297.

Mohajerani MH, Sivakumaran S, Zacchi P, Aguilera P, Cherubini E (2007) Correlated network activity enhances synaptic efficacy via BDNF and the ERK pathway at immature CA3 CA1 connections in the hippocampus. *Proc Natl Acad Sci U S A* 104:13176-13181.

Mok SY, Nadasdy Z, Lim YM, Goh SY (2012) Ultra-slow oscillations in cortical networks in vitro. *Neuroscience* 206:17-24.

Molina LA, Skelin I, Gruber AJ (2014) Acute NMDA receptor antagonism disrupts synchronization of action potential firing in rat prefrontal cortex. *PLoS One* 9:e85842.

Molosh AI, Johnson PL, Spence JP, Arendt D, Federici LM, Bernabe C, *et al.* (2014) Social learning and amygdala disruptions in Nf1 mice are rescued by blocking p21-activated kinase. *Nat Neurosci* 17:1583-1590.

Monyer H, Burnashev N, Laurie DJ, Sakmann B, Seeburg PH (1994) Developmental and regional expression in the rat brain and functional properties of four NMDA receptors. *Neuron* 12:529-540.

Moosmang S, Haider N, Klugbauer N, Adelsberger H, Langwieser N, Müller J, *et al.* (2005) Role of hippocampal Cav1. 2 Ca2+ channels in NMDA receptor-independent synaptic plasticity and spatial memory. *Journal of Neuroscience* 25:9883-9892.

Morishita E, Masuda S, Nagao M, Yasuda Y, Sasaki R (1997) Erythropoietin receptor is expressed in rat hippocampal and cerebral cortical neurons, and erythropoietin prevents in vitro glutamate-induced neuronal death. *Neuroscience* 76:105-116.

Mummery C, Ward-van Oostwaard D, Doevendans P, Spijker R, van den Brink S, Hassink R, *et al.* (2003) Differentiation of human embryonic stem cells to cardiomyocytes: role of coculture with visceral endoderm-like cells. *Circulation* 107:2733-2740.

Mundy P (2003) Annotation: the neural basis of social impairments in autism: the role of the dorsal medial-frontal cortex and anterior cingulate system. *J Child Psychol Psychiatry* 44:793-809.

Muratore CR, Srikanth P, Callahan DG, Young-Pearse TL (2014) Comparison and Optimization of hiPSC Forebrain Cortical Differentiation Protocols. *PLoS One* 9:e105807.

Naisbitt S, Kim E, Tu JC, Xiao B, Sala C, Valtschanoff J, *et al.* (1999) Shank, a novel family of postsynaptic density proteins that binds to the NMDA receptor/PSD-95/GKAP complex and cortactin. *Neuron* 23:569-582.

Neale BM, Kou Y, Liu L, Ma'ayan A, Samocha KE, Sabo A, *et al.* (2012) Patterns and rates of exonic de novo mutations in autism spectrum disorders. *Nature* 485:242-245.

Newman EA (2015) Glial cell regulation of neuronal activity and blood flow in the retina by release of gliotransmitters. *Philos Trans R Soc Lond B Biol Sci* 370.

Nicholas CR, Chen J, Tang Y, Southwell DG, Chalmers N, Vogt D, *et al.* (2013) Functional maturation of hPSC-derived forebrain interneurons requires an extended timeline and mimics human neural development. *Cell Stem Cell* 12:573-586.

Nolan MF, Malleret G, Dudman JT, Buhl DL, Santoro B, Gibbs E, *et al.* (2004) A behavioral role for dendritic integration: HCN1 channels constrain spatial memory and plasticity at inputs to distal dendrites of CA1 pyramidal neurons. *Cell* 119:719-732.

Nowak L, Bregestovski P, Ascher P, Herbet A, Prochiantz A (1984) Magnesium gates glutamate-activated channels in mouse central neurones. *Nature* 307:462-465.

Nowak LG, Azouz R, Sanchez-Vives MV, Gray CM, McCormick DA (2003) Electrophysiological classes of cat primary visual cortical neurons in vivo as revealed by quantitative analyses. *J Neurophysiol* 89:1541-1566.

Odawara A, Katoh H, Matsuda N, Suzuki I (2016) Physiological maturation and drug responses of human induced pluripotent stem cell-derived cortical neuronal networks in long-term culture. *Sci Rep* 6:26181.

Odawara A, Saitoh Y, Alhebshi AH, Gotoh M, Suzuki I (2014) Long-term electrophysiological activity and pharmacological response of a human induced pluripotent stem cell-derived neuron and astrocyte co-culture. *Biochem Biophys Res Commun* 443:1176-1181.

Okamoto N, Kubota T, Nakamura Y, Murakami R, Nishikubo T, Tanaka I, *et al.* (2007) 22q13 Microduplication in two patients with common clinical manifestations: a recognizable syndrome? *Am J Med Genet A* 143A:2804-2809.

Okita K, Ichisaka T, Yamanaka S (2007) Generation of germline-competent induced pluripotent stem cells. *Nature* 448:313.

Okita K, Nakagawa M, Hyenjong H, Ichisaka T, Yamanaka S (2008) Generation of mouse induced pluripotent stem cells without viral vectors. *Science* 322:949-953.

Oram Cardy JE, Flagg EJ, Roberts W, Roberts TP (2005) Delayed mismatch field for speech and non-speech sounds in children with autism. *Neuroreport* 16:521-525.

Orive G, Hernández RM, Gascón AR, Igartua M, Pedraz JL (2003) Controversies over stem cell research. *TRENDS in Biotechnology* 21:109-112.

O'Roak BJ, Vives L, Fu W, Egerton JD, Stanaway IB, Phelps IG, *et al.* (2012) Multiplex targeted sequencing identifies recurrently mutated genes in autism spectrum disorders. *Science* 338:1619-1622.

Pan Y, Chen J, Guo H, Ou J, Peng Y, Liu Q, *et al.* (2015) Association of genetic variants of GRIN2B with autism. *Sci Rep* 5:8296.

Paşca SP, Portmann T, Voineagu I, Yazawa M, Shcheglovitov A, Paşca AM, *et al.* (2011) Using iPSC-derived neurons to uncover cellular phenotypes associated with Timothy syndrome. *Nat Med* 17:1657-1662.

Patel AJ, Honoré E (2001) Properties and modulation of mammalian 2P domain K⁺ channels. *Trends Neurosci* 24:339-346.

Patel TP, Man K, Firestein BL, Meaney DF (2015) Automated quantification of neuronal networks and single-cell calcium dynamics using calcium imaging. *J Neurosci Methods* 243:26-38.

Pavlov I, Savtchenko LP, Song I, Koo J, Pimashkin A, Rusakov DA, Semyanov A (2014) Tonic GABAA conductance bidirectionally controls interneuron firing pattern and synchronization in the CA3 hippocampal network. *Proc Natl Acad Sci U S A* 111:504-509.

Peça J, Feliciano C, Ting JT, Wang W, Wells MF, Venkatraman TN, *et al.* (2011) Shank3 mutant mice display autistic-like behaviours and striatal dysfunction. *Nature* 472:437-442.

Pellerin L, Bouzier-Sore AK, Aubert A, Serres S, Merle M, Costalat R, Magistretti PJ (2007) Activity-dependent regulation of energy metabolism by astrocytes: an update. *Glia* 55:1251-1262.

Peñagarikano O, Abrahams BS, Herman EI, Winden KD, Gdalyahu A, Dong H, *et al.* (2011) Absence of CNTNAP2 leads to epilepsy, neuronal migration abnormalities, and core autism-related deficits. *Cell* 147:235-246.

Pfisterer U, Kirkeby A, Torper O, Wood J, Nelander J, Dufour A, *et al.* (2011) Direct conversion of human fibroblasts to dopaminergic neurons. *Proceedings of the National Academy of Sciences* 108:10343-10348.

Phelan K, Boccutto L, Rogers RC, Sarasua SM, McDermid HE (2015) Letter to the editor regarding Disciglio *et al.*: Interstitial 22q13 deletions not involving SHANK3 gene: A new contiguous gene syndrome. *American Journal of Medical Genetics Part A* 167:1679-1680.

Phelan K, McDermid HE (2012) The 22q13.3 Deletion Syndrome (Phelan-McDermid Syndrome). *Mol Syndromol* 2:186-201.

Phelan MC, Rogers RC, Saul RA, Stapleton GA, Sweet K, McDermid H, *et al.* (2001) 22q13 deletion syndrome. *Am J Med Genet* 101:91-99.

Pickard L, Noël J, Henley JM, Collingridge GL, Molnar E (2000) Developmental changes in synaptic AMPA and NMDA receptor distribution and AMPA receptor subunit composition in living hippocampal neurons. *J Neurosci* 20:7922-7931.

Piton A, Jouan L, Rochefort D, Dobrzyniecka S, Lachapelle K, Dion PA, *et al.* (2013) Analysis of the effects of rare variants on splicing identifies alterations in GABAA receptor genes in autism spectrum disorder individuals. *Eur J Hum Genet* 21:749-756.

Platkiewicz J, Brette R (2010) A threshold equation for action potential initiation. *PLoS Comput Biol* 6:e1000850.

Polo JM, Liu S, Figueroa ME, Kulalert W, Eminli S, Tan KY, *et al.* (2010) Cell type of origin influences the molecular and functional properties of mouse induced pluripotent stem cells. *Nat Biotechnol* 28:848-855.

Postea O, Biel M (2011) Exploring HCN channels as novel drug targets. *Nat Rev Drug Discov* 10:903-914.

Prè D, Nestor MW, Sproul AA, Jacob S, Koppensteiner P, Chinchalongporn V, *et al.* (2014) A time course analysis of the electrophysiological properties of neurons differentiated from human induced pluripotent stem cells (iPSCs). *PLoS One* 9:e103418.

Przewlocki R, Parsons KL, Sweeney DD, Trotter C, Netzeband JG, Siggins GR, Gruol DL (1999) Opioid enhancement of calcium oscillations and burst events involving NMDA receptors and L-type calcium channels in cultured hippocampal neurons. *J Neurosci* 19:9705-9715.

Quian Quiroga R (2009) What is the real shape of extracellular spikes? *J Neurosci Methods* 177:194-198.

Quian Quiroga R, Nadasdy Z, Ben-Shaul Y (2004) Unsupervised Spike Detection and Sorting with Wavelets and Superparamagnetic Clustering. *Neural Comput* 16:1661-1687.

Raichman N, Ben-Jacob E (2008) Identifying repeating motifs in the activation of synchronized bursts in cultured neuronal networks. *J Neurosci Methods* 170:96-110.

Rakic P (2009) Evolution of the neocortex: a perspective from developmental biology. *Nat Rev Neurosci* 10:724-735.

Rambhatla L, Chiu C-P, Kundu P, Peng Y, Carpenter MK (2003) Generation of hepatocyte-like cells from human embryonic stem cells. *Cell transplantation* 12:1-11.

Rasband MN (2010) The axon initial segment and the maintenance of neuronal polarity. *Nature Reviews Neuroscience* 11:552-562.

Raymond GV, Bauman ML, Kemper TL (1996) Hippocampus in autism: a Golgi analysis. *Acta Neuropathol* 91:117-119.

RDevelopment C (2012) TEAM 2009: R: A language and environment for statistical computing. *Vienna, Austria. Internet: <http://www.R-project.org>*.

Rebsam A, Seif I, Gaspar P (2002) Refinement of thalamocortical arbors and emergence of barrel domains in the primary somatosensory cortex: a study of normal and monoamine oxidase a knock-out mice. *J Neurosci* 22:8541-8552.

Regehr WG, Pine J, Cohan CS, Mischke MD, Tank DW (1989) Sealing cultured invertebrate neurons to embedded dish electrodes facilitates long-term stimulation and recording. *J Neurosci Methods* 30:91-106.

Reiersen AM, Todd RD (2008) Co-occurrence of ADHD and autism spectrum disorders: phenomenology and treatment. *Expert Rev Neurother* 8:657-669.

Ren J, Guo W (2012) ERK1/2 regulate exocytosis through direct phosphorylation of the exocyst component Exo70. *Dev Cell* 22:967-978.

Richards M, Tan S, Fong CY, Biswas A, Chan WK, Bongso A (2003) Comparative evaluation of various human feeders for prolonged undifferentiated growth of human embryonic stem cells. *Stem Cells* 21:546-556.

Risher WC, Eroglu C (2012) Thrombospondins as key regulators of synaptogenesis in the central nervous system. *Matrix Biol* 31:170-177.

Rivera C, Voipio J, Payne JA, Ruusuvuori E (1999) The K⁺/Cl⁻-co-transporter KCC2 renders GABA hyperpolarizing during neuronal maturation. *Nature* 397:251.

Robinson EB, Lichtenstein P, Anckarsäter H, Happé F, Ronald A (2013) Examining and interpreting the female protective effect against autistic behavior. *Proc Natl Acad Sci U S A* 110:5258-5262.

Robinson JT, Jorgolli M, Shalek AK, Yoon MH, Gertner RS, Park H (2012) Vertical nanowire electrode arrays as a scalable platform for intracellular interfacing to neuronal circuits. *Nat Nanotechnol* 7:180-184.

Rodríguez JI, Kern JK (2011) Evidence of microglial activation in autism and its possible role in brain underconnectivity. *Neuron Glia Biol* 7:205-213.

Rodríguez-Molina V, Patiño J, Vargas Y, Sánchez-Jaramillo E, Joseph-Bravo P, Charli JL (2014) TRH regulates action potential shape in cerebral cortex pyramidal neurons. *Brain Res* 1571:1-11.

Ronald A, Hoekstra RA (2011) Autism spectrum disorders and autistic traits: a decade of new twin studies. *Am J Med Genet B Neuropsychiatr Genet* 156B:255-274.

Roybon L, Lamas NJ, Garcia-Diaz A, Yang EJ, Sattler R, Jackson-Lewis V, et al. (2013) Human stem cell-derived spinal cord astrocytes with defined mature or reactive phenotypes. *Cell Rep* 4:1035-1048.

R R, Lepistö T, Shestakova A, Vanhala R, Alku P, Nääätänen R, Yaguchi K (2003) Speech--sound-selective auditory impairment in children with autism: they can perceive but do not attend. *Proceedings of the National Academy of Sciences* 100:5567-5572.

De Rubeis S, He X, Goldberg AP, Poultney CS, Samocha K, Cicek AE, et al. (2014a) Synaptic, transcriptional and chromatin genes disrupted in autism. *Nature* 515:209-215.

De Rubeis S, He X, Goldberg AP, Poultney CS, Samocha K, Ercument Cicek A, et al. (2014b) Synaptic, transcriptional and chromatin genes disrupted in autism. *Nature* 515:209-215.

Rudy B, McBain CJ (2001) Kv3 channels: voltage-gated K⁺ channels designed for high-frequency repetitive firing. *Trends Neurosci* 24:517-526.

Rushton DJ, Mattis VB, Svendsen CN, Allen ND, Kemp PJ (2013) Stimulation of GABA-induced Ca²⁺ influx enhances maturation of human induced pluripotent stem cell-derived neurons. *PLoS One* 8:e81031.

Rusu SI, Borst JG (2011) Developmental changes in intrinsic excitability of principal neurons in the rat medial nucleus of the trapezoid body. *Dev Neurobiol* 71:284-295.

Sadakata T, Furuichi T (2009) Developmentally regulated Ca²⁺-dependent activator protein for secretion 2 (CAPS2) is involved in BDNF secretion and is associated with autism susceptibility. *Cerebellum* 8:312-322.

Sanchez-Vives MV, McCormick DA (2000) Cellular and network mechanisms of rhythmic recurrent activity in neocortex. *Nat Neurosci* 3:1027-1034.

Sanders SJ, Murtha MT, Gupta AR, Murdoch JD, Raubeson MJ, Willsey AJ, et al. (2012) De novo mutations revealed by whole-exome sequencing are strongly associated with autism. *Nature* 485:237-241.

Sandin S, Lichtenstein P, Kuja-Halkola R, Larsson H, Hultman CM, Reichenberg A (2014) The familial risk of autism. *JAMA* 311:1770-1777.

Sans N, Petralia RS, Wang YX, Blahos J, Hell JW, Wenthold RJ (2000) A developmental change in NMDA receptor-associated proteins at hippocampal synapses. *J Neurosci* 20:1260-1271.

Santilli G, Lamorte G, Carlessi L, Ferrari D, Rota Nodari L, Binda E, et al. (2010) Mild hypoxia enhances proliferation and multipotency of human neural stem cells. *PLoS One* 5:e8575.

Schierberl K, Hao J, Tropea TF, Ra S, Giordano TP, Xu Q, et al. (2011) Cav1.2 L-type Ca²⁺ channels mediate cocaine-induced GluA1 trafficking in the nucleus accumbens, a long-term adaptation dependent on ventral tegmental area Ca(v)1.3 channels. *J Neurosci* 31:13562-13575.

Schindelin J, Arganda-Carreras I, Frise E, Kaynig V, Longair M, Pietzsch T, et al. (2012) Fiji: an open-source platform for biological-image analysis. *Nat Methods* 9:676-682.

Schizophrenia Working Group of the Psychiatric Genomics Consortium (2014) Biological insights from 108 schizophrenia-associated genetic loci. *Nature* 511:421-427.

Schlick B, Flucher BE, Obermair GJ (2010) Voltage-activated calcium channel expression profiles in mouse brain and cultured hippocampal neurons. *Neuroscience* 167:786-798.

Schmeisser MJ, Ey E, Wegener S, Bockmann J, Stempel AV, Kuebler A, et al. (2012) Autistic-like behaviours and hyperactivity in mice lacking ProSAP1/Shank2. *Nature* 486:256-260.

Schmitz N, Rubia K, Daly E, Smith A, Williams S, Murphy DG (2006) Neural correlates of executive function in autistic spectrum disorders. *Biol Psychiatry* 59:7-16.

Schmunk G, Nguyen RL, Ferguson DL, Kumar K, Parker I, Gargus JJ (2017) High-throughput screen detects calcium signaling dysfunction in typical sporadic autism spectrum disorder. *Sci Rep* 7:40740.

Schubert E, Sander J, Ester M, Kriegel HP, Xu X (2017) DBSCAN Revisited, Revisited: Why and How You Should (Still) Use DBSCAN. *ACM Transactions on Database Systems (TODS)* 42:19.

Schumann CM, Amaral DG (2006) Stereological analysis of amygdala neuron number in autism. *J Neurosci* 26:7674-7679.

- Sebat J, Lakshmi B, Malhotra D, Troge J, Lese-Martin C, Walsh T, *et al.* (2007) Strong association of de novo copy number mutations with autism. *Science* 316:445-449.
- Sedmak G, Jovanov-Milošević N, Puskarjov M, Ulamec M, Krušlin B, Kaila K, Judaš M (2015) Developmental Expression Patterns of KCC2 and Functionally Associated Molecules in the Human Brain. *Cereb Cortex*.
- de Sena Cortabitarte A, Degenhardt F, Strohmaier J, Lang M, Weiss B, Roeth R, *et al.* (2017) Investigation of SHANK3 in schizophrenia. *Am J Med Genet B Neuropsychiatr Genet* 174:390-398.
- Serio A, Bilican B, Barmada SJ, Ando DM, Zhao C, Siller R, *et al.* (2013) Astrocyte pathology and the absence of non-cell autonomy in an induced pluripotent stem cell model of TDP-43 proteinopathy. *Proceedings of the National Academy of Sciences* 110:4697-4702.
- Shah M, Haylett DG (2000) Ca(2+) channels involved in the generation of the slow afterhyperpolarization in cultured rat hippocampal pyramidal neurons. *J Neurophysiol* 83:2554-2561.
- Shaltouki A, Peng J, Liu Q, Rao MS, Zeng X (2013) Efficient generation of astrocytes from human pluripotent stem cells in defined conditions. *Stem Cells* 31:941-952.
- Shcheglovitov A, Shcheglovitova O, Yazawa M, Portmann T, Shu R, Sebastiano V, *et al.* (2013) SHANK3 and IGF1 restore synaptic deficits in neurons from 22q13 deletion syndrome patients. *Nature* 503:267-271.
- Sheridan SD, Theriault KM, Reis SA, Zhou F, Madison JM, Daheron L, *et al.* (2011) Epigenetic characterization of the FMR1 gene and aberrant neurodevelopment in human induced pluripotent stem cell models of fragile X syndrome. *PLoS One* 6:e26203.
- Shi Y, Kirwan P, Livesey FJ (2012a) Directed differentiation of human pluripotent stem cells to cerebral cortex neurons and neural networks. *Nat Protoc* 7:1836-1846.
- Shi Y, Kirwan P, Smith J, Robinson HP, Livesey FJ (2012b) Human cerebral cortex development from pluripotent stem cells to functional excitatory synapses. *Nat Neurosci* 15:477-86, S1.
- Silver I, Erecińska M (1998) Oxygen and ion concentrations in normoxic and hypoxic brain cells. *Adv Exp Med Biol* 454:7-16.
- Simms ML, Kemper TL, Timbie CM, Bauman ML, Blatt GJ (2009) The anterior cingulate cortex in autism: heterogeneity of qualitative and quantitative cytoarchitectonic features suggests possible subgroups. *Acta Neuropathol* 118:673-684.
- Sirén AL, Fratelli M, Brines M, Goemans C, Casagrande S, Lewczuk P, *et al.* (2001) Erythropoietin prevents neuronal apoptosis after cerebral ischemia and metabolic stress. *Proc Natl Acad Sci U S A* 98:4044-4049.
- Smith SE, Zhou YD, Zhang G, Jin Z, Stoppel DC, Anderson MP (2011) Increased gene dosage of Ube3a results in autism traits and decreased glutamate synaptic transmission in mice. *Sci Transl Med* 3:103ra97.
- Solso S, Xu R, Proudfoot J, Hagler DJ, Campbell K, Venkatraman V, *et al.* (2016) Diffusion Tensor Imaging Provides Evidence of Possible Axonal Overconnectivity in Frontal Lobes in Autism Spectrum Disorder Toddlers. *Biol Psychiatry* 79:676-684.
- Sottile V, Thomson A, McWhir J (2003) In vitro osteogenic differentiation of human ES cells. *Cloning & Stem Cells* 5:149-155.
- South M, Ozonoff S, McMahon WM (2007) The relationship between executive functioning, central coherence, and repetitive behaviors in the high-functioning autism spectrum. *Autism* 11:437-451.
- Spira ME, Hai A (2013) Multi-electrode array technologies for neuroscience and cardiology. *Nat Nanotechnol* 8:83-94.
- Splawski I, Timothy KW, Sharpe LM, Decher N, Kumar P, Bloise R, *et al.* (2004) Ca(V)1.2 calcium channel dysfunction causes a multisystem disorder including arrhythmia and autism. *Cell* 119:19-31.
- Stacpoole SRL, Bilican B, Webber DJ, Luzhynskaya A, He XL, Compston A, *et al.* (2011) Derivation of neural precursor cells from human ES cells at 3% O₂ is efficient, enhances survival and presents no barrier to regional specification and functional differentiation. *Cell death and differentiation* 18:1016.
- Stadtfeld M, Nagaya M, Utikal J, Weir G, Hochedlinger K (2008) Induced pluripotent stem cells generated without viral integration. *Science* 322:945-949.
- Staerk J, Dawlaty MM, Gao Q, Maetzel D, Hanna J, Sommer CA, *et al.* (2010) Reprogramming of human peripheral blood cells to induced pluripotent stem cells. *Cell Stem Cell* 7:20-24.
- Stella N, Tencé M, Glowinski J, Prémont J (1994) Glutamate-evoked release of arachidonic acid from mouse brain astrocytes. *J Neurosci* 14:568-575.
- Straub H, Köhling R, Frieler A, Grigat M, Speckmann EJ (2000) Contribution of L-type calcium channels to epileptiform activity in hippocampal and neocortical slices of guinea-pigs. *Neuroscience* 95:63-72.
- Studer L, Csete M, Lee SH, Kabani N, Walikonis J, Wold B, McKay R (2000) Enhanced proliferation, survival, and dopaminergic differentiation of CNS precursors in lowered oxygen. *J Neurosci* 20:7377-7383.
- Subramanian J, Morozov A (2011) Erk1/2 inhibit synaptic vesicle exocytosis through L-type calcium channels. *J Neurosci* 31:4755-4764.
- Sun JJ, Kilb W, Luhmann HJ (2010) Self-organization of repetitive spike patterns in developing neuronal networks in vitro. *Eur J Neurosci* 32:1289-1299.
- Szatmari P, Paterson AD, Zwaigenbaum L, Roberts W, Brian J, Liu XQ, *et al.* (2007) Mapping autism risk loci using genetic linkage and chromosomal rearrangements. *Nat Genet* 39:319-328.
- Takada N, Pi HJ, Sousa VH, Waters J, Fishell G, Kepecs A, Osten P (2014) A developmental cell-type switch in cortical interneurons leads to a selective defect in cortical oscillations. *Nat Commun* 5:5333.
- Takahashi K, Tanabe K, Ohnuki M, Narita M, Ichisaka T, Tomoda K, Yamanaka S (2007) Induction of pluripotent stem cells from adult human fibroblasts by defined factors. *Cell* 131:861-872.

Takahashi K, Yamanaka S (2006) Induction of pluripotent stem cells from mouse embryonic and adult fibroblast cultures by defined factors. *Cell* 126:663-676.

Takekawa T, Isomura Y, Fukui T (2010) Accurate spike sorting for multi-unit recordings. *Eur J Neurosci* 31:263-272.

Tang X, Kim J, Zhou L, Wengert E, Zhang L, Wu Z, *et al.* (2016) KCC2 rescues functional deficits in human neurons derived from patients with Rett syndrome. *Proc Natl Acad Sci U S A* 113:751-756.

Telezhkin V, Schnell C, Yarova P, Yung S, Cope E, Hughes A, *et al.* (2016) Forced cell cycle exit and modulation of GABAA, CREB, and GSK3 β signaling promote functional maturation of induced pluripotent stem cell-derived neurons. *Am J Physiol Cell Physiol* 310:C520-C541.

Tetreault NA, Hakeem AY, Jiang S, Williams BA, Allman E, Wold BJ, Allman JM (2012) Microglia in the cerebral cortex in autism. *Journal of autism and developmental disorders* 42:2569-2584.

Thomas CA, Springer PA, Loeb GE, Berwald-Netter Y, Okun LM (1972) A miniature microelectrode array to monitor the bioelectric activity of cultured cells. *Exp Cell Res* 74:61-66.

Thomson JA, Itskovitz-Eldor J, Shapiro SS, Waknitz MA, Swiergiel JJ, Marshall VS, Jones JM (1998) Embryonic stem cell lines derived from human blastocysts. *Science* 282:1145-1147.

Tian C, Ambroz RJ, Sun L, Wang Y, Ma K, Chen Q, *et al.* (2012) Direct conversion of dermal fibroblasts into neural progenitor cells by a novel cocktail of defined factors. *Curr Mol Med* 12:126-137.

Tippens AL, Pare J-F, Langwieser N, Moosmang S, Milner TA, Smith Y, Lee A (2008) Ultrastructural evidence for pre- and postsynaptic localization of Cav1.2 L-type Ca $^{2+}$ channels in the rat hippocampus. *Journal of Comparative Neurology* 506:569-583.

Tremblay R, Lee S, Rudy B (2016) GABAergic Interneurons in the Neocortex: From Cellular Properties to Circuits. *Neuron* 91:260-292.

Tsai PT, Hull C, Chu Y, Greene-Colozzi E, Sadowski AR, Leech JM, *et al.* (2012) Autistic-like behaviour and cerebellar dysfunction in Purkinje cell Tsc1 mutant mice. *Nature* 488:647-651.

Tuchman R, Rapin I (2002) Epilepsy in autism. *The Lancet Neurology* 1:352-358.

Tu JC, Xiao B, Naisbitt S, Yuan JP, Petralia RS, Brakeman P, *et al.* (1999) Coupling of mGluR/Homer and PSD-95 complexes by the Shank family of postsynaptic density proteins. *Neuron* 23:583-592.

Tyzio R, Ivanov A, Bernard C, Holmes GL, Ben-Ari Y, Khazipov R (2003) Membrane potential of CA3 hippocampal pyramidal cells during postnatal development. *J Neurophysiol* 90:2964-2972.

Uchino S, Wada H, Honda S, Nakamura Y, Ondo Y, Uchiyama T, *et al.* (2006) Direct interaction of post-synaptic density-95/Dlg/ZO-1 domain-containing synaptic molecule Shank3 with GluR1 α -amino-3-hydroxy-5-methyl-4-isoxazole propionic acid receptor. *J Neurochem* 97:1203-1214.

Uhlén M, Fagerberg L, Hallström BM, Lindskog C, Oksvold P, Mardinoglu A, *et al.* (2015) Proteomics. Tissue-based map of the human proteome. *Science* 347:1260419.

Ullian EM, Christopherson KS, Barres BA (2004) Role for glia in synaptogenesis. *Glia* 47:209-216.

Vaags AK, Lionel AC, Sato D, Goodenberger M, Stein QP, Curran S, *et al.* (2012) Rare deletions at the neurexin 3 locus in autism spectrum disorder. *Am J Hum Genet* 90:133-141.

van de Leemput J, Boles NC, Kiehl TR, Corneo B, Lederman P, Menon V, *et al.* (2014) CORTECON: a temporal transcriptome analysis of in vitro human cerebral cortex development from human embryonic stem cells. *Neuron* 83:51-68.

van Kooten IA, Palmen SJ, von Cappeln P, Steinbusch HW, Korr H, Heinsen H, *et al.* (2008) Neurons in the fusiform gyrus are fewer and smaller in autism. *Brain* 131:987-999.

Vargas-Caballero M, Robinson HP (2004) Fast and slow voltage-dependent dynamics of magnesium block in the NMDA receptor: the asymmetric trapping block model. *J Neurosci* 24:6171-6180.

Vargas DL, Nascimbene C, Krishnan C, Zimmerman AW, Pardo CA (2005) Neuroglial activation and neuroinflammation in the brain of patients with autism. *Ann Neurol* 57:67-81.

Vato A, Bonzano L, Chiappalone M, Cicero S, Morabito F, Novellino A, Stillo G (2004) Spike manager: a new tool for spontaneous and evoked neuronal networks activity characterization. *Neurocomputing* 58:1153-1161.

Vicidomini C, Ponzoni L, Lim D, Schmeisser MJ, Reim D, Morello N, *et al.* (2017) Pharmacological enhancement of mGlu5 receptors rescues behavioral deficits in SHANK3 knock-out mice. *Mol Psychiatry* 22:784.

Vorstman JAS, Parr JR, Moreno-De-Luca D, Anney RJL, Nurnberger JI, Hallmayer JF (2017) Autism genetics: opportunities and challenges for clinical translation. *Nat Rev Genet* 18:362-376.

Waga C, Okamoto N, Ondo Y, Fukumura-Kato R, Goto Y, Kohsaka S, Uchino S (2011) Novel variants of the SHANK3 gene in Japanese autistic patients with severe delayed speech development. *Psychiatr Genet* 21:208-211.

Wagenaar DA, Pine J, Potter SM (2006) An extremely rich repertoire of bursting patterns during the development of cortical cultures. *BMC Neurosci* 7:11.

Wang C, Shimizu-Okabe C, Watanabe K, Okabe A, Matsuzaki H, Ogawa T, *et al.* (2002) Developmental changes in KCC1, KCC2, and NKCC1 mRNA expressions in the rat brain. *Brain Res Dev Brain Res* 139:59-66.

Wang D, Grillner S, Wallén P (2013) Calcium dynamics during NMDA-induced membrane potential oscillations in lamprey spinal neurons--contribution of L-type calcium channels (CaV1.3). *J Physiol* 591:2509-2521.

Wang L, Meece K, Williams DJ, Lo KA, Zimmer M, Heinrich G, *et al.* (2015) Differentiation of hypothalamic-like neurons from human pluripotent stem cells. *J Clin Invest* 125:796-808.

- Wang X, Bey AL, Katz BM, Badea A, Kim N, David LK, *et al.* (2016) Altered mGluR5-Homer scaffolds and corticostriatal connectivity in a Shank3 complete knockout model of autism. *Nat Commun* 7:11459.
- Wang X, McCoy PA, Rodriguiz RM, Pan Y, Je HS, Roberts AC, *et al.* (2011) Synaptic dysfunction and abnormal behaviors in mice lacking major isoforms of Shank3. *Hum Mol Genet* 20:3093-3108.
- Wang X, Xu Q, Bey AL, Lee Y, Jiang YH (2014) Transcriptional and functional complexity of Shank3 provides a molecular framework to understand the phenotypic heterogeneity of SHANK3 causing autism and Shank3 mutant mice. *Mol Autism* 5:30.
- Watanabe K, Kamiya D, Nishiyama A, Katayama T, Nozaki S, Kawasaki H, *et al.* (2005) Directed differentiation of telencephalic precursors from embryonic stem cells. *Nat Neurosci* 8:288-296.
- Watanabe K, Ueno M, Kamiya D, Nishiyama A, Matsumura M, Wataya T, *et al.* (2007) A ROCK inhibitor permits survival of dissociated human embryonic stem cells. *Nat Biotechnol* 25:681-686.
- Wegiel J, Kuchna I, Nowicki K, Imaki H, Wegiel J, Marchi E, *et al.* (2010) The neuropathology of autism: defects of neurogenesis and neuronal migration, and dysplastic changes. *Acta Neuropathol* 119:755-770.
- Weiss LA, Escayg A, Kearney JA, Trudeau M, MacDonald BT, Mori M, *et al.* (2003) Sodium channels SCN1A, SCN2A and SCN3A in familial autism. *Mol Psychiatry* 8:186-194.
- Werling DM, Geschwind DH (2013) Understanding sex bias in autism spectrum disorder. *Proceedings of the National Academy of Sciences* 110:4868-4869.
- Wernig M, Meissner A, Foreman R, Brambrink T, Ku M, Hochedlinger K, *et al.* (2007) In vitro reprogramming of fibroblasts into a pluripotent ES-cell-like state. *Nature* 448:318.
- Westenbroek RE, Hoskins L, Catterall WA (1998) Localization of Ca²⁺ channel subtypes on rat spinal motor neurons, interneurons, and nerve terminals. *J Neurosci* 18:6319-6330.
- Wheeler DG, Groth RD, Ma H, Barrett CF, Owen SF, Safa P, Tsien RW (2012) Ca V 1 and Ca V 2 channels engage distinct modes of Ca²⁺ signaling to control CREB-dependent gene expression. *Cell* 149:1112-1124.
- White JA, McKinney BC, John MC, Powers PA, Kamp TJ, Murphy GG (2008) Conditional forebrain deletion of the L-type calcium channel CaV1.2 disrupts remote spatial memories in mice. *Learning & memory* 15:1-5.
- White SW, Oswald D, Ollendick T, Scahill L (2009) Anxiety in children and adolescents with autism spectrum disorders. *Clin Psychol Rev* 29:216-229.
- Wilson HL, Wong AC, Shaw SR, Tse WY, Stapleton GA, Phelan MC, *et al.* (2003a) Molecular characterisation of the 22q13 deletion syndrome supports the role of haploinsufficiency of SHANK3/PROSAP2 in the major neurological symptoms. *J Med Genet* 40:575-584.
- Wilson HL, Wong ACC, Shaw SR, Tse WY, Stapleton GA, Phelan MC, *et al.* (2003b) Molecular characterisation of the 22q13 deletion syndrome supports the role of haploinsufficiency of SHANK3/PROSAP2 in the major neurological symptoms. *Journal of medical genetics* 40:575-584.
- Wiser O, Bennett MK, Atlas D (1996) Functional interaction of syntaxin and SNAP-25 with voltage-sensitive L- and N-type Ca²⁺ channels. *The EMBO journal* 15:4100.
- Wiser O, Trus M, Hernández A, Renström E, Barg S, Rorsman P, Atlas D (1999) The voltage sensitive L-type Ca²⁺ channel is functionally coupled to the exocytotic machinery. *Proc Natl Acad Sci U S A* 96:248-253.
- Wong TK, Fung PC, Chua SE, McAlonan GM (2008) Abnormal spatiotemporal processing of emotional facial expressions in childhood autism: dipole source analysis of event-related potentials. *Eur J Neurosci* 28:407-416.
- Won H, Lee HR, Gee HY, Mah W, Kim JI, Lee J, *et al.* (2012) Autistic-like social behaviour in Shank2-mutant mice improved by restoring NMDA receptor function. *Nature* 486:261-265.
- Xu Y, Wang L, Liu YZ, Yang Y, Xue X, Wang Z (2016) GABAergic Interneurons are Required for Generation of Slow CA1 Oscillation in Rat Hippocampus. *Neurosci Bull* 32:363-373.
- Yang M, Bozdagi O, Scattoni ML, Wöhr M, Roullet FI, Katz AM, *et al.* (2012) Reduced excitatory neurotransmission and mild autism-relevant phenotypes in adolescent Shank3 null mutant mice. *J Neurosci* 32:6525-6541.
- Yi F, Danko T, Botelho SC, Patzke C, Pak C, Wernig M, Südhof TC (2016) Autism-associated SHANK3 haploinsufficiency causes Ih channelopathy in human neurons. *Science* 352:aaf2669.
- Ylä-Outinen L, Heikkilä J, Skottman H, Suuronen R, Aänismaa R, Narkilahti S (2010) Human cell-based micro electrode array platform for studying neurotoxicity. *Front Neuroeng* 3.
- Yoo AS, Sun AX, Li L, Shcheglovitov A, Portmann T, Li Y, *et al.* (2011) MicroRNA-mediated conversion of human fibroblasts to neurons. *Nature* 476:228-231.
- Young DM, Schenk AK, Yang SB, Jan YN, Jan LY (2010) Altered ultrasonic vocalizations in a tuberous sclerosis mouse model of autism. *Proc Natl Acad Sci U S A* 107:11074-11079.
- Yuen RK, Merico D, Cao H, Pellecchia G, Alipanahi B, Thiruvahindrapuram B, *et al.* (2016) Genome-wide characteristics of de novo mutations in autism. *NPJ Genom Med* 1:160271-1602710.
- Yu J, Vodyanik MA, Smuga-Otto K, Antosiewicz-Bourget J, Frane JL, Tian S, *et al.* (2007) Induced pluripotent stem cell lines derived from human somatic cells. *Science* 318:1917-1920.
- Yu PB, Deng DY, Lai CS, Hong CC, Cuny GD, Bouxsein ML, *et al.* (2008) BMP type I receptor inhibition reduces heterotopic ossification. *Nat Med* 14:1363-1369.
- Yu X, Shacka JJ, Eells JB, Suarez-Quian C, Przygodzki RM, Beleslin-Cokic B, *et al.* (2002) Erythropoietin receptor signalling is required for normal brain development. *Development* 129:505-516.

- Zamponi GW, Striessnig J, Koschak A, Dolphin AC (2015) The Physiology, Pathology, and Pharmacology of Voltage-Gated Calcium Channels and Their Future Therapeutic Potential. *Pharmacol Rev* 67:821-870.
- Zecevic N, Hu F, Jakovcevski I (2011) Interneurons in the developing human neocortex. *Dev Neurobiol* 71:18-33.
- Zhang Y, Bonnan A, Bony G, Ferezou I, Pietropaolo S, Ginger M, *et al.* (2014) Dendritic channelopathies contribute to neocortical and sensory hyperexcitability in *Fmr1(-/-)* mice. *Nat Neurosci* 17:1701-1709.
- Zhang Y, Pak C, Han Y, Ahlenius H, Zhang Z, Chanda S, *et al.* (2013) Rapid single-step induction of functional neurons from human pluripotent stem cells. *Neuron* 78:785-798.
- Zhou T, Benda C, Dunzinger S, Huang Y, Ho JC, Yang J, *et al.* (2012) Generation of human induced pluripotent stem cells from urine samples. *Nat Protoc* 7:2080-2089.
- Zhou Y, Kaiser T, Monteiro P, Zhang X, Van der Goes MS, Wang D, *et al.* (2016) Mice with Shank3 Mutations Associated with ASD and Schizophrenia Display Both Shared and Distinct Defects. *Neuron* 89:147-162.
- Zikopoulos B, Barbas H (2010) Changes in prefrontal axons may disrupt the network in autism. *Journal of Neuroscience* 30:14595-14609.
- Zucker RS (1999) Calcium-and activity-dependent synaptic plasticity. *Curr Opin Neurobiol* 9:305-313.

Appendix 1

Protocol to differentiate hPS cells into cortical neural progenitors

Written by members of the laboratory of
Prof. Jack Price, Institute of Psychiatry, King's College London

Standard Operating Procedure

TC.32

Differentiating iPSCs to Neural Progenitors

Document history

Version No	Effective Date	Details of change	Approved by	Status
1	11/4/2014	-		ARCHIVED
2	20/6/2014	Details regarding biological replicates added; AA2P treatment from D12 onwards		ARCHIVED
3	28/09/14	AA2P treatment from D12 onwards removed from protocol; replaced 1 μ M DM with 100nM LDN193189		ACTIVE

1 PURPOSE

The purpose of this SOP is to describe the procedure for differentiating iPSCs to neural progenitors.

2 INTRODUCTION

iPSCs are plated in 6 well plates at high density and treated with two inhibitors of SMAD signalling – Dorsomorphin and SB431542 – for 7 days to induce neural conversion. Subsequent passaging allows for expansion of progenitors which may then be differentiated to neurons or cryopreserved.

3 DEFINITIONS

SMADi; SMAD Inhibitor

Rocki; Rock Inhibitor

DMEM; Dubecco's Modified Eagle Medium

HBSS; Hank's Balanced Salt Solution

NP; neural passage

4 RESPONSIBILITY

It is the responsibility of the Lab Manager or designates to ensure that all staff comply with the SOP till the end of their post. To minimize the chance of contamination, all manipulations of reagents and cells in open containers are performed using appropriate aseptic cell culture techniques in the Microbiological safety cabinet by personnel trained in safe aseptic cell culture techniques.

5 PRODUCTION MATERIALS AND EQUIPMENT

5 mL/10mL serological pipette

p10/p200/p1000 micropipettes

6-well tissue culture treated plate

Culture media and reagents

Geltrex (Life Technologies; A1413302)

HBSS (Invitrogen; 14170146)

Versene (Lonza; BE17-711E)

E8 Medium (Life Technologies; A1517001)

Ri (Sigma; Y0503)

Accutase (Invitrogen; a1110501)

N2 Supplement (Life Technologies; 17502-048)

DMEM (Sigma; D6421)

B27 Supplement (Life Technologies; 17504-044)

Neurobasal Medium (Life Technologies; 21103-049)

Glutamax (Life Technologies; 35050-038)

SB431542 (Cambridge Bioscience; ZRD-SB-50)

LDN193189 (Sigma; SML0559)

6 PROCEDURE

NOTE - For experiments requiring them, a biological replicate is defined as a culture that has been passaged independently since at least D7. See *Biological Replicates: Example Schematics* for visual representation. As three biological replicates are required, a minimum of three (thereafter, multiples of three) wells must be neutralised at D0.

Day -1

*Note: Plate iPSCs in E8 medium onto 6 well geltrex-coated plates, at a density that will ensure cells reach approaching 100% confluence within 24 hours of plating **24 hours prior to desired neutralisation start time**. Cells should be ~60% confluent prior to replating.*

See Appendix for details regarding timing - If cells do not reach total confluence by D-1 +3d, discard them. Allowing cells to remain at high confluence for longer periods of time diminishes iPSC quality and results in variable growth across the well, as well interfering with the timing of subsequent passages. iPSC passage number must fall between 20 – 50 at the start of neutralisation.

1. Inspect iPSCs for quality and estimate passage ratio.
2. Coat plates with geltrex (see TC.27: Preparation and coating of geltrex). While plates are incubating, remove any differentiating iPSCs.
3. Aspirate total volume of media from each well, and rinse with HBSS at room temperature (RT) (1mL/well) to remove calcium.
4. Add 1mL/well RT versene (EDTA) and incubate (37°C; 5% CO₂; 5% O₂) for 3-5 minutes. Periodically check plates for signs of colonies detaching.
5. Aspirate total volume of versene and replace with 1mL/well RT E8 media. Working rapidly, use a cell lifter to gently detach colonies from plate.
6. Using a 1000µL pipette, carefully pipette up and down **once** (collect cells, pipette suspension across well, collect) to achieve a homogenous suspension of large iPSC clusters.

Note: Breaking the colonies up too much will delay iPSCs in reaching 100% confluence.

7. Using the same procedure, collect suspension from all wells into a 50mL tube. With a 10mL stripette add to existing cell suspension the correct volume of RT E8, such that you have twice the volume of suspension as you do geltrex coated wells.
8. Aspirate geltrex and aliquot E8 across plates at 1mL/well.
9. Using a 10mL stripette transfer (a well at a time) 2mL cell suspension to each well.
10. Rock plates to distribute cells evenly across wells, and incubate (37°C; 5% CO₂; 5% O₂) for 24 hours.
11. Following 24 hour incubation, check plates. If cells are not approaching 100% confluent/are

loosely packed or appear to have suffered during passage, change media (3ml/well RT E8) and wait an additional day before neuralisation.

Day 0

Note: Cells must be 100% confluent, or approaching 100% confluence prior to start of neuralisation. Inducing neuralisation while cells are <100% confluent will result in differentiation towards neural crest or nonspecific cells.

12. Aspirate total volume of E8 medium from each well, and replace with 2mL/well warm 50% N2/50% B27 + 100nM LDN193189 + 10µM SB43 (SMAD inhibitors (SMADi)) (henceforth referred to as “neuralisation medium”). Incubate plate for 24 hours (37°C; 5% CO₂; 20% O₂).
13. Following 24 hour incubation, aspirate neuralisation medium and replace with 2mL/well warm neuralisation medium. Incubate plate for 24 hours (37°C; 5% CO₂; 20% O₂). Continue replacing medium every 24 hours until **Day 7**, or until **formation of a uniform neuroepithelial sheet** occurs.

Note: A substantial amount of cell death occurs within the first 24 hours of neuralisation; shake plates to resuspend dead cells prior to aspirating medium on Day 1. Cell layer thickens during initial stage of neuralisation – take care when changing media (especially from ~ Day 5 onwards), as forceful pipetting can cause cell layer to detach from plate.

Day 7 - np1

Note: At this stage cells must be passaged 1:1.

14. Remove plate(s) from incubator and allow to equilibrate to room temperature (~10 minutes). At the same time, remove HBSS from fridge.
15. Aspirate total volume of medium from each well, and rinse with 1mL/well cool (~10°C) HBSS. Let sit for 30 seconds.
16. Remove total volume of HBSS and add 1mL/well cold (4°C) accutase (keep protected from light). Immediately transfer plate to incubator and incubate for 2 – 5 minutes (37°C; 5% CO₂; 20% O₂), until material can be lifted with gentle pipetting.
17. Prepare 15mL tubes containing RT DMEM at twice the volume of accutase to be added to the tubes.
18. Using a p1000 micropipette, attempt to lift all cells by pipetting up and down as gently and as little as possible no more than 5 times.

Note: Any remaining attached cells can be collected by rinsing the plate with 1mL/well RT DMEM.

19. Collect cells in accutase, and transfer directly into DMEM.

Note: Do this one well at a time (i.e. collect cells and transfer to DMEM before detaching cells from

adjacent well) to minimize exposure of cells to accutase. Avoid exposing cells to air – do not introduce air bubbles; transfer cells in accutase directly into DMEM. Attempt to produce a homogenous suspension of large cell clusters.

20. Rinse plates with DMEM (1mL/well). Add to tube(s) containing accutase/DMEM/cells. Invert tubes to mix.
21. Centrifuge cell suspension (900 RPM for 2 minutes) and carefully remove supernatant, leaving ~50µL atop pelleted cells.
22. Add RT DMEM (at a volume equal to the number of wells transferred to the tube) to tube, and gently flick/shake to resuspend pellet.

Note: Pellet should resuspend very easily – if it doesn't, try to break it up by pipetting up and down gently with a 10mL stripette. If it still doesn't resuspend, continue on to step 23 regardless.

23. Centrifuge cell suspension (900 RPM for 2 minutes).
24. Prepare plates. Aspirate geltrex and aliquot fresh neuralisation medium + 10µM ROCKi across plates at 1mL/well.
25. Carefully remove supernatant from tubes, leaving <50µL atop pelleted cells. Add RT neuralisation medium + 10µM ROCKi to tube, at a volume equal to the number of wells passaged. Resuspend by gently pipetting up and down using a 10mL stripette.

Note: If pellet failed to resuspend during step 22, it probably won't resuspend at this point. Pipette up and down with a 10mL stripette to break up pellet as much as possible, and allow any cell clusters that fail to resuspend to settle to the bottom of the tube. Try not to carry these over to your new plate – remove any unbroken clusters that are transferred using a p100 pipette.

26. Aliquot cell suspension across plates (1mL/well, one well at a time). Rock plate to distribute cells, and incubate for 24 hours (37°C; 5% CO₂; 20% O₂).
27. Following incubation, remove total volume of medium and replace with 2mL/well N2:B27 **ONLY** (i.e. discontinue use of SMADi). Incubate plate (37°C; 5% CO₂; 20% O₂) for 24 hours. Continue replacing medium with fresh N2:B27 every 24 hours until **Day 12**.

Day 12 – np2

28. Passage cells at Day 12, following steps 14 – 27 and replating 1:1 in N2:B27 + 10µM ROCKi. Continue replacing medium with fresh N2:B27 every 24 hours until **Day 15/16**.

Day 15/16 – np3

29. Passage cells at Day 15/16, following steps 14 – 27 and replating 2:3 in N2:B27 + 10µM ROCKi.

Note: Passaging cells as clusters at Days 7 and 12 is critical for survival of the culture. Following Day 15/16 cells can and should be passaged as single cells, to promote proliferation and further differentiation. To this end, previous restrictions implemented in order to minimise fragmentation of the cell layer should now be removed. Use RT HBSS and accutase, and use a p1000 micropipette to fully dissociate cells. Cells may be resuspended using a 5mL stripette. From this point forward, centrifuge cells at 1250RPM for 2 minutes when passaging.

N.B. – np3 falls on a Friday to allow cells to grow to confluence over the weekend. To this end, Days 15/16 are treated as equivalent (no distinction is made between passaging cells for np3 at Day 15 and doing so at D16 – any cultures that were previously out of step may be re-synchronized at this point.

30. Continue replacing medium with fresh N2:B27 every 24 hours until Day 18/19.

Day 18/19 – np4

28. Passage cells at Day 18/19, following steps 14 – 27 and replating 1:2 in N2:B27 + 10 μ M ROCKi.

29. Gently shake flasks to evenly distribute cells, and incubate (37°C; 5% CO₂; 20% O₂) for 24 hours.

PROCEED TO TC.37 “TERMINAL PLATING OF NEURAL PROGENITORS”

7 DATA ANALYSIS

n/a

8 APPENDICES

Timings

To avoid weekend work beyond media changes, it is advised to stick to the following schedule:

Week 1

Monday – No action

Tuesday – Day -1 – Replate cells so that they are ready to be neuralised on Wednesday

Wednesday – Day 0 OR Day -1 – Begin neuralisation OR continue to allow iPSCs to grow to confluence

Thursday – Day 1 OR Day 0 – Change media OR begin neuralisation

Friday – Day 2 OR Day 1 – Change media

Saturday – Day 3 OR Day 2 – Change media

Sunday – Day 4 OR Day 3 – Change media

Week 2

Monday – Day 5 OR Day 4 – Change media

Tuesday – Day 6 OR Day 5 – Change media

Wednesday – Day 7 OR Day 6 – Np1 OR Change media

Thursday – Day 8 OR Day 7 – Change media OR Np1

Friday – Day 9 OR Day 8 – Change media

Saturday – Day 10 OR Day 9 – Change media

Sunday – Day 11 OR Day 10 – Change media

Week 3

Monday – Day 12 OR Day 11 – Np2 OR Change media

Tuesday – Day 13 OR Day 12 – Change media OR Np2

Wednesday – Day 14 OR Day 13 – Change media

Thursday – Day 15 OR Day 14 – Change media

Friday – Day 16 OR Day 15 – Np3 passage 2:3

Saturday – Day 17 OR Day 16 – Change media

Sunday – Day 18 OR Day 17 – Change media

Week 4

Monday – Day 19 OR Day 18 – Np4 - passage 1:2

Tuesday – Day 20 OR Day 19 – Change media. Prepare plates for terminal plating.

Wednesday – Day 21 OR Day 20 – Terminally plate or freeze cells